UNIVERSITÀ
DEGLI STUDI
DI PADOVA

Università degli Studi di Padova

Dipartimento di Science Chimiche

Scuola di Dottorato in Scienze Molecolari

Ciclo XXXII

CLEAVAGE OF PHOSPHATE DIESTERS BY FUNCTIONALIZED GOLD NANOPARTICLES: FROM SIMPLE MODELS TO PLASMID DNA

Direttore della Scuola: Ch.mo. Prof. Leonard J. Prins

Supervisore: Ch.mo. Prof. Paolo M. Scrimin

Dottoranda: Joanna Częścik

Funding

Molecular Tools for Nucleic Acid Manipulation

*for Biological Intervention (**MMBio**)*

This project has received funding from the European Union's Horizon 2020 research and innovation programme under the Marie Skłodowska-Curie grant agreement **No 721613**.

Table of Contents

Abbreviations

K_M	Michaelis-Menten Constant
K_i	Inhibition Constant
k_2	Second-order Rate Constant
k_{cat}	Catalyst Rate Constant
v_0	Initial Velocity/Rate of the Reaction
v_{max}	Maximal Velocity/Rate of the Reaction
A	Adenine
ACN	Acetonitrile
AIBN	*α,α′*-Azoisobutyronitrile
AP	Alkaline Phosphatase
ApA	Adenylyl-3′,5′-adenosine
ApU	Adenylyl-3′,5′-uridine
Asp	Aspartate
ATP	Adenosine 5′-triphosphate
BAPA	Bis-(2-amino-pyridinyl-6-methyl)amine
BNP	Bis-*p*-nitrophenyl Phosphate
Boc-on	2-(Tert-butoxycarbonyloxyimino)-2-phenylacetonitrile
C	Cytosine
CAPS	3-[Cyclohexylamino]1-propanesulfonic Acid
CD spectroscopy	Circular Dichroism Spectroscopy
CHES	2-[*N*-cyclohexylamino]ethanesulfonic Acid
Collidine	2,4,6-Trimethylpyridine
Cyclen	1,4,7,9-Tetraazacyclododecane
DCM	Dichloromethane
DIC	*N,N′*-Diisopropylcarbodiimide
DIPEA	*N,N′*-Diisopropylethylamine

DMP	Dimethyl Phosphate
DNA	Deoxyribonucleic Acid
EDC*HCl	*N*-(3-Dimethylaminopropyl)-*N*′-ethyl-carbodiimide Hydrochloride
EDTA	Ethylenediaminetetraacetic Acid
EPPS	4-(2-Hydroxyethyl)-1- piperazine-propanesulfonic Acid
Fmoc	Florenylmethyloxycarbonyl
G	Guanine
HEPES	4-(2-Hydroxyethyl)-1-piperazineethanesulfonic Acid
His	Histidine
HOBt	Hydroxybenzotriazole
HPNP	2-Hydroxypropyl *p*-nitrophenyl Phosphate
LAH	Lithium Aluminium Hydride
LEFR	Linear Free Energy Relationships
Leu	Leucine
LG	Leaving Group
MES	2-Morpholinoethanesulfonic Acid
MNP	*p*-Nitrophenyl Phosphate Monoester
mTHP	Methoxy-tetrahydropyranyl
$NaBH_4$	Sodium Borohydride
NMP	1-Methyl-2-pyrrolidone
NMR	Nuclear Magnetic Resonance
Oxyma	Ethyl cyano(7ydroxyamino)acetate
Pbf	2,2,4,6,7-Pentamethyldihydrobenzofuran-5-sulfonyl
PEG	Polyethylene Glycol
PNP	*p*-Nitrophenoxide
RNA	Ribonucleic acid
RP HPLC	Reversed Phase High-Performance Liquid Chromatography

RT	Room Temperature
Rt	Retention time
SDS	Sodium Dodecyl Sulfate
Ser	Serine
T	Thymine
TACN	1,4,7-Triazacyclononane
TAE	Tris-acetate-ethylenediaminetetraacetic Acid
TEA	Triethylamine
TEG	Triethylene Glycol
TEM	Transmission Electron Microscopy
TFA	Trifluoroacetic Acid
TGA	Thermogravimetric Analysis
THF	Tetrahydrofuran
Thr	Threonine
TOABr	Tetraoctylammonium bromide
TS	Transition state
U	Uracil
UMP	Uridine monophosphate
UpA	Uridylyl-3′,5′-adenosine
UpPNP	Uridine 3′-*p*-nitrophenyl
UpU	Uridylyl-3′,5′-uridine

Abstract

For many decades, scientists have attempted to understand and replicate nuclease efficiency. These enzymes are responsible for the cleavage of phosphodiester bonds, bonds that constitute the backbone of nucleic acids. By studying nuclease active sites, as well as reported examples of artificial enzymes able to cleave DNA and RNA models, chemists aim to achieve systems possessing better catalytic properties.

Designing artificial nucleases which can overcome the structural complexity and compete with the efficiency observed in Nature's enzymes can be achievable with complex, nevertheless easy to prepare architectures, like gold nanoparticles (AuNPs). Indeed, functionalized AuNPs are one of the most attractive architectures reported so far in terms of phosphodiester cleavage. The necessity for a multistep synthesis can be easily overcome by using thiols as passivating agents that strongly interact with the metal cluster. By precisely tuning the organic thiol structures, it is possible to modulate AuNPs functionalization and properties of the reaction environment. Moreover, taking advantage of supramolecular chemistry principles, multivalency of gold nanoparticles may provide the cooperativity of several active and identical groups, enhancing the catalytic efficiency.

Herein, studies on the cleavage of DNA and RNA models, such as:

- ✓ 2-hydroxypropyl-*p*-nitrophenyl phosphate (HPNP)
- ✓ bis-*p*-nitrophenyl phosphate (BNP)
- ✓ uridine 3'-(LG) phosphates

and easy to manipulate DNA (plasmid pBR322 DNA), using self-assembled gold nanoparticles (AuNPs) are presented. Five different catalytic systems (**AuNP1-5**) were functionalized with at least one zinc complex of 1,4,7-triazacyclononane (TACN), either connected to a hydrocarbon chain (**AuNP1,2**) or decorated with different

flanking species (a second Zn(II) complex, triethyleneoxymethyl derivative or the guanidinium unit of arginine; **AuNP3-5**).

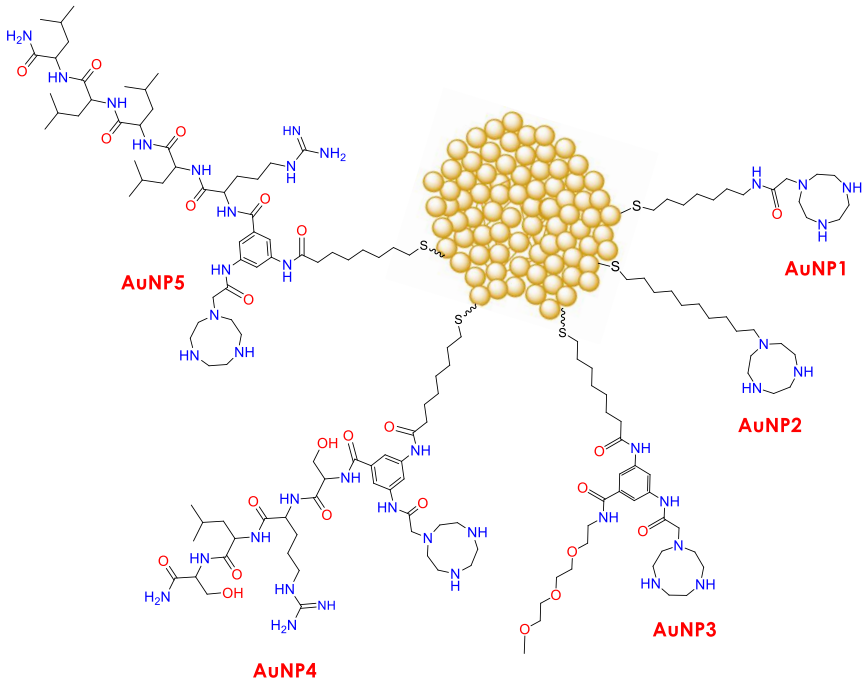

In particular, *chapters 1-3* describe the fundamental aspects of phosphates and nucleic acids, as well as cover the most relevant features contributing to the acceleration of the hydrolysis of nucleic acids by artificial nucleases. Furthermore, the principles of gold nanoparticles, including their properties, synthetic methods, application, as well as techniques of their characterisation are described.

Chapter 4 covers the synthesis and kinetic studies on the hydrolysis of 2-hydroxypropyl *p*-nitrophenyl phosphate. Performed Michaelis-Menten-like kinetics, Zn(II) titration, pH-profiles, kinetic isotopic effect as well as competitive inhibition with dimethyl phosphate enabled the proposal of two mechanisms towards the cleavage of HPNP, based on type of catalytic units present on the AuNP monolayer. Studied AuNPs were able to hydrolyse HPNP almost 1 million times compared to background reaction, being so far one of the most efficient systems cleaving this RNA model substrate.

Chapter 5 reports the results of the cleavage of bis-*p*-nitrophenyl phosphate and pBR322 DNA, as a DNA model substrate (the former one) and an example of a real

polymer (the latter one). Thorough studies revealed significant differences in AuNPs catalytic activity in the hydrolysis of BNP and plasmid DNA. Among all studied nanozymes, only a Y-shaped species decorated with a peptide comprising serine and arginine in its sequence (**AuNP4**) was able to efficiently convert the supercoiled DNA into its nicked form in less than 3-4 hours at 35 μM concentration. Interestingly, in the hydrolysis of much simpler model BNP, the most reactive were nanozymes **AuNP1-3**, displaying only a minimal efficiency in the plasmid DNA cleavage.

Chapter 6 reports studies dedicated to the leaving group departure from uridine 3'-(LG) phosphates with the most efficient in HPNP and BNP cleavage, **AuNP1**. Final results of the hydrolysis of chosen nucleotides were presented in the form of Brønsted plot, displaying no change throughout the explored pK*a* range of leaving groups. Furthermore, a great negative value of the Brønsted constant suggested a significant development of anionic charge in the transition state (β_{LG} = -0.86).

Taking advantage of the reactivity and ease in monitoring the cleavage of uridine 3'-*p*-nitrophenyl phosphate, more detailed UV-Vis-based kinetic studies in the presence of either **AuNP1** or the zinc complex of 1,3-di(1,4,7-triazonan-1-yl)propan-2-ol Zn_2(**4e**) were performed, providing additional information about Zn(II)-TACN interactions with uracil. Moreover, the reactivity and catalytic properties of **AuNP1** *vs* Zn_2(**4e**) in nucleotide cleavage revealed that, due to conformational flexibility, nanoparticles **1** were able to easily accommodate bulky substrates, contrary to what happens with the rigid Zn_2(**4e**).

The presented supramolecular systems appear to be among the best reported catalysts for the cleavage of studied nucleic acids model substrates. Mechanistic investigations afforded a detailed information of the way AuNPs hydrolyse phosphodiester linkages. It has been demonstrated that the proper design and synthesis of nanoparticles may embrace significant factors that make nucleases one of the most efficient enzymes encountered in Nature.

Chapter 1

1. *What Governs the Importance of Nucleic Acids? A Brief History of DNA and RNA: Structure, Stability and Cleavage.*

There are two types of nucleic acids found in cells: DNA (deoxyribonucleic acid) and RNA (ribonucleic acid), both of which play a pivotal role for a cell function, and therefore, are the essence of life on Earth. Simply speaking, they control the genetic information that makes every organism what it is. Similar to other macromolecules such as peptides and polysaccharides, DNA and RNA are long biopolymers made up of multiple similar units, in their case called nucleotides. Each nucleotide consists of a nitrogen base, sugar moiety and the phosphodiester bond (*Fig.1.1.*).

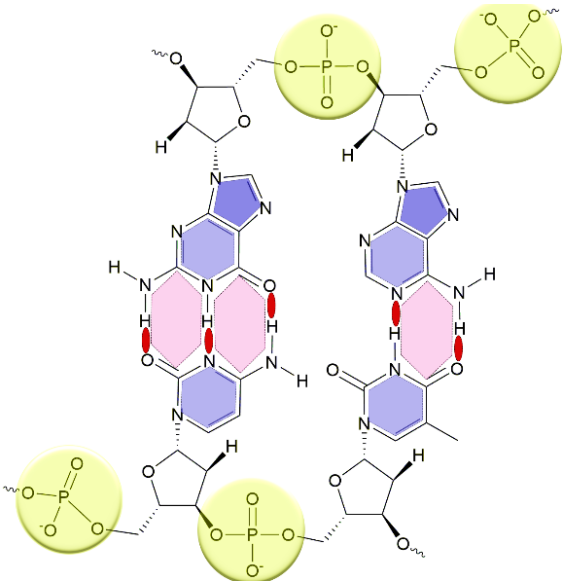

Fig.1.1. The schematic representation of DNA structure and base pairs formation *via* hydrogen bonding.

There are five different molecules belonging to DNA and RNA nucleobases, derived from either a purine (adenine (A) and guanine (G)) or pyrimidine (cytosine (C), thymine (T) and uracil (U)). The ability to form base pairs can be attributed to

hydrogen bonds and π-π stacking interactions which constitutes the fundament of a long-chain helical-like structure of nucleic acids. Like an alphabet is used to create words, the order of nucleobases in DNA forms a language of cells, and this language is biologically expressed in the form of genes. Particularly, genes are fundamental for proteins' synthesis (which is a main function of RNA). In terms of sugar moieties, nucleic acids possess a ribose as a foundation. DNA uses its modified version deprived of 2'-oxygen (deoxyribose). This makes this nucleic acid less polar (more hydrophobic) than RNA. The last, 3rd moiety constituting a nucleotide unit is a phosphodiester bond, which was Nature's solution to protect nucleic acids from rapid hydrolysis. Indeed, the phosphorus of a phosphate diester being surrounded by a cloud of negative charge does efficiently repulse nucleophilic attack by anions. That is why DNA and RNA reveal an extremely high resistance and sluggish reactivity under physiological conditions, which is vital for their biological function.

Excluding their many similarities, nucleic acids differ not only in their function, the presence of either thymine (DNA) or uracil (RNA) and single vs. double stranded nature, but also in their stability. As mentioned above, the structure of DNA is very similar to that of RNA with the main difference in sugar moiety. This has been found to account for a massive difference in nucleic acids reactivity. Ribose, possessing a hydroxyl group at 2' position, leads to a faster degradation of RNA vs. DNA at higher pH than 2-3. The -OH can play the role of internal nucleophile attacking a phosphorus atom and therefore performing RNA cleavage through a cleavage of the adjacent phosphate. Thus, by removing the hydroxyl from ribose, DNA avoids being easily broken down. As with everything in Nature, this difference has a rational explanation: RNA plays a short-term role sending messages and synthesising proteins as part of gene expression, thus the 2'-hydroxyl group helps to decompose RNA quickly, effectively switching the affected genes to their *off state*. DNA however, being a genetic backbone of living organisms, must retain greater stability. That is why Nature has deprived it from any internal sources which can lead to its potential degradation. Indeed, the most reliable estimates on the stability of the phosphodiester bond, based

on high temperature studies on simple models phosphates, indicate that the hydrolytic half-life of RNA and DNA is in the range of approximately 100 years and millions of years at neutral pH, respectively.[1], [2]

Nature, however, always requires an equilibrium and therefore, nucleic acid backbones must be cleavable as well. That ensures the manipulation, repair and synthesis of DNA and RNA. Nucleases, being one of the most efficient enzymes within Nature, are responsible for very effective hydrolysis of phosphodiesters.

2. *Nucleases – Nature's Backbone-Breaking Agents.*

Nucleases (also known as phosphodiesterases) are indispensable to life. They play an integral role of DNA replication (the 5′ to 3′ exo- and endonucleases have to remove RNA primers as well as the 3′ to 5′ exonuclease for proofreading), recombination and repair.[3], [4] Moreover, nuclease activity is needed for the site-specific recombination, topoisomerization or RNA splicing.[5],[6] During these processes, a phosphodiester linkage is temporarily broken and either reformed after strand passing or transferred to a new target. Furthermore, DNA and RNA degradation is pivotal for microbial defence mechanisms, programmed cell death or for avoiding overexpression of already synthesised protein.[7]

DNA and RNA present two types of phosphodiester cleavage: 3′ or 5′ of a scissile phosphate. The principle of that cleavage lies in the nucleophilic substitution; however, the structure and hydrolytic mechanism of phosphodiesterases is much more complex. The structure of nucleases is mostly based on proteins and in many cases, the presence of at least one metal ion is often required for enzymes catalytic activity. Based on the substrate preference, nucleases can be divided into DNase and RNase or, depending on whether the 5′ or 3′ end is required for a DNA's or RNA's

recognition, we have an exo- and endonucleases. Accordingly, there is no simple way to classify these enzymes.

Nevertheless, as presented in *Fig.1.2.*, all nucleases can cleave one of the two bridging P-O bonds (3′ (a) or 5′ (b)) in DNA and RNA. The commonly accepted approach is based on a general acid-base catalysis, where a nucleophile is activated by its deprotonation (by a general base) and leaving group protonation, which facilitates its departure as an alcohol (by a general acid).

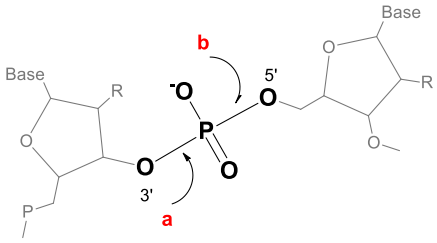

Fig.1.2.

The phosphodiester hydrolysis can be divided into three steps: nucleophilic attack, formation of the penta-coordinated species or transition state and lastly, the cleavage of the scissile bond. Eventually, it results with the formation of either 5′ or 3′ phosphates and 5′ or 3′-OH groups.

In terms of nucleophiles, nucleases may utilize a deprotonated water molecule or hydroxyl. As already mentioned, due to the presence of the 2′-OH group in ribose, RNA is already encompassed with a species attacking the phosphorus atom. Afterwards, the formation of 2′,3′-cyclic phosphate occurs, which is consecutively hydrolysed yielding a 3′-phosphate or occasionally a 2′-phosphate.[8], [9]

For DNA cleavage (more in *Chapter 5*), it was observed that the side chains of serine, tyrosine and histidine were serving as nucleophiles to form a covalent DNA protein-phosphate intermediate. This species can be subsequently resolved by either the hydrolysis via two-step cleavage or phosphoryl transfer reaction back to DNA due to recombination and topoisomerization.[10], [11]

Nevertheless, because of a vast variety of classes of nucleases, the way they are accelerating the hydrolysis of phosphodiester bond cannot be just limited to above described examples.

3. *Phosphates: The Champions of Natural Selection. Differences Between Mono, Di and Tri-Phosphoesters.*

Phosphates are not only present in nucleic acids as it is described above, but also they stand for the principal reservoirs of bio-chemical energy (ATP, creatine phosphate) or being a part of intermediary metabolite structures. Furthermore, they are relevant in biochemical syntheses and degradation.[12] Consequently, phosphates are essential for the existence of living organisms.

In 1958 Davis in his work entitled *The importance of being ionized* explained the relevance of phosphates.[13] Living organisms have to conserve all of their metabolites within the membrane's cell, otherwise they may get diffused and lost by dilution in water outside the mother cell. Thus, the greater the charge possessed by these molecules, the greater the chance they will not pass through a membrane. Most ionized molecules like salts or species with p*K*a less than 4 remain in their ionized form at physiological pH. The p*K*a of phosphoric acid and phosphomono- and diesters are in the range of 1.3-2.2, thus phosphates can be easily trapped within cells.[14] It may also explain why Nature did not chose phosphotriesters as a fundament of genetic material; not only they can be hydrolysed faster than other phosphates, but also the fact that they are not ionized may result with their escape from cells.[15] Additionally, the presence of a negative charge sharply diminishes the rate of nucleophilic attack on the ester, which stands for the stability of nucleic acids. Triesters of phosphoric acid are deprived of that property.

Apart from Davis, Westheimer and Warshel added two more relevant factors explaining the phenomena of phosphates, further adding to their importance. The first one published in 1983 a work titled *Why nature chose phosphates*, focused mostly on the high stability of phosphates towards hydrolytic cleavage (which allows for the protection of genetic information).[12] The second published more recently (2013) *Why nature really chose phosphates*, analysed the possibility of control of the reactivity of phosphates towards faster and slower reactions by exploiting the electrostatics.[16]

Comparing the phosphomono- and diesters there is a great difference in terms of their acidity and mechanistic behaviour towards non-enzymatic hydrolysis. A phosphodiester is the strongest acid among all phosphate esters (pKa~1.3) ensuring the ionized form of nucleic acids at physiological pH. In the non-enzymatic basic hydrolysis, phosphomonoesters proceed *via* S_N2-like mechanism being in their most favoured, mono-deprotonated form. Upon nucleophilic attack, monoesters form a transition state where one available proton serves as an intramolecular general acid, therefore stabilizing a charge build-up on the leaving group (alcohol) in the rate determining step. The situation looks different with phosphodiesters, where there is no proton to serve as a general acid. Consequently, intermediates release the leaving group as an alkoxide, which can be further protonated due to a proton transfer.

4. *Phosphate Esters Cleavage – Mechanisms of the Phosphoryl Transfer.*

Even the simplest phosphoesters can be hydrolysed through a variety of mechanisms. Phosphate mono-, di-, and triesters undergo a hydrolytic cleavage through different mechanisms, transition states, revealing distinct degrees of bond formation, breaking and distribution of charge. A preferred mechanism may be additionally complicated by other features, such as level of esterification, solvent choice and pH. To simplify the understanding of relatively complex phosphate cleavage, attention will be focused on the most commonly accepted phosphoryl-transfer mechanisms: dissociative, associative and concerted (*Fig.1.3.*).[17]

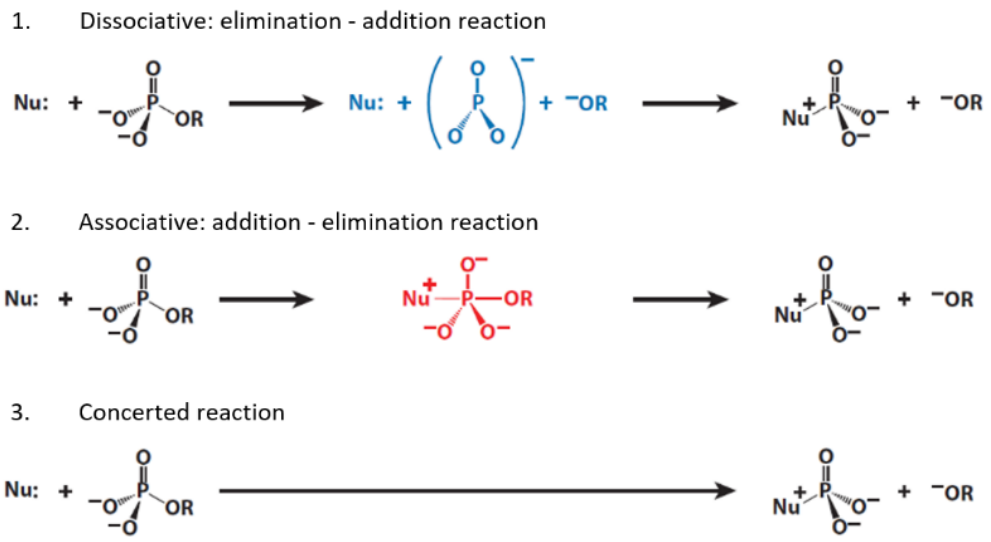

Fig.1.3. Mechanistic pathways of phosphoryl-transfer mechanisms: dissociative, associative and concerted.

The hydrolysis of phosphate monoesters is generally thought to proceed *via* loose, dissociative species with a great degree of a charge build-up on the leaving group and limited nucleophile impact.[18] Therefore, a dissociative mechanism is a stepwise elimination-addition with a metaphosphate intermediate, upon formation overtakes the nucleophilic attack. As a natural consequence, monoesters display both larger dependence on leaving group reactivity and smaller on nucleophile (β_{LG} = -1.23 for hydrolysis reactions and β_{NUC} = 0.13 for substituted pyridines attacking 4-nitrophenyl phosphate; all kinetic data were collected at different pH taking into account the fraction of free amine according to its p*K*a).[19], [20]

In terms of phosphodiesters, the hydrolysis occurs mostly *via* a more synchronous transition state. The total bond order of the phosphorus atom to the leaving group resembles the one in the ground state. Diester reactions have usually a relatively large, negative β_{LG} values (e.g. β_{LG} = -0.97 for the hydrolysis of a series of diaryl phosphates) which indicates a substantial bond breaking between the departing oxygen and phosphorus in TS. Taking also into consideration a nucleophile dependence

(β_{NUC} = 0.37 for 2,4-dinitrophenyl LG) it is clear that the phosphodiester cleavage is concerted, involving simultaneous bond formation and bond cleavage.[21]

Lastly, phosphotriester hydrolysis follows the associative mechanism, which is a stepwise addition-elimination with a stable penta-coordinate intermediate. In that mechanism, the nucleophilic attack overtakes the formation of an unstable transition state. Phosphotriesters exhibit, on the contrary to previous cases, an increased sensitivity to nucleophile and a decreased one to the leaving group departure (β_{LG} = -0.4 for the hydroxide nucleophile and β_{NUC} = 0.61 for substituted pyridines and 2,4-dinitrophenyl LG).[15] Interestingly, di- and triesters reveal equal dependence on the p*K*a of oxyanions nucleophiles (β_{NUC} = 0.3 for 2,4-dinitrophenyl LG) meaning that the phosphodiester cleavage with an oxyanion nucleophile requires a more associative transition state to overcome electrostatic repulsion between nucleophile and the negatively charged phosphoryl centre. All presented mechanistic pathways are based on a great variety of studies relying on isotope effects or LEFR (linear free energy relationships).[17], [22]

Probably the most convenient way to depict all of possible mechanisms are More O'Ferrall-Jencks diagrams (*Fig.1.4.*).[17] In a two-dimensional reaction coordinate diagram, the phosphate esters (reactants) are located in the lower left corner, the products of hydrolysis in the upper right. Bond breaking and formation proceeds along the x- and y-axis, respectively. Notably, a transition state constitutes a maximum along the reaction pathway, but a minimum in the direction perpendicular to the reaction pathway (saddle point).[17] Therefore, More O'Ferrall-Jencks diagrams depict the continuum of possible reaction pathways between the two extremes of a dissociative mechanism (lower right corner) and associative (upper left corner).

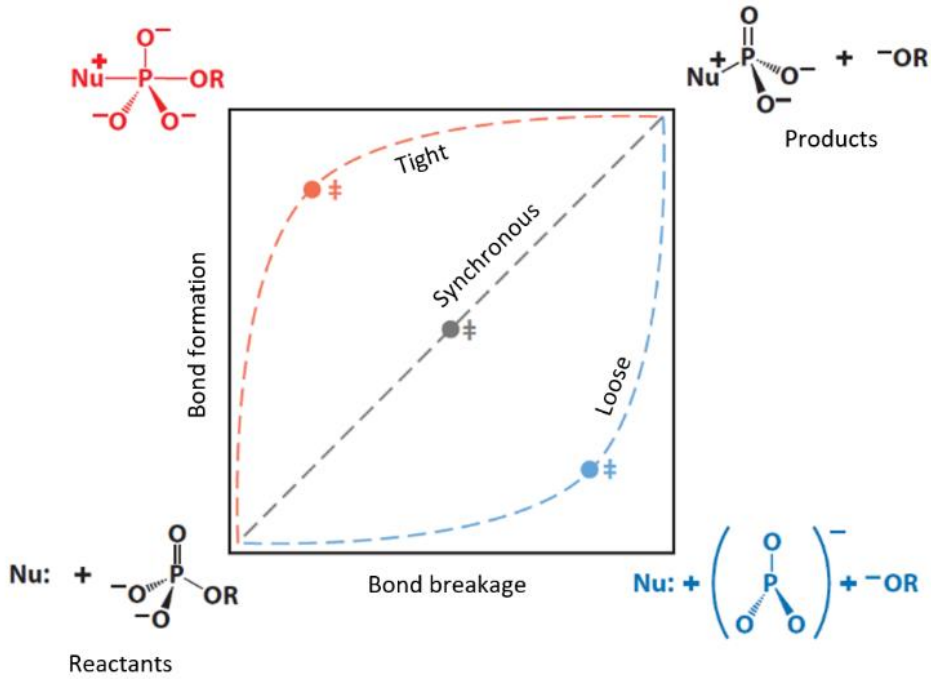

Fig.1.4. Two-dimensional More O'Ferrall-Jencks reaction coordinate diagram for phosphates cleavage.

In the particular case of RNA cleavage, the mechanism of hydrolysis is dependent on the conditions; in the base-catalysed cleavage (*Fig.1.5.*), firstly an intramolecular attack of deprotonated 2'-OH occurs followed by the formation of a dianionic penta-coordinated cyclic phosphate. Since that intermediate is highly negative and unstable, the next step is a straight departure of the leaving group being in its apical position (Westheimer rule) yielding two products: cyclic phosphate and alkoxide.[23]

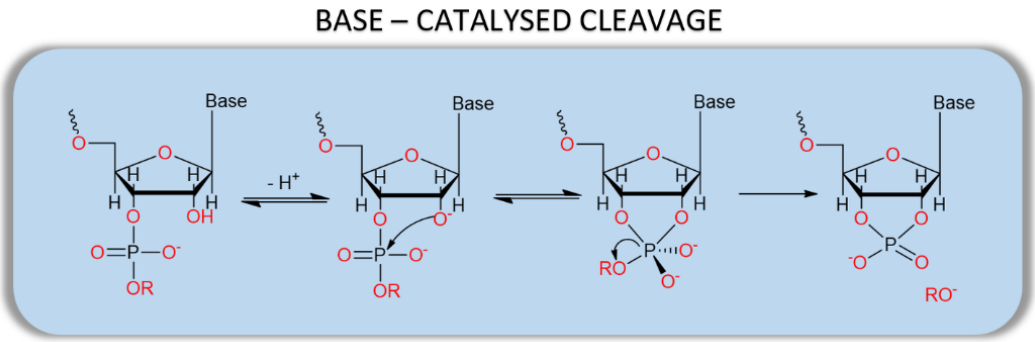

Fig.1.5. The mechanism of the base-catalysed RNA cleavage.

A pH-independent cleavage (where 2'-hydroxyl is the nucleophile, not a hydroxide) a proton transfer to a non-bridging phosphate oxygen occurs simultaneously with a nucleophilic attack (*Fig.1.6.*). Since formed penta-coordinated intermediate is stable enough to pseudo-rotate, its isomerisation can proceed via A_N + D_N (associative) pathway, which may result in either a further departure of the leaving group, yielding the cyclic phosphate product, or with a formation of the isomer of the starting phosphate. Thus, a change of the mechanism may be substantially induced by the protonation/lack of protonation of the nucleophile.

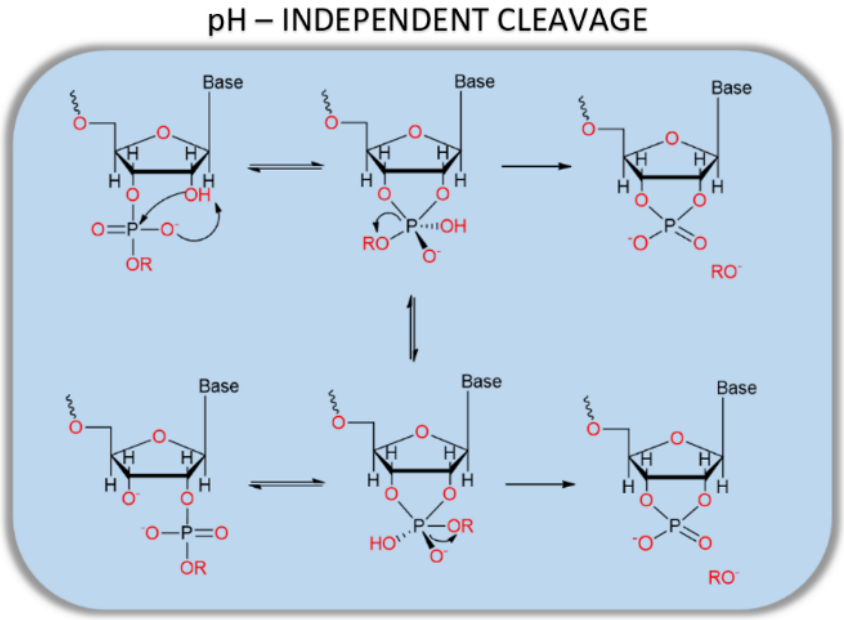

Fig.1.6. The mechanism of the pH-independent RNA cleavage.

5. *LFER – a Powerful Tool Providing the Insight into the Nature of Transition States.*

To date, no experimental methods have been developed which allows for direct visualization of a transition state for any reactions in solution. Indeed, on contrary to intermediate, a transition state is represented as local maximum on the reaction coordinate diagram (*Fig.1.7.*) and its lifetime lasts for just one bond vibration cycle. However, kinetic studies may be a great tool to understand the properties of a transition state, what in consequence may give direct information about the reaction rate determining step.

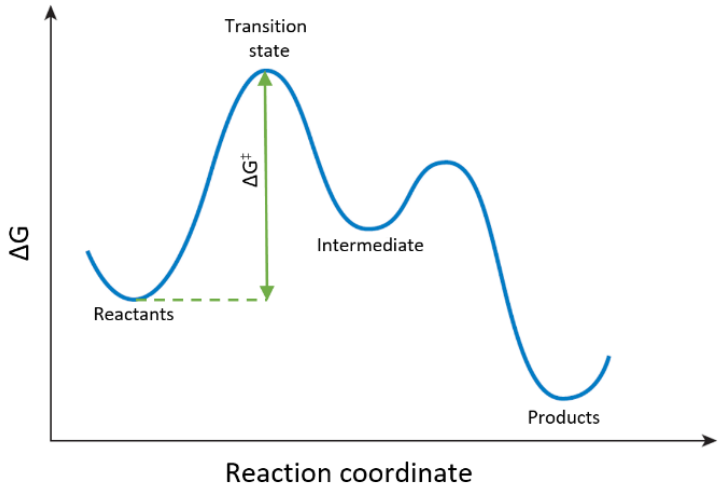

Fig.1.7.

Probably the most powerful experimental method is to study the linear free energy relationships (LFER), making quantitative inferences about the nature of transition state's bonding, geometry and charge distribution.[24] The idea behind LFER is quite intuitive: if a chemical bond is broken or formed in a TS, the change from reactants to transition state in electron density and charge will take place. Adding the electron-donating groups will destabilize developing negative charge and stabilize a positive one, whereas the electron donating groups will have the opposite effect.[25] Hence, to comprehend the charge build-up in the transition state, the studies on different leaving groups bearing both, electron-donating and withdrawing groups should be performed. For instance, in a tight transition state with a little bond cleavage to the LG, electron-donating groups give a large rate increases, on contrary to loose TS, where electron-withdrawing groups enhances the reaction rate constant.

In practice, LFER is usually reported as a function of the logarithm of the reaction rate constant log(k) vs logarithm of p*K*a of the leaving groups (or nucleophiles). The slopes

of so-called Bronsted plots (β) may provide a better insight into the type of TS (loose TS – steep β, tight TS – shallow β), reveal a presence of intermediates (in the shape of convex points) and in general, may help to elucidate the role of the LG (or nucleophiles) in the reaction's rate determining step.[17]

The variations between different LG and how they may contribute to the cleavage rates of phosphate esters may be simply presented with the hydrolysis of the phenyl phosphate dianion (*Fig.1.8.*).

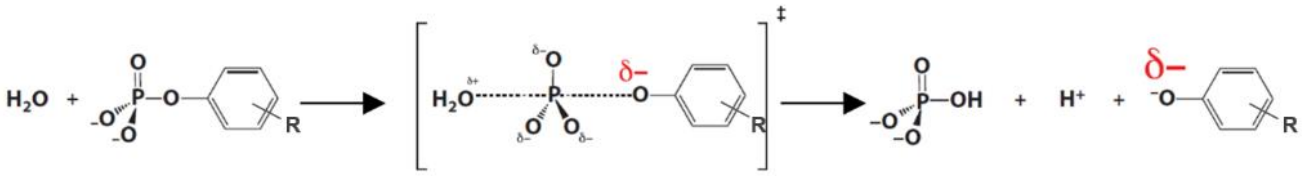

Fig.1.8. Mechanistic pathway of the cleavage of phenyl phosphate dianion.

The hydrolysis starts with the P-O bond breakage to the phenolate LG, what results with net charge equal to -1 on phenolate oxygen. Adding the electron-withdrawing LG such as nitro group (*Fig.1.9.*) stabilizes not only a developing negative charge on phenolate oxygen, but also a phenolate product in overall equilibrium.

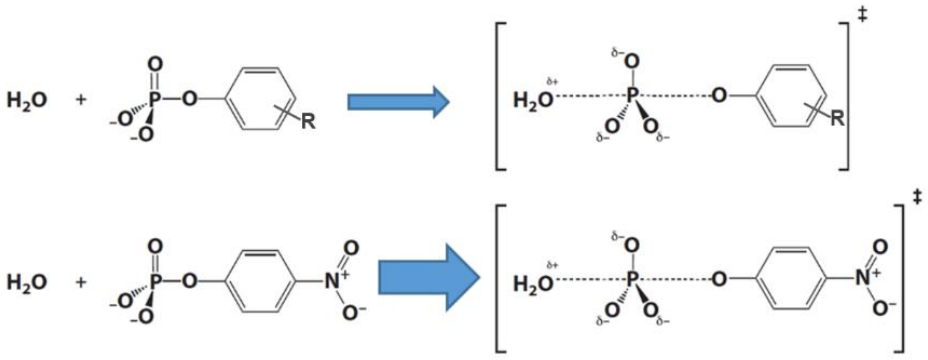

Fig. 1.9. Stabilization of the negative charge on phenolate oxygen with and without EWG.

Simply speaking, the better the leaving group in the phosphate cleavage (lower p*K*a), the faster the reaction and the more stabilized are the final products. Specifically, for the phenyl phosphate dianion example, the presence of the nitro group lowers the p*K*a of the leaving group, which substantially facilitates the departure of the LG as an aryloxide or oxyanion, without the need of its prior protonation (specifically, if departure of the leaving group is the rate determining step or is involved in the rate-determining step in concerted mechanism).

6. *References of Chapter 1.*

[1] P. Jarvinen, M. Oivanen, H. Lonnberg, *The Journal of Organic Chemistry* **1991**, *56*, 5396-5401.

[2] G. K. Schroeder, C. Lad, P. Wyman, N. H. Williams, R. Wolfenden, *Proceedings of the National Academy of Sciences of the United States of America* **2006**, *103*, 4052-4055.

[3] H. I. Kao, R. A. Bambara, *Critical reviews in biochemistry and molecular biology* **2003**, *38*, 433-452.

[4] B. Shen, P. Singh, R. Liu, J. Qiu, L. Zheng, L. D. Finger, S. Alas, *BioEssays : news and reviews in molecular, cellular and developmental biology* **2005**, *27*, 717-729.

[5] J. J. Champoux, *Annual review of biochemistry* **2001**, *70*, 369-413.

[6] J. C. Wang, *Nature reviews. Molecular cell biology* **2002**, *3*, 430-440.

[7] W. Yang, *Quarterly reviews of biophysics* **2011**, *44*, 1-93.

[8] J. Abelson, C. R. Trotta, H. Li, *The Journal of biological chemistry* **1998**, *273*, 12685-12688.

[9] R. T. Raines, *Chem Rev* **1998**, *98*, 1045-1066.

[10] N. D. Grindley, K. L. Whiteson, P. A. Rice, *Annual review of biochemistry* **2006**, *75*, 567-605.

[11] J. A. Stuckey, J. E. Dixon, *Nature structural biology* **1999**, *6*, 278-284.

[12] F. H. Westheimer, *Science (New York, N.Y.)* **1987**, *235*, 1173-1178.

[13] B. D. Davis, *Archives of biochemistry and biophysics* **1958**, *78*, 497-509.

[14] M. Wojciechowski, T. Grycuk, J. M. Antosiewicz, B. Lesyng, *Biophys J* **2003**, *84*, 750-756.

[15] S. A. Khan, A. J. Kirby, *Journal of the Chemical Society B: Physical Organic* **1970**, 1172-1182.

[16] S. C. Kamerlin, P. K. Sharma, R. B. Prasad, A. Warshel, *Q Rev Biophys* **2013**, *46*, 1-132.

[17] J. K. Lassila, J. G. Zalatan, D. Herschlag, *Annual review of biochemistry* **2011**, *80*, 669-702.

[18] M. F. Mohamed, F. Hollfelder, *Biochimica et Biophysica Acta (BBA) - Proteins and Proteomics* **2013**, *1834*, 417-424.

[19] A. J. Kirby, W. P. Jencks, *Journal of the American Chemical Society* **1965**, *87*, 3209-3216.

[20] A. J. Kirby, A. G. Varvoglis, *Journal of the American Chemical Society* **1967**, *89*, 415-423.

[21] A. J. Kirby, M. Younas, *Journal of the Chemical Society B: Physical Organic* **1970**, 1165-1172.

[22] W. W. Cleland, A. C. Hengge, *Chemical Reviews* **2006**, *106*, 3252-3278.

[23] F. H. Westheimer, *Accounts of Chemical Research* **1968**, *1*, 70-78.

[24] M. Huang, D. M. York, *Phys Chem Chem Phys* **2014**, *16*, 15846-15855.

[25] ain *Free Energy Relationships in Organic and Bio-Organic Chemistry* (Ed.: A. Williams), The Royal Society of Chemistry, **2003**, pp. 1-16; bin *Free Energy Relationships in Organic and Bio-Organic Chemistry* (Ed.: A. Williams), The Royal Society of Chemistry, **2003**, pp. 55-74.

Chapter 2

1. *Metallonucleases in Phosphate Ester Cleavage.*

As mentioned in *Chapter 1*, there is no single "recipe" for nucleases' hydrolytic success. There are myriad ways in which they accelerate phosphate cleavage. However, among all of the subclasses, a great interest has been devoted to a superfamily of nucleases possessing in their active sites divalent metal ions, called metallonucleases.[1], [2] The established mechanisms where metal ions are enhancing the phosphodiester cleavage include, for instance, a Lewis acid activation, the ability to facilitate the formation of the nucleophile, decreasing the electrostatic repulsions or improving the ability of the leaving group to depart.[3], [4] Below described examples illustrate versatility and importance of metal ions in Nature's nucleases.

Enzymes known as Ribonucleases H are hydrolysing the RNA of RNA-DNA hybrids. The most studied example, isolated from *Escherichia Coli,* is a 17.6 kDa protein (*Fig. 2.1.*). Its active site consists of four negatively charged amino acid residues (aspartates and glutamate, so called DEDD motif). For the maximal hydrolytic efficiency, at least one or two metal ions and one water molecule are required (sometimes the additional histidine residue is conserved).[5] In most cases, both metal ions are coordinated by the acidic DEDD motif. One metal (usually Mg^{2+}) is essential for a substrate-assisted nucleophile formation and the release of product, whereas the second metal may destabilize the enzyme–substrate complex, promoting the

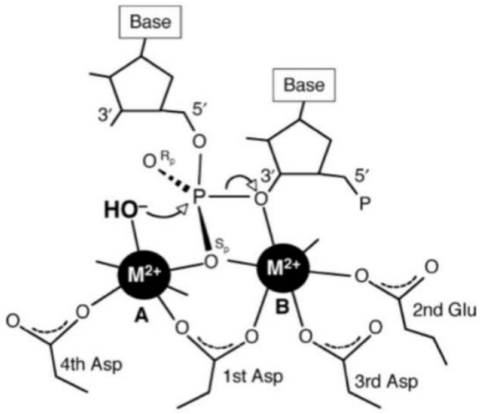

Fig.2.1.

phosphoryl transfer. In that way, the hydrophobic pocket for the substrate recognition and binding, as well as the presence of metal ions, can lead a good environment for the negatively charged RNA.

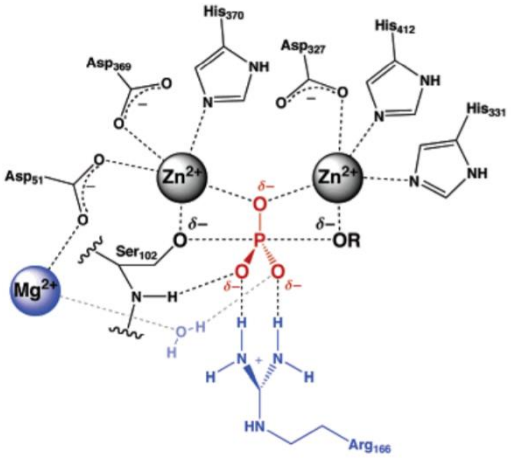

Fig.2.2.

Another example is Alkaline Phosphatase (AP), the enzyme of the 1960's, also isolated from *Escherichia Coli* bacteria (*Fig.2.2.*). In terms of function, AP is dephosphorylating organic species (i.e. it is responsible for the hydrolysis of a phosphate moiety from organic compounds) and it is active in alkaline environments (pH > 7.5).[6] The active site of AP constitutes a dimer composed of two identical inactive subunits with a total molecular weight 86 kDa. One subunit contains two zinc atoms (being c.a. 4 Å apart), one magnesium which is vital for the catalytic function (however, magnesium is not taking part in the hydrolysis but it contributes to the electrostatic potential around the active site).[7], [8] One zinc is penta-coordinated to His-331, His-412, two oxygens of Asp-327 and one of the phosphate substrate. The second tetra-coordinated zinc binds His-370, one oxygen of phosphate substrate, Asp-369 and Asp-51.

There are several roles suggested for two Zn(II) ions in the active site. They may bind phosphate esters and stabilize a formed intermediate upon Ser-102 nucleophilic attack or facilitate a departure of the leaving group (alcohol) by lowering p*K*a of a zinc-bound water molecule. Furthermore, metal ions may assist in release of phosphates (after nucleophilic attack of a water molecule).[9]

Apart from Alkaline Phosphatase, nucleases like Phospholipase C, P1 nuclease, Phosphodiesterase or Ser/Thr Phosphatase also do require the presence of at least two Zn(II) in their active sites. [10], [11], [12], [13]

The reason behind Nature's choice of these particular element which constitutes the active site of many nucleases will be explained in detail in the next paragraph.

2. *Zn(II) – the Most Promiscuous Lewis Acid for DNA and RNA Cleavage? Features of the 'Best' Metal Ion in Phosphate Hydrolysis.*

Among all divalent metal ions such as magnesium, cobalt, copper or iron, zinc (Zn^{2+}) seems to be the most attractive option for enzymatic DNA and RNA hydrolysis. It has been demonstrated to be essential for the growth, development and differentiation of all types of life.[14] Interestingly, after iron, it is the most abundant trace metal in the human body: an average 70 kg man contains 2.3 g of Zn(II).[15] Since the discovery of Carbonic Anhydrase II in 1940 by Keilin and Mann, more than 300 zinc enzymes (covering all six classes of enzymes) have been discovered.[16], [17]

In terms of zinc properties, one may be thinking they are not exceptional compared to other metals present in nucleases. However, Zn(II) has a *d* orbital totally filled which means it does not participate in redox reactions and is eager to accept a pair of electrons making it a good Lewis acid. With the lack of redox chemistry, Zn(II) is stable in biological environments. The *d*-shell orbital of zinc has low energetic barriers to multiple equally accessible coordination geometries, that can be used to alter the reactivity of the metal ion. An attractive and useful property of Zn(II) is also rapid ligand exchange, allowing for an efficient dissociation of the product required for fast turnover.[18]

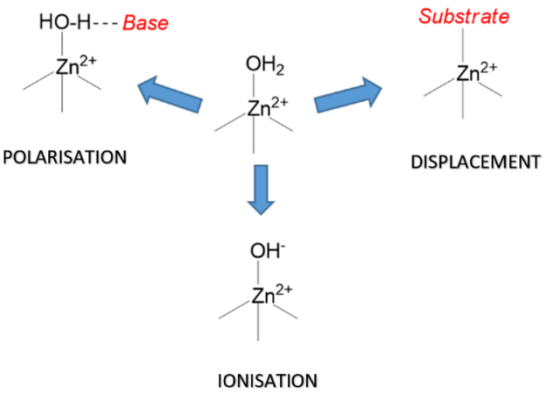

Fig.2.3.

When present in enzymatic active sites, zinc exists with an open coordination sphere, thus zinc-binding polyhedra contain at least one water molecule apart from three or four other ligands, depending on the metal geometry. A zinc-bound water molecule is a vital part of metallonucleases catalytic sites and, indeed, it can have several functions: activation for the nucleophilic attack by lowering the p*K*a (a nucleophile can be generated by a coordination of water to Zn(II), that shifts the dissociation equilibrium towards hydroxide formation), polarizability by a base or displacement by a substrate (*Fig.2.3.*).

However, not only zinc-coordinated water plays a role in catalysis. Indeed, there are two types of modes describing how metal ions can enhance the efficiency of the phosphoesters cleavage, these are known as direct and indirect (*Figs.2.4., 2.5.*).[19]

Direct modes involve the activation of the electrophile, nucleophile or leaving group. Taking Zn(II) directly coordinated to phosphate carbonyl group as an example, it can act as a Lewis acid by removing the electron density, facilitating the nucleophilic attack and stabilizing the transition state. Coordinated to the leaving group, it is promoting its departure of the LG (as an alkoxide). If the nucleophile constitutes a water/alcohol molecule, coordinated Zn(II) can decrease its p*K*a facilitating nucleophile deprotonation therefore making nucleophilic attack more favourable even at neutral pH.

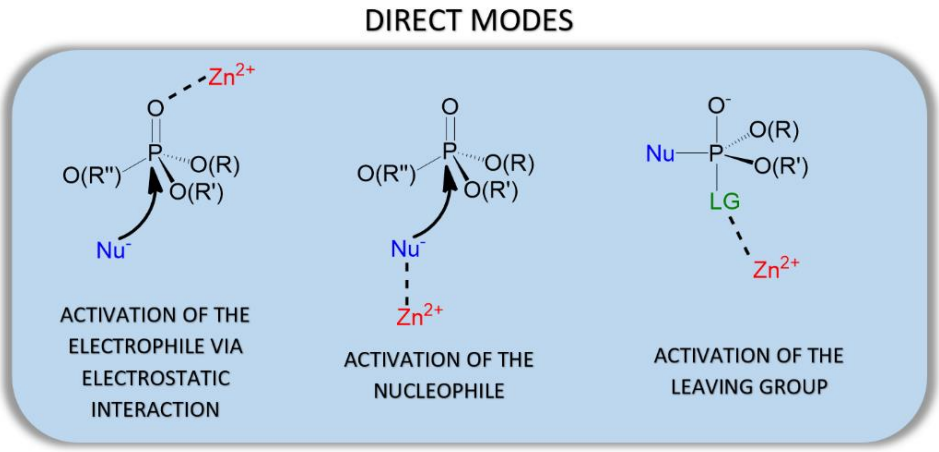

Fig.2.4. Direct modes of the phosphate esters cleavage in the presence of Zn(II).

Indirect modes include the general acid or base catalysis and template effect. Since due to the metal-ion coordination a water molecule is more acidic, it is more prone to transfer a proton to the leaving group (especially the one with a low p*K*a), stabilizing the negative charge and facilitating LG departure. Zinc-hydroxide however, can play the role of the general base by deprotonating water molecule (nucleophile), attacking the phosphate ester. In terms of the template effect, zinc brings the electrophile and nucleophile into a close proximity, which results in a reduction of electrostatic repulsion.

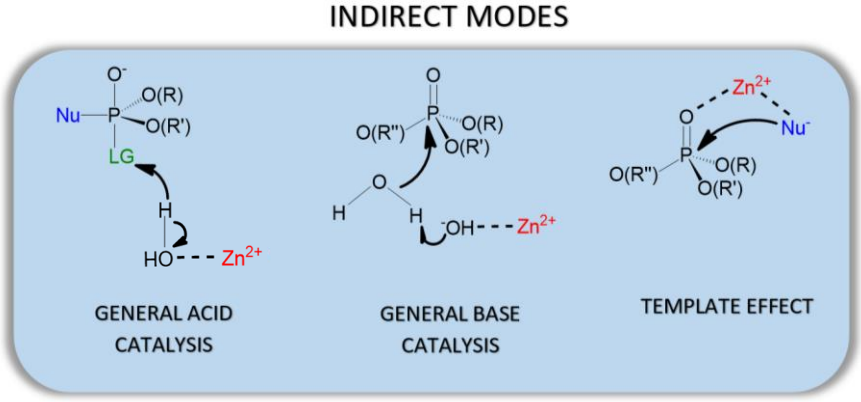

Fig.2.5. Indirect modes of the phosphate esters cleavage in the presence of Zn(II).

3. *How to Replicate Nature's Efficiency? Relevant Features Which May Accelerate the Hydrolysis of Nucleic Acids by Artificial Metallonucleases*.

For more than 4 decades, scientists have attempted to understand and replicate nucleases efficiency. By studying their active sites as well as reported examples of artificial enzymes able to cleave DNA and RNA models, chemists aim to achieve systems possessing a variety of catalytic properties.[20], [5], [21]

The application of the artificial nucleases is truly impressive. Phosphodiester cleavage is crucial for degradation of foreign, viral DNA. Nature-mimic systems, when attached to a nucleic acid recognition sequence, can play the role of artificial restriction enzymes that cut DNA in restriction sites. Moreover, artificial nucleases can be incorporated into therapeutic agents that are able to selectively bind or efficiently cleave the specific sequence of DNA or RNA of viruses or bacteria. Such properties can be relevant for a design of anti-infective drugs. They may help against a wide variety of human disorders, including osteoporosis, cancer, cystic fibrosis and depression, employed in pesticides' detoxification and chemical weapons.[22],[23] The information detailing mechanistic studies of phosphodiester cleavage may lead to better a understanding of the chemistry of one of Nature's most efficient and complex catalytic systems.

Despite the fact that many artificial nucleases have been described and some of them already found an application, we are not even approaching enzyme's rate acceleration using available bio-chemical tools. Possibly, a deeper and better understanding of the relevant factors that are affecting nuclease efficiency may contribute to the design of game-changing technology in phosphodiester cleavage.

However, enzymes are very complex and dynamic systems changing their conformations for catalytic purposes. Therefore, they present a flexibility not shown by synthetic models. Furthermore, nucleases, in particular, are able to provide a full package of features making the phosphate cleavage extremely efficient, for instance:

a) Nucleophile and species able to activate it;
b) Hydrogen bond donors stabilizing transition states;
c) Microenvironment in the active site, different from water in which enzymes are usually operating (ensuring stronger electrostatic interactions);
d) Metal ions which can facilitate a departure of the leaving group, activate the electrophile/nucleophile or decrease electrostatic repulsions.

Regarding metal ions, enzymatic active sites are perfectly adapted to host a variety of metals at physiological pH, without their precipitation as hydroxides. What is more, once the hydrolysis has occurred, products can be easily released from the active site and an enzyme is immediately prepared to start another catalytic cycle (in kinetic terminology this phenomenon is called 'turnover').

Studies on Nature's nucleases have been able to pick up a key mechanistic aspects which can undoubtedly contribute to preparation of more efficient catalysts for DNA and RNA cleavage. In particular, these aspects can result in a more elaborate and accurate engineering of catalytic sites. This goal can be achievable by taking advantage of supramolecular chemistry, nanochemistry and their governing principles.

4. *References of Chapter 2.*

[1] J. A. Cowan, *Chemical Reviews* **1998**, *98*, 1067-1088.

[2] J. A. Doudna, T. R. Cech, *Nature* **2002**, *418*, 222-228.

[3] R. L. Baldwin, *Protein Science* **2000**, *9*, 207-207.

[4] D. Herschlag, W. P. Jencks, *Biochemistry* **1990**, *29*, 5172-5179.

[5] T. Tadokoro, S. Kanaya, *The FEBS journal* **2009**, *276*, 1482-1493.

[6] D. E. Wilcox, *Chemical Reviews* **1996**, *96*, 2435-2458.

[7] J. A. Reynolds, M. J. Schlesinger, *Biochemistry* **1969**, *8*, 588-593.

[8] J. E. Coleman, *Annual review of biophysics and biomolecular structure* **1992**, *21*, 441-483.

[9] J. G. Zalatan, T. D. Fenn, A. T. Brunger, D. Herschlag, *Biochemistry* **2006**, *45*, 9788-9803.

[10] C. Little, A.-B. Otnäss, *Biochimica et Biophysica Acta (BBA) - Enzymology* **1975**, *391*, 326-333.

[11] J. F. Murray, L. L. Robert, *Cold Spring Harbor Monograph Archive; Volume 25 (1993): Nucleases, 2nd ed.* **1993**.

[12] L. S. Beese, T. A. Steitz, *The EMBO journal* **1991**, *10*, 25-33.

[13] J. Goldberg, H. B. Huang, Y. G. Kwon, P. Greengard, A. C. Nairn, J. Kuriyan, *Nature* **1995**, *376*, 745-753.

[14] W. Maret, *Adv Nutr* **2013**, *4*, 82-91.

[15] R. A. McCance, E. M. Widdowson, *The Journal of Physiology* **1942**, *101*, 44-85.

[16] D. W. Christianson, *Advances in protein chemistry* **1991**, *42*, 281-355.

[17] D. Keilin, T. Mann, *The Biochemical journal* **1940**, *34*, 1163-1176.

[18] F. A. Cotton, G. Wilkinson, C. A. Murillo, M. Bochmann, R. Grimes, *Advanced inorganic chemistry, Vol. 6*, Wiley New York, **1988**.

[19] F. Mancin, P. Scrimin, P. Tecilla, *Chemical Communications* **2012**, *48*, 5545-5559.

[20] B. Stec, K. M. Holtz, E. R. Kantrowitz, *Journal of molecular biology* **2000**, *299*, 1303-1311.

[21] J. Weston, *Chemical Reviews* **2005**, *105*, 2151-2174.

[22] N. Mitic, S. J. Smith, A. Neves, L. W. Guddat, L. R. Gahan, G. Schenk, *Chem Rev* **2006**, *106*, 3338-3363.

[23] Y. Yamamoto, A. Uehara, A. Watanabe, H. Aburatani, M. Komiyama, *ChemBioChem* **2006**, *7*, 673-677.

Chapter 3

1. *Small is the New Big. Principles of Nanotechnology. Properties of Metallo-nanoparticles.*

Even though the nanoworld cannot be seen by the naked eye, it has absolutely dominated the science field. The term 'nanotechnology' should not be defined only in terms of the length scale. Obviously, it automatically confines to the matter at the nanoscale, more specifically dimensions between 1 and 100 nm, however it offers the ability to see and control individual atoms and molecules, as well as imaging, modelling and arranging matter at these small scales. Indeed, it is truly fascinating how matters such as solids, liquids or gasses can reveal different and unusual physical, biological and chemical properties at the nanoscale.

A high surface area (SA) is a relevant property of nanomaterials that should be highlighted. It may be clearly illustrated on a solid cube possessing sides of 1 cm and 6 cm^2 of total SA. If the same cube was filled with 1 nm sized cubes on a side, that would equal 10^{21} nm-sized cubes, each one having a 6 nm^2 SA. The original surface area of 6 cm^2 would be increased to 6000 m^2, which is comparable to the size of a football field. Therefore, it should not be surprising that unique properties and benefits from tailoring the structures of materials at the atomic level result in a variety of applications of nanomaterials. These include sensing, electronics, medicine, energy conversion, cosmetics and much more.[1], [2], [3], [4], [5]

A big surface area coupled with improved reactivity and the possibility of atomic precision tailoring were the driving force for utilizing nanoparticles for the creation of superior catalysts. Particularly, a very important role in that field is played by gold nanoparticles: they are commonly used as catalysts in many chemical reactions, such as CO, H_2 and methanol oxidation, NO and CO_2 reduction, epoxidation of propylene,

hydrochlorination of acetylene to vinyl chloride or homogenous catalysts in the transformation of organic molecules.[6], [7], [8], [9], [10] Apart from the high surface area effect, metallonanoparticles reveal another interesting features like redox potential, ionisation and cohesive or electron conductivity.[11], [12], [13], [14], [15], [16]

Because of a small size and metallic nature, metallonanoparticles behave differently than bulk material, due to so called quantum-effects.[17] One of the most important phenomena depicting their optoelectronic properties is the Surface Plasmon Resonance, i.e. collective oscillations of mobile electrons in metallic nanoparticles being excited by an external electric field (light).[18] Accordingly, depending on dimension of the gold core, the colour of AuNPs may differ. That is due to the shifting and broadening the plasmonic band at 500-520 nm towards longer wavelengths (what is observable for nanoparticles bigger than 3 nm), which elicits a colour-shift or change (*Fig.3.1.*).[1] Thus, based on the metal, size and shape of nanoparticles, they can absorb the light at distinctive resonance frequencies. Moreover, metallonanoparticle optoelectronic properties can be observed fluorescence measurements, since they can act as a fluorescence quencher.[19]

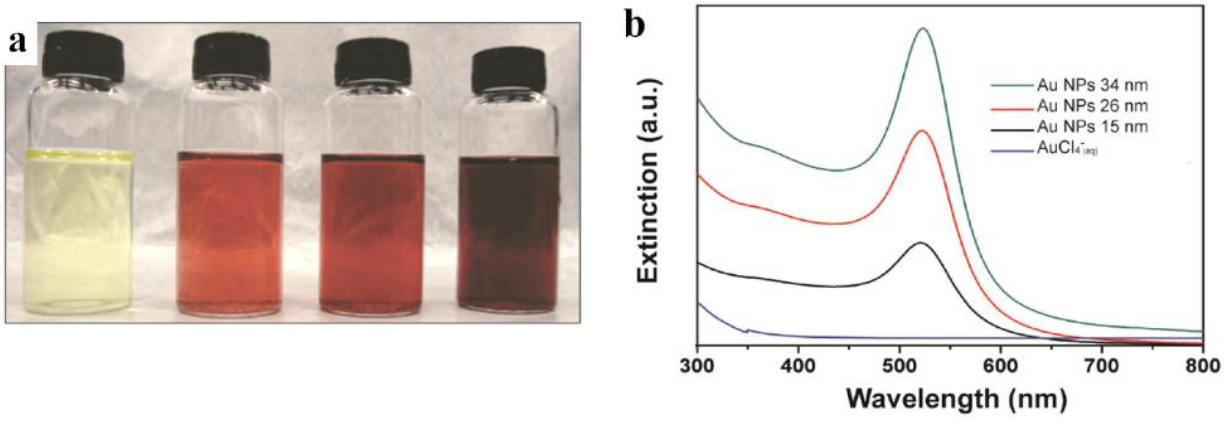

Fig.3.1. $AuCl_{4^{-}(aq)}$ solution (left) and aqueous suspensions of AuNPs in three sizes (15 ± 2.2, 26 ± 2.4, 34 ± 3.0 nm in diameter) (*a*) and their UV-Vis extinction spectra (*b*).

The surface of gold nanoparticles can be coated (thus, functionalized) with organic molecules (for instance thiols), constituting monolayer. Furthermore, carefully chosen organic units as well as their relatively close proximity from each other on the gold platform may result in cooperativity (describing how the binding of one ligand influences a receptor's affinity toward further binding interactions) and multivalency (i.e. simultaneous binding of multiple receptors to multiple ligands).[20] Consequently, these properties can lead a generation of multifunctional architectures. Additionally, cautiously selected structures of thiols can self-organize, yielding the formation of patches, stripes or they can just be randomly distributed.[21]

Upon proper tailoring coating monolayer, functionalisation of the gold surface is relatively easy and additionally it may contribute to enhanced binding of targets. Particularly, it has been reported that functionalized AuNPs may create hydrophobic pockets similar to those present in enzymes active sites, which can stabilize occurring electrostatic and nucleophile-electrophile interactions.[22] These pockets are characterized by a lower polarity environment, compared to a bulk water.

2. *Gold Nanoparticles - Evolution in Metodology of their Synthesis.*

As mentioned before, metal nanoparticles differ from their corresponding bulk analoges in many ways, which stands for their unique behaviour. In essence, brand new properties of metal nanoparticles are ruled by so-called quantum effects. The high and tunable performances arise from the nanoparticles' features, either individual or combined. Indeed, their properties strongly depend on the composition, shape, size and structure. During solution-phase synthesis, all of these parameters can be controlled yielding the predicted nanomaterial.

There exist two main approaches which describe the basic concept of metal nanoparticle synthesis (*Fig.3.2.*).[1] ,,Top-down" is based on the concept where the

synthesis starts from a large chunk of material which can be cut and trimmed until the desired nanoarchitecture is reached. Usually this type of approach is associated with physical processing techniques, like lithography, molecular beam epitaxy or vapor decomposition.[23], [24]

The second method called ,,bottom-up", begins at the atomic scale, thus the desired nanomaterial is built from the ground up. It is associated with chemistry and synthesis, and therefore less expensive, can be controlled by manipulating many experimental parameters and is more commonly utilized than the ,,top-down" approach.

However, the ,,top-down" and ,,bottom-up" procedures are not the only factors that should be taken into consideration when planning the synthesis of metallonanoparticles. Excluding the methods controlling shape, size, functionalization and stability, factors such as reducing agents, solvent or temperatures must also be considered.

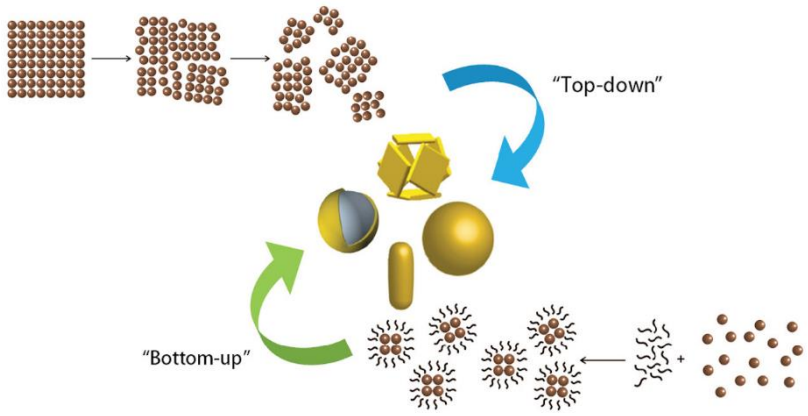

Fig.3.2. Schematic representation of ,,top-down" and ,,bottom-up" approaches in the nanoparticles synthesis.

In 1953 Turkevitch reported studies of the nucleation and the growth stage in the synthesis of colloidal gold.[25] As a source of gold atoms, he used a water solution of tetrachloroauric acid and sodium citrate as a reducing and stabilizing agent (due to its

negative charge). However, this method possesses a few limitations. It does not allow the synthesis of nanoparticles smaller than 5 nm, in addition, the reaction must be performed at very high temperatures. Such conditions lead to difficulties in controlling the size (low monodispersity), concentration and final yield of nanoparticles formed.

In the early 90s, Brust and Schiffrin developed a new revolutionary synthetic method which was based on Au-S interaction, which is stronger than Au-COO-. That resulted in the creation of more stable nanoparticles, able to be dried and re-dissolved without changing their chemical properties. A typical synthesis starts with $HAuCl_4$ which is transferred from aqueous to organic medium (toluene) using a phase-transfer agent, like tetraoctylammonium bromide (TOABr).[26] Subsequently, sodium borohydride reduces gold (III) to gold (0) in the presence of dodecanethiol. In this methodology, the first step constitutes the reduction of gold (III) to gold (I) by thiols (which results with formation of $[Au(SR)]_n$ polymers), followed by reduction of gold (I) to gold (0) by sodium borohydride. Compared to Turkevich's method, this one allows for the synthesis of nanoparticles within a size range of 1.5-5 nm (by manipulating the ratio between gold and thiols). Milder reaction conditions (RT-0°C) leads to an overall greater control of the dispersion and higher yields.

An additional protocol was presented by Peng and Scrimin independently, being a tuned Brust-Schiffrin method (*Scheme 3.3.*).[27],[28] After transferring Au(III) from a water solution to an organic medium by TOABr, dioctylamine is added to stabilise formed nanoparticles. Dioctylamine has however, additional purposes. Its amount allows for the control of nanoparticles size and, because of weaker Au-N than Au-S interactions, functionalized gold nanoparticles can be easily obtained by exchanging dioctylamine with thiols. Contrary to the Brust-Schiffrin method, it allows for the creation of water-soluble AuNPs, which is particularly important for their application and further usefulness in medicine and biology.

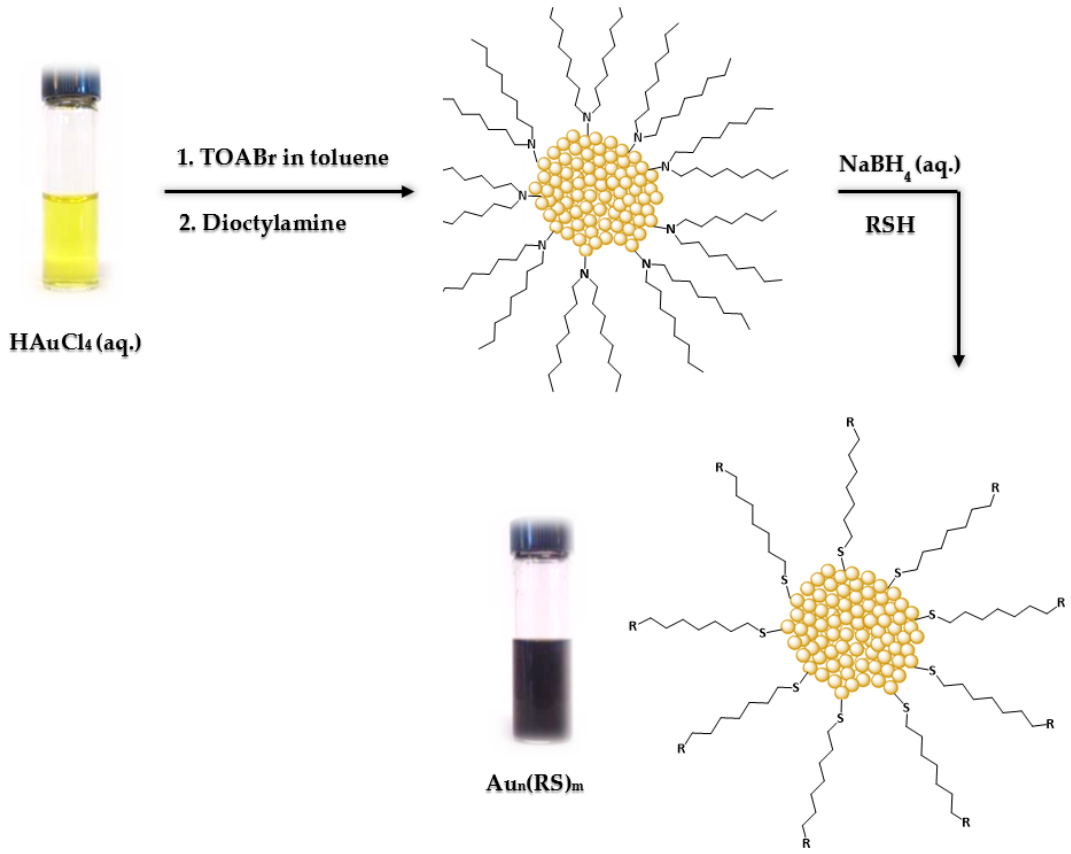

Scheme 3.3. Peng and Scrimin's method of the synthesis of self-assembled gold nanoparticles.

However, despite many positive changes that have occurred within 70 years, there are still some points in the synthesis of AuNPs requiring improvements. None of the presented methods allows for the creation of monodispersed particles. Furthermore, in terms of mixed monolayers, lack of control in their morphology may result with different binding sites for molecular accommodation.

3. Principal Techniques of AuNPs Characterisation.

Because of the nano-size, gold nanoparticles require specific, more advanced instrumentation and techniques for their characterisation.

Transmission Electron Microscopy (TEM) allows for the measurement of the size of nanoparticles with a diameter smaller than 5 nm. In this microscopy technique, a beam of electrons is transmitted through a sample deposited on a relatively electron transparent substrate (like a thin carbon-coated micro-grid).[29] The final image is formed upon interactions between the electrons and the sample, as the beam is transmitted through a specimen. TEM results are usually depicted as function of a number of particles and their average size.

Another commonly used technique is the Thermogravimetric Analysis (TGA), in which changes of the sample's weight are monitored as the function of increased temperature. Therefore, TGA allows for the determination of the amount of organic monolayer surrounding metallonanoparticles since upon thermal decomposition of the organic part only the metal core remains unaltered under high temperature conditions. The final result, in conjunction with the established size of the nanoparticles, enables determination of the AuNPs' chemical formula.

In terms of rapid evaluation of the presence of larger clusters, the Ultraviolet-Visible Spectrophotometry (UV-Vis) is utilized. A plasmonic band at 500-520 nm indicates a presence of bigger than 3-5 nm nanoparticles (see *paragraph 1*).

Lastly, the Nuclear Magnetic Resonance Spectroscopy (NMR) and diffusion-filtered experiments provide two key pieces of information. First of all, they prove the formation of functionalized gold nanoparticles in the shape of broad signals. This phenomenon takes place due to several copies of the same molecules and increased relaxation time. Additionally, the comparison of ^{1}H NMR and ^{1}H diffusion-filtered NMR spectra helps to evaluate AuNP purity (sharp peaks indicate either a presence of solvents or organic impurities).

Aim of the Project

Self-Assembled Gold Nanoparticles as Artificial Metallonucleases.

Designing artificial nucleases which can overcome the structural complexity and compete with the efficiency observed in Nature's enzymes seems to be achievable with less elaborate architectures, like gold nanoparticles. The necessity for a multistep synthesis can be easily overcome by already introduced self-assembly of simple catalytic units on the gold surface, therefore constituting a multivalent and functional monolayer (see *paragraph 1*). Particularly, thiols that are anchored on the gold support, reveal a limited mobility and being conformationally constrained, can act in a cooperative fashion which is expected in catalysis. Moreover, the presence of metal ion complexes constituting AuNPs monolayer can result in the formation a bimetallic site. Last but not least, a proper design and synthesis may yield with water-soluble gold nanoparticles, which can create a local microenvironment with a polarity lower than that of the bulk water. All of these properties can substantially contribute to acceleration of the phosphodiester cleavage (see *Chapter 2*, *paragraph 3*).

The last two decades provided us with some great examples of gold nanoparticles in phosphodiester hydrolysis. A special attention has been devoted to AuNPs bearing azacrown macrocycle derivatives, which are known to strongly bind transition metal ions, such as zinc.[30], [31], [32] These supramolecular architectures are one of the most efficient artificial systems hydrolysing the DNA and RNA backbone, cleaving it almost one million times faster compared to background reactions. However, the complexity of phosphodiester cleavage, i.e. numbers of factors, parameters, conditions that have to be taken into account to succeed in their hydrolysis (i.e. facilitating a departure of the leaving group, providing a nucleophile or its activation, enhancing electrostatic interactions by lowering dielectric constant of the 'catalytic pocket', stabilization of the transition state), makes the nanoworld doors still open to improvement already reported artificial nucleases and to understanding of Nature's mechanistic choices.

Herein I present my studies on the cleavage of DNA and RNA models using self-assembled gold nanoparticles. Five different catalytic systems (**AuNP1-5**) were prepared upon Peng-Scrimin's protocol, yielding nanoparticles within the range of 1-2 nm in diameter. (*Fig.3.4.*).

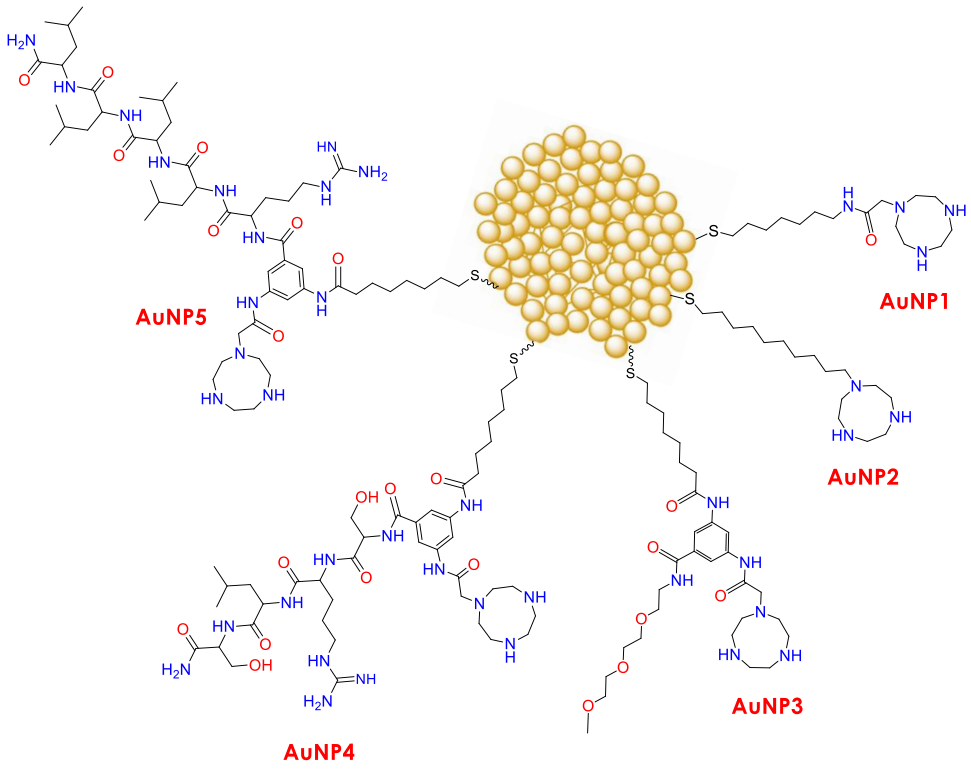

Fig.3.4. Synthesized self-assembled gold nanoparticles **AuNP1-5**.

Their design was based on key features making Nature's enzymes efficient in phosphodiester cleavage as well as on already established studies on artificial metallonucleases.[33], [34], [35] The source of multiple bimetallic sites wass ensured by the presence of 1,4,7-triazacyclononane (TACN) known for its strong binding of transition metal ions such as Zn(II).[36] Zinc, as already mentioned, is naturally present in the active sites of nucleases, lacks of relevant redox chemistry in physiological conditions and has strong Lewis-acid properties (see *Chapter 2*). With these factors in mind, zinc appeared to be an optimal choice of metal for creating artificial nucleases.

Additionally, the phosphate cleavage occurs at the interface between the bulk aqueous solution and pseudophase formed by the AuNPs monolayer. Therefore, as already mentioned, it ensures a less polar environment, resembling enzymes active sites.[28]

Structurewise, **AuNP1,2** thiols were decorated with TACN followed by a C_{10} (T2) or C_7 (T1) hydrocarbon chains, in the second case enriched with amide functionality (*Scheme 3.5.*). It has been already presented by Diez-Castellnou that a monolayer composed by such simple, similar thiols reveals a high reactivity towards phosphodiester cleavage.[32]

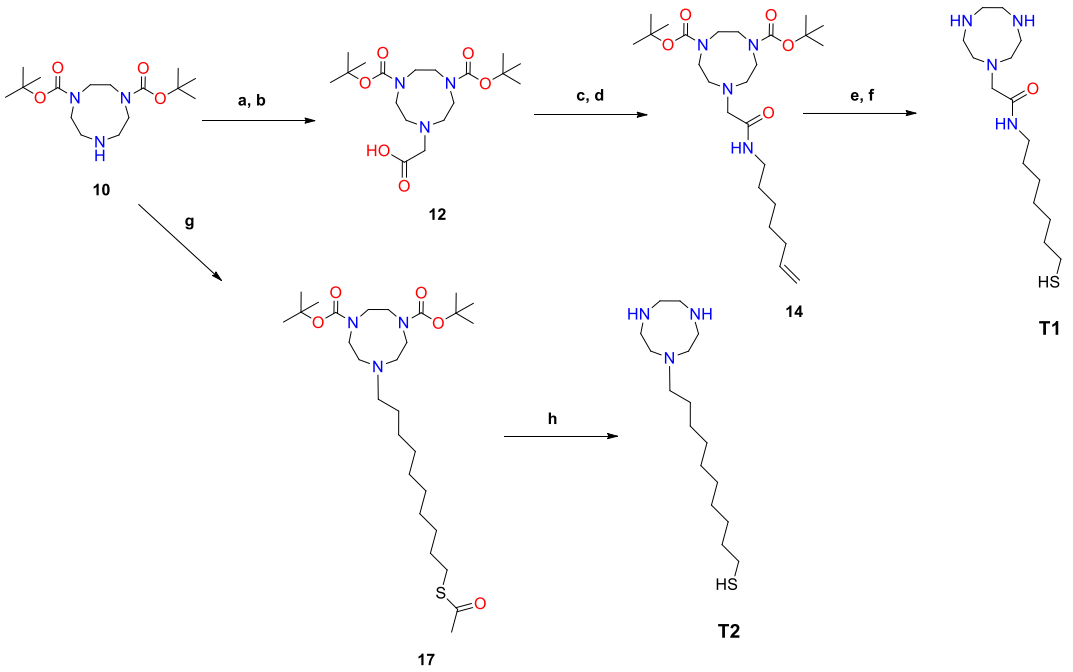

Scheme 3.5. Synthetic route of Y-shaped thiols 1,2 (**T1**, **T2**).

a: 2-Br-methylacetate, Cs_2CO_3 in $ACN_{(anhyd.)}$, N_2, overnight, RT; **b**: 1M NaOH in MeOH, 2h, RT; **c**: pentafluorophenol, EDC·HCl in $DCM_{(anhyd.)}$, N_2, overnight, RT; **d**: hept-6-en-1-ammonium chloride, DIPEA in $DCM_{(anhyd.)}$, N_2, overnight, RT; **e**: 2,2-dimethoxy-1,2-diphenylethan-1-one, thioacetic acid in MeOH, hv=254 nm, 1h, RT; **f**: 6M HCl in EtOH, 2h, reflux; **g**: 10-bromothioacetate, K_2CO_3, $NaHCO_3$ in ACN, 4h, 40°C; **h**: 1M HCl in EtOH, 2h, reflux.

Thiols of higher complexity, coating **AuNP3-5**, resemble in their shape the letter Y, and hereon in was described as Y-shaped monolayer (*Scheme 3.6.*). Their structure was based on 3,5-diaminobenzoic acid which was functionalized in all cases with a part constituting a derivative of 8-mercaptooctanoic acid (responsible for the Au-S interactions) and a TACN moiety (for Zn(II) complexation). A third 'arm' was composed by either 2-(2-(2-methoxyethoxy)ethoxy)ethanamine (ensuring solubility in water) and peptides with 4-5 amino acid residues (serine, arginine and leucine).

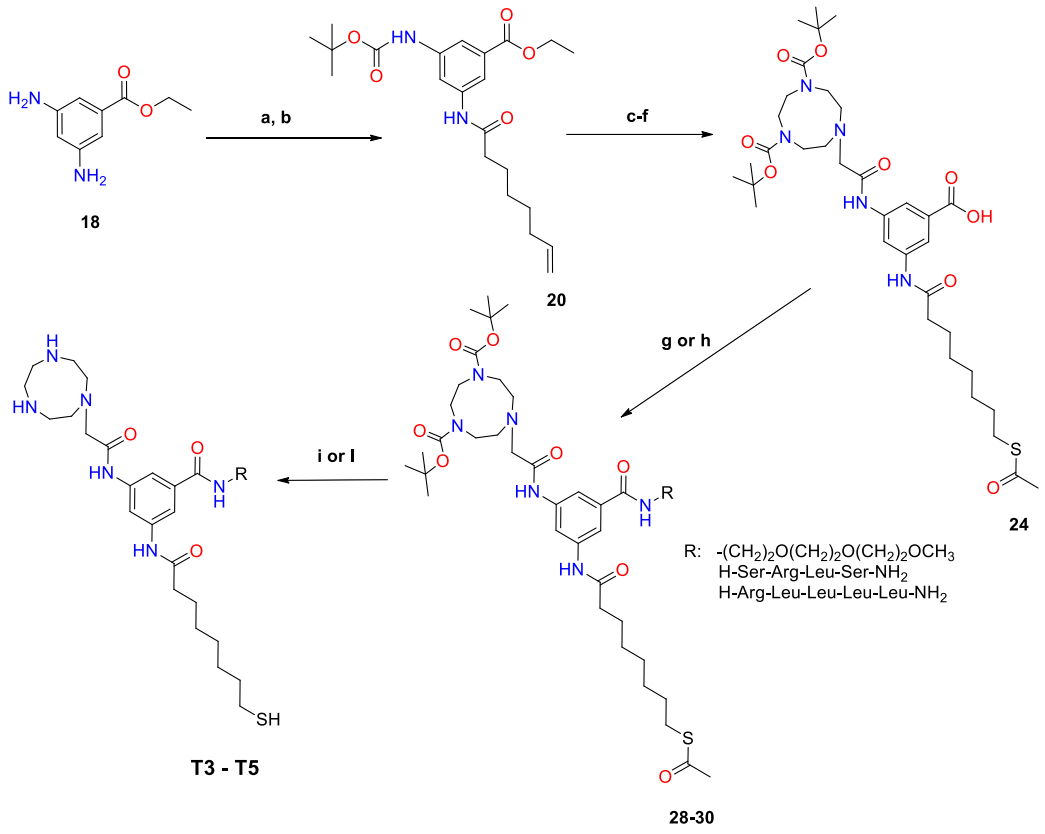

Scheme 3.6. Synthetic route of Y-shaped thiols 3-5 (**T3-T5**).

a: Boc anhydride, Et_3N, in dioxane/water, overnight, RT; **b**: octan-7-enoic acid, EDC·HCl, HOBt, Et_3N, in $ACN_{(anhyd.)}$, N_2, overnight, RT; **c**: TFA in DCM, 2h, RT; **d**: **12** is converted to the activated ester with pentafluorophenol, EDC·HCl in $DCM_{(anhyd.)}$, N_2, overnight, RT and then coupled with **21** in the presence of DIPEA, $DCM_{(anhyd.)}$, N_2, 2 days, reflux; **e**: 1M NaOH in EtOH, 2h, RT; **f**: Thioacetic acid, AIBN, in toluene, overnight, reflux; **g**: 2-(2-(2-methoxyethoxy)ethoxy)ethan-1-amine, Et_3N, EDC·HCl, HOBt in $DCM_{(anhyd.)}$, N_2, overnight, RT, for the synthesis of **25**; **h**: peptide, DIC, oxyma, 2,4,6-trimethylpyridine in DMF, overnight, RT, for **26** and **27**; **i**: CH_3ONa in $MeOH_{(anhyd.)}$, N_2, 2h, RT for the synthesis of **T3** precursor; **l**: 95% TFA, 2.5% TRIS, 2.5% H_2O, 2h, RT, then NH_3 in $MeOH_{(anhyd.)}$, N_2, overnight, RT for the synthesis of **T4** and **T5**.

The choice of amino acids was inspired by active sites of Nature's nucleases as well as their planned and desired functions. Arginine (being an active component of the catalytic centre of some nucleases, like topoisomerase) can participate in proton transfer from the attacking 2'-OH to non-bridging phosphoryl oxygen, which may serve as a weak general acid and stabilize the transition state via phosphates' hydrogen bonding.[37],[38] Moreover, it maintains a positive charge in a wide range of pH (the p*K*$_a$ value of Arg side chain is ~ 12.5), that may affect the stabilization of electrostatic interactions. Serine however, is a hydrogen bond donor and may serve as an internal nucleophile and finally, leucine can help to create a more hydrophobic environment, which should stabilize nucleophile-electrophile electrostatic interactions.

Apart from standard kinetic experiments, which were performed to elucidate nanoparticles catalytic importance, for the first time the studies on the leaving group departure from uridine 3'-alkyl or aryl phosphates were reported, catalyzed by the most efficient nanozyme. Obtained results were compared with already reported artificial nucleases, proving a great efficiency in phophodiester cleavage by presented here AuNPs.

4. *References of Chapter 3.*

[1] R. S. Geonmonond, A. Silva, P. H. C. Camargo, *Anais da Academia Brasileira de Ciencias* **2018**, *90*, 719-744.

[2] A. S. Aricò, P. Bruce, B. Scrosati, J.-M. Tarascon, W. van Schalkwijk, *Nature Materials* **2005**, *4*, 366-377.

[3] P. K. Jain, K. S. Lee, I. H. El-Sayed, M. A. El-Sayed, *The journal of physical chemistry. B* **2006**, *110*, 7238-7248.

[4] G. Baffou, R. Quidant, *Chemical Society Reviews* **2014**, *43*, 3898-3907.

[5] V. Polshettiwar, B. Baruwati, R. S. Varma, *Chemical communications (Cambridge, England)* **2009**, 1837-1839.

[6] M. Haruta, T. Kobayashi, H. Sano, N. Yamada, *Chemistry Letters* **1987**, *16*, 405-408.

[7] M. Haruta, N. Yamada, T. Kobayashi, S. Iijima, *Journal of Catalysis* **1989**, *115*, 301-309.

[8] M. Haruta, *Catalysis Today* **1997**, *36*, 153-166.

[9] G. J. Hutchings, *Journal of Catalysis* **1985**, *96*, 292-295.

[10] Y. Ito, M. Sawamura, T. Hayashi, *Journal of the American Chemical Society* **1986**, *108*, 6405-6406.

[11] M. Wuithschick, A. Birnbaum, S. Witte, M. Sztucki, U. Vainio, N. Pinna, K. Rademann, F. Emmerling, R. Kraehnert, J. Polte, *ACS Nano* **2015**, *9*, 7052-7071.

[12] C. Chu, J. S. Na, G. N. Parsons, *J Am Chem Soc* **2007**, *129*, 2287-2296.

[13] M. C. Daniel, D. Astruc, *Chem Rev* **2004**, *104*, 293-346.

[14] J. Turkevich, P. C. Stevenson, J. Hillier, *Discussions of the Faraday Society* **1951**, *11*, 55-75.

[15] S. Yapar, M. Oikonomou, A. H. Velders, S. Kubik, *Chemical Communications* **2015**, *51*, 14247-14250.

[16] O. R. Miranda, X. Li, L. Garcia-Gonzalez, Z. J. Zhu, B. Yan, U. H. Bunz, V. M. Rotello, *J Am Chem Soc* **2011**, *133*, 9650-9653.

[17] P. P. Edwards, J. M. Thomas, *Angewandte Chemie (International ed. in English)* **2007**, *46*, 5480-5486.

[18] C. Cobley, Y. Xia, *Elements* **2009**, *5*, 309-313.

[19] M. Grzelczak, J. Pérez-Juste, P. Mulvaney, L. M. Liz-Marzán, *Chemical Society Reviews* **2008**, *37*, 1783-1791.

[20] J. D. Badjić, A. Nelson, S. J. Cantrill, W. B. Turnbull, J. F. Stoddart, *Accounts of Chemical Research* **2005**, *38*, 723-732.

[21] A. M. Jackson, J. W. Myerson, F. Stellacci, *Nat Mater* **2004**, *3*, 330-336.

[22] L. Riccardi, L. Gabrielli, X. Sun, F. De Biasi, F. Rastrelli, F. Mancin, M. De Vivo, *Chem* **2017**, *3*, 92-109.

[23] D. R. Walt, *Nature Materials* **2002**, *1*, 17-18.

[24] A. Biswas, I. S. Bayer, A. S. Biris, T. Wang, E. Dervishi, F. Faupel, *Advances in colloid and interface science* **2012**, *170*, 2-27.

[25] J. Turkevich, P. C. Stevenson, J. Hillier, *The Journal of Physical Chemistry* **1953**, *57*, 670-673.

[26] M. Brust, M. Walker, D. Bethell, D. J. Schiffrin, R. Whyman, *Journal of the Chemical Society, Chemical Communications* **1994**, 801-802.

[27] N. R. Jana, X. Peng, *Journal of the American Chemical Society* **2003**, *125*, 14280-14281.

[28] F. Manea, C. Bindoli, S. Polizzi, L. Lay, P. Scrimin, *Langmuir : the ACS journal of surfaces and colloids* **2008**, *24*, 4120-4124.

[29] C. Kumara, V. R. Jupally, A. Dass, in *Gold Clusters, Colloids and Nanoparticles I* (Ed.: D. M. P. Mingos), Springer International Publishing, Cham, **2014**, pp. 155-187.

[30] F. Manea, F. B. Houillon, L. Pasquato, P. Scrimin, *Angewandte Chemie (International ed. in English)* **2004**, *43*, 6165-6169.

[31] G. Zaupa, C. Mora, R. Bonomi, L. J. Prins, P. Scrimin, *Chemistry – A European Journal* **2011**, *17*, 4879-4889.

[32] M. Diez-Castellnou, F. Mancin, P. Scrimin, *Journal of the American Chemical Society* **2014**, *136*, 1158-1161.

[33] O. Iranzo, A. Y. Kovalevsky, J. R. Morrow, J. P. Richard, *Journal of the American Chemical Society* **2003**, *125*, 1988-1993.

[34] G. Feng, D. Natale, R. Prabaharan, J. C. Mareque-Rivas, N. H. Williams, *Angewandte Chemie (International ed. in English)* **2006**, *45*, 7056-7059.

[35] C. T. Liu, A. A. Neverov, R. S. Brown, *Journal of the American Chemical Society* **2008**, *130*, 13870-13872.

[36] E. L. Hegg, J. N. Burstyn, *Inorganic Chemistry* **1996**, *35*, 7474-7481.

[37] M. R. Redinbo, L. Stewart, P. Kuhn, J. J. Champoux, W. G. Hol, *Science (New York, N.Y.)* **1998**, *279*, 1504-1513.

[38] S. Mikkola, T. Lönnberg, H. Lönnberg, *Beilstein Journal of Organic Chemistry* **2018**, *14*, 803-837.

Chapter 4

1. *The Concept of Simple Nucleic Acids' Models in Phosphodiester Cleavage.*

As the efficient design and synthesis of artificial nucleases is paramount to this work, one should not forget about DNA and RNA models, which are crucial components of phosphodiester cleavage studies. Indeed, direct hydrolysis of nucleic acids is not only labour and financially expensive, but also, keeping in mind their great stability, it is particularly difficult to perform hydrolysis of DNA and RNA with non-enzymatic systems.

To facilitate studies on phosphodiester cleavage, scientists are utilizing nucleic acids models in the form of simple molecules. Although dinucleoside-3',5'-monophosphates as the nucleic acid unit may be the obvious choice, their kinetic studies are relatively laborious (HPLC chromatography has to be used to study the content of samples withdrawn at proper intervals). Therefore, many research groups prefer to work with more convenient molecules, like 2-hydroxypropyl *p*-nitrophenyl phosphate (HPNP) or bis-*p*-nitrophenyl phosphate (BNP), being RNA and DNA model substrates, respectively.

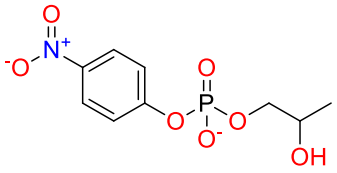

HPNP

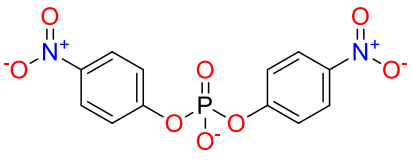

BNP

Their hydrolysis can be followed by UV-Vis spectrophotometry: once cleaved, HPNP and BNP release *p*-nitrophenoxide (which has a characteristic yellow colour) allowing for its detection at 400 nm. In the case of HPNP, it has additionally an internal

nucleophile (hydroxyl group) as RNA does, whereas BNP is deprived of it, having a *p*-nitrophenyl moiety instead.

However, one should bear in mind that *p*-nitropenoxide has a p*Ka* 8 units lower than that of the alcohol 5'-linked in RNA and DNA, making it a better leaving group.[1] Therefore, the rate limiting step of RNA/DNA cleavage and HPNP/BNP hydrolysis is likely to be different. Moreover, the acyclic HPNP is much less reactive than the ribonucleoside monophosphate bearing the same leaving group.[1] Nevertheless, for the initial screening of phosphodiester cleavage, both HPNP and BNP are still one of the most convenient nucleic acids' models.

2. *HPNP – Synthesis, Stability and its pH-dependent Cleavage.*

On the contrary to BNP, HPNP is not commercially available and its synthesis is particularly challenging. Due to the presence of the internal nucleophile, the synthesis should either encompass the protection of hydroxyl group until the final step or be relatively fast to minimize the intramolecular nucleophilic attack on the phosphorus atom. Moreover, HPNP is sensitive to high pH and temperature, which should be taken into account when planning reaction conditions of the final synthetic step and storage.

The first approach of HPNP synthesis was influenced by protocols reported by Prestwich and Kantrowitz independently (*Scheme 4.1.*).[2], [3], [4]

It starts with the esterification of 2-(benzyloxy)-propanoic acid with ethanol. Afterwards, product (**1**) is reduced with lithium aluminium hydride to alcohol (**2**) and then phosphorylated with dimethyl chlorophosphate. Subsequent demethylation of (**3**) and further condensation with *p*-nitrophenol yields with 2-(benzyloxy)propyl (4-nitrophenyl) phosphate (**5**). The last step requires dealkylation of (**5**) with BBr_3,

however it results with a very low yield (~4%) and additionally it is necessary for the crude to be purified by HPLC.

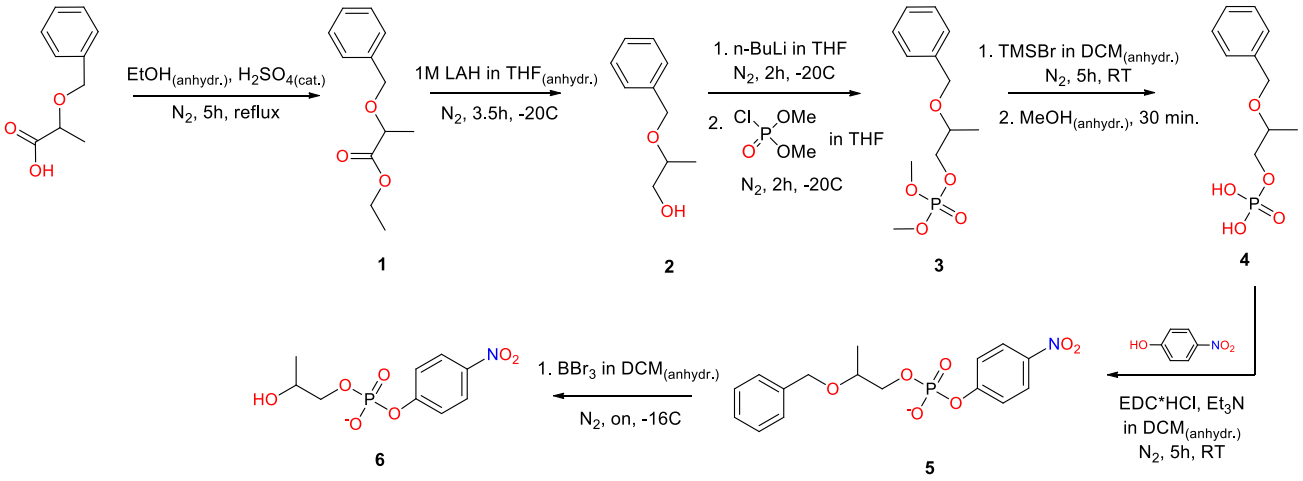

Scheme 4.1. The first pathway of HPNP synthesis.

The second method based on Brown's protocol (dating 1965) comprises of just one synthetic step, however the work-up is much more sensitive and demanding than any from the multiple-step approach (*Scheme 4.2.*).[5] It is based on a 2-day reaction between *p*-nitrophenyl phosphate (upon passing its sodium salt through an ion exchange column) with an excess of 1,2-epoxypropane. The work-up firstly requires the removal of non-reacted epoxide, passing the crude through an ion exchange column. Following this, careful adjustment of pH to 6.5-7.0 (slightly more basic pH results in the hydrolysis of HPNP), precipitation with ethanol, concentration of the filtrate and lastly, its precipitation with 10% solution of ethanol in acetone.

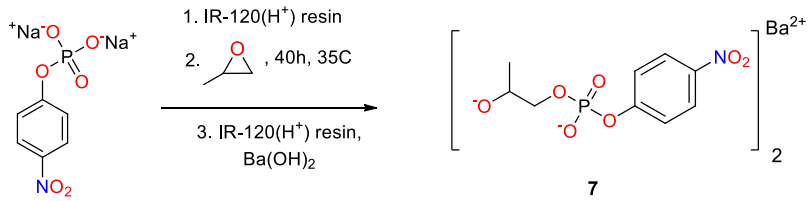

Scheme 4.2. The second pathway of HPNP synthesis.

Since the cleavage of HPNP is based on the intramolecular nucleophilic attack, it is important to document its behaviour at different pH (background reaction), without any catalysts (*Fig.4.3.*). At neutral pH (6.5-7.5), the hydrolysis of HPNP is relatively slow compared to basic pH (from 8.5-9.0 onwards), where the percentage of cleaved HPNP increases exponentially.

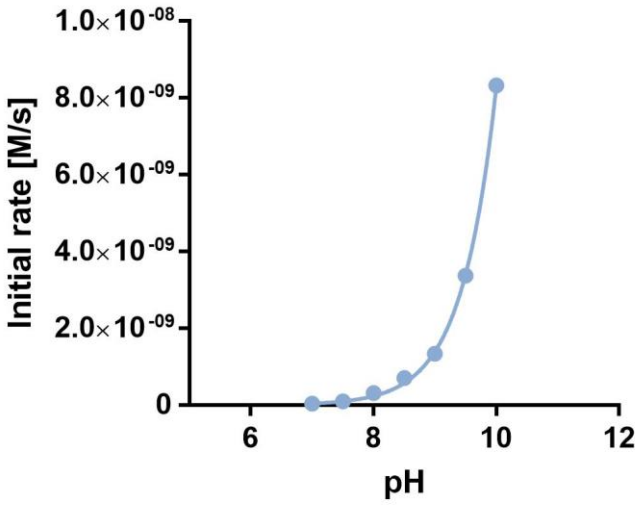

Fig.4.3. pH-rate profile of spontaneous HPNP cleavage.
Conditions: [HPNP] = 1.2×10^{-3} M, [buffers] = 1.0×10^{-2} M ,25 °C in H_2O.

3. *From Years to Seconds – The Cleavage of HPNP by Artificial Metallonucleases.*

In 1999 Chin estimated the relative importance of different factors affecting the reaction rate of phosphodiester cleavage.[6] He claimed that the most important contributions should be first, activation of the nucleophile (10^8-fold), then leaving group (10^6-fold), followed by Lewis acid activation (10^2-fold). Interestingly, in 2017 Mancin revised Chin's estimations, reporting a larger contribution for the leaving group departure assistance (up to 10^6-fold) and a lower for the nucleophile activation (10^2-fold).[7] In any case, if the sum of these contributions were totalled, the given rate

acceleration would almost approach those of enzymes. However, the creation of artificial nucleases able to combine all of the previously mentioned activation modes has not been so far reported, and more often one or two simultaneous contributions are achievable. Therefore, it should not be surprising that bimetallic complexes can be even hundreds of times more efficient in phosphodiester cleavage than their monometallic counterparts. [8], [9], [10], [11], [12], [13]

One example of mono vs. bimetallic catalysts in the cleavage of HPNP was presented by Hamilton *et al*. (*Fig.4.4.*).[14] Two dinuclear Cu(II) complexes (**4c** and **4d**) were prepared by linking Cu(**4a**) and Cu(**4b**) through an amide group. Both cases reveal much higher activity when compared with their corresponding mononuclear equivalents in HPNP cleavage (the second Cu(II) ion increases the activities of Cu_2(**4c**) and Cu_2(**4d**) by 51- and 67- fold, respectively, relative to Cu(**4b**) and the second Cu(II) ion increases the activities of Cu_2(**4d**) by 24-fold relative to Cu(**4a**)).

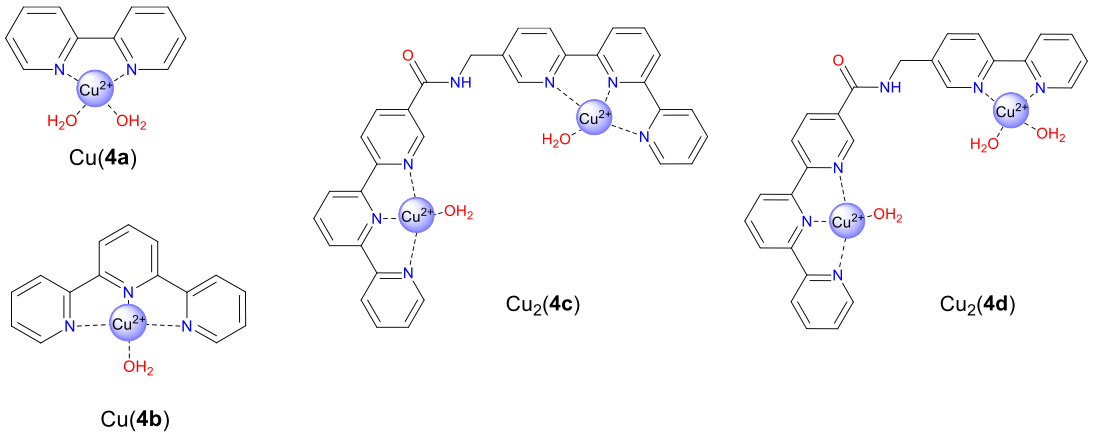

Fig.4.4.

Since two metal ions may cooperate in many different ways to promote phosphodiester cleavage, pH rate profiles for di- and mononuclear complexes were studied to achieve a greater understanding of the mechanisms involved. It has been established that in the case of bis-terpyridine complex Cu_2(**4c**), the main contributing factor was a double Lewis acid activation and double general base catalysis. The

terpyridine-bipyridine system Cu_2(**4d**) was found to operate via single Lewis acid activations and a double general base catalysis (*Scheme 4.5.*).

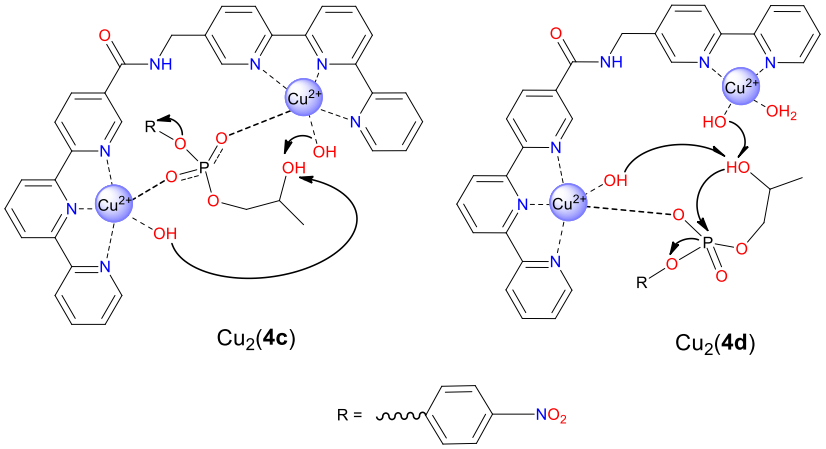

Scheme 4.5. Proposed mechanisms for Cu_2(**4c**)/Cu_2(**4d**)-catalysed hydrolysis of HPNP.

Since the discovery of enhanced efficiency of phosphodiester cleavage by bimetallic complexes against their monometallic counterparts, many examples depicting the cooperativity between two metal ions combined in one system have been published.

In terms of HPNP cleavage, it is impossible not to begin with the example of Morrow and Richard from 2003, whose simple concept yielded great efficiency within their systems of phosphodiester hydrolysis (*Fig.4.6.*, Zn_2(**4e**)).[15]

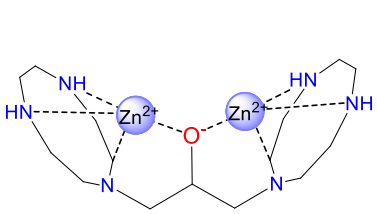

Zn_2(**4e**)

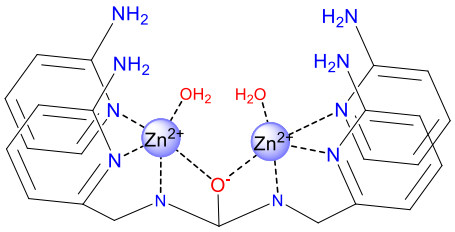

Zn_2(**4f**)

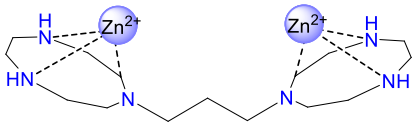

Zn_2(**4g**)

Catalyst (as the zinc complex)	Medium	k_{cat} [s^{-1}]	K_M [mM]	k_2 [M^{-1} x s^{-1}]
4e	H_2O	0.0041	16	0.025
4f	H_2O	0.017	0.32	53
4g	MeOH	2300	8.3	275000

Fig.4.6. and *Table 4.7.*

Their concept is based on bimetallic catalyses ensured by the presence of oxo-bridged-dinuclear complexes which are able to maintain an optimal distance between two Zn(II) ions (3.66 Å) also found in Nature's nuclease active sites.[16] The presence of an ionized alkoxide bridge shields from undesired electrostatic repulsions, keeping metal ions in a position allowing for a double Lewis acid activation. *Nota bene*, Zn_2(**4e**) reveals two orders of magnitude the efficiency in HPNP cleavage than its mononuclear analogue (at pH 7.61 the second order rate constants are 25 x 10^{-2} and 0.13 x 10^{-2} M^{-1} x s^{-1} for a di and mononuclear complexes, respectively).

In 2006 Williams presented the complex of *N,N,N',N'*-tetrakis(6-aminopyridine-2-ylmethyl)-1,3-diaminopropan- 2-ol combining both double Lewis acid activity and H-bond donors stabilizing the transition state (*Fig.4.6.*, Zn_2(**4f**)).[17] Not only does Zn_2(**4f**) hydrolyse HPNP 700 times faster than its monometallic counterpart, but also

it is 2000 times more efficient than Zn_2(**4e**) (comparing the second order rate constants; *Table 4.7.*). The authors claimed that half of the acceleration came from the binding affinity (due to hydrogen bonds) and half from the intra-complex reactivity enhancement. Furthermore, Zn_2(**4f**) is also able to catalyse the isomerization of UpU, indicating an associative mechanism involving a phosphorane intermediate.[18] Therefore, the cooperation between two Zn(II) and hydrogen bonds may assist in decreasing the charge on the phosphoryl group.

A milestone in realizing enzyme-like activity using artificial systems came from studies within the Brown group in 2008.[19] Brown presented a poorly organized catalyst Zn_2(**4g**) (*Fig.4.6.*), which is the same as Zn_2(**4e**) but without the oxo-bridge. It was determined that this was depriving the complex from its catalytic properties, i.e. double Lewis acid activation: and indeed, in water Zn_2(**4g**) is almost inactive towards HPNP cleavage. However, dissolved in alcohols like methanol or ethanol, Zn_2(**4g**) is approaching enzymatic efficiency (*Table 4.7.*). This finding can be attributed to the stabilization of electrostatic interaction between the positive Zn(II) and anionic phosphates, maximized in a low dielectric constant medium. Indeed, the alcohol-like environment resembles the one found in enzyme active sites, which is different than the aqueous medium where biologically active molecules function.

The simplified concepts presented above were the inspiration for the creation of much more complex supramolecular systems. One of the first examples was a calix[4]arene scaffold introduced by Reinhoudt *et al.*, substituted in the upper rim with one, two or three 2,6-bis-(aminoethyl)pyridine units (*Fig.4.8.*).[20] This supramolecular architecture Zn_2(**4h**) was able to achieve a remarkable acceleration of the hydrolysis of HPNP, being almost 32000-times faster comparing to uncatalysed systems at pH 7.0 and 25°. The key to success lies in three aspects: firstly, the flexibility of the upper rim allows for the formation of tri-metallic complex and a hydrophobic cage formed by flexible upper rim units. Secondly, this cage can host *p*-nitrophenyl groups, thus transforming the intermolecular process into pseudo-intramolecular. Lastly, the tunability of the lower

rim may help with solubility of the whole complex in water. What is also worth mentioning is the fact that the reactivity of tri and bimetallic systems was comparable, thus the third metal does not play a significant role in HPNP cleavage.

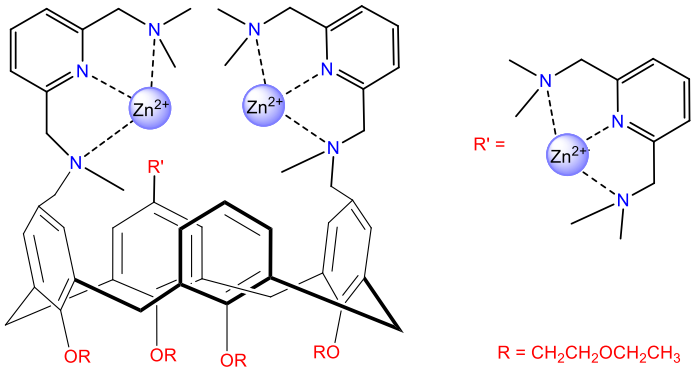

Zn_2(**4h**)

Fig.4.8.

The examples presented thus far were taking advantage of cooperativity between two metal ions in HPNP cleavage. However, looking at nuclease active sites, a bimetallic interaction is not the only way that Nature copes with efficient phosphodiester cleavage. The following examples combine a guanidinium unit and 1,4,7-triazacyclononane (TACN) complexes (TACN-Zn(II)/Cu(II)), where the hydroxy-form of a ligated metal ion plays the role of a general base.

The first metal complex of (**4i**) is a simple system based on *m*-xylene linker.[21] Interestingly, TACN complexed with Zn(II) and Cu(II) revealed different degrees of cooperation between catalytic units in HPNP hydrolysis (in DMSO-water (4:1 v/v)). At 5 mM bi-functional catalyst concentration, the rate enhancement relative to background hydrolysis was 1 x 10^4 -fold and 4 x 10^4 -fold for Zn(II) and Cu(II), respectively. The pH dependent kinetics showed a sigmoidal profile with p*Ka* 8.94 (TACN-Cu(II)) and 8.60 (TACN-Zn(II)), confirming a deprotonation of a metal-coordinated water molecule acting as a general base and therefore accelerating HPNP hydrolysis. At pH regions where water deprotonation occurs, the guanidinium unit

stays positively charged which also may promote the electrophilic activation of phosphates.

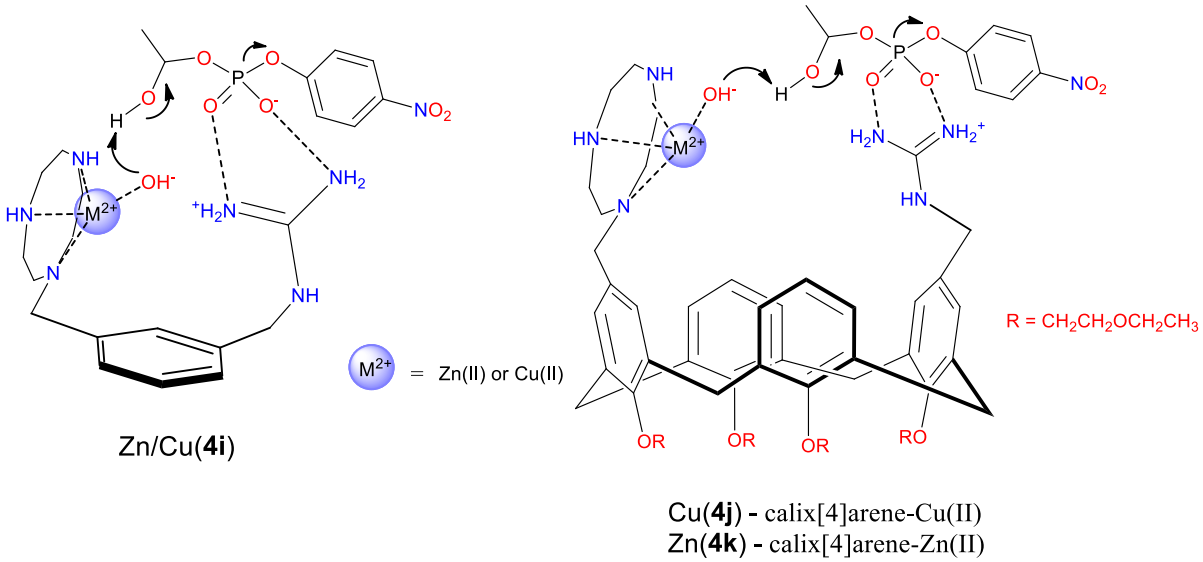

Fig.4.9.

Improvement of the above presented complex has been achieved using cone-calix[4]arene as a platform.[22] The catalytic efficiency of Cu(**4j**) was 10^3 times higher than that of the mono-functional control TACN-Cu(II), indicating a large degree of cooperation between catalytic units. In this case, the substantial catalytic efficiency was possible due to a high level of adaptability resulting from the conformational mobility of these supramolecular scaffolds. Eventually, it was established that the catalyst Cu(**4j**) was 40-times more active than Cu(**4i**) in HPNP cleavage.

The Zn(II) complex of (**4k**) was only five times more effective than the corresponding complex of TACN, which shows a moderate degree of synergism between catalytic units regardless of utilized scaffold.

The above cases exhibit phosphodiester cleavage of HPNP occurring within a single catalytic site. The number of active catalytic sites placed on one scaffold can be substantially increased utilizing self-assembled gold nanoparticles. As described in *Chapter 3*, not only can these nanoparticles provide multiple-bimetallic sites, but also

the variety of anchored thiols enables for unlimited functionalities which may create a hydrophobic environment enhancing electrostatic interactions.

In 2011 Scrimin and co-workers reported the reactivity of series of gold nanoparticles containing different ratios of the catalytic unit TACN-Zn(II) (**4l**) and inert triethyleneglycol (TEG) (**4m**, *Fig.4.10.*).[23] Their catalytic activity was tested towards the cleavage of HPNP, reaching the maximum values for Michaelis-Menten parameters k_{cat} and K_M of 6.7 x 10^{-3} s^{-1} and 3.1 x 10^{-4} M respectively.

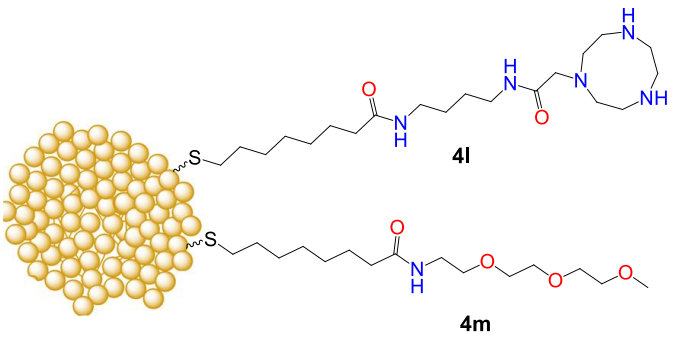

Fig.4.10.

It was shown that up to the molar fraction of Zn(**4l**) (x_{A1}) 0.4 in the mixed monolayers, the first order rate constant was increasing and afterwards it remained constant, whereas K_M was decreasing exponentially. That effect originates from the cooperativity between two TACN-Zn(II) catalytic units, additionally proving a great importance of double Lewis acid activation in phosphodiester cleavage, and also from increased substrate affinity with the catalyst. What also was observed from k_{cat} and K_M trends is the random distribution of thiols of Zn(**4l**) and (**4m**) on the common platform (see *Chapter 3*, *paragraph 1*) and, as indicated and confirmed by theoretical analysis and control experiments, in the case of clustering both k_{cat} and K_M values remain constant through the whole range of x_{A1}. Nevertheless, the catalytic site is more or less the same over the range of studied mole fractions.

Three years later the same group presented a series of relatively similar structure-wise nanoparticles, but manipulating the length of the alkyl chain between two amide groups (in one case the alkyl chain was replaced by TEG; *Fig.4.11.*).[24] It has been proven that by a single modification of the coating thiol's structure, i.e. by increasing the length of the alkyl chain, it is possible to obtain a microenvironment with a polarity lower than that of bulk water. This stabilizes the electrostatic interaction by the metal ion and even more the dianionic transition state, that certainly accelerates the hydrolysis of HPNP. Comparing Zn(**4l**) with Zn(**4p**), not only did k_{cat} increase c.a. 6 folds, but also the affinity to RNA model substrate increased 3 times (*Table 4.12.*), making Zn(**4p**) one of the most efficient HPNP cleavers reported in the literature so far.

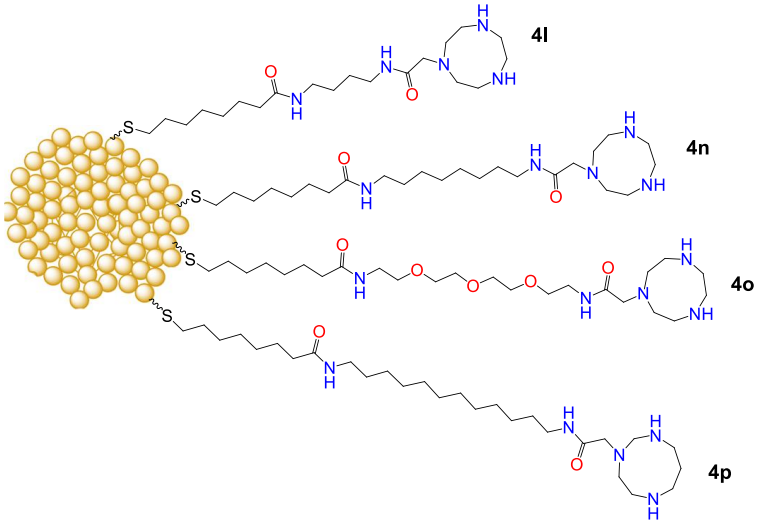

Catalyst as the zinc complex	k_{cat} [s^{-1}]	K_M [mM]	k_2 [M^{-1} x s^{-1}]
4l	0.036	0.58	62
4n	0.212	0.40	437
4o	0.019	0.38	50
4p	0.196	0.30	638

Fig.4.11., Table 4.12.

From *Table 4.12.* very similar values of K_M for all AuNPs are observable. Thus, it implies that elongation and structural modification of thiols do not significantly affect the binding site preorganization. Therefore, the reason behind diverse catalytic activities of nanozymes arises from different reactivity of fully formed substrate-enzyme complex. Thus, what stands for increased reactivity of HPNP cleavage using Zn(**4n**) and Zn(**4p**) is their pseudophase formed by the coating monolayer, which enhances the metal ion-substrate interaction and desolvates the nucleophile. Interestingly, creation of more hydrophobic environments to accelerate the phosphodiester cleavage was also pointed out by Brown *et al*., in the previously described Zn_2(**4g**) case (*Fig.4.6.*).[19]

4. *Kinetic Experiments of the Cleavage of HPNP in the Presence of Nanozymes* ***AuNP1-5****.*

Herein presented kinetic studies are the result of experiments based on spectrophotometrically monitored cleavage of HPNP, catalysed by **AuNP1-5**. In all cases, the concentration of nanozymes was much lower than the substrate – therefore, to simplify the complexity of kinetic studies, the experiments were performed under so called pseudo-first order conditions

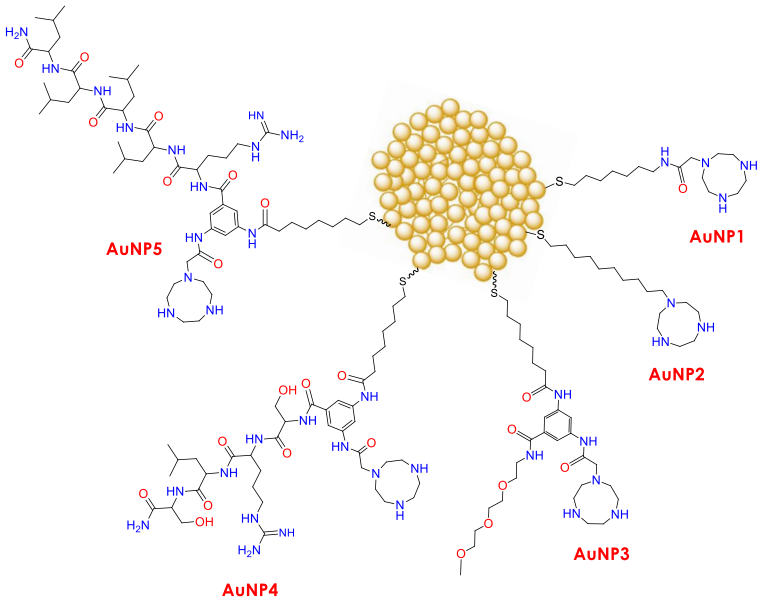

From obtained UV-Vis data, being the function of increasing absorbance at 400 nm against passing time, the initial velocity/rate of the reaction has been calculated and utilized as a common parameter for all kinetic profiles. It is considered as a velocity measured before more than ~10% of the substrate has been converted to the product. Consequently, many undesired factors and effects can be minimized, such as reversible reactions, inhibition of nanoparticles by product or progressive inactivation of the nanozyme.

a) Cooperativity Between Adjacent Functional Groups – Zn(II) Titration.

To establish the exact concentration of TACN groups in synthetized AuNPs, Zn(II)-dependent kinetic experiments were performed at constant HPNP and nanoparticles concentrations (*Fig.4.13.*). [Zn(II)] values, at which nanoparticles reactivity plateaued, were considered as the saturation concentrations of all TACN units present in nanoparticles. In all cases, the maximum catalytic activity was observed when all triazacyclononane moieties coating the gold core were complexed with zinc ions. Additionally, it is important to note that *Fig.4.13.* represents data that were normalized for all AuNPs, thus at the same concentration of Zn(II) ions.

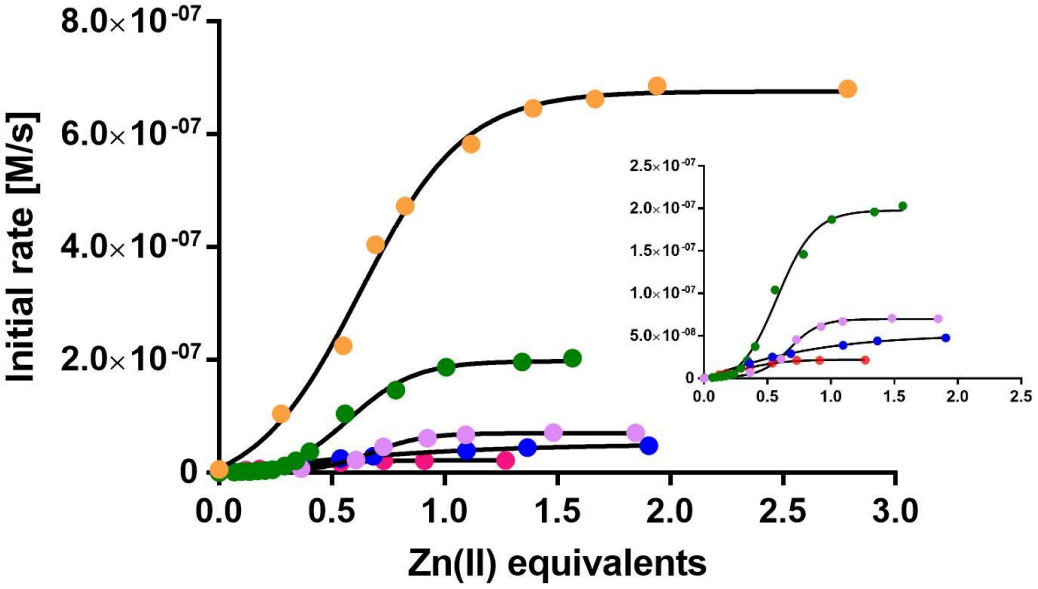

Fig.4.13. Zn(II)-dependence in the cleavage of HPNP by **AuNP1-5**.
Conditions: [HPNP] = 1.0 x 10^{-3} M, [HEPES] = 1.0 x 10^{-2} M, pH = 7.5, T = 40°C in H_2O.
Symbols code: **AuNP1** orange, **AuNP2** green, **AuNP3** pink, **AuNP4** dark blue, **AuNP5** red.

The shape of the kinetic titration curves indicates a possible mechanism of the AuNPs' catalytic efficiency. Previous literature reports that the sigmoidal shape reflects bimetallic cooperativity, which is the case of **AuNP1-3**. At low Zn(II) loading, monometallic complexes are formed first, which is logical as these are more favourable

due to electrostatic repulsions. As soon as Zn(II)-TACN complexes start to create bimetallic units, a substantial increase in the catalytic efficiency is observed.

Zn(II) titration in the presence of **AuNP4,5** revealed not a sigmoidal but saturation profile, which one may consider as a lack of cooperation between two metal ions. In terms of structure, thiols coating nanoparticles **4** and **5** possess arginine in their peptide sequences, and therefore, a positively charged guanidinium group. Guanidinium functionality is inactive itself in the hydrolysis of HPNP, however upon Zn(II) addition the catalytic activity increases until all TACN units are complexed with the metal ion.

The cooperativity between the guanidinium unit and metal ion complexes which catalyse the cleavage of phosphodiester linkages is already established within literature (see Chapter 4, *Fig.4.9.*). However, an important factor which has not been suitably addressed is whether the bimetallic catalysis could be substantially more efficient than that resulted from a flanking guanidinium moiety and a single metal centre. Based on results of performed kinetic studies with **AuNP1-5** (*Fig.4.13.*), in HPNP cleavage the bimetallic catalysis is more efficient than the one obtained with a guanidinium unit and metal ion complex.

In the case of the Y-shaped nanoparticles **AuNP3**, apart from Zn(II)-TACN complexes there are no more species which may constitute the active site of the catalyst, therefore it should not be surprising that the PEG-decorated nanoparticles reveal the same behaviour as **AuNP1,2.** Importantly, the density of Zn(II) ions in the case of Y-shaped nanoparticles is lower due to 'dilution' by other constituent moieties (peptide or triethyleneoxymethyl derivative) which makes the cooperation of two adjacent catalytic units less favourable. That is why, despite the same catalytic behaviour, **AuNP3** are less efficient in HPNP cleavage than **AuNP1,2**.

It has to be pointed out that whenever the concentration of nanoparticles will be mentioned throughout this work, it will be referred to the concentration of TACN-ligand present on AuNPs' monolayer. It is to allow to quantitatively access the role of metal complexes once they are confined on the surface of nanoparticles.

*b) Michaelis-Menten-like Kinetic Experiments in the Cleavage of HPNP by **AuNP1-5**.*

The catalytic efficiency of five synthesized nanoparticles complexed with Zn(II) was studied by following the cleavage of increasing concentration of HPNP (*Fig.4.14.*). As previously mentioned (see *Chapter 4*, *paragraph a*), the nanozymes' catalytic efficiency is governed by their composition, therefore, the concentrations of the catalysts were normalized according to number of metallic sites (**AuNP1-3**: bimetallic and **AuNP4,5** monometallic catalysis). Additionally, *Table 4.16.* comprises established and calculated kinetic parameters.

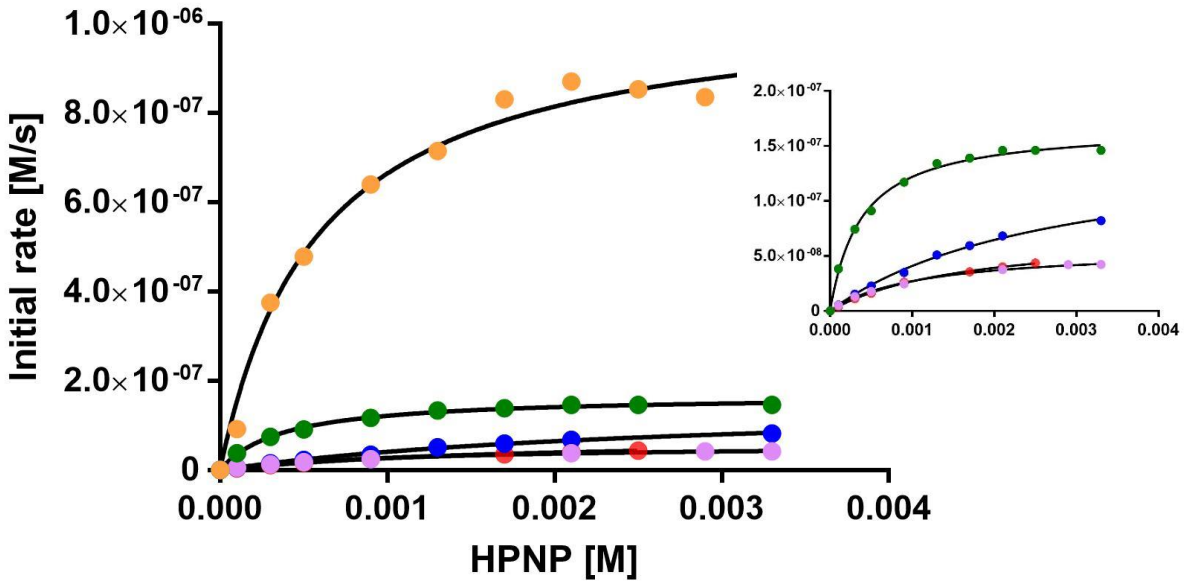

Catalyst	k_{cat} [s^{-1}]	k_2 [l×mol^{-1}×s^{-1}]	K_M [mM]	[a] k_{rel}
AuNP1	0.193	331	0.58	9.7 x 10^5
AuNP2	0.031	81.6	0.38	1.5 x 10^5
AuNP3	0.010	9.39	1.1	5.3 x 10^4
AuNP4	0.014	5.14	2.7	6.9 x 10^4
AuNP5	0.006	3.85	1.7	3.3 x 10^4

Fig.4.14. Table 4.15. Michaelis-Menten kinetic studies on the cleavage of HPNP by **AuNP1-5** and calculated kinetic parameters. Conditions: [nanozyme] = 2.5 x 10^{-5} M, [HEPES] = 1.0 x 10^{-2} M, pH = 7.5, T = 40°C in H_2O. [a] $k_{rel} = \frac{k_{cat}}{k_{uncat}}$, $k_{uncat} = 2.0 \times 10^{-7}\ s^{-1}$.[25]
Symbols code: **AuNP1** orange, **AuNP2** green, **AuNP3** pink, **AuNP4** dark blue, **AuNP5** red.

Upon analysis of collected data it is evident that the most efficient nanoparticles in HPNP cleavage are **AuNP1**. They are as active as, and structurally similar to, the previously reported nanozymes by Scrimin et al. (see *Fig.4.11.*). Existing as one of the most effective catalysts for the hydrolysis of HPNP, **AuNP1** are able to accelerate the cleavage of RNA models almost one million times faster compare to the background reaction. The comparison with **AuNP2** indicates that an amide moiety plays a relevant role in the efficiency of the cleavage but it does not dramatically change the affinity to the substrate. However, taking into account the second-order rate constants, **AuNP1** is a four-fold better catalyst than **AuNP2**.

From the analysis of Michaelis-Menten constants K_M (the introduction to Michaelis-Menten kinetics, see *the Appendix to Chapter 4*), HPNP has a better affinity for **AuNP1,2** than for the higher-complexity nanoparticles **AuNP3-5**. Indeed, it was already reported that phosphodiesters bind strongly to cationic Zn(II) rather than ammonium ions, for instance in the form of guanidinium group present in **AuNP4,5**.[26] In the case of **AuNP3**, a dilution of the metal ion complexes on the monolayer makes an access to bimetallic sites less available, which is likely responsible for their lower affinity towards HPNP.

The comparison of oligopeptide-decorated gold nanoparticles reveals that there is not a big difference in terms of their reactivity towards the cleavage of HPNP. The better catalytic performance of **AuNP4** over **AuNP5** may be reasoned through the improved positioning of the guanidinium moiety in relation to TACN. The **AuNP5** arginine is separated by one amino acid from the monometallic site compared to **AuNP4**, making the cooperation of functional units in that catalytic site less efficient.

*c) pH–dependent Kinetics of HPNP Hydrolysis by **AuNP1,2** and **4**.*

To better understand the catalytic phenomena of gold nanoparticles, additional analysis of pH-dependence of HPNP hydrolysis by **AuNP1,2,4** was done (*Fig.4.16.*). Collected data were fitted with the equation (1):

$$k_2 = \frac{k\varphi[TACN{\cdot}Zn(II)]tot}{\left(1+\frac{[H^+]}{K_{a1}}+\frac{K_{a2}}{[H^+]}\right)+k_H[H^+]} \qquad (1)$$

Where $k\varphi$ is the observed reaction rate, K_{a1} and K_{a2} are the first and second relevant deprotonation constants and k_H is the constant of the acid catalysed background reaction. In all cases, the second order rate constant vs pH exhibited a bell-shaped profile, which indicates that there are two kinetically relevant proton exchanges having either a positive (K_{a1}) or negative (K_{a2}) impact on the catalytic efficiency.

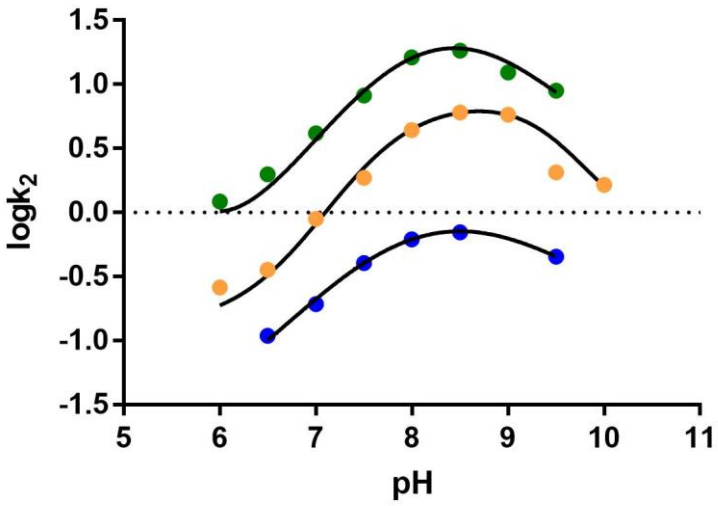

Fig.4.16. The function of the second order rate constant vs pH of the hydrolysis of HPNP by **AuNP1,2,4**. Conditions: [nanozyme] = 1.4 - 3.5 x 10^{-3} M, [HPNP] = 1.0 x 10^{-3} M, [buffers] = 1.0 x 10^{-2} M, T = 40°C in H_2O. Symbols code: **AuNP1** orange, **AuNP2** green, **AuNP4** dark blue.

K_{a1} and K_{a2} may reflect a deprotonation of two TACN-Zn(II)-bound water molecules, as schematically depicted in *Scheme 4.17.*:

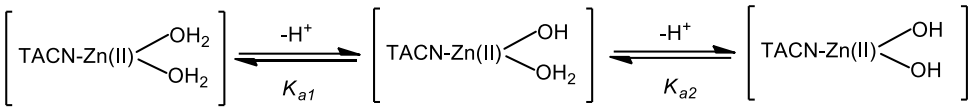

Scheme 4.17.

The first deprotonation of water molecule (K_{a1}) allows the substrate (HPNP) binding and release of remaining water molecule, having a positive impact on the catalytic efficiency (*Scheme 4.18).*

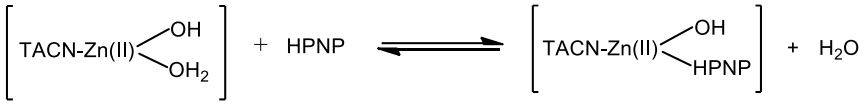

Scheme 4.18.

On the other hand, further increase of pH deprotonates the second water molecule (K_{a2}), what saturates the coordination sphere of Zn(II) (*Scheme 4.19.*) This may deactivate the catalyst due to less favoured replacement of the metal bound hydroxide with the substrate, hampering the formation of the substrate-catalyst complex.

Scheme 4.19.

The hydrolysis of HPNP catalysed by either **AuNP1** or **AuNP2** reveals a fairly similar set of pK*a*, being 7.9, 9.3 and 7.8 and 9.2, respectively. The first deprotonation (K_{a1}) may be associated with the activation of nucleophile, i.e. the hydroxyl group of HPNP. Therefore, it reflects the increase of the catalytic efficiency. The second deprotonation (K_{a2}) refers to already mentioned formation of the second $^{-}$OH bound to Zn(II), which saturates its coordination sphere.

The pH-dependent kinetics catalysed by **AuNP4** show two kinetically relevant deprotonations with p*K*a 7.5 and 10.1, according to the equation (1). The first one, similar to that established for **AuNP1,2** refers to activation of internal nucleophile of HPNP. The fact that this value is slightly lower than 7.8-7.9 (calculated for **AuNP1,2**) may be a consequence of the increased local pH due to the presence of a positively charged guanidinium moiety or charge influence on the p*K*a value of the zinc bound water. On the other hand, the second deprotonation with p*K*a 10.1 is higher than in the previous systems, which may be associated with deprotonation of the guanidinium ion with p*K*a = 12.5. This value may be decreased on the monolayer of **AuNP4** because of the presence of positively charged Zn(II) complexes. The deprotonation of the guanidinium functionality may be detrimental due to the loss of interaction with the phosphate group of HPNP, occurring via electrostatic interaction.

d) Competitive Inhibition Studies and Kinetic Isotopic Effect.

Previous literature has established that binding affinity of probes present on the monolayer of gold nanoparticles is caused not only by electrostatic interactions, but also interactions with the hydrophobic part of the monolayer. Accordingly, the hydrophobic contribution in the cleavage of HPNP by **AuNP1** and **AuNP2** have been additionally studied. Since HPNP has a non-polar aromatic unit attached to the phosphate group, this functionality easily penetrates the hydrophobic monolayer of gold nanoparticles. Indeed, not only the surface of nanozymes is relevant from the catalytic point of view, but also the area in closer proximity to the gold core.

To explore the hydrophobic contribution of the cleavage of HPNP by gold nanoparticles, competitive inhibition studies were performed in the presence of increasing concentrations of DMP (dimethyl phosphate), *Fig.4.20*. The experiments were performed under sub-saturation conditions for HPNP and the concentration of inhibitor in solution was not perturbed by the amount bound to the catalyst.

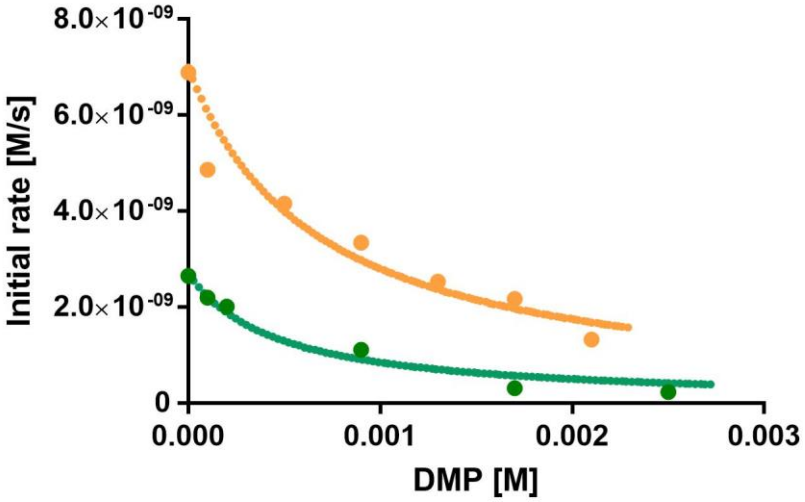

Fig.4.20. Inhibition kinetics of the hydrolysis of HPNP by **AuNP1** and **AuNP2** by progressive addition of dimethyl phosphate. Conditions: [nanozyme] = 2.5 × 10^{-5} M, [HEPES] = 1.0 × 10^{-2} M, [HPNP] = 1.0 x 10^{-5} M; pH = 7.5, 40 °C in H_2O.
Symbols code: **AuNP1** orange, **AuNP2** green.

The apparent inhibition constants K_i were calculated using the equation (2):

$$\frac{k_\psi}{k_0} = \frac{1}{1 + K_i[\mathrm{DMP}]} \qquad (2)$$

where k_0 is the reaction rate in the absence of DMP, k_ψ is the reaction rate at certain concentration of DMP and K_i is the binding constant of DMP to AuNPs. Their established values (23.3 mM and 38.5 mM for **AuNP1** and **AuNP2**, respectively) indicate that there is a better binding of DMP to **AuNP1** than **AuNP2**, being the opposite result of their affinity to HPNP. The lower affinity to nanoparticles however

do not affect the catalytic efficiency of **AuNP1**, which is much more reactive than **AuNP2**.

Since dimethyl phosphate and 2-hydroxypropyl *p*-nitrophenyl phosphate alter in terms of hydrophobicity, their interaction with the monolayer is different. DMP is not prone to enter the hydrophobic part of nanoparticles (due to lack of non-polar functionality), hence it prefers to stay at AuNPs' surface. HPNP however, possessing the aromatic unit, is more eager to penetrate the monolayer, where the catalysis likely takes place (thus, HPNP reveals here a higher binding constant than DMP). Therefore, gold nanoparticles are creating a microenvironment which stabilizes electrostatic interactions occurring during hydrolysis, resembling enzymes' active sites.

The potential proton transfer relevance at the rate limiting step was explored. The pH and pD dependent hydrolysis of HPNP in the presence of **AuNP1** were performed either in H_2O or D_2O (*Fig.4.21.*).

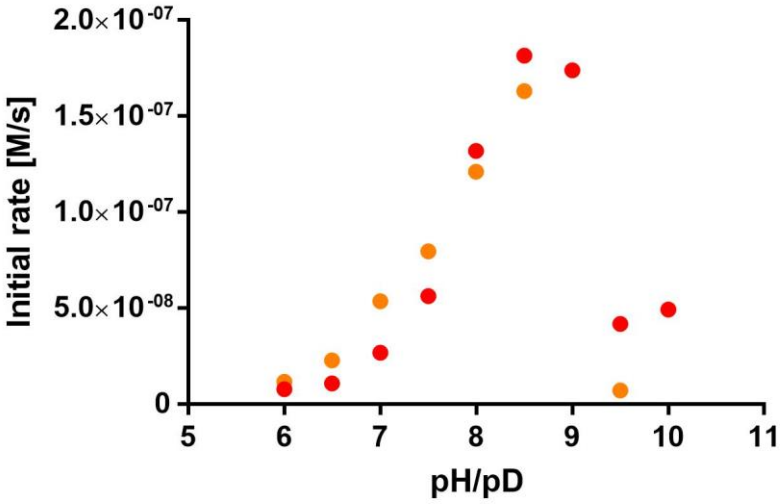

Fig.4.21. pH/pD-rate profile of the cleavage of HPNP by **AuNP1**. Conditions: [nanozyme] = 1.7×10^{-5} M, [buffers] = 1.0×10^{-2} M, [HPNP] = 1.2×10^{-3} M, 25 °C in H_2O/D_2O.
Symbols code: **AuNP1** in H_2O red, **AuNP1** in D_2O orange.

The proton transfer may occur via deprotonation of the nucleophile by the hydroxide bound to Zn(II)-TACN complex, automatically implying its activation. The obtained results depicted in *Fig.4.21.* clearly indicate a lack of proton transfer at the rate determining step of the hydrolysis of HPNP – indeed, both pH and pD profiles are almost superimposable. The presented kinetic studies also exclude any similar involvement by the amide bond, connecting Zn(II)-TACN complex to the alkyl chain.

5. *Concluding Remarks and The Proposed Mechanisms of the Cleavage of HPNP by **AuNP1-5**.*

On the basis of the described studies, it is evident that the presented nanoparticles catalyse the cleavage of HPNP following two different mechanisms, depending on catalytic units present on the AuNP monolayer (*Fig.4.22.*). **AuNP1-3** utilize two Zn(II) ions which form bimetallic sites; **AuNP4,5** however, use a single Zn(II) ion and the guanidinium group of the arginine, present in the peptide sequence of each of Y-shaped thiols. This finding was confirmed by Zn(II)-dependent kinetics (*Fig.4.13.*), where **AuNP1-3** exhibited a sigmoidal profile indicating bimetallic cooperativity, whereas **AuNP4,5** demonstrated a saturation profile. This particular result may be considered as a catalysis involving a single metal ion. Both proposed mechanisms require the initial binding of HPNP to the catalytic site of nanoparticles, according to performed Michaelis-Menten kinetics (*Fig.4.14.*).

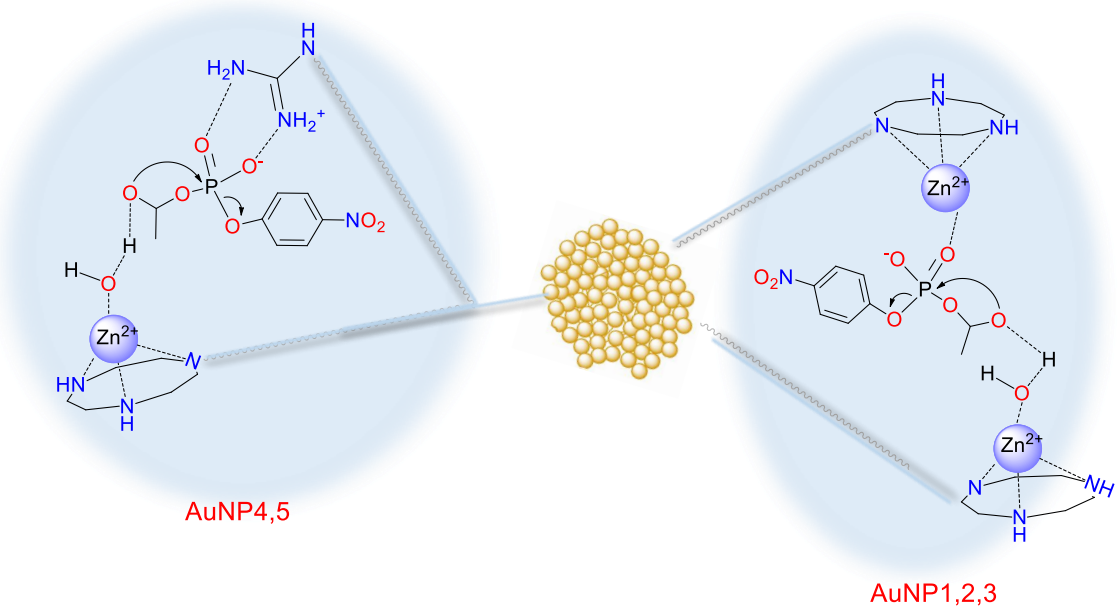

Fig.4.22. The proposed mechanism of HPNP cleavage by either bimetallic sites (**AuNP1-3**; right) or a single zinc ion and guanidinium moiety (**AuNP4-5**; left). In both cases one of Zn(II) acts as a general base catalyst.

In both mechanisms, deprotonation of the hydroxyl group of HPNP is accelerated by a coordination to Zn(II)-bound water molecule (mediating a contact between the metal ion and the hydroxopropyl-OH group), resulting in an electrostatic stabilization and lowering of p*Ka* of the nucleophile. It is unlikely that the activation occurs via general-base catalysis, since no proton transfer at the rate determining step was detected (*Fig.4.21.*). Additionally, the catalysis performed at pH levels higher than 9.0-9.5 indicated that in the case of bimetallic nanoparticles, the coordination sphere of Zn(II) was saturated by deprotonation of the second metal-bound water molecule. Consequently, the coordination of the substrate by nanozyme is less favoured, diminishing its efficiency. In the case of peptide-decorated nanoparticles, working at very basic conditions may give deprotonation the guanidinium moiety. This would result in a lack of desired electrostatic interaction within phosphates. The catalysis likely occurs inside the monolayer of gold nanoparticles, a finding suggested by inhibition kinetics with dimethyl phosphate, depicting a high hydrophobic contribution during the cleavage of HPNP.

The presented supramolecular systems appear to be among the best performing catalysts for the cleavage of the RNA model substrate, HPNP. Indeed, **AuNP1** are 1.3-fold better in terms of k_2 than the nanozyme reported by Diez-Castellnou Zn(**4e**) and 6.2-fold better than the so far most efficient dinuclear Zn(II) complex Zn_2(**4f**) presented by Williams.[24], [27] While 1.3-fold of a difference is likely within the experimental error, 6.2-fold increase of the efficiency can be considered as significant. Furthermore, gained knowledge from performed mechanistic studies enabled a greater understanding of the way in which AuNPs hydrolyse the phosphodiester bond. Multiple functional units can be anchored to one system at an optimal distance from each other, resulting in unique microenvironments. These provide a great catalytic efficiency in phosphodiester cleavage, in comparison to reported simple organic complexes as well as more advanced supramolecular systems, such as calixarenes.

Appendix to *Chapter 4*

Introduction to the Michaelis-Menten Model in Enzyme-Catalysed Reactions.

The enzyme-like behaviour of gold nanoparticles in the phosphodiester cleavage can be demonstrated by the titration of a substrate at a constant concentration of a catalyst.

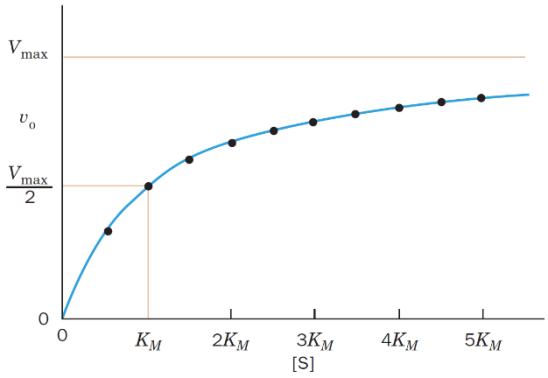

Fig.4.23. The plot of the initial velocity vs. the substrate concentration of a simple Michaelis-Menten reaction.

The result of this kind of experiment is the saturation function (more specifically, the rectangular hyperbola) as depicted in *Fig.4.23.*.[28] It can be mathematically described as the expression called the Michaelis-Menten equation (after the names of Leonor Michaelis and Maud Menten), which is one of the best-known models of enzyme kinetics[29]:

$$v = \frac{d[P]}{dt} = \frac{V_{max}\,[S]}{K_M + [S]} \qquad (3)$$

where v is the rate of reaction at certain time, V_{max} represents the maximum rate that can be achieved by a catalyst/enzyme under saturation conditions (i.e. when the concentration of a substrate $[S]$ is much higher than enzyme's), K_M, being the Michaelis-Menten constant, reflects the concentration of a substrate at which the reaction rate is equal $0.5\,V_{max}$. The constant is not dependent on the concentration of an enzyme, however it is affected by the temperature, pH as well as the type of substrate.

The equation (3) has its fundaments in a general, two-step reaction scheme (4). As was firstly reported in 1902 by Adrian Brown, the enzymatic reaction comprises a substrate (S) interacting with an enzyme (E), eventually forming (ES) complex.[30] That reaction

is followed by a decomposition of (ES) to form a product (P) and free enzyme. The rate of (ES) formation is determined by k_I and the reverse reaction by k_{-I}. The breakdown of (ES) and formation of (P) is represented by the rate constant k_{II}.

$$E + S \underset{k_{-I}}{\overset{k_I}{\rightleftharpoons}} ES \overset{k_{II}}{\rightarrow} P + E \tag{4}$$

In order to explicitly integrate the Michaelis-Menten equation (3) based on scheme (4), a few simplifying approximations should be applied, such as:

1) Rapid equilibrium approximation: $k_{-I} \gg k_{II}$, $thus\ K_S \sim K_M = \frac{k_{-I}}{k_I} = \frac{[E][S]}{[ES]}$ (K_S refers to a dissociation constant, K_M is a binding constant), meaning that a substrate binding and dissociation occur more rapidly than a product formation;
2) Steady state approximation: $\frac{d[ES]}{dt} = 0$, meaning that the concentration of an enzyme remains approximately unchanged;
3) Free ligand approximation: $[S] \approx [S]_T = [S] + [ES]$, where the total enzyme concentration $[ES]$ is usually much smaller than substrate's, therefore a depletion of S in binding to enzyme is relatively small and the concentration of a free substrate $[S]$ can be approximated by the total concentration of substrate $[S]_T$;
4) Conservation conditions: $[E]_T = [E] + [ES]$, where $[E]_T$ is the total enzyme concentration, $[E]$ is equal to free enzyme concentration and $[ES]$ refers to the concentration of enzyme bound to a substrate.[31], [32], [28]

In terms of reaction order, that strongly depends on the amount of substrate. At low substrate concentration $[S] << K_M$ the reaction rate varies linearly with $[S]$ (first-order kinetics), whereas at the last stage of catalytic process, when $[S] >> K_M$, the reaction

becomes strongly independent of $[S]$ (zero-order kinetics), reaching its maximum when all enzyme is bound to a substrate (V_{max}).

The Michaelis-Menten kinetic profile enables the researcher to establish relevant parameters providing a measure of an enzyme's catalytic efficiency. K_M has another important meaning: the enzyme's affinity for its substrate. Therefore, if an enzyme has a low K_M value, it reaches the maximal catalytic efficiency at low substrate concentration, thus reflecting a high enzyme-substrate affinity. On the contrary, high Michaelis-Menten constant means a low enzyme-substrate affinity, therefore the concentration of a substrate has to be relatively high to increase the statistical chances to bind to an enzyme.

Knowing V_{max} and the total concentration of an enzyme $[E_T]$, the catalytic constant k_{cat} (also known as the turnover number) can be calculated:

$$k_{cat} = \frac{V_{max}}{[E_T]} \tag{5}$$

Lastly is the second-order rate constant of the enzymatic reaction k_2 (known in the field of biochemistry as the specificity constant), which can be established utilizing k_{cat} and K_M:

$$k_2 = \frac{k_{cat}}{K_M} \tag{6}$$

k_2 is a measure how efficiently an enzyme converts substrates into products. Particularly, the second-order rate constant depends on both, strength of the substrate-enzyme binding and the intrinsic efficiency of substrate conversion into product.

6. *References of Chapter 4.*

[1] S. Mikkola, T. Lönnberg, H. Lönnberg, *Beilstein Journal of Organic Chemistry* **2018**, *14*, 803-837.

[2] L. Qian, Y. Xu, H. Arai, J. Aoki, T. M. McIntyre, G. D. Prestwich, *Organic Letters* **2003**, *5*, 4685-4688.

[3] Y. Xu, L. Qian, G. D. Prestwich, *Org Lett* **2003**, *5*, 2267-2270.

[4] J. Eldo, S. Heng, E. R. Kantrowitz, *Bioorganic & Medicinal Chemistry Letters* **2007**, *17*, 2086-2090.

[5] D. M. Brown, D. A. Usher, *Journal of the Chemical Society (Resumed)* **1965**, 6558-6564.

[6] N. H. Williams, B. Takasaki, M. Wall, J. Chin, *Accounts of Chemical Research* **1999**, *32*, 485-493.

[7] M. Diez-Castellnou, A. Martinez, F. Mancin, in *Advances in Physical Organic Chemistry, Vol. 51* (Eds.: I. H. Williams, N. H. Williams), Academic Press, **2017**, pp. 129-186.

[8] N. H. Williams, W. Cheung, J. Chin, *Journal of the American Chemical Society* **1998**, *120*, 8079-8087.

[9] P. Molenveld, J. F. J. Engbersen, H. Kooijman, A. L. Spek, D. N. Reinhoudt, *Journal of the American Chemical Society* **1998**, *120*, 6726-6737.

[10] T. Gajda, A. Jancsó, S. Mikkola, H. Lönnberg, H. Sirges, *Journal of the Chemical Society, Dalton Transactions* **2002**, 1757-1763.

[11] W. H. Chapman, R. Breslow, *Journal of the American Chemical Society* **1995**, *117*, 5462-5469.

[12] P. Molenveld, J. F. J. Engbersen, D. N. Reinhoudt, *European Journal of Organic Chemistry* **1999**, *1999*, 3269-3275.

[13] C. He, S. J. Lippard, *Journal of the American Chemical Society* **2000**, *122*, 184-185.

[14] S. Liu, A. D. Hamilton, *Bioorganic & Medicinal Chemistry Letters* **1997**, *7*, 1779-1784.

[15] O. Iranzo, A. Y. Kovalevsky, J. R. Morrow, J. P. Richard, *Journal of the American Chemical Society* **2003**, *125*, 1988-1993.

[16] W. N. Lipscomb, N. Sträter, *Chemical Reviews* **1996**, *96*, 2375-2434.

[17] G. Feng, D. Natale, R. Prabaharan, J. C. Mareque-Rivas, N. H. Williams, *Angewandte Chemie International Edition* **2006**, *45*, 7056-7059.

[18] H. Linjalahti, G. Feng, J. C. Mareque-Rivas, S. Mikkola, N. H. Williams, *Journal of the American Chemical Society* **2008**, *130*, 4232-4233.

[19] C. T. Liu, A. A. Neverov, R. S. Brown, *Journal of the American Chemical Society* **2008**, *130*, 13870-13872.

[20] P. Molenveld, J. F. J. Engbersen, D. N. Reinhoudt, *Angewandte Chemie International Edition* **1999**, *38*, 3189-3192.

[21] R. Salvio, R. Cacciapaglia, L. Mandolini, *The Journal of Organic Chemistry* **2011**, *76*, 5438-5443.

[22] R. Salvio, S. Volpi, R. Cacciapaglia, A. Casnati, L. Mandolini, F. Sansone, *The Journal of Organic Chemistry* **2015**, *80*, 5887-5893.

[23] G. Zaupa, C. Mora, R. Bonomi, L. J. Prins, P. Scrimin, *Chemistry – A European Journal* **2011**, *17*, 4879-4889.

[24] M. Diez-Castellnou, F. Mancin, P. Scrimin, *Journal of the American Chemical Society* **2014**, *136*, 1158-1161.

[25] G. Zaupa, C. Mora, R. Bonomi, L. J. Prins, P. Scrimin, *Chemistry (Weinheim an der Bergstrasse, Germany)* **2011**, *17*, 4879-4889.

[26] D. O. Corona-Martínez, P. Gomez-Tagle, A. K. Yatsimirsky, *The Journal of Organic Chemistry* **2012**, *77*, 9110-9119.

[27] G. Feng, D. Natale, R. Prabaharan, J. C. Mareque-Rivas, N. H. Williams, *Angewandte Chemie (International ed. in English)* **2006**, *45*, 7056-7059.

[28] D. Voet, J. G. Voet, in *Biochemistry*, 4th ed ed. (Eds.: D. Voet, J. G. Voet), John Wiley and Sons, Hoboken, NJ, **2011**.

[29] L. Menten, M. I. Michaelis, *Biochem Z* **1913**, *49*, 5.

[30] A. J. Brown, *Journal of the Chemical Society, Transactions* **1902**, *81*, 373-388.

[31] G. E. Briggs, J. B. S. Haldane, *Biochemical Journal* **1925**, *19*, 338.

[32] F. C. Wedler, *International Journal of Chemical Kinetics* **1976**, *8*, 159-159.

Chapter 5

1. *Even Stable Can Sometimes Be Unstable - The Hydrolytic vs. Oxidative Pathway of DNA Cleavage and Its Model Substrates.*

From all possible mechanistic pathways of DNA cleavage, oxidative is the most effective (*Fig. 5.1.*). However, despite the attractiveness of oxidative cleaving agents, there are two reasons explaining why their applicability is limited.[1] The oxidative cleavage yields toxic oxygen species (generally hydroxyl radical species of O_2 (OH)), which can cause difficulties in determining the exact location of targeted secondary structures.[2] Moreover, it results with inconsistent fragments of DNA compared to products formed upon cleavage by natural metallonucleases, i.e. 5'-phosphates and 3'-hydroxyls.[3] Lastly, oxidative cleavage can be potentially devastating to normal cell physiology. It may lead to mutagenesis and/or cell death due to damage of all four nucleobases or/and deoxyribose sugars.[2], [4]

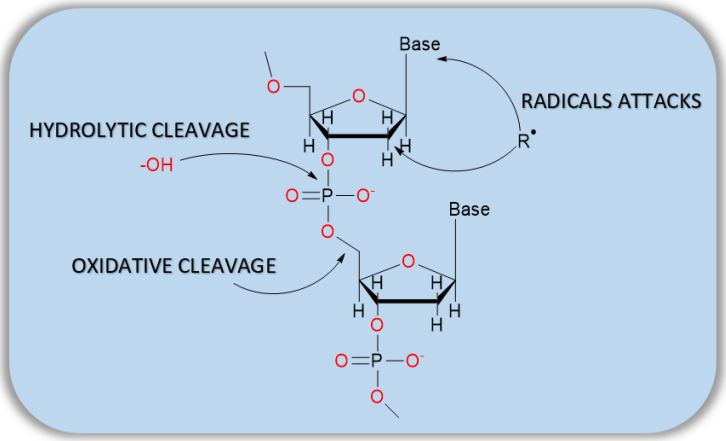

Fig.5.1. Possible pathways of DNA cleavage.

It is, therefore, seemingly obvious why design of artificial nucleases should take into account the redox chemistry of utilized metal ions (like Cu(II), Mn(II) or Fe(III)).[5], [6] The reactivity of oxidizing agents strongly depends on cofactors such as molecular

oxygen, hydrogen peroxide or sources of diffusible radicals, hence their absence should be excluded from the first instance when the hydrolytic pathway is studied. However, literature can provide us with some unexpected examples of C-O cleavage by seemingly oxidative-resistant metal complexes. The first reported case was presented by Reedijk *et al.,* who observed such a behaviour in the presence of the $[Zn_2(pyrimol)_2]^+$ complex.[7] Even though this peculiar behaviour may be due to the pyrimol ligand reactivity, it is a serious warning to look out for the oxidative cleavage of DNA model substrates.

The concept of simple model substrates serves to predict mechanistic behaviour (like hydrolysis, interaction with another chemical species or stability) of their more robust and complex equivalents. However, even with the use of simple organic compounds, some complications are inevitable, especially in terms of deoxyribonucleic acid models. In the previous case of the RNA model, HPNP, C-O cleavage is not observed due to the presence of an internal nucleophile and increased steric hindrance at the carbon.[8] In the case of DNA models however, C-O cleavage is relatively common. Employing dimethyl phosphate (DMP), Westheimer *et al*. established the rate constant of DNA hydrolysis.[9, 10] It has since been found by Bunton *et al*. that most of the reaction proceeded via nucleophilic attack at carbon with C-O cleavage and not the desired P-O bond cleavage.[11] Since then the actual cleavage of DMP has been of keen interest and under experimental probe. Eventually, the most reliable research based on DMP cleavage, by extrapolation of high temperature kinetic data are reporting that the half-life of DNA is 130000 years at 25°C and pH 6.8.[12] However, this number refers mainly to C-O cleavage, serving as an upper limit for DNA hydrolysis.

As mentioned in *Chapter 4*, very convenient simple nucleic acids models constitute molecules possessing aryloxy substituents. In addition to their increased reactivity (due to the presence of a good leaving group), it has been found that in their case C-O cleavage is suppressed and thus the reaction rates of P-O cleavage can be determined directly.[7]

a) Bis-para-nitrophenyl Phosphate (BNP)

One of the commonly used DNA model previously mentioned is bis-*para*-nitrophenyl phosphate (BNP). This commercially available compound is hydrolysed in water with a half-life of 1300 years at pH 7.0 and 25°C, which can be conveniently monitored by UV-Vis spectrophotometry.[13] Its hydrolysis has been extensively studied since 1990, when the first BNP cleavage by a simple mononuclear Zn(**5a**) and Zn(**5b**) complexes was reported by Trögler and Rosch (*Fig. 5.2.*).[14] However, the obtained acceleration in BNP cleavage was very modest (2 and 53-fold rate acceleration over the background reaction at pH 7.0 and 75°C).

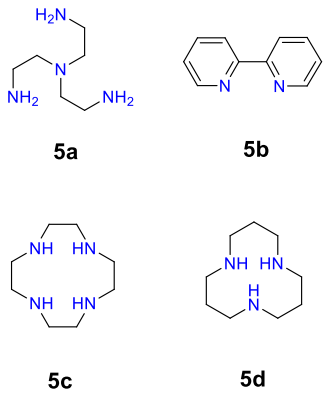

Fig.5.2.

Following studies by Kimura and Koike who noticed a strong binding of a nitrogen atom containing macrocycles to the transition metal ions, a new era of simple catalysts for the cleavage of nucleic acids models began.[15] Using Zn(II) coordinated 1,4,7,10-tetraazacyclododecane Zn(**5c**) and 1,5,9-triazacyclododecane Zn(**5d**) complexes (*Fig. 5.1.*), the rate acceleration of BNP cleavage was substantially increased comparing to previously introduced complexes (by 100-fold and 2000-fold compared to the background reaction, respectively). The superiority of Zn(**5d**) was attributed to its ability to lower the p*K*a of a zinc bound water molecule at physiological pH (p*K*a = 7.9).[16] However, in the case of Zn(**5c**), the catalytic efficiency was suppressed due to the saturation of binding sites of the metal ion by nitrogen atoms, revealing at

the same time the p*K*a of zinc-bound water molecule similar to that of Zn(**5d**) (p*K*a = 7.3). Unfortunately, authors claimed that the phosphoryl transfer of BNP was too complex to allow for the full explanation of reaction mechanism.

The same authors presented in their next studies a new and improved complex, being a benzyl alcohol-pendant cyclen complexed with Zn(II) bearing a chiral carbon, adjacent to the phenyl group (**5e**, *Fig. 5.3.*).[16]

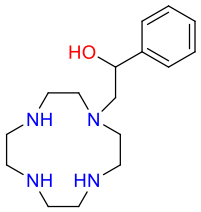

5e

Fig.5.3.

Due to performed studies such as potentiometric titrations, pH-profiles or analysis of crystal structures, authors were able to conclude the mechanism of cleavage of BNP by Zn(**5e**). Firstly, at pH 7.4 the hydroxyl group of the benzyl alcohol is activated by coordination to Zn(II). In such a way, the first ester group of BNP is immediately hydrolysed, making Zn(**5e**) 125 times more efficient than the Zn(II)-activated water molecule of (**5c**). At pH 9.0 the second relevant deprotonation occurs, meaning a generation of the nucleophile from the Zn(II)-coordinated water molecule. This deprotonation results in the intramolecular transesterification, which is 45000 times faster than the cleavage of ethyl *para*-nitrophenyl phosphate with zinc-bound hydroxide of (**5c**). However, Zn(**5e**) cannot be fully considered as a catalyst, since the product *para*-nitrophenyl phosphate, coordinated to the complex, was inert under standard conditions and led to inactivation of the metal chelate. Nevertheless, the authors presented the elucidation of the collaborative role of alkoxide (belonging to the ligand) and Zn(II), which resembles at the same time the active site of Alkaline Phosphatase bearing serine and Zn(II) functionalities.

In 2004 Chin compared the reactivity of bis-(pyridylmethyl) amine derivatives complexed with Zn(II) in the cleavage of BNP (*Fig. 5.4.*).[17] Apart from the previously introduced concept of a ligand bearing an alcoholic group that acts as a nucleophile (or a metal-bound water molecule playing the same role), the presence of H-bond donating groups was additionally studied.

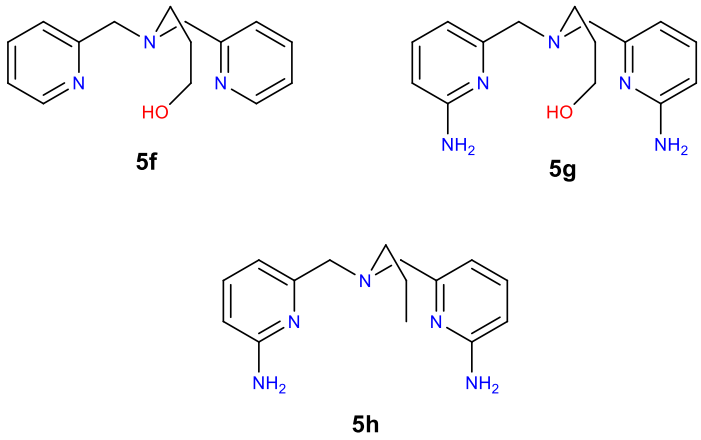

Fig.5.4.

It has been shown that the cooperation between different functional organic groups in conjunction with metal ion activation yields a great increase efficiency in phosphodiester cleavage. Bell-shaped pH profiles indicated firstly, the formation of the active nucleophile (metal-bound hydroxide or alkoxide, first p*K*a), and upon further increase of pH, a drop in the reactivity, due to saturation of the coordination site of the metal ion (formation of a Zn(II)-bound hydroxide, second p*K*a). Further analysis confirmed the highest efficiency in BNP cleavage by Zn(**5g**), being able to accelerate the hydrolysis almost six orders of magnitude faster compared to the rate of BNP spontaneous cleavage (at pH 7.0 and 25°C). Interestingly, the contribution of the alkoxide as a nucleophile is roughly 17-fold higher than a metal-bound hydroxide, caused by weaker solvation of the oxygen atom (steric hindrance of the hydrophobic alkyl moiety). However, an even greater effect emerges from H-bond donors (**5g**, **5h**), resulting in a 230-fold higher catalytic efficiency. The presented rough mechanistic

studies on BNP cleavage by Zn(**5g**) assumed nucleophilic attack of the Zn(II)-bound alkoxide and stabilization of the transition state primary amine groups of the ligand.

Three years later the same group proposed a full mechanistic explanation of BNP cleavage discussed bis-(pyridylmethyl)amine derivatives, based on DFT calculations, ^{31}P NMR and UV-Vis studies.[18] The nature of the reaction products were found to be strictly dependent on the active nucleophile. Using as nucleophile a zinc-bound water molecule, as in the case of Zn(**5h**), only *p*-nitrophenyl phosphate monoester (MNP) and *p*-nitrophenoxide were detected, as expected from the clean hydrolytic cleavage of BNP. However, MNP binds more strongly to the catalyst than BNP, hence the catalytic efficiency of Zn(**5h**) was decreased by *p*-nitrophenyl phosphate monoester inhibition. In the case of the zinc-bound alkoxide of (**5f**, **5g**) acting as a nucleophile, *O*-phosphorylated ligand was formed as the result of transesterification (*Fig. 5.5.*). Furthermore, neither *O*-phosphorylated ligand nor MNP underwent further cleavage.

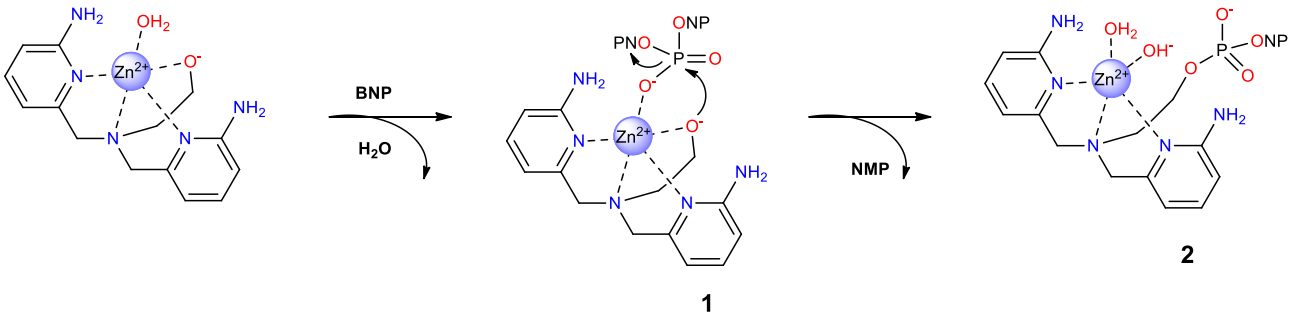

Fig.5.5.

However, the fate of the reaction did not depend only on the type of nucleophilic species, but also on the amount of substrate vs. catalyst. In the presence of an excess of BNP not only the formation of the *O*-phosphorylated complex was observed, but also a slow release of *p*-nitrophenoxide and the formation of MNP (*Fig. 5.6.*). As the *O*-phosphorylated ligand did not hydrolyse further and a zinc-bound hydroxide could still serve as a nucleophile, the formation of MNP could only result from BNP

hydrolysis. Therefore, the second hydrolysis, occurring due to an excess of BNP, resembled the cleavage in the presence of Zn(**5h**).

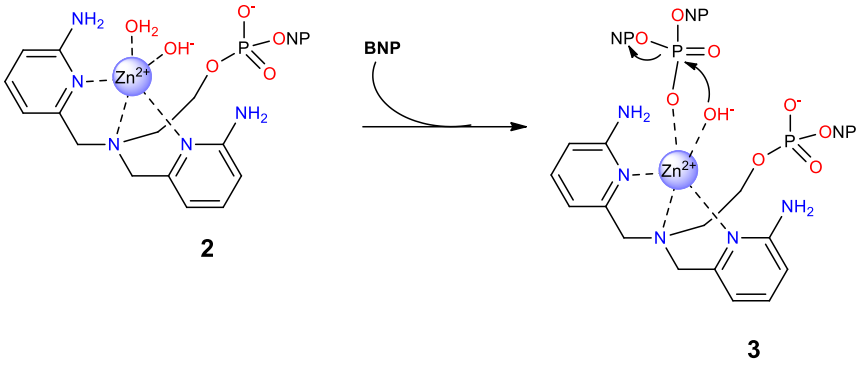

Fig.5.6.

On the contrary, working with an excess of the catalyst Zn(**5g**) resulted in two equivalents of PNP released from one BNP molecule (*Fig. 5.7.*). Since no more BNP was added, the only source of the second *p*-nitrophenoxide must be the hydrolysis of the phosphorylated hydroxopropyl arm.

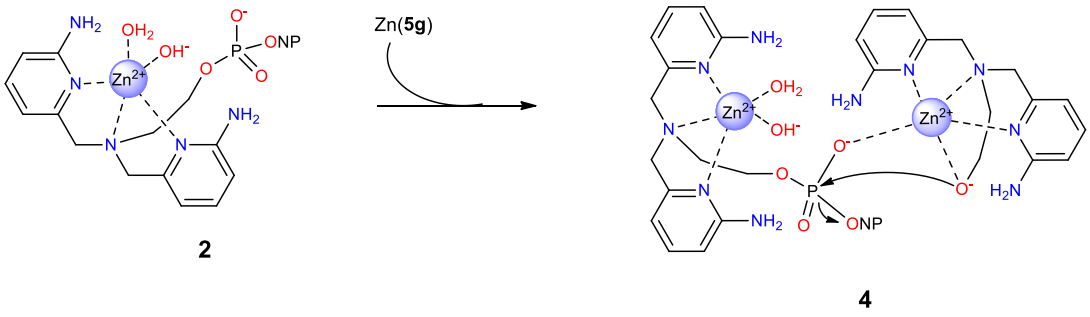

Fig.5.7.

Based on the previous studies, the BNP cleavage in excess of Zn(**5g**) could be hydrolysis of the phosphorylated hydroxypropyl arm by a second Zn(II)-bound alkoxide, followed by formation of a dimer (**5g** complexes linked by a phosphate bridge).

As already mentioned, Nature often relies on two or more metal ions in enzyme active sites, to enhance the effectiveness of phosphodiester cleavage. The cooperative action of metal ions in BNP cleavage was first explored in 1995 by Breslow and Chapman.[19] Since then, scientists have been utilizing bimetallic functionality to create even more efficient artificial nucleases.

To better understand the role of metal alkoxide- and metal hydroxide-containing models in phosphodiester cleavage, Guo *et al.* studied the efficiency of bimetallic Zn(II) complexes of phenolate ligands decorated with two pyridylmethyl amine moieties and hydroxylethyl arms (**5i**) in BNP cleavage (*Fig. 5.8.*).[20]

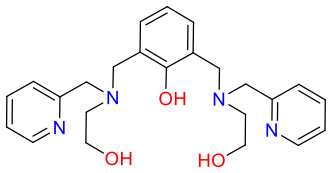

5i

Fig.5.8.

Potentiometric studies of Zn_2(**5i**) revealed two relevant p*K*a values, 7.2 and 8.1. The former one was ascribed to deprotonation of alcoholic hydroxyl, whereas the latter to deprotonation of a zinc-coordinated water molecule. Furthermore, the pH-dependent cleavage of BNP displayed a sigmoidal profile with a turning point at p*K*a 7.1, what strongly suggests that the alcoholic hydroxyl may be the active species responsible for the hydrolysis. Accordingly, the mechanism of BNP cleavage by Zn_2(**5i**) proposed by the authors involves the phosphodiester coordination to two metal ions linked by a phenolate bridge, followed by attack of the deprotonated alcoholic hydroxyl on the phosphorus centre. The established catalytic constant k_{cat} = 4.6 x 10^{-6} s^{-1} at pH 7.2 and 50°C for Zn_2(**5i**) means a 10^5-fold acceleration of the spontaneous cleavage of BNP.

In terms of BNP cleavage by AuNPs, just two examples have been reported so far. In 2008 Scrimin *et al.* presented functionalized gold nanoparticles coated with thiols bearing bis-(2-amino-pyridinyl-6-methyl)amine (BAPA) derivatives complexed with zinc (*Fig. 5.9.*).[21] Due to the presence of primary amino groups and pyridinyl moieties complexed with the metal ion, the system was combining both, H-bond donors and Lewis acid activation. To increase water solubility, a thiol bearing a tri(ethyleneglycol) unit was also introduced by thiol-exchange technique. In particular, two different nanoparticles compositions were created bearing a different ratio of thiol (**5j**) and (**5k**) (1:9 and 4:6).

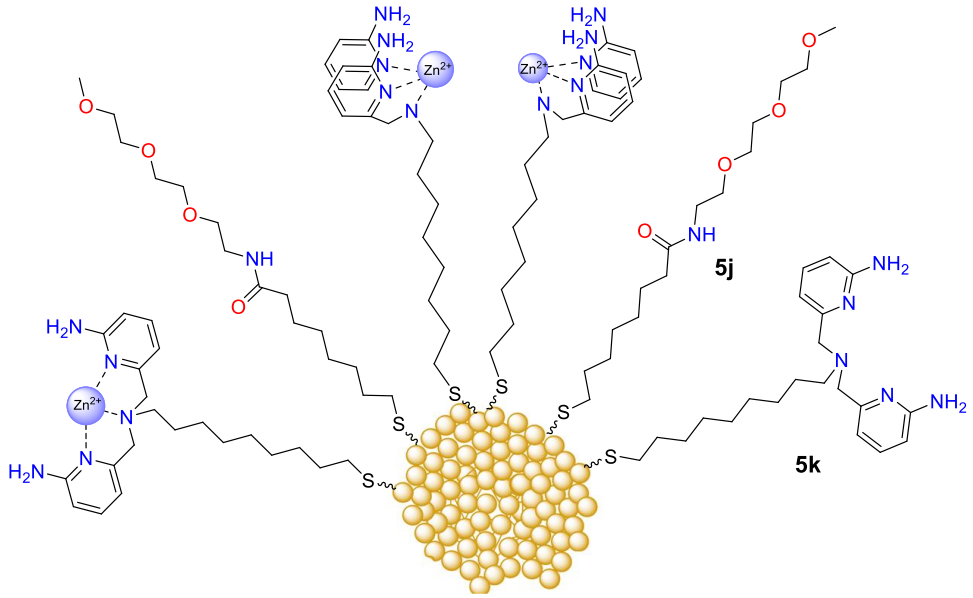

Fig.5.9.

Zn(II) titration for both nanozymes at pH 8.0 revealed an interesting behaviour of the catalytic species. After addition of one equivalent of zinc, the reactivity immediately reached a plateau, meaning full binding of the metal ion to the catalytic unit. Moreover, the authors observed a non-monotonic increase of the reaction rate toward saturation, that was attributed to the presence of two spontaneously formed active species (mono- and bimetallic), dependent on the metal ion loading. Additionally, the impact of pH

on the catalytic efficiency of BNP cleavage was studied. It was noticed with nanozymes bearing a higher percentage of thiol (**5k**), that the pH influence was relatively small in the interval 7.0-9.5, indicating the formation of relevant nucleophilic species under these conditions.

The studied inhibition with dimethyl phosphate established that a great part of the catalytic efficiency of BAPA-decorated AuNPs was due to enhanced binding and a relevant hydrophobic contribution. At pH 8.0 and 40°C, Zn(II)-BAPA decorated nanoparticles cleaved BNP from 62000 to 58000 times faster compared to the background reaction ($k_2 = 1.4$ s^{-1} x M^{-1}), being the most efficient Zn(II)-based catalyst for BNP cleavage reported so far.

One year later the same group proposed another system for BNP cleavage, this time based on gold nanoparticles complexed with cerium (*Fig. 5.10.*).[22] The reason behind the use of this particular metal ion was not accidental; cerium is known for its ability to form a stable tetravalent oxidation state. However, it is able to cleave DNA without any oxidative mechanisms.[23], [24] Furthermore, it has fast ligand exchange and a high coordination number (up to 12). Ce(IV) itself can reduce the half-life of DNA from millions of years to a few hours and it forms hydroxopolymers and hydroxoxomplexes below pH 4.0;[25] above this pH it precipitates as cerium hydroxide, forming a gel. Even though some lanthanide gels are extremely reactive towards the cleavage of phosphodiester bonds, their reproducibility and characterisation are rather poor.[25], [26]

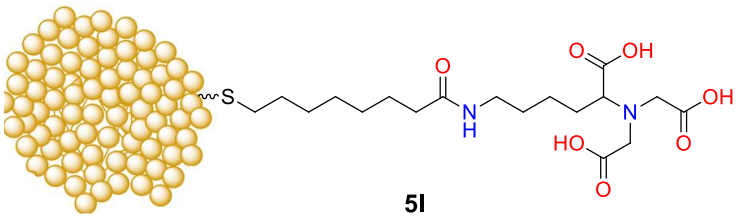

Fig.5.10

In order to obtain a more stable system, Ce(IV) was complexed on a surface of gold nanoparticles bearing a tetradentate polycarboxylate ligand (**5l**). The sigmoidal shape upon Ce(IV) titration in the presence of BNP reflects the highest reactivity of the system once all ligands are fully complexed with the metal ion. The sigmoidal trend also indicates the cooperativity of more than one metal species. Additional confirmation by Michaelis-Menten kinetics, revealed a saturation profile. However, comparing calculated k_2 values for BNP cleavage catalysed by Ce(**5l**) with its cleavage by the aqueous cerium salt $Ce(NH_4)_2(NO_3)_6$ (0.3 vs. 1.6 s^{-1} x M^{-1} at 25°C), it is clear that the AuNP-based system was less reactive than uncomplexed Ce(IV). Nevertheless, nanoparticles complexed with cerium were still much more efficient in BNP cleavage than their zinc counterparts.

b) Plasmid DNA

Even though commonly used bis-*para*-nitrophenyl phosphate as a DNA model substrate has many advantages, it does not reflect a realistic behaviour of the nucleic acid towards nucleophilic attack. Supercoiled plasmid DNA, found in bacterial cells, appears to be a more reliable candidate.[27]

One single strand scission transforms the supercoiled DNA (form I) to a nicked form (relaxed circular, form II), while a second cut on the complementary strand (within a limited number of nucleobases) produces a linear DNA (form III, *Fig.5.11.*).[28] All forms can be separated by gel electrophoresis, which is a commonly used technique for rapid kinetic analysis and studies of nucleic acid cleavage.

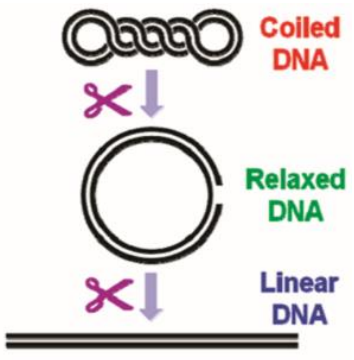

Fig.5.11.

As previously mentioned, an oxidative pathway of DNA cleavage may occur due to the presence of metal ions capable of redox chemistry. Additionally, most of the enzymes rely on Lewis acid metals in phosphoryl transfer reactions. However, Nature presents us with a few exceptions. Some of the nucleases base their efficiency on simply the presence of amino acids in their active site. Human DNA Topoisomerase I for instance, activates the phosphodiester groups of DNA by electrostatic interactions of two arginine residues, whereas the cleavage occurs by nucleophilic attack of tyrosine's hydroxyl group.[29] In the case of Staphylococcal nuclease (SNase), the guanidinium functionality imparts over 10^{16}-fold rate enhancement for DNA hydrolysis.[30]

The idea of metal-free cleaving reagents possessing both guanidinium and hydroxyl groups, has been reported by Göbel and Xu independently (*Fig.5.12.*).[31], [32] The former one presented guanidinium alcohols bearing a naphthol derivative (**5m**, **5n**), whereas the latter author depicted the activity of 1,4,7-triazacyclononane containing guanidino-ethyl and hydroxyethyl side arms (**5o**). All catalysts were tested towards the hydrolysis of the pUC19 plasmid DNA.

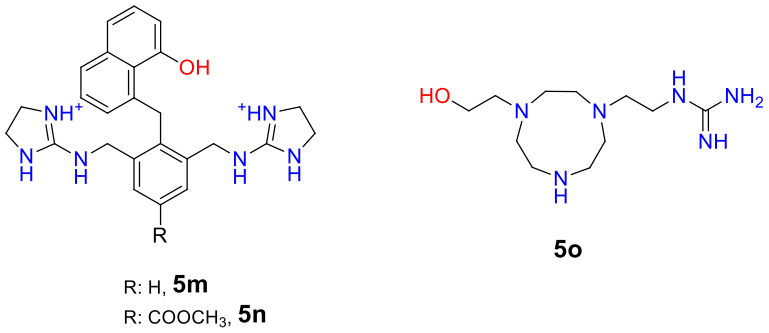

Fig.5.12.

After a 20-hour incubation at 37°C and pH 7.0, 10 mM of either (**5m**) or (**5n**) converted roughly 40% of pUC19 into its open-circular form II. At the same time, no linear form was observed. An additional experiment using the presence of EDTA proved that the

efficiency of both ligands were independent of metal ions. As the authors claimed, the pathway of pUC19 hydrolysis could result from different mechanisms, the most probable one, however, was the nucleophilic substitution at the phosphorus atom.

The reactivity of structurally simpler ligand (**5o**) surpasses (**5m, 5n**). 18-hour incubation with pUC19 at 37°C, pH 7.2 and 0.14 mM concentration gave formation of both, nicked and linear forms of DNA. The established first-order rate constant ($k_{max} = 0.16$ h^{-1}) meant a 10^7-fold rate acceleration over uncatalyzed hydrolysis of double-stranded DNA. Interestingly, the non-guanidinium equivalent of (**5o**) was just 2.5 times slower and had almost 2 times weaker affinity to the substrate.

Surprisingly enough, the reactivity of Zn(II) complex of (**5o**), studied under the same conditions, was lower than for its non-metallic counterpart. The justification of such behaviour is twofold. Firstly, the cleavage of DNA may be inhibited due to formation of the Zn(II)-bound complex with the guanidinium functionality (which was previously noticed by Kimura *et al*.).[33] Secondly, the additional pH-dependent studies revealed a different behaviour of the (**5o**) and Zn(**5o**) catalysts. The comparison of both first-order rate constants at pH 6.0 under the same conditions showed a 10-times higher efficiency in the plasmid cleavage for the metal complex. Referring again to Kimura's studies, the authors claimed that since the guanidinium group does not bind zinc at weakly acidic conditions, it may promote the phosphodiester cleavage at pH 6.0 by electrostatic interaction. Moreover, also (**5o**) hydroxide may benefit from the presence of Zn(II) due to its decreased p*K*a and thus, increased nucleophilic activity.

Based on Burstyn's pioneering studies which depicted the reactivity of the Cu(II)-TACN complex in phosphodiester cleavage, Spiccia *et al*. reported the efficiency of two artificial metallonucleases, based on Cu(II)-TACN complexes, featuring additional pairs of ethyl- or propyl-guanidinium pendants, in pBR322 plasmid DNA cleavage (*Figure 5.13*.). [34], [35]

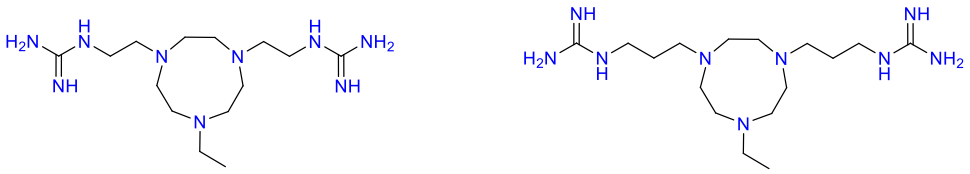

5p **5u**

Fig.5.13.

Excess of the copper (II) complex of either (**5p**) or (**5u**) (150 μM) was incubated with plasmid DNA (39 μM) for 24 hours at 37°C and pH 7.0. Both catalysts were able to convert between 60-75% of the initial supercoiled form I into the open-circular form II, where Cu(**5u**) showed a slightly higher reactivity than Cu(**5p**). The doubly nicked linear form was not observed. Moreover, additional experiments confirmed that there was no observed reactivity of non-metalated (**5p**)/(**5u**) ligands or $CuCl_2$ in plasmid cleavage. Therefore, the catalytic activity in DNA hydrolysis came exclusively from the metal complexes.

As a control, the cleavage of pBR322 by the $[Cu(TACN)(OH_2)_2]^{2+}$ complex was performed under the same conditions. It yielded 40% conversion of the form I to II, showing a similar result as Cu(**5p**) and a slightly lower reactivity than for Cu(**5u**). Such a modest performance of (**5p**) and (**5u**) complexes may be due to unfavourable steric interactions of both catalysts with the double-helix structure, which excludes a potential positive contribution from the guanidinium group.

pH-profiles revealed a bell-shaped trend with the highest activity at pH 7.0 for both catalysts. That pH not only allows the guanidinium functionality to maintain its positive charge, but also allows the metal-bound hydroxide to play the role of nucleophile. At the same time, it is possible that at pH 7.0 the guanidinium group is bound to the metal ion or it is likely responsible for the competitive binding, what could explain a relatively modest performance of Cu(**5p**) and Cu(**5u**). Upon comparison with similar systems bearing two guanidinium groups (on more rigid,

aromatic scaffolds), Cu(**5p**) and Cu(**5u**) have either a significantly lower or relatively similar activity towards plasmid DNA cleavage.[36], [37], [38]

Taking into consideration previous studies and reported literature examples, the same group presented a new strategy, which was aimed at improving the already proposed Cu(II)-TACN complexes bearing a guanidinium moiety.[28] Since the most reactive species towards phosphodiester cleavage were based at that time on the more rigid pendants (preventing from the coordination of guanidine to the copper (II) centre and reducing the competition of phosphate binding between the copper(II) and guanidinium moiety), a single pendant seemed to be more preferable due to lack of unfavourable steric interactions. The authors designed three new copper(II) based complexes featuring *o*-, *m*- and *p*-xylylguanidine pendant groups (*Fig. 5.14.*, **5r-5t**)

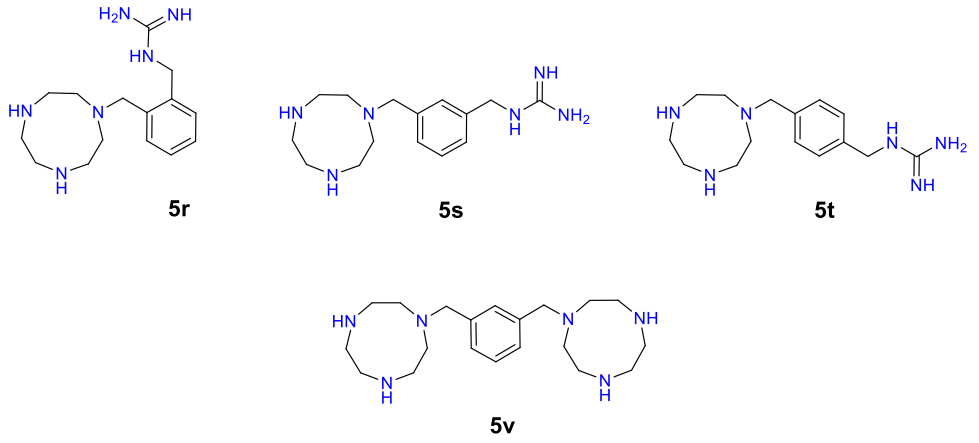

Fig.5.14.

To elucidate the character of plasmid DNA catalyst interaction, CD spectroscopy studies were performed. This technique is useful in monitoring changes in DNA conformation in solution and may provide some information about the binding interactions with nucleic acids. For the copper(II) complexes of (**5r**-**5t**) a substantial degree of distortion of the initial DNA structure was observed, whereas for Cu(**5r**)

these were slightly smaller. In summary, all catalysts gave electrostatic interactions with DNA and an effect on the nucleic acid conformation.

The reactivity of Cu(**5r-5t**) complexes was assessed by incubating them with the plasmid DNA pBR322 at 37°C, pH 7.0 (catalyst concentration was equal to 150 μM). In all cases a conversion of form I to form II was observed and, in addition, form III for the catalyst Cu(**5r**). Comparing all complexes, Cu(**5r**) revealed a significantly higher reactivity, which can be explained by the greater acidity of its complex (p*K*a-s of metal complexes of **5r** = 6.4, **5s-5t** = 7.0), promoting the deprotonation of a metal-coordinated water molecule acting as a nucleophile. The rate constant of Cu(**5r**) is almost 3-4 times higher than Cu(**5s-5t**), making it one of the most attractive catalysts reported so far for the plasmid DNA cleavage.

It is also worth analysing the reactivity of a bimetallic analogue of (**5r**) deprived of the guanidinium group. Akkaya *et al*. reported the aromatic complex (*Figure 5.14*., **5v**) bearing two *m*-TACN units complexed with Zn(II).[39] Its reactivity was studied towards the hydrolysis of pKSHT plasmid DNA (incubated for 24 hours at pH 7.5 and 50°C with a 5 mM Zn_2(**5v**)). Both nicked and linear forms were detected and the calculated rate constant (2.3 x 10^{-5} h^{-1}) meant a million-fold acceleration over uncatalyzed hydrolysis rate of DNA. Since Cu(**5r**) and Zn_2(**5v**) reactivity was studied at different conditions and substrates, their direct comparison is relatively difficult. However, both of these metal-based catalysts revealed a great efficiency in plasmid cleavage, showing that both, mono- and bimetallic systems, if carefully designed, may both be equally very active.

Another interesting example of mono and binuclear catalysts for phosphodiester cleavage was reported by Scrimin *et al.* (*Fig.5.15*.).[40] Design of the platforms (**5w**-**5z**) was based on a peptide backbone: the bimetallic system was represented by two heptapeptides bearing two TACN units and either the acetyl group protecting the *N*-terminus (**5w**) of the peptide or an acridine intercalating moiety (**5x**). The monometallic pentapeptide-based catalyst possesses one TACN unit and the acridine

functionality (**5y**). As a comparison, simple monometallic TACN-based catalysts were also provided (**5a'-5b'**).

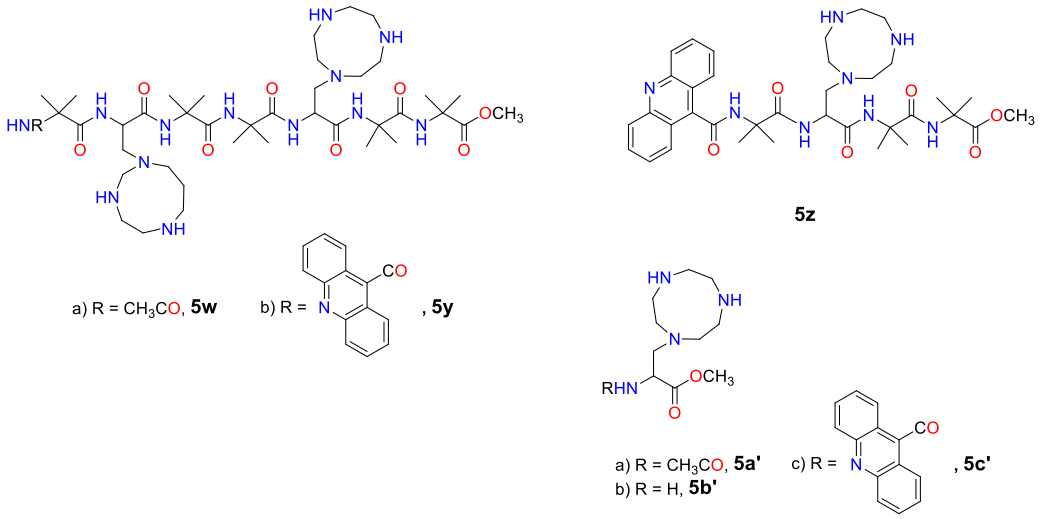

Fig.5.15.

The incubation of Zn(II) complexes of (**5w-5y**) with pBR322 plasmid DNA for 24 hours at 37°C and pH 7.0 gave a conversion of the supercoiled form I into both, nicked and linear forms (II and III, respectively). The implementation of the intercalating agent, known for its strong interaction with nucleic acids, did not result in a major change of reactivity. Working with lower concentrations, Zn_2(**5y**) was found to be more efficient than Zn_2(**5w**) and, on the other hand, slightly less efficient when its concentration was substantially increased. A possible explanation of such behaviour provided by the authors was a strong binding with DNA at low Zn_2(**5y**) concentration (via phosphate-metal ion interactions and additional intercalation of the acridine ring) and the formation of peptide dimers or larger aggregates at higher Zn_2(**5y**) concentrations. The importance of the substrate affinity in the catalytic performance was additionally supported by the results of pBR322 cleavage by Zn(**5a'-5c'**) - the most efficient complex in the plasmid hydrolysis there was Zn(**5c'**) with the acridine ring.

Comparison of the reactivity of Zn_2(**5y**) and Zn_2(**5z**) reveals a more efficient performance with bimetallic system in plasmid cleavage. Indeed, the measured rate constant for Zn_2(**5y**) indicated 10 million-fold rate acceleration over the uncatalyzed DNA hydrolysis. Remarkably, when just 3.5 μM of the Zn_2(**5y**) complex was needed to cleave 50% of form I of the plasmid, while with Zn(**5a'**) 80 μM was needed to achieve the same result under similar conditions. Based on additional kinetic studies, the authors related the catalytic success of Zn_2(**5y**) to the strong binding of Zn(II) to TACN, a decreased p*K*$_a$ of the zinc-bound water molecule playing the role of a nucleophile and to the spatial positioning of two Zn(II)-TACN functionalities. It was found that the peptide was folded in the 3_{10}-helical conformation, and thus two TACN units were able to face each other allowing for the accommodation and interaction with the phosphate substrate and the formation of a bimetallic system.

The last literature example is the aforementioned supramolecular scaffold AuNP Zn(**5k**), which appeared to cleave efficiently not only BNP, but also plasmid DNA.[21] Incubation of pBR322 for 24 hours at 37°C and pH 7.0 with 15 μM of AuNPs Zn(**5k**) yielded the rate constant 2×10^{-6} s^{-1}, thus 5-fold acceleration over uncatalyzed DNA hydrolysis. Even though it is not the most efficient reported catalyst, it is intriguing that the cleavage with AuNPs Zn(**5k**) resulted a higher amount (approximately 50% higher) of linear DNA than its nicked form. This behaviour is relatively common for enzymes, but not for artificial nucleases. Considering that the composition of the monolayer enabled just a fraction of the active bimetallic complexes to interact with the plasmid DNA (due to geometric reasons), the catalytic performance of these gold nanoparticles builds a strong foundation for further improvement of supramolecular scaffolds toward the efficient cleavage of plasmid DNA.

*2. BNP Cleavage by **AuNP1-4**. The Michaelis-Menten and pH-dependent Profiles.*

Following the very promising results of HPNP hydrolysis by studied nanoparticles, it was important to explore their efficiency with more challenging nucleic acid model substrates, i.e. bis-*para*-nitrophenyl phosphate. Due to the lack of a hydroxyl group (like in HPNP), an artificial nuclease designed for the cleavage of BNP should be able not only to provide a nucleophile, but also activate the substrate itself. As already mentioned, all presented gold nanoparticles possess Zn(II)-bound water molecules and additionally –OH-serine groups in the case of **AuNP4**, which can attack the phosphorus atom; furthermore, the presence of H-bond donors and zinc as the Lewis-acid may serve to activate both, electrophile and nucleophile.

Firstly, 1.0 x 10^{-5} M **AuNP1-4** were incubated with increasing amount of bis-*para*-nitrophenyl phosphate for 24 hours at pH 8.0 and 40°C. In almost all cases, precipitation of gold nanoparticles was observed, apart from at the lowest titrated concentration of BNP (1.0 x 10^{-4} M). Accordingly, this concentration enabled a rough comparison of initial rates for four nanoparticles, presented in *Fig. 5.16.*

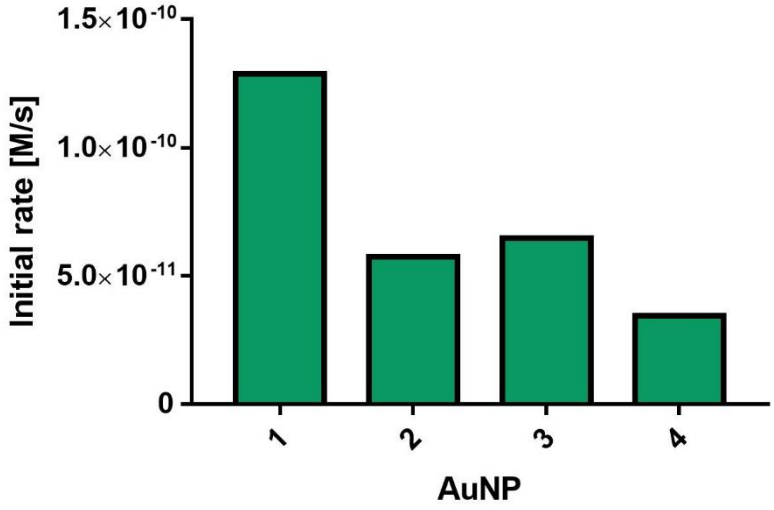

Fig.5.16. The initial rates of the cleavage of BNP by **AuNP1-4**. Conditions: [nanozyme] = 1.0 x 10^{-5} M, [BNP] = 1.0 x 10^{-4} M, [EPPS] = 1.0 x 10^{-2} M, pH = 8.0, T = 40°C in H_2O.

As in the cleavage of HPNP, the most efficient nanoparticles were **AuNP1** with the least effective being **AuNP4** (almost 4-times slower than **AuNP1**). In terms of nanoparticles **2** and **3**, they revealed at these particular conditions a surprisingly high reactivity, acting only two times less efficiently than may have been caused by the neutralization of the charged nanoparticles, the next studies were performed at 3-times higher concentration of AuNPs (3.0×10^{-5} M). These conditions enabled for the full investigation of BNP hydrolysis by **AuNP1-3**. Therefore, Zn(II)-titration (*Fig. 5.17.*) and Michaelis-Menten-like kinetics (*Fig. 5.18*) (with calculated kinetic parameters (*Table 5.19.*)) were performed. Additionally, the pH-profile for the most active nanozyme in *Fig. 5.20.* was explored. In the case of **AuNP4** however, a precipitation was observed throughout the whole studied range of BNP concentrations, disabling further studies.

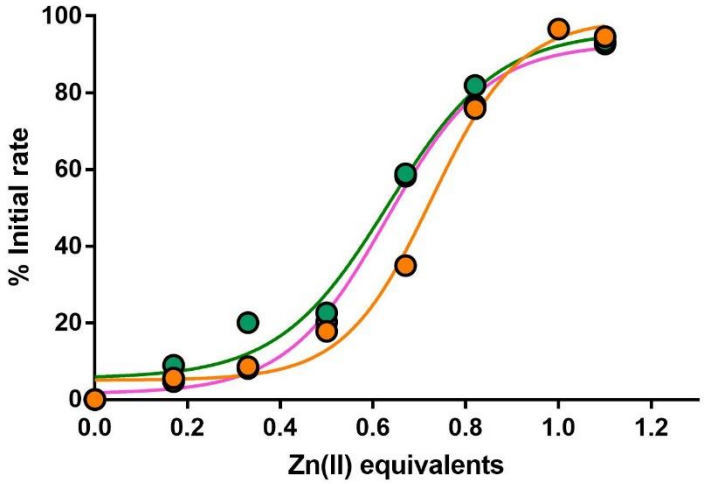

Fig.5.17. Zn(II) dependence in the cleavage of BNP by **AuNP1-3**.
Conditions: [nanozyme] = 3.0×10^{-5} M, [BNP] = 1.0×10^{-4} M, [EPPS] = 1.0×10^{-2} M, pH = 8.0, T = 40°C in H_2O.
Symbols code: **AuNP1** orange, **AuNP2** green, **AuNP3** pink.

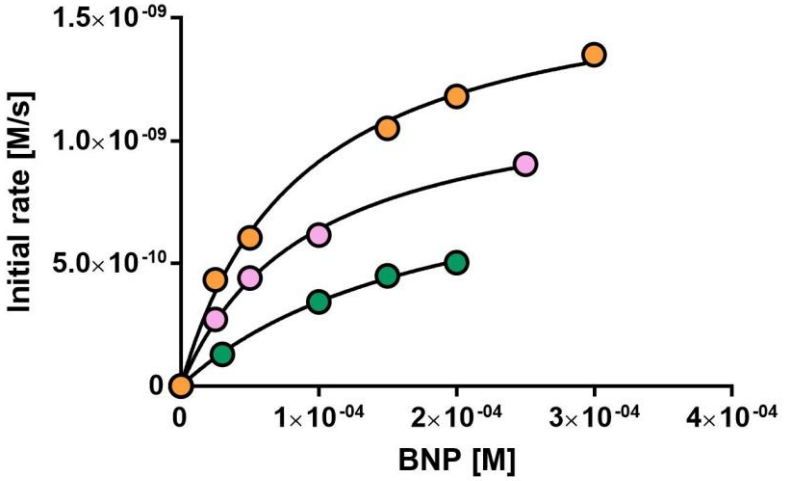

Catalyst	k_{cat} [s^{-1}]	k_2 [l×mol^{-1}×s^{-1}]	K_M [mM]	[a] k_{rel}
AuNP1	1.1 x 10^{-4}	1.3	8.6 x 10^{-2}	7.1 x 10^{6}
AuNP2	6.6 x 10^{-5}	0.35	1.9 x 10^{-1}	4.2 x 10^{6}
AuNP3	8.2 x 10^{-5}	0.89	9.3 x 10^{-2}	5.1 x 10^{6}

Fig. 5.18. Table 5.19. Michaelis-Menten kinetic studies on the cleavage of BNP by **AuNP1-3** and calculated kinetic parameters. Conditions: [nanozyme] = 3.0 x 10^{-5} M, [EPPS] = 1.0 x 10^{-2} M, pH = 8.0, T = 40°C in H_2O.

[a] $k_{rel} = \frac{k_{cat}}{k_{uncat}}$, $k_{uncat} = 1.6\ x\ 10^{-11}\ s^{-1}$.[13]

Symbols code: **AuNP1** orange, **AuNP2** green, **AuNP3** pink.

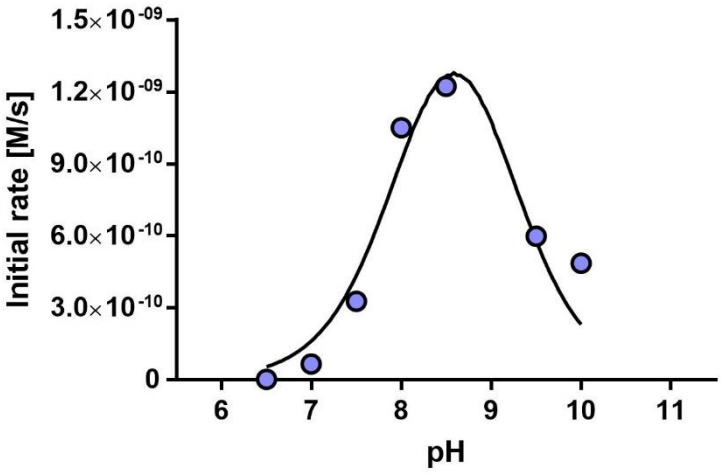

Fig. 5.20. The function of initial rate *vs* pH of the hydrolysis BNP by **AuNP1.**
Conditions: [**AuNP1**] = 3.0 x 10^{-3} M, [BNP] = 1.5 x 10^{-4} M, [buffers] = 1.0 x 10^{-2} M, T = 40°C in H_2O.
Data fitted with the equation: $v_\varphi = \frac{v_{max}}{\frac{[H^+]}{K_a^1}+1+\frac{K_a^2}{[H^+]}}$.

All studied nanoparticles were able to accelerate the hydrolysis of BNP from 4- up to 7- 10^7 times compared to uncatalysed reaction, which makes **AuNP1-3** the most active artificial nucleases in BNP hydrolysis reported thus far. They reveal a fairly similar affinity to the studied DNA model (c.a. 0.1 mM), and the second-order rate constant (0.35 – 1.3 l x mol^{-1} x s^{-1}), which may suggest a relatively similar mechanism for their catalytic performance. Zn(II)-dependent kinetic experiments revealed a sigmoidal profile, as for the case of HPNP cleavage by **AuNP1-3** (*Chapter 4*, *Fig.4.13*.). Thus, at low zinc loading monometallic complexes are formed first, and full catalytic efficiency is observed once all TACN units are complexed with zinc, creating bimetallic units. Therefore, the concentrations of **AuNP1-3** were normalized accordingly to two metal ion system present within the catalytic site.

Additional studies of pH-dependent kinetics revealed a bell-shape-like profile suggestive of two critical p*Ka* values, 8.1 and 9.1 (*Fig.5.20.*). The catalysis occurring at neutral conditions is much slower than under basic conditions, indicating the importance of the first deprotonation, which is likely to be activation of the nucleophile (a zinc bound water molecule). The second deprotonation, as in case of HPNP, can mean a saturation of the coordination sphere of the metal, therefore blocking additional interaction with the substrate.

*3. pBR322 Plasmid DNA cleavage by **AuNP1-5**.*

*a) The First Screening – Incubation of pBR322 plasmid DNA with **AuNP1-5**.*

The ability of AuNPs to cleave DNA was assessed by incubating them with pBR322 plasmid DNA at 37°C for 24 hours with and without Zn(II) as a control (*Fig. 5.21*). Conversion of the supercoiled form I to the relaxed circular form II was monitored by agarose gel electrophoresis and subsequently quantified (the agarose gel pictures: see *Chapter 7*, *E.32*.).

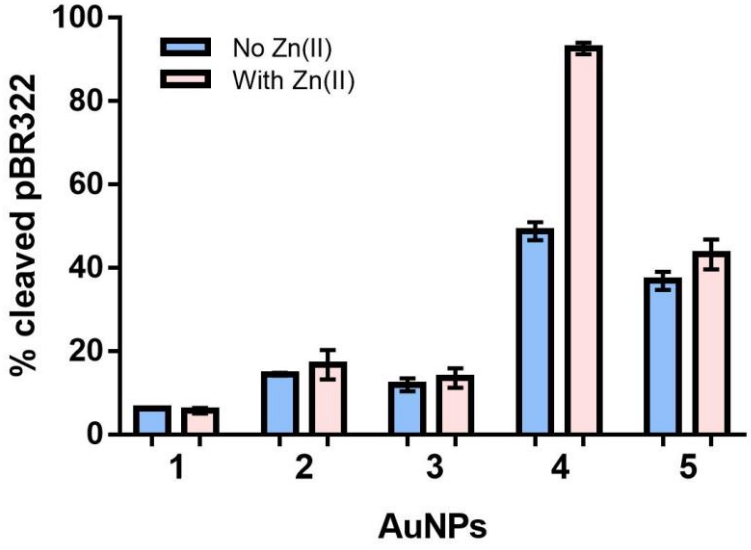

Fig. 5.21. Percentage of plasmid cleavage after 24-hour incubation with **AuNP1-5**.
Conditions: [nanozyme] = 45 μM, [pBR322 DNA] = 19.3 μM/bp, [HEPES] = 20 mM, 37°C, pH 7.5 in H_2O.

A massive decrease in the intensity of the band due to form I after 24-hour incubation with **AuNP4** was accompanied by the appearance and intensification of a band corresponding to form II. Surprisingly, 50% of the hydrolytic activity could be associated to **AuNP4** without any metal ion. An intriguing result was found with **AuNP5,** both with and without Zn(II). The results revealed 40-50% of catalytic efficiency in the cleavage of plasmid DNA, in both cases. In terms of the rest of studied nanoparticles, they showed a fairly modest efficiency in pBR322 cleavage, contrary to the previously established results of BNP cleavage.

*b) Concentration, Time and pH-dependence of pBR322 Cleavage by **AuNP4**.*

In order to fully investigate the efficiency of **AuNP4**, the plasmid DNA was firstly incubated with nanozymes **4** for 1 hour (*Fig. 5.22.*; the agarose gel picture: see *Chapter 7*, *E.33.*) Since the minimal studied concentration of **AuNP4** enabling for the best catalytic performance was 35 μM, that concentration was up-taken as the optimum. Moreover, the observed linear tendency is in accordance with a greater amount of phosphate-nanoparticle interactions upon **AuNP4** titration, yielding the increase of catalytic efficiency.

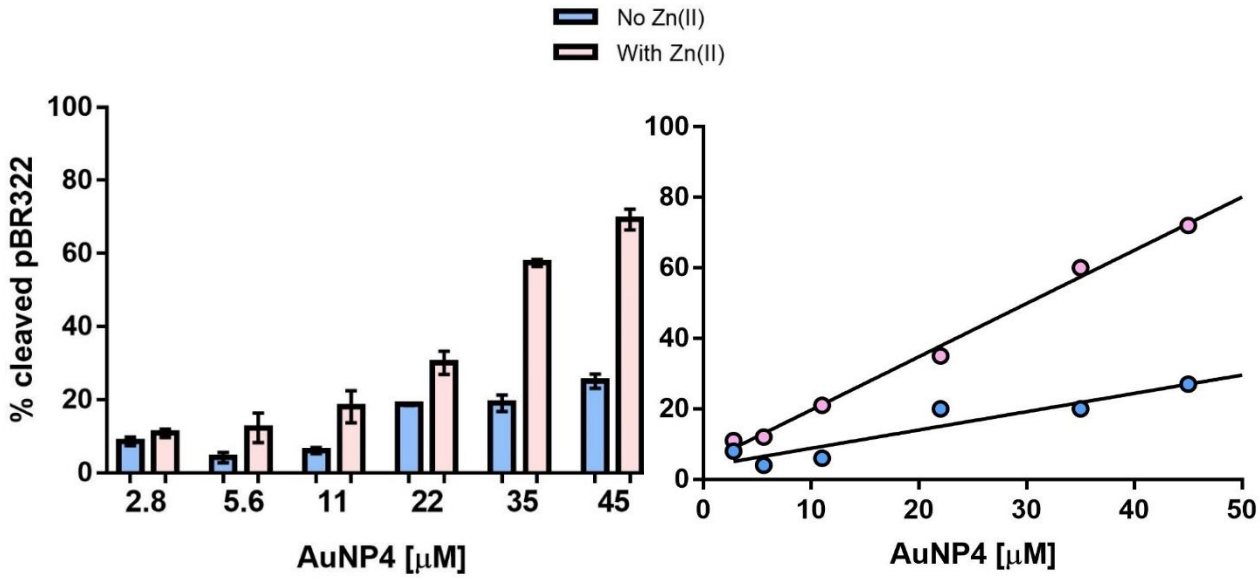

Fig. 5.22. The percentage of plasmid cleavage by **AuNP4** after 1-hour incubation. Conditions: [pBR322 DNA] = 19.3 μM/bp, [HEPES] = 20 mM, 37°C, pH 7.5 in H_2O.

Afterwards, pH- and time-dependent kinetics were collected (*Fig. 5.23.*). The former studies revealed that the highest efficiency of **AuNP4** was at pH 6.5-7.5. Interestingly, the plasmid DNA cleavage was more effective in a wider pH range when compared to BNP. In terms of time dependence, the plateau was reached after a 3-hour incubation with 35 μM of nanoparticles, meaning that the half-life of pBR322 plasmid DNA upon **AuNP4** cleavage is ca. 1.5 hours. In all the cases, mostly the formation of the open-circular plasmid DNA (form II) was observed.

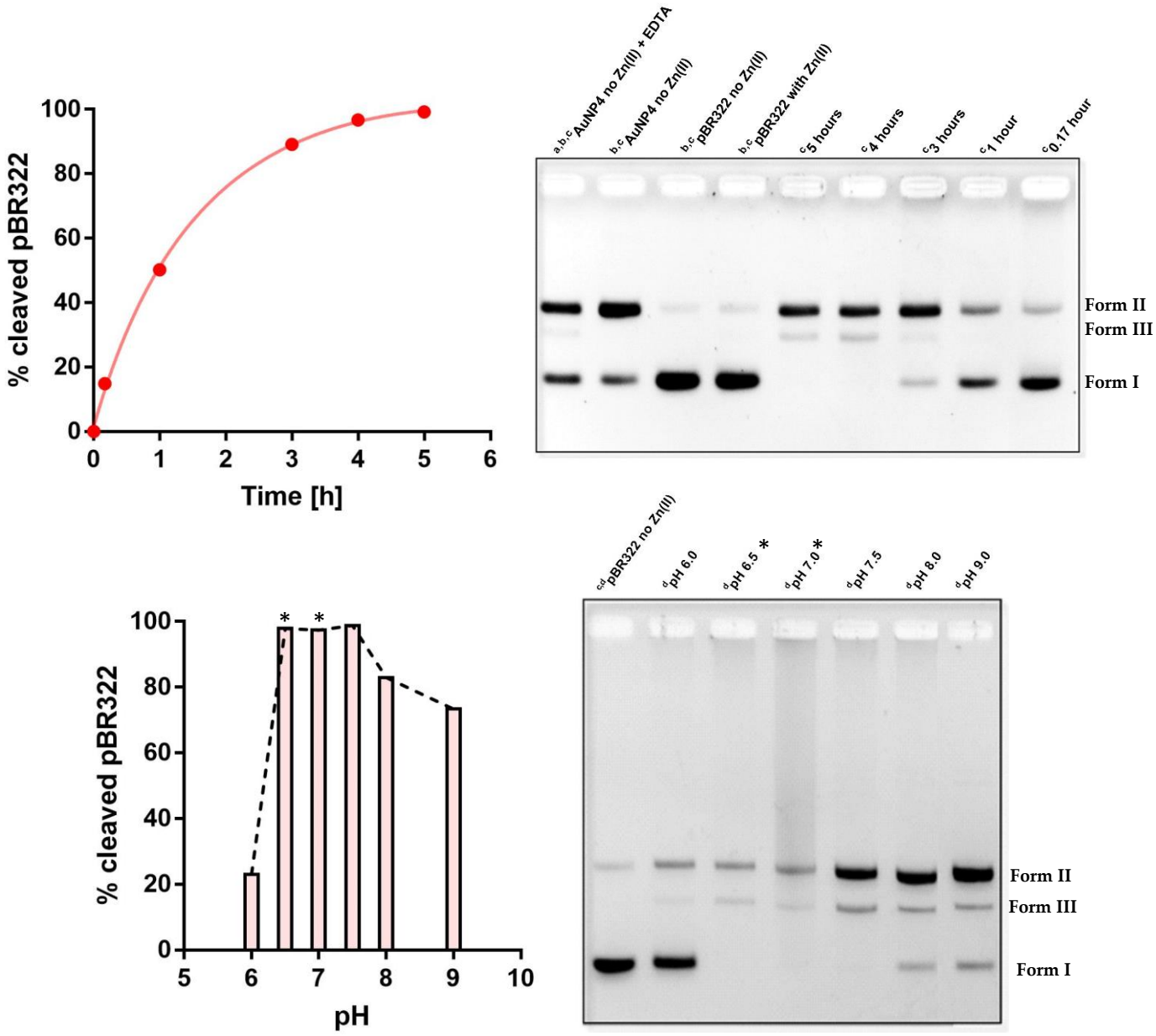

Fig. 5.23. Agarose gels electrophoresis and their quantification upon time (upper) and pH (lower) dependent kinetics of pBR322 DNA cleavage by **AuNP4**. Conditions: [nanozyme] = 35 μM, [pBR322 DNA] = 19.3 μM/bp, [buffers] = 20 mM, 37°C in H_2O.

[a]12.5 μM EDTA, [b]5-hour incubation, [c]pH 7.5, [d]3.5-hour incubation.

*Note: Bands at pH 6.5 and 7.0 turned out to be weaker compared to remaining bands, which may indicate a partial loss of plasmid DNA, possibly due to precipitation. Therefore, estimated %cleaved pBR322 are compromised and based on eventually obtained bands.

Since substantial cleavage of pBR322 was observed without Zn(II) (see Fig.*5.21-5.22.*), an additional control was performed in the presence of EDTA to exclude any metal ions present in the **AuNP4** stock solution before complexation with Zn(II) (*Fig.5.23.*,

upper agarose gel picture). The obtained result indicated that **AuNP4** uncomplexed with zinc is indeed able to partially cleave plasmid DNA.

*c) Zn(II)-dependent Kinetics of pBR322 Cleavage by **AuNP4**.*

In order to explore the nature of the Zn(II)-TACN complex in plasmid DNA cleavage, pBR322 was incubated for 3 hours at pH 7.5 and 37°C with **AuNP4**, complexed with an increasing concentration of zinc ions (*Fig. 5.24.*).

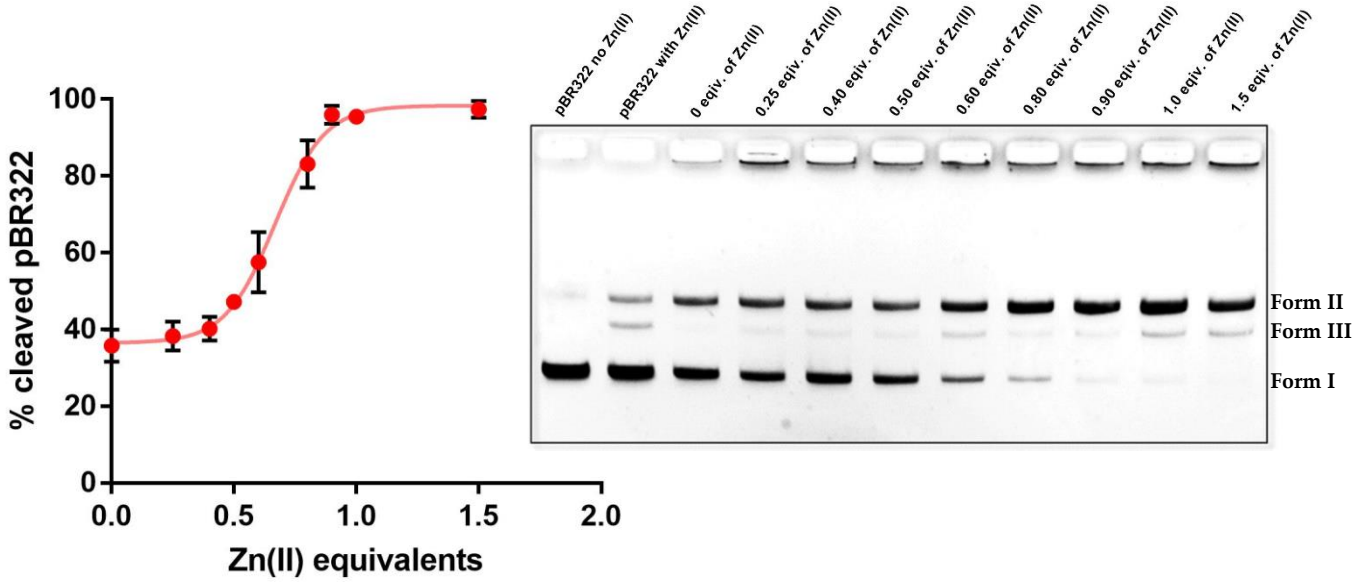

Fig. 5.24. Agarose gel electrophoresis and its quantification upon Zn(II)-dependent kinetics of pBR322 DNA cleavage by **AuNP4**. Conditions: [nanozyme] = 35 μM, [pBR322 DNA] = 19.3 μM/bp, [HPNP] = 20 mM, 3 hours, pH 7.5, 37°C in H_2O.

The Zn(II) titration gave a sigmoidal shape profile, indicating a bimetallic catalysis and showing the greatest efficiency once all TACN were complexed with the metal ion. As experienced with the previous studies, **AuNP4** deprived of Zn(II) approached almost 40% of a single cleavage of pBR322 after 3-hour incubation. Nevertheless, the supercoiled plasmid DNA was fully converted into its nicked form only in the presence of Zn(II) complexing all TACN units.

4. ***AuNP6*** *– Synthesis and Reactivity Towards the Cleavage of pBR322.*

Since **AuNP4** are decorated with a peptide possessing two serine moieties, the cleavage activity may be the result of the nucleophilic properties of the serine hydroxyl groups. As mentioned before, natural nucleases do not always rely on the presence of metal ions in their active sites (for instance human DNA Topoisomerase I), utilizes the intrinsic properties of amino acids instead. Accordingly, to explore the catalytic efficiency of nanoparticles decorated with just the peptide part of **AuNP4**, the new nanozymes **AuNP6** were synthesized (*Fig. 5.25.*). Subsequently, the plasmid DNA was incubated with increasing concentrations **AuNP6**.

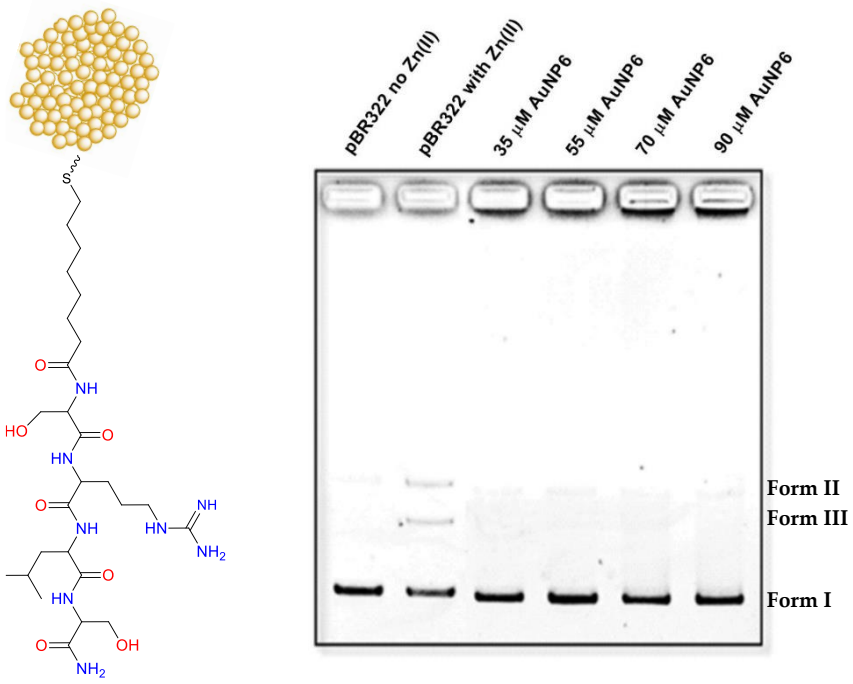

Fig. 5.25. The structure of **AuNP6** and agarose gel electrophoresis of pBR322 DNA after 3-hour incubation with **AuNP6**. Conditions: [pBR322 DNA] = 19.3 μM/bp, [HEPES] = 20 mM, 37°C, pH 7.5 in H_2O.

The final result showed a lack of hydrolytic reactivity of **AuNP6** even at very high concentrations. The observed phenomenon may be explained as the result of tight packing of peptide-based thiols constituting the monolayer of nanoparticles thus not leaving any room for a complex with plasmid DNA formation.

5. Concluding Remarks.

Among all studied nanozymes, only Y-shaped species decorated with peptide containing serine and arginine in its sequence (**AuNP4**) was able to efficiently convert the supercoiled DNA into its nicked form. Interestingly, in the hydrolysis of much simpler nucleic acids' models like HPNP or BNP, their reactivity was relatively modest comparing to other nanoparticles.

Additional studies such as concentration and time dependence demonstrated that **AuNP4** can cleave plasmid DNA in less than 3-4 hours at 35 μM concentration. In order to further understand the observed phenomenon, Zn(II)- and pH-dependent kinetics were subsequently performed. The latter revealed that the greatest efficiency in cleavage of pBR322 occurs in the range of pH 6.5-7.5, where the first deprotonation of Zn(II) coordinated water takes place and the guanidinium moiety still remains positively charged. Zn(II) titration gave a sigmoidal shape profile, indicating a bimetallic catalysis and showing the greatest efficiency once all TACN were complexed with Zn(II). To understand the catalytic importance of utilized peptides, **AuNP6**, being an equivalent to **AuNP4** but deprived of the aromatic connecting unit and TACN moiety, were synthesized. Incubation of the plasmid DNA with an increasing concentration of nanozymes **6** showed a lack of hydrolytic reactivity, even at very high concentrations.

Taking into account these studies, there are key factors making nanozymes efficient towards the hydrolysis of plasmid DNA. The maximum efficiency is observed when all TACN's are complexed with Zn(II), which one may consider as a proof that the most active species is bimetallic. However, bimetallic catalysis is not enough by itself in cleavage of plasmid DNA, since a very modest hydrolysis was observed for the remaining nanoparticles. It can be suggested that the observed maximum efficiency is due to the cooperativity between Lewis-acid properties of Zn(II) and arginine and serine present in the peptide. Furthermore, almost 50% cleavage with **AuNP4** could be observed without any metal ion which may be caused by the nucleophilic activity

of serine and strong interaction between arginine and phosphates. Arginine, present in natural nuclease active sites, may serve as a weak general acid and stabilize the transition state *via* hydrogen bonding to phosphates and/or electrostatic interaction.[41] However, arginine itself is not enough to ensure the catalytic efficiency – indeed, the comparison of **AuNP4** and **AuNP5** proves that the lack of serine on nanoparticles, with maintaining the presence of arginine, yielded much lower efficiency of plasmid cleavage.

The observed contrast in reactivity of nanoparticles in the cleavage of DNA model substrate and the real polymer may be elucidated on the basis of their structure. Bis-*para*-nitrophenyl phosphate possesses just one phosphate moiety and two good leaving groups, which departure does not need to be activated by a catalyst. The plasmid DNA, on the contrary is composed by thousands of phosphodiester units, which statistically increases the probability of a single cleavage. However, since it is built from nucleotides, the plasmid DNA is deprived of good leaving groups, making plasmid hydrolysis more challenging. The additional presence of the guanidinium group, being located just in front of Zn(II)-TACN complex, can probably yield a more efficient cooperation between Lewis acid and electrostatic interactions, which may be crucial in the case of multiple phosphodiesters linked together.

6. *References of Chapter 5.*

[1] Q. Jiang, N. Xiao, P. Shi, Y. Zhu, Z. Guo, *Coordination Chemistry Reviews* **2007**, *251*, 1951-1972.

[2] S. G. K.R, B. B. Mathew, C. N. Sudhamani, H. S. B. Naik, *Biomedicine and Biotechnology* **2014**, *2*, 1-9.

[3] C. Liu, L. Wang, *Dalton Transactions* **2009**, 227-239.

[4] S. Maynard, S. H. Schurman, C. Harboe, N. C. de Souza-Pinto, V. A. Bohr, *Carcinogenesis* **2009**, *30*, 2-10.

[5] D. S. Sigman, A. Mazumder, D. M. Perrin, *Chemical Reviews* **1993**, *93*, 2295-2316.

[6] J. C. Joyner, J. Reichfield, J. A. Cowan, *Journal of the American Chemical Society* **2011**, *133*, 15613-15626.

[7] P. U. Maheswari, S. Barends, S. Özalp-Yaman, P. de Hoog, H. Casellas, S. J. Teat, C. Massera, M. Lutz, A. L. Spek, G. P. van Wezel, P. Gamez, J. Reedijk, *Chemistry – A European Journal* **2007**, *13*, 5213-5222.

[8] S. A. Melnychuk, M.Sc. thesis, Queen's University (Canada) (Ann Arbor), **2008**.

[9] J. Kumamoto, J. R. Cox, F. H. Westheimer, *Journal of the American Chemical Society* **1956**, *78*, 4858-4860.

[10] P. C. Haake, F. H. Westheimer, *Journal of the American Chemical Society* **1961**, *83*, 1102-1109.

[11] C. A. Bunton, M. M. Mhala, K. G. Oldham, C. A. Vernon, *Journal of the Chemical Society (Resumed)* **1960**, 3293-3301.

[12] A. Radzicka, R. Wolfenden, *Science (New York, N.Y.)* **1995**, *267*, 90.

[13] J. Chin, M. Banaszczyk, V. Jubian, X. Zou, *Journal of the American Chemical Society* **1989**, *111*, 186-190.

[14] M. A. De Rosch, W. C. Trogler, *Inorganic Chemistry* **1990**, *29*, 2409-2416.

[15] T. Koike, E. Kimura, *Journal of the American Chemical Society* **1991**, *113*, 8935-8941.

[16] E. Kimura, Y. Kodama, T. Koike, M. Shiro, *Journal of the American Chemical Society* **1995**, *117*, 8304-8311.

[17] M. Livieri, F. Mancin, U. Tonellato, J. Chin, *Chemical Communications* **2004**, 2862-2863.

[18] M. Livieri, F. Mancin, G. Saielli, J. Chin, U. Tonellato, *Chemistry – A European Journal* **2007**, *13*, 2246-2256.

[19] W. H. Chapman, R. Breslow, *Journal of the American Chemical Society* **1995**, *117*, 5462-5469.

[20] J. Chen, X. Wang, Y. Zhu, J. Lin, X. Yang, Y. Li, Y. Lu, Z. Guo, *Inorganic Chemistry* **2005**, *44*, 3422-3430.

[21] R. Bonomi, F. Selvestrel, V. Lombardo, C. Sissi, S. Polizzi, F. Mancin, U. Tonellato, P. Scrimin, *Journal of the American Chemical Society* **2008**, *130*, 15744-15745.

[22] R. Bonomi, P. Scrimin, F. Mancin, *Organic & Biomolecular Chemistry* **2010**, *8*, 2622-2626.

[23] K. Makoto, S. Tetsuro, K. Teruyuki, T. Naoya, S. Jun, Y. Morio, **1994**, *23*, 1025-1028.

[24] M. Komiyama, N. Takeda, Y. Takahashi, H. Uchida, T. Shiiba, T. Kodama, M. Yashiro, *Journal of the Chemical Society, Perkin Transactions 2* **1995**, 269-274.

[25] M. Komiyama, N. Takeda, H. Shigekawa, *Chemical Communications* **1999**, 1443-1451.

[26] A. L. Maldonado, A. K. Yatsimirsky, *Organic & Biomolecular Chemistry* **2005**, *3*, 2859-2867.

[27] I. Bertini, *Bioinorganic chemistry*, University Science Books, Mill Valley, Calif., **1994**.

[28] L. Tjioe, A. Meininger, T. Joshi, L. Spiccia, B. Graham, *Inorganic Chemistry* **2011**, *50*, 4327-4339.

[29] M. R. Redinbo, L. Stewart, P. Kuhn, J. J. Champoux, W. G. J. Hol, *Science (New York, N.Y.)* **1998**, *279*, 1504.

[30] R. Krämer, *Coordination Chemistry Reviews* **1999**, *182*, 243-261.

[31] S. Ullrich, Z. Nazir, A. Büsing, U. Scheffer, D. Wirth, J. W. Bats, G. Dürner, M. W. Göbel, *Chembiochem : a European journal of chemical biology* **2011**, *12*, 1223-1229.

[32] X. Sheng, X.-M. Lu, J.-J. Zhang, Y.-T. Chen, G.-Y. Lu, Y. Shao, F. Liu, Q. Xu, *The Journal of Organic Chemistry* **2007**, *72*, 1799-1802.

[33] S. Aoki, K. Iwaida, N. Hanamoto, M. Shiro, E. Kimura, *Journal of the American Chemical Society* **2002**, *124*, 5256-5257.

[34] E. L. Hegg, J. N. Burstyn, *Coordination Chemistry Reviews* **1998**, *173*, 133-165.

[35] L. Tjioe, T. Joshi, J. Brugger, B. Graham, L. Spiccia, *Inorganic Chemistry* **2011**, *50*, 621-635.

[36] T. Gupta, S. Dhar, M. Nethaji, A. R. Chakravarty, *Dalton Transactions* **2004**, 1896-1900.

[37] J. He, P. Hu, Y.-J. Wang, M.-L. Tong, H. Sun, Z.-W. Mao, L.-N. Ji, *Dalton Transactions* **2008**, 3207-3214.

[38] Y. Shao, X. Sheng, Y. Li, Z.-L. Jia, J.-J. Zhang, F. Liu, G.-Y. Lu, *Bioconjugate Chemistry* **2008**, *19*, 1840-1848.

[39] F. Nihan Aka, M. S. Akkaya, E. U. Akkaya, *Journal of Molecular Catalysis A: Chemical* **2001**, *165*, 291-294.

[40] C. Sissi, P. Rossi, F. Felluga, F. Formaggio, M. Palumbo, P. Tecilla, C. Toniolo, P. Scrimin, *Journal of the American Chemical Society* **2001**, *123*, 3169-3170.

[41] S. Mikkola, T. Lönnberg, H. Lönnberg, *Beilstein Journal of Organic Chemistry* **2018**, *14*, 803-837.

Chapter 6

1. *How Studying Leaving Group Departure May Provide Insight into the Mechanism of the Phosphodiester Cleavage?*

As already mentioned in *Chapter 4*, HPNP is one of the most common RNA model substrates. Although it provided us with many useful observations so far, one should bear in mind that *p*-nitrophenoxide is not only a much better leaving group (LG) than 5′-linked nucleoside, but also it does not require any protonation while departing from a penta-coordinated phosphate. That is contrary to 5′-nucleosides which, being less acidic, may benefit from the stabilization of the negative charge at the leaving C-5′-alkoxy oxygen of the rate-determining transition state.[1] What is more, the intramolecular nucleophile in HPNP is more flexible than the 2′-alkoxide in nucleotides and has a higher p*K*a value.[2] Therefore, the hydrolytic fate of HPNP may not necessarily represent the optimum choice for understanding the cleavage of nucleotides.

The seemingly straightforward mechanism of the hydrolysis of RNA via nucleophilic attack of the 2′-OH group, yielding the formation of penta-coordinated phosphorane, may vary depending on conditions. Lönnberg *et al.* presented in 1997 studies on the cleavage of the uridine 3′- phosphates bearing different alkyl leaving groups (*Fig.6.1.*) in the aqueous acidic and alkaline environments.[3] The hydronium and hydroxide ion-catalysed cleavage was performed in 0.5 M HCl and 0.01-1.0 M NaOH at 25°C.

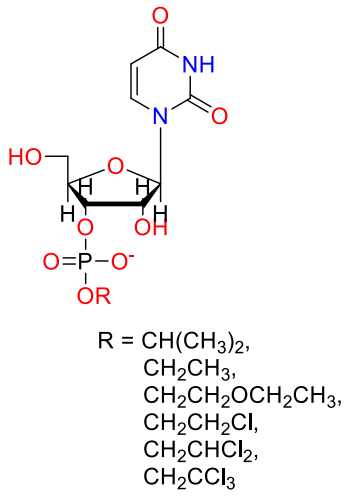

Fig.6.1.

It was observed that at the acidic conditions, uridine 2′,3′-cyclic phosphate was not accumulated, but hydrolysed to a mixture of uridine 2′- and 3′- phosphates.

β_{LG} values for cleavage and isomerization (calculated on the basis of Brønsted plots, -0.12 and -0.18 respectively) showed a similar dependence on the leaving group departure in the formation of uridine 2′- and 2′,3′-cyclic phosphates (*Fig.6.2.*). Furthermore, the rate of cleavage highly depended on the polar nature of the LG, which departed as an alcohol, not alkoxide ion. The isomerization was also relatively prone to the polar nature of alkyl leaving groups. Their increasing electronegativity seemed to favour the isomerization over the cleavage.

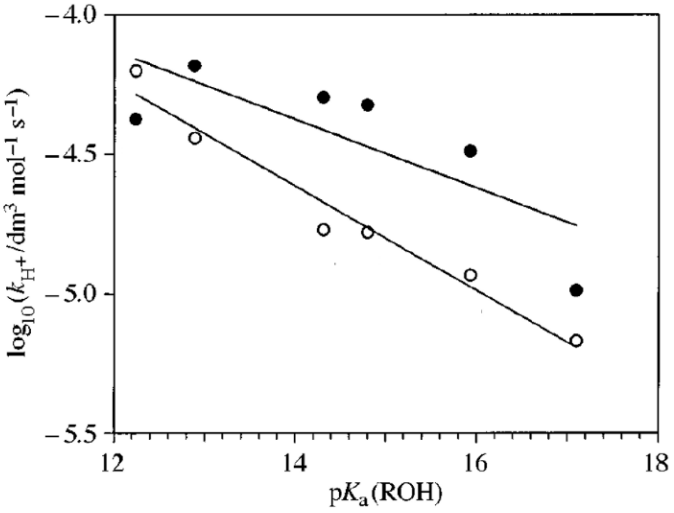

Fig.6.2. The Brønsted plot of esterified alcohols for the transesterification of uridine 3′-alkyl phosphates to uridine 2′-alkyl phosphates (◦) and uridine 2′,3′-cyclic phosphate (●) under acidic conditions.

For the hydroxide ion-catalysed cleavage, no isomerization to 2′-alkyl phosphates was observed. It may be due to the formation of unstable dianionic species, which is immediately hydrolysed to the cyclic phosphate. The highly negative β_{LG} value -1.28 strongly indicates that alkoxy ions were well-developed in the transition state (*Fig.6.3.*). Therefore, occurring mechanism may proceed *via* formation of dianionic phosphorane followed by the repulsion of the leaving group as an alkoxide, yielding 2′,3′-cyclic phosphate.

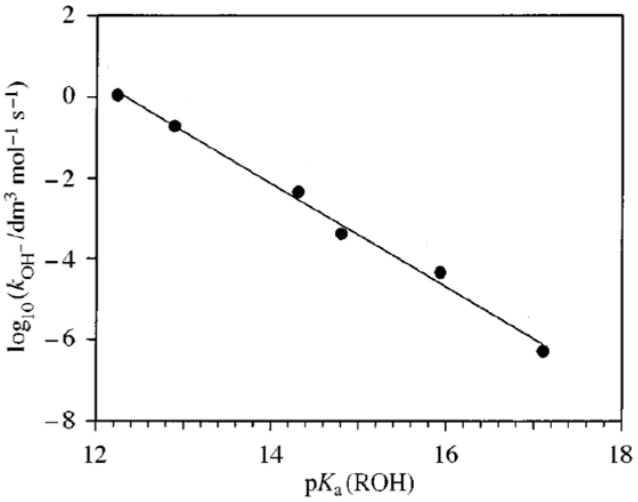

Fig.6.3. The Brønsted plot of esterified alcohols for the transesterification of uridine 3′-alkyl phosphates to uridine 2′,3′-cyclic phosphate under basic conditions.

The same research group studied the leaving group departure in metal ion promoted cleavage of uridine 3′-alkyl and aryl phosphates (*Fig. 6.4.*).[4] The hydrolysis was performed at pH 5.6, 25°C or 90°C with 10 mM Zn^{2+} aquo ions. In the presence of metal ion no isomerization occurred for both, alkyl and aryl LGs (no stable intermediate was formed), resembling in this sense the base-catalysed cleavage.[5], [6]

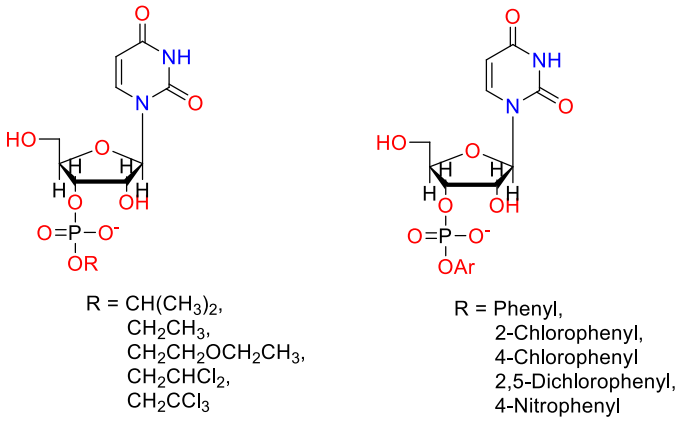

Fig.6.4.

The rate enhancement in the presence of zinc was detected as the efficiency of the leaving group was decreasing. It was already mentioned that under acidic conditions alkyl LGs were departing as alcohols (β_{LG} = -0.12) and that process was independent

from the acidity of leaving groups. Under alkaline conditions results were different: LGs were departing as alkoxides (the observed β_{LG} value was high, -1.28) and the cleavage was strongly dependent on the acidity of leaving groups. Thus, the comparison with the β_{LG} value determined for the hydrolysis of uridine 3'-alkyl phosphates in the presence of Zn^{2+} aquo ion (-0.32, *Fig. 6.5. (a)*) implies that the metal ion may assist (protonate) the departure of alkyl leaving groups through a bound water molecule, acting as a general acid. The fact that no phosphate migration was observed suggests likewise a deprotonation of the attacking nucleophile, and therefore the formation of a dianionic phosphorane. This, together with the increased rate of the Zn(II) promoted cleavage upon increasing pH, may suggest a base catalysis.

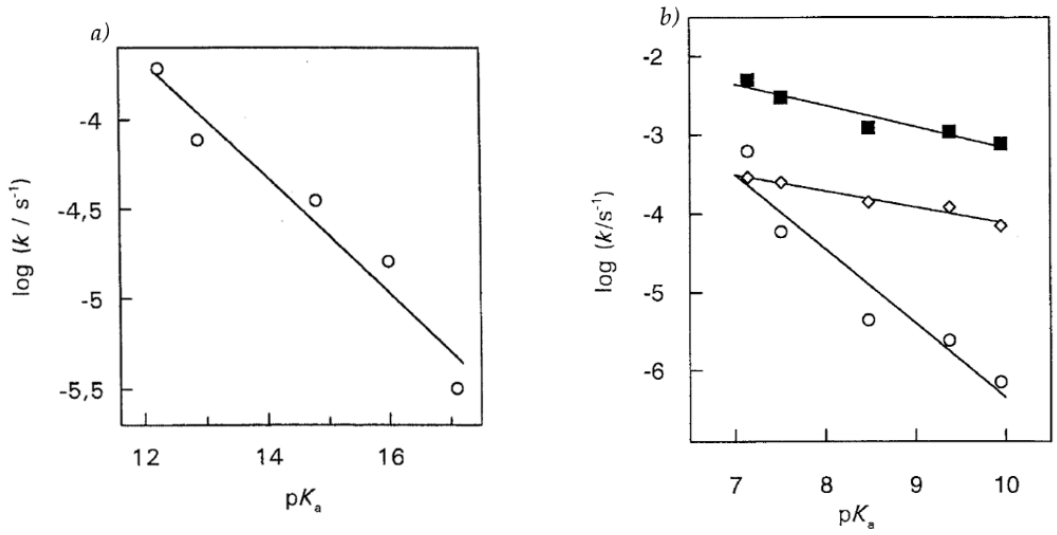

Fig.6.5. Brønsted plots of the cleavage of uridine 3'-alkyl (left) and -aryl (right) phosphates. (◦): Zn^{2+} catalysed cleavage, (◊): buffer and pH-independent cleavage in formic acid buffer at pH 3.5, (▪): acid-catalysed cleavage.

The situation with aryl leaving groups was significantly different, since obtained β_{LG} value in the presence of Zn^{2+} was highly negative (-0.90, *Fig.6.5.(b)*). Furthermore, on the contrary to alkyl LGs, the value for Zn(II)-promoted cleavage of aryl esters was more negative compared to that in the absence of zinc (reported by Williams β_{LG} values for the hydroxide ion-catalysed and buffer dependent cleavage were -0.54 and -0.59,

respectively).[7] Furthermore, the acid-catalysed and buffer independent hydrolysis of uridine 3′-aryl phosphates revealed even less negative β_{LG} values (-0.27 and -0.20, respectively). These results strongly support the hypothesis regarding departure of aryl LGs as alkoxides. Consequently, the Zn^{2+} aquo ion does little to enhance departure of aryloxide leaving groups, however, it likely acts as a general base deprotonating the 2′-hydroxyl. Similarly, as in the case of uridine 3′-alkyl phosphates, no isomerization was observed. It is evident here that metal ions may play the role of intra-complex base catalyst, as is well supported by literature.[8], [9], [10], [11], [12], [13]

Artificial metallonucleases are usually endowed with ligands able to bind metal ions. Indeed, this allows for the functionality of metals at neutral and basic pH, preventing their precipitation as hydroxides. In the case of Zn^{2+}, its complexes with azacrowns (e.g. cyclen ([12]aneN$_3$) or TACN, ([9]aneN$_3$)), bipyridine, terpyridine and their derivatives have been commonly used. Mikkola *et al*. reported laborious studies on the cleavage of uridine 3′-aryl and alkyl phosphates by various mono- and bimetallic complexes (*Fig.6.6.*).[14]

Based on results of uridine 3′-(LG) phosphates cleavage with 2 mM zinc complexes of (**6a**), (**6b**) and (**6d-6g**) at pH 6.9 and 90°C, authors proposed three different ligand-based groups. Group A consists of Zn^{2+} complexes of (**6a**) and (**6c**), which have a high proportion of the hydroxo form. Accordingly, they are good catalysts for more acidic leaving groups, where protonation is not needed. As a consequence, group A can enhance the phosphodiester cleavage by general base catalysis. Zn(**6d**-**6g**) belonging to the group C, can substantially enhance the reaction rate only with very poor leaving groups. Therefore, group C favours their protonation and acts as a general acid catalyst. Group B includes the zinc complex of (**6b**), which provides both, hydroxo and aquo forms. As a consequence, it may play the role of a bi-functional catalyst, following a general base/acid route. Moreover, group B shows a consistent enhancement in the cleavage activity as the leaving group becomes poorer (*Fig.6.6.*).

Additionally, it was concluded that apart from Zn(**6g**), none of the zinc complexes were able to stabilize the penta-coordinated phosphorane and neutralize its negative

charge, thus the formation of dianionic species (and therefore, no isomerisation) was observed.

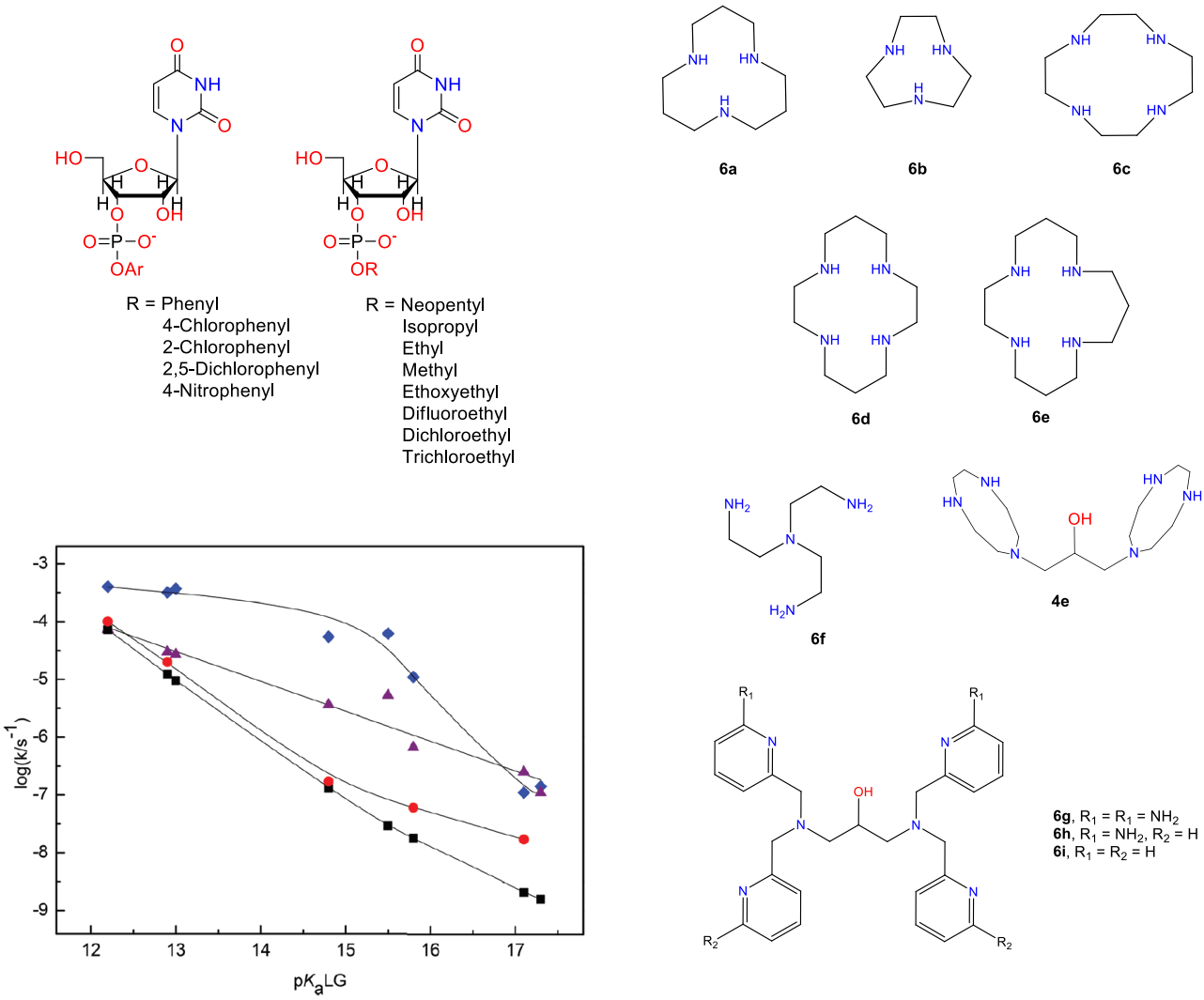

Fig.6.6. The Brønsted plot of the cleavage of uridine 3′-aryl and -alkyl phosphates by Zn^{2+} complexes of (**6a**,**6b**) and (**6d**). Squares: uncatalysed cleavage, circles: Zn^{2+}-(**6d**), trangles: Zn^{2+}-(**6b**), diamonds: Zn^{2+}-(**6a**).

Based on more detailed studies, the authors claimed that departure of the leaving group was rate-determining for a general acid-base catalysed hydrolysis of uridine 3′-alkyl phosphates, being dependent on the acidity of both, catalyst and leaving group. The situation was different with uridine 3′-aryl phosphates cleaved by monometallic complexes. As the enhancement was bigger when the acidity of LGs was increasing, a step-wise mechanism was proposed (where the catalytic efficiency was enhanced as a

difference between energy barriers of individual steps was increasing). Therefore, for aryl leaving groups, a more likely rate-limiting step was the nucleophilic attack.

Bimetallic catalysis can be much more efficient than a monometallic, due to the simultaneous interaction between two positively charged metal ions. Double activation makes the phosphate more electrophilic and stabilized by enhanced interactions.[15], [16], [17] However, the authors claimed that both bimetallic and monometallic catalysts were following very similar trends in leaving group departure. As mononuclear complexes, bimetallic catalysts were more active when the acidity of the leaving group was increased. Comparing the reactivity of zinc complexes of (**6g**) and (**6i**), the difference between them was decreasing when the leaving group was becoming poorer, characteristic of general acid catalysis. In the case of zinc complexes of (**6b**) and (**4e**), the catalytic difference could be attributed to their different p*K*a values (9.2 and 7.8, respectively). Therefore, Zn_2(**4e**) can act as a general-base catalyst, whereas its monometallic counterpart may be more prone to protonate the leaving group at neutral conditions, acting as a general-acid catalyst.

In the case of the zinc complexes of (**6g**) and (**6i**), compared to the difference between (**6b**) and (**4e**) was decreasing as the leaving group was becoming less acidic. However, for aryl LGs, a difference was diminishing as the acidity of LGs was increasing. In other words, a dissimilarity decreases as the nucleophilic attack becomes more clearly the rate-determining step.

As already presented in *Chapter 4*, Zn_2(**4f**) is one of the most efficient reported artificial metallonuclease in the cleavage of simple nucleic acid models. This is due to functional groups capable of hydrogen bond formation, the oxo-bridge placing two metal ions in an optimal position enhancing their cooperativity, the double Lewis acid activation that decreases the p*K*a value of the metal coordinated water molecule and protonation of the leaving group that may be substantially facilitated.[18], [19] Williams *et al*. decided to

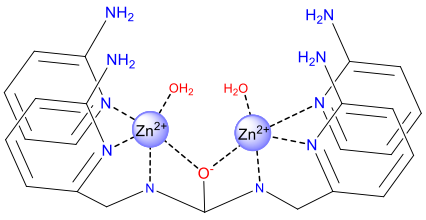

Zn_2(**4f**)

continue studies with Zn_2(**4f**), this time in order to evaluate the effect of different leaving groups, on both the cleavage and isomerization of uridine 3′-phosphates (*Fig.6.7.*).[2]

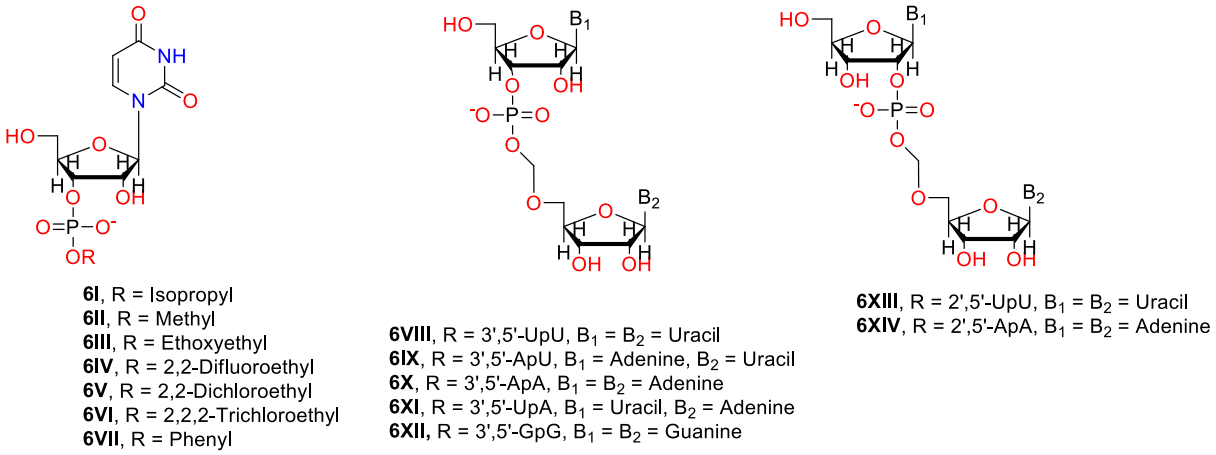

Fig.6.7.

Zn_2(**4f**) was able to catalyse both the isomerisation and cleavage of uridine 3′-phosphates, more efficiently for the latter one (except for the substrate (**6I**) that possesses the worst leaving group). Interestingly, the better the leaving group was, the lower was the proportion of isomerisation (*Fig.6.8.(a)*). Additional studies performed in the presence of exclusively the Zn^{2+} aquo ions showed that the absence of Zn_2(**4f**) drastically decreased the catalytic efficiency in phosphodiester cleavage and the metal aquo ion did not promote isomerisation.

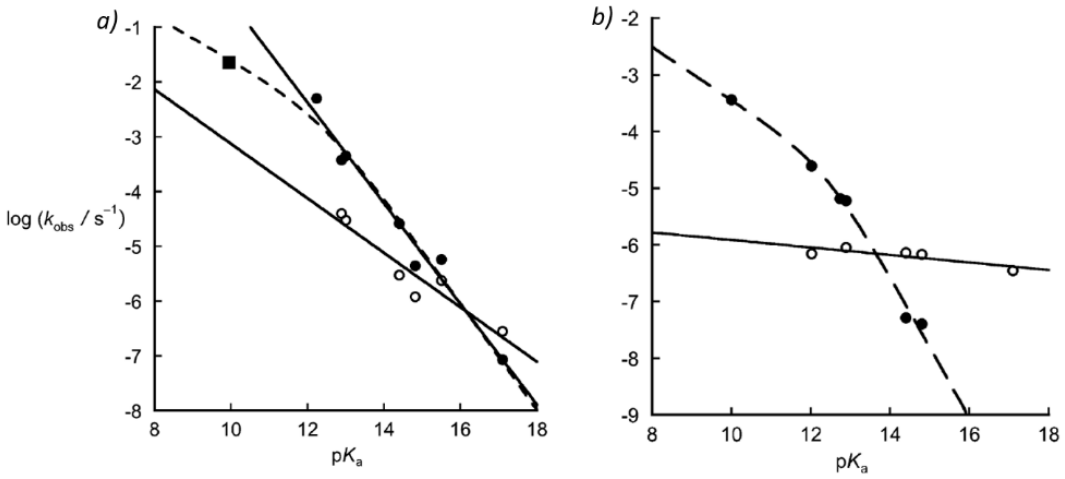

Fig.6.8. The Brønsted plot of the cleavage and isomerisation of uridine 3′-(**6I-6VII**) phosphates by (Zn_2**4f**, *a)*) and spontaneous cleavage at pH 6.5 at 90°C (*b*).
a) ● Zn_2(**4f**)-promoted cleavage, ◦ Zn_2(**4f**)-promoted isomerisation, ▪ Zn_2(**4f**)-promoted cleavage of (**6VII**).
b) ● cleavage of (**6III-6VII**, **6VIII**), ◦ isomerisation of (**6I**, **III, IV, VII** and **6VIII**).

Spontaneous cleavage and isomerisation of uridine 3′-phosphoesters presented in *Fig.6.8.(b)* clearly differentiate from each other. The cleavage does not depend linearly on pK*a* of the leaving group revealing a convex point at pK*a* 12.4., which also agrees with results of hydroxide promoted cleavage.[20] The breakpoint occurs when rates of phosphorane's breakdown to products or the starting material are equal.
Taking all data together, authors claimed that Zn_2(**4f**) acts as an electrophilic catalyst and the cleavage mechanism involves a proton transfer from 2′-OH to zinc-coordinated hydroxide, followed by the formation of penta-coordinated phosphorane intermediate and the general-acid-catalysed departure of the leaving group.

Additional studies were aimed at determination of whether the interactions between Zn_2(**4f**) and nucleobases are significant factors. Reported results by Lönnberg, Hamilton and Komiyama clearly indicate that the interaction with a nucleic acid base may either enhance (for instance by stabilisation of the reactive conformation) or decrease (competing with binding of the metal ion complex to the phosphate) the efficiency in phosphodiester cleavage.[21],[22],[23] In the case of Zn_2(**4f**), no significant effect was observed in the presence of various 3′,5′-dinucleoside monophosphates

(**6VIII**-**6XII**), therefore there were no relevant interactions between the catalyst and nucleobases. In terms of 2′,5′-isomers (**6XIII**, **6XIX**), they were 5-times slower than their 3′,5′-isomers (**6VIII** and **6X**). This finding was justified by a higher p*K*a of the 3′-hydroxide compared to the 2′-equivalent and weaker interactions of Zn_2(**4f**) with 2′,5′-isomers.

2. *Studies on the Nucleobase-Specific Interactions with Aza-Macrocycles in the Cleavage of Nucleosides 3'-phosphates.*

The molecular recognition of nucleic acids constituents via hydrogen bond pairing, hydrophobic, electrostatic and π-π interactions is responsible for a myriad of relevant biochemical processes.[24],[25],[26] In the case of phosphate hydrolysis, the interaction of nucleobases with commonly used metal complexes of aza-macrocycles may be either beneficial or detrimental for the catalytic efficiency.

One of the pioneers in the macrocyclic polyamine-nucleobase chemistry is Prof. Kimura. He has been studying in particular uracil/thymine-Zn(II)cyclen (1,4,7,10-tetraazacyclododecane) interactions, showing not only their specificity and chemistry, but also potential applications.[27], [28], [29], [30] For instance, Kimura presented bis-(Zn(II)-cyclen) complexes linked by an aromatic unit playing the role of highly selective diotopic receptors for a variety of uracil and thymine nucleotides, which were aimed to increase the efficacy of some drugs.[31]

In terms of features of cyclen-Zn(II) interactions, not only did the complexation by cyclen substantially reduce the p*Ka* of the zinc-coordinated water molecule in comparison to the metal aquo ion, but also zinc, affected by the macrocyclic coordination, promoted a deprotonation of sulfonamides (pKa~ 7-11) and carboxamides (pKa~14). Therefore, the interaction between the anionic $–NHSO_2-$ or –NCO- and the Lewis acid is significantly stronger (*Fig.6.9.*).[32], [33], [34]

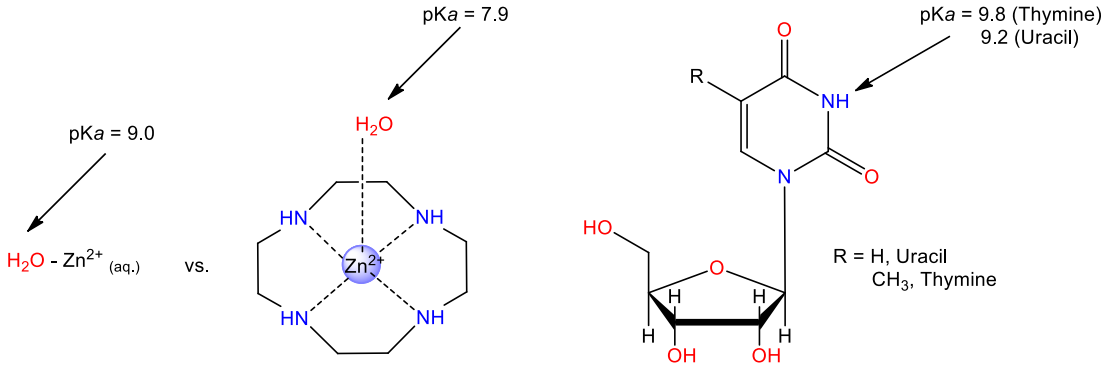

Fig.6.9.

Accordingly, when Zn(II)-cyclen is interacting with the imide's proton (like in uracil's or thymine's), zinc firstly dissociates that proton, yielding a Zn(II)-N$^-$(3) bond. Simultaneously, the carbonyls at C(2) and C(4), with their free electron pairs, act as acceptors for the acidic –NH hydrogens of cyclen at complementary positions (*Fig.6.10.*). The presented concept is commonly accepted and now called Kimura's three point recognition model.

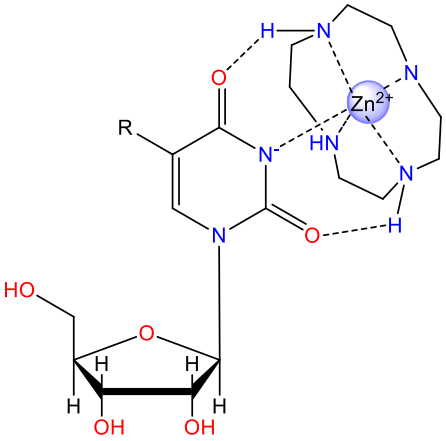

Fig.6.10.

Additional studies showed that interactions between Zn(II)-cyclen and remaining nucleobases (adenine, guanine and cytosine) are much weaker than with uracil and thymine. This is due to either lack of a basic imide site (adenine or cytosine) or repulsion between the zinc-aza-macrocycle complex and the –NH group (C(2), guanine), making the Zn(II)-N$^-$(3) interaction weaker, thus preventing strong binding.

Studies on the recognition of uridine with zinc-aza-macrocycles of (**6a**,**6c**,**6j**,**6k**,**6l**) (*Fig. 6.11.*), as well as its relevance in the phosphodiester cleavage, was explored by Morrow *et al*.[35]

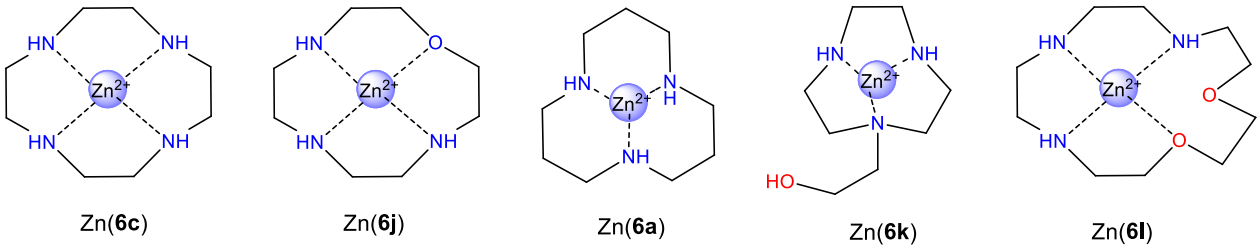

Fig.6.11.

The estimated pK*a* values for zinc-coordinated water molecules of (**6a, 6c, 6j-6l**) vary roughly about one pK*a* unit. Interestingly, the correlation between the coordination number of each studied aqua complexes and the pK*a* of the water ligand has been observed. The higher the coordination number (as 5 or 6 for TACN derivatives), the lower was the affinity to hydroxide ion. Accordingly, complexes with lower coordination numbers (as 4 or 5 for Zn(**6a**)) had higher affinity to the coordinated hydroxide and therefore lower water ligand pK*a* values.[36], [37]

The uracil binding constants with zinc complexes of aza-macrocycles varied nearly 3-orders of magnitude ($\log K_{U^-}$= 4-5 for Zn(**6c**), Zn(**6j**) and Zn(**6a**) and for Zn(**6k**) and Zn(**6l**) $\log K_{U^-}$= 2-3). Furthermore, no straightforward correlation between the uracil anion binding strength to studied aza-macrocycles and the types of donor groups or macrocycle sizes has been observed. However, as the pK*a* of a water-ligand was decreased, the binding constant for the uracil anion was increasing. Another noted observation in terms of Zn(II)-macrocycle binding properties were steric factors. It was pointed out that the 'more open' the coordination sphere, the stronger was the interaction with bulky uracil. Therefore, Zn(**6a**) seemed to be more promising complex than Zn(**6k**).

Additional uridine inhibition experiments performed for HPNP cleavage in the presence Zn(**6j**), Zn(**6a**) and Zn(**6k**) revealed competitive binding between the uracil anion and the phosphate unit. Established effective binding constants for uracil bound to zinc aza-macrocycle complexes were larger than for phosphate diesters. Therefore,

the phosphate hydrolysis, in the presence of a single unit of the aza-macrocycle zinc complex, may be drastically inhibited.

The analysis of above described studies yields the conclusion that the design of a phosphodiester cleaving agent encompassed with a nucleoside-base selectivity function is a challenging task. One reported example (already presented in *Chapter 4* in *Fig. 4.4*, Cu_2(**4d**)) is a bis-Cu(II) complex based on covalently linked terpyridine and bipyridine ligands, showing a high selectivity for adenine.[38] The observed phenomenon was attributed to π-π stacking interaction between the nucleoside base and the bipyridine-Cu(II) unit.

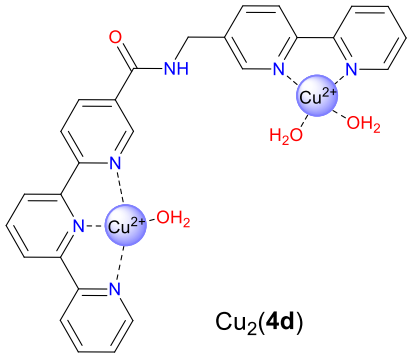

Cu_2(**4d**)

Lönnberg *et.al*, however, were the first to apply aza-macrocycle units to artificial metallonuclease architectures that were not only selective to uracil, but also efficient in phosphodiester bond hydrolysis.[21]

The authors have been studying the selectivity of five di-nucleating Zn_2(**6m**) and one tri-nucleating Zn_3(**6n**) zinc complexes with either two or three 1,5,9-triazacyclododecan-3-yloxy units (*Fig. 6.12*) in the cleavage of ApA, ApU, UpA and UpU.

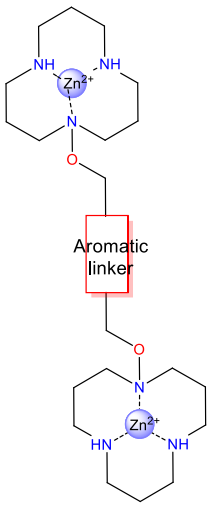

Zn_2(**6m**)

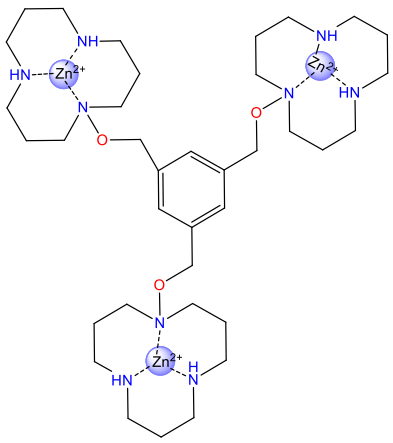

Zn_2(**6n**)

Fig.6.12.

The complexes Zn_2(**6m**) containing two 1,5,9-triazacyclododecane moieties revealed a base selectivity with the studied dinucleoside 3′,5′-monophosphates. Unsurprisingly, the weakest interaction was reported with ApA (due to feasible Zn_2(**6m**)-nucleobase stacking interaction), being cleaved only slightly more rapidly by Zn_2(**6m**) than by the single zinc 1,5,9-triazacyclododecane complex. Cleavage of ApU and UpA by Zn_2(**6m**) revealed that just one uracil base was sufficient to anchor Zn^{2+}[12]aneN_3 to the substrates, while the other Zn(II)-macrocycle moiety acted as an intra-complex catalyst. It was able to cleave the neighbouring phosphodiester bond, reaching even up to 100-fold rate acceleration compared to that obtained with a monomeric complex. It should not be surprising that in the case of UpU no change in the cleavage rate was observed, since all cleaving species were engaged in the uracil anion binding. Intuitively, a third azacrown group could restore the cleavage activity due to the availability of another zinc-1,5,9-triazacyclododecane complex to participate in the effective phosphate cleavage (*Fig. 6.13.(a)*). Indeed, Zn_3(**6n**) at 1.5 mM concentration was able to accelerate the cleavage of UpU 50-times as efficiently as its bifunctional counterpart at a concentration of 1.0 mM (*Fig. 6.13.(b)*).

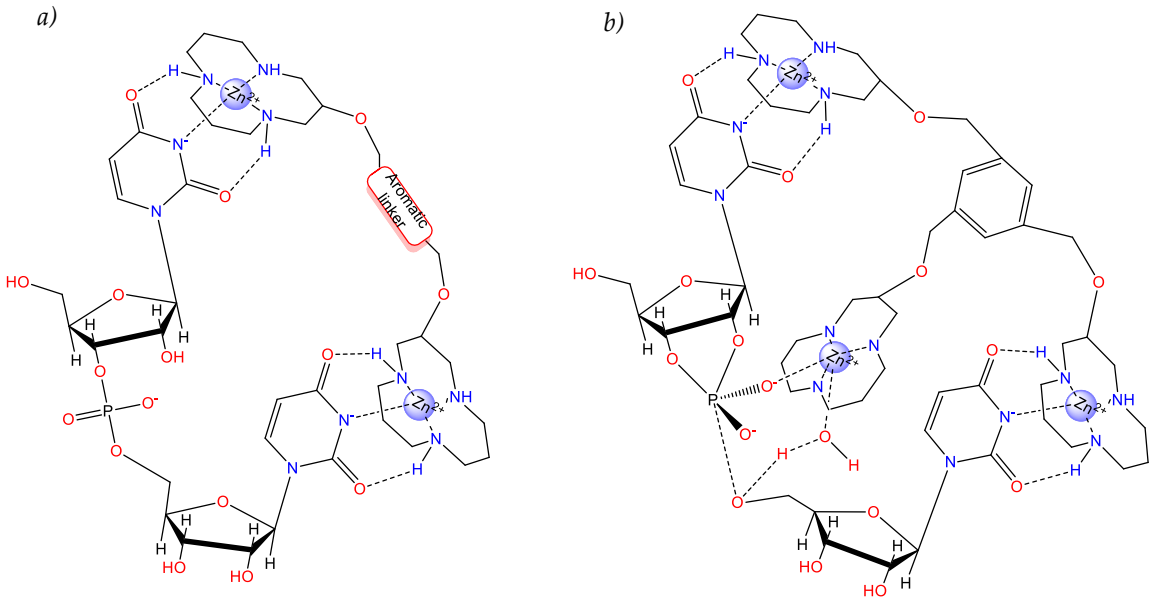

Fig.6.13. Assumed interactions of Zn_2(**6m**) (*a*) and Zn_3(**6n**) (*b*) complexes with UpU.

3. *Leaving Group Effect in the Phosphodiester Cleavage by **AuNP1**.*

To establish the importance of the leaving group departure in phosphodiester cleavage by self-assembled gold nanoparticles, a library of uridine 3′-(LG) phosphates was synthesized (*Scheme 6.14.*). Six RNA models bearing either alkyl or aryl leaving group covered a 6-unit range of p*K*a values (**LG**$_1$-**LG**$_6$).[39] Cleavage was performed in the presence of our most efficient nanozyme in the cleavage of HPNP, **AuNP1**.

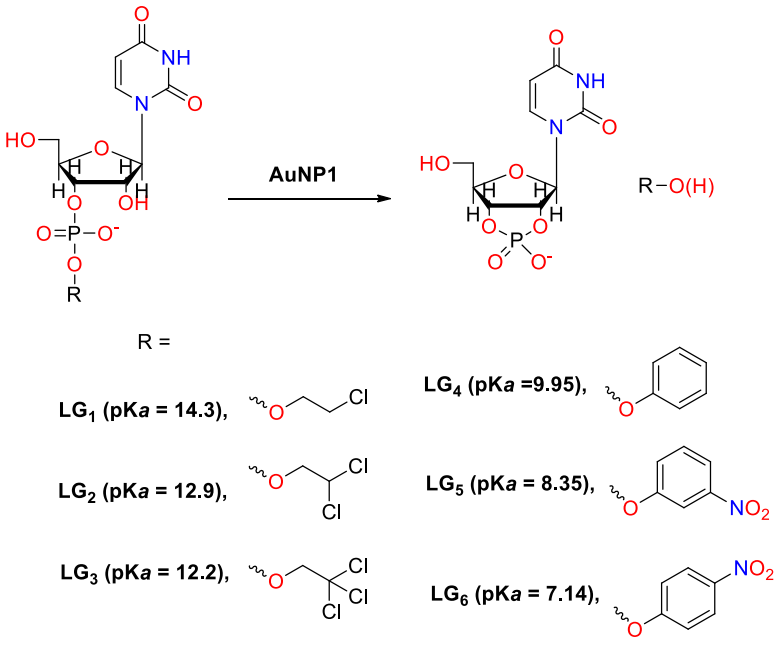

Scheme 6.14. The hydrolysis of uridine 3′-alkyl (**LG**$_1$-**LG**$_3$) and aryl (**LG**$_4$-**LG**$_6$) phosphates by **AuNP1**.

a) The Synthesis of Uridine 3′-(LG) phosphates.

The synthesis of uridine 3′-(LG) phosphates was influenced by Strömberg's and Saffhill's protocols, reported independently.[40], [41]

It starts with the acid-catalysed exchange between uridine and trimethyl orthoester, which gives 2′,3′-*O*-methoxyarylidene derivative. Subsequent hydrolysis and reaction with the excess of 4-methoxy-5,6-dihydro-2*H*-pyran yields the bisketal ester (**33**). After treatment with methanolic sodium methoxide, (**34**) is phosphonylated with pyridinium *H*-pyrophosphonate, generated in situ from phosphorous acid and pivaloyl chloride as a condensing agent. In this form, *H*-phosphonate (**35**) can be consecutively coupled with desired alcohols, oxidized and deprived of mTHP protecting groups under mild acidic conditions (*Scheme 6.15.).*

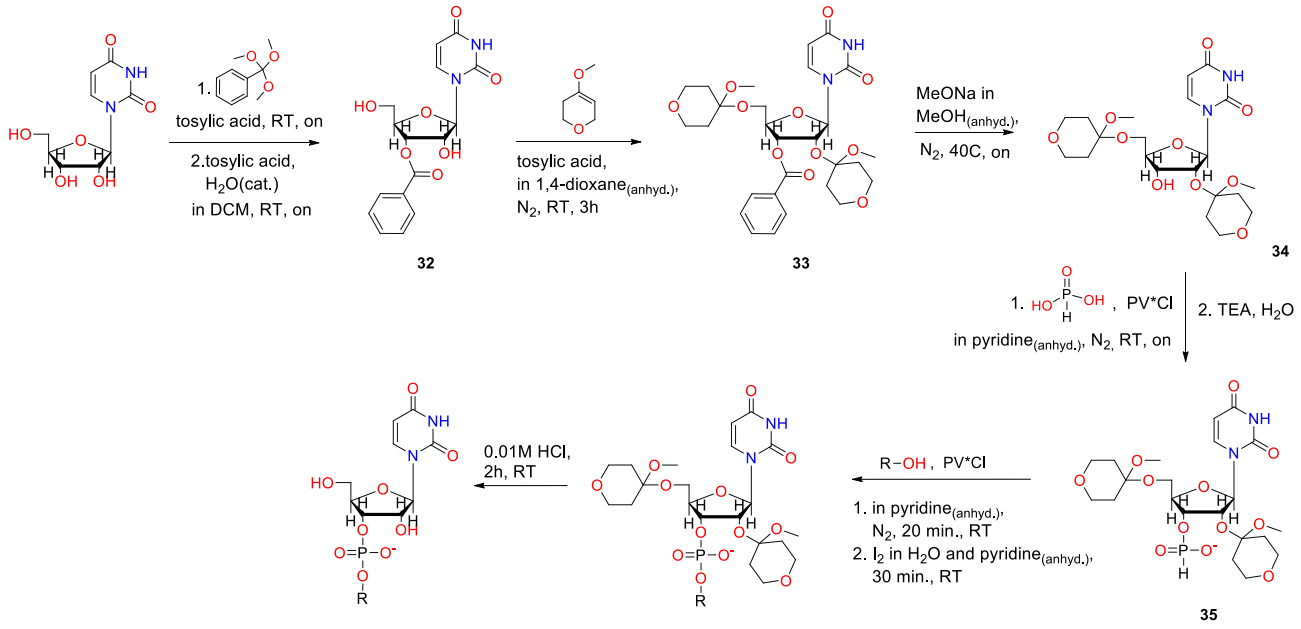

Scheme 6.15. The pathway of the synthesis of uridine 3′-(LG) phosphates.

During the very early stage of uridine 3′-(LG) phosphate synthesis, 2′- and 5′-OH groups had to be protected, in order to exclusively functionalize the 3′-hydroxyl unit. The protecting group needs to fulfil certain conditions; its removal should be

performed under mild acidic conditions to avoid the cleavage and isomerization of phosphodiester linkages.[42] Furthermore, there is an advantage if the protecting group is symmetrical, not leading mixtures of diastereoisomeric nucleoside derivatives, avoiding possible isomeric contaminations. All of these requirements are fulfilled by a methoxy-tetrahydropyranyl (mTHP) group.

Phosphonylation of protected nucleosides may be performed in a several ways, depending on the substrate's reactivity and solubility, reaction conditions, efficiency or developed side products.[43] The reported protocols include, for instance, phosphorus trichloride as the reagent system, transesterification of diphenyl *H*-phosphonate with protected nucleosides, salicyl-chlorophosphite as the phosphonylating agent or pyridinium *H*-pyrophosphonate, generated *in situ* from phosphorus acid and a condensing agent.[44], [45], [46], [47] The latter route appeared to be the most suitable in the synthesis of uridine 3'-(LG) phosphates protected with mTHP groups.

b) *The Analysis of the Hydrolysis of Uridine 3'-(LG) Phosphates.*

The hydrolysis of uridine 3'-(LG) phosphates was monitored by either UV-Vis spectroscopy or analytical HPLC. UV-Vis enabled for the observation of meta- and para- nitrophenoxides (**LG$_5$**, **LG$_6$**), at 238 and 400 nm respectively. HPLC however, equipped with UV-detection (at 260 nm), allowed for analysis of the disappearance of substrates (**LG$_1$**-**LG$_4$**) and appearance of products.[40] Since uridine 3'-(LG) phosphates with (**LG$_5$**) and (**LG$_6$**) were much more reactive under established reaction conditions than the remaining nucleotides, their reactivities were estimated based on linear extrapolation (Arrhenius plot) performed at 20-30°C (see *Chapter 7*, *Fig.E.42.*).

Due to the poor reactivity under the explored conditions of the substrate with the leaving group (**LG$_1$**), it could not be studied when using **AuNP1** as a catalyst. After a

long incubation period at 40°C, **AuNP1** degradation became relevant. Accordingly, this problem rendered the monitoring of the kinetic experiments scarcely reliable. Unfortunately, the increase of the temperature may have resulted in degradation of **AuNP1**, which possibly was faster than the cleavage process for that substrate.

A thorough analysis of HPLC chromatograms enabled a better understanding of the evolution of nucleotides' hydrolysis catalysed by **AuNP1**. The original 3'-phosphate diester evolved to the cyclic phosphate (**2**), which was eventually hydrolysed to two uridine monophosphates (3'-UMP (**3**) and 2'-UMP (**4**)) (*Fig.6.16.*). According to Gajda *et al.*, the reaction of the hydrolysis of (**2**) exhibits a clear preference for 2'O-P over 3'O-P bond cleavage by artificial nucleases.[48] Indeed, on the course of all performed kinetic experiments with HPLC, it was observed that (**3**) and (**4**) were formed in a ca. 2:1 ratio.

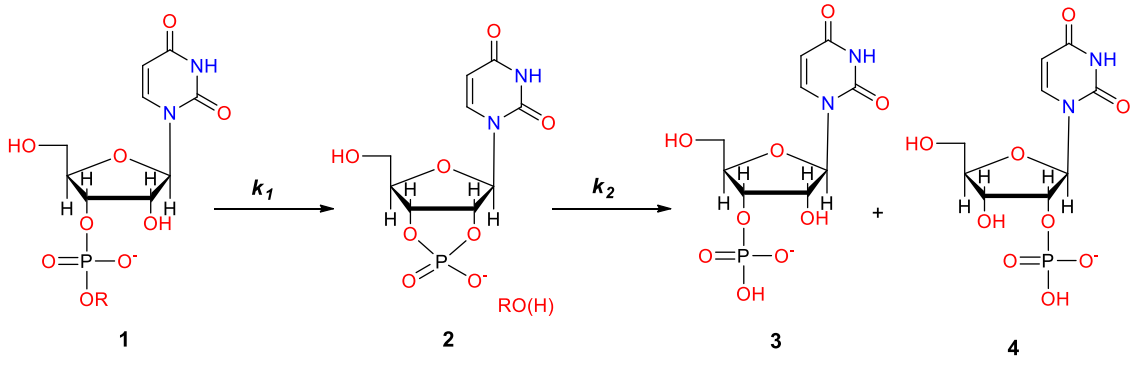

Fig.6.16. The steps of the cleavage of uridine 3'-(LG) phosphates (**1**) by **AuNP1**, proceeding *via* formation of the cyclic phosphate (**2**) and its hydrolysis to uridine 3'- and 2'-phosphates (**3**) and (**4**).

Fig.6.17 reports the change of the composition of the reaction mixtures in time for the substrates followed *via* HPLC. The significant variability of collected data points is a clear consequence (as already mentioned) of the fact that all reactions were carried out at 40°C for many hours/days. Therefore, the data may be affected by the stability of gold nanoparticles, sensitive to high temperatures. Moreover, AuNPs were not

removed before analytical runs and therefore, utilized conditions for compound separation could have resulted in **AuNP1** interference with the analysis. Nevertheless, it did not hamper the determination of relatively reliable rate constants.

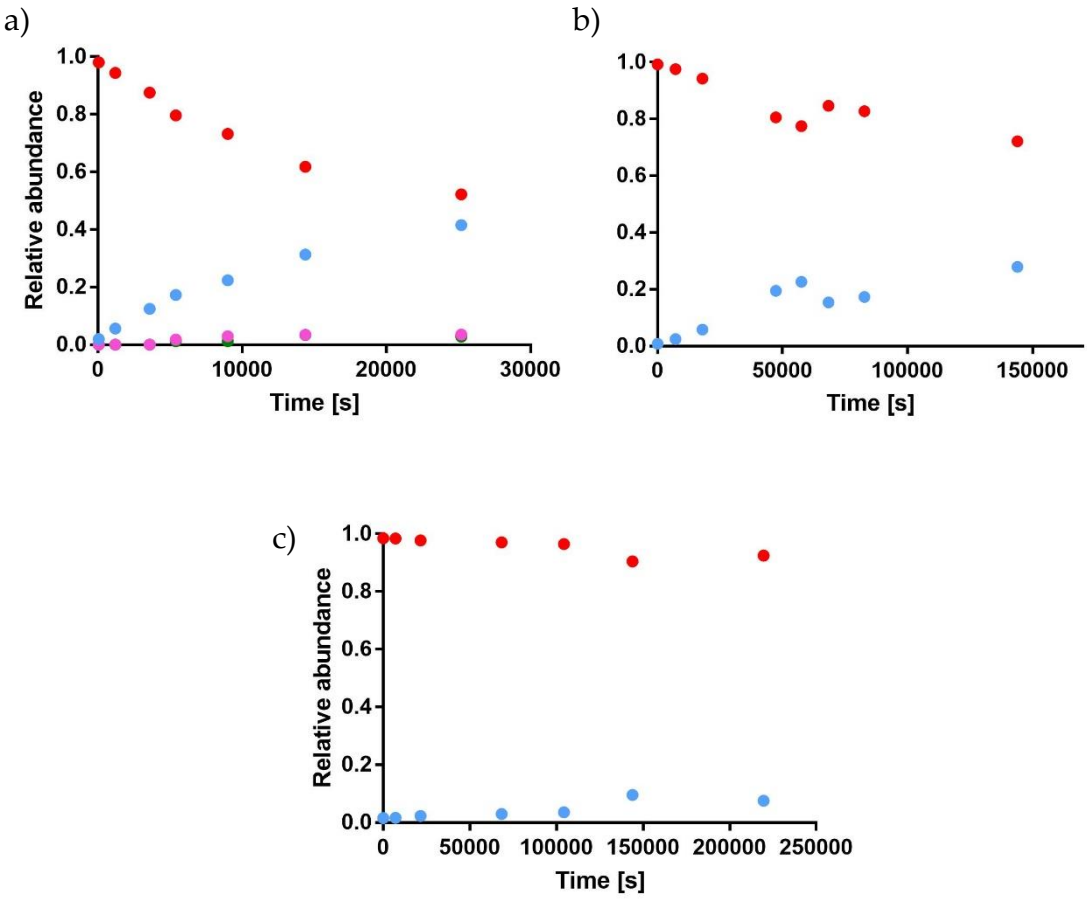

Fig.6.17. The cleavage of uridine 3′-(**LG**) phosphates (a, **LG**$_4$), (b, **LG**$_3$) and (c, **LG**$_2$) by **AuNP1** as the function of relative abundance *vs* time.
Red: uridine 3′-(**LG**) phosphate (**1**); blue: uridine 2′,3′-phosphate (**2**); pink: uridine 3′-phosphate (**3**); green: uridine 2′-phosphate (**4**) (mostly superimposed by the pink (**3**)).

In order to elucidate the mechanism of AuNP-catalysed cleavage of uridine 3′-(LG) phosphates, the function of log(k) *vs* pK*a* of different leaving groups is presented in a so called Brønsted plot (*Fig.6.18*).

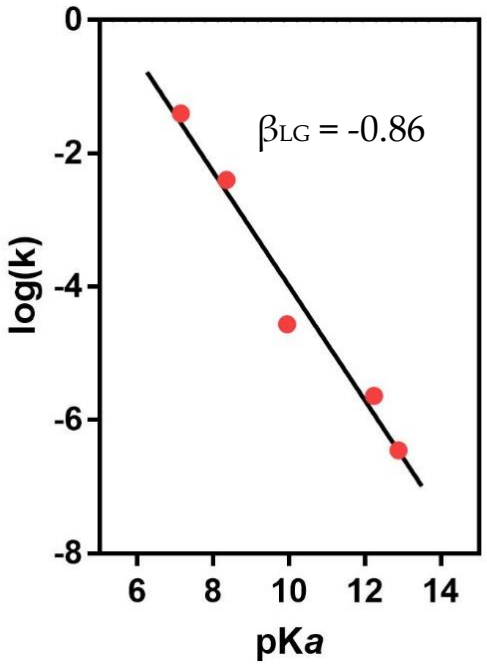

Fig.6.18. The Brønsted plot of uridine 3′-(LG) phosphates hydrolysis promoted by **AuNP1**. Conditions: [**AuNP1**] = [Zn(II)] = 5.0 x 10^{-6} M, [nucleosides]= 3.0 x 10^{-5} M, [HEPES]= 0.01 M, pH 7.5, 40°C in H_2O (R-square = 0.96326).

The profile of the Brønsted plot is linear with a slope equal to -0.86. The data for three aromatic and two aliphatic leaving groups (**LG_2-LG_6**) fits on the same straight line, suggesting that in the explored pK*a* interval there is no change of mechanism. Presented results are different from those reported by Lönnberg *et al*. (see *paragraph 1*), showing the phosphate cleavage catalysed by Zn(II) aqua ions at pH 5.6. In that case the authors reported two different β_{LG} for aromatic and aliphatic leaving groups with values of -0.90 and -0.32, respectively. Accordingly, the β_{LG} value -0.86 here presented is comparable to that reported for the aromatic leaving groups. This may suggest a significant development of the anionic charge in the transition state. Furthermore, this is consistent with a transition state where there is little (if any) proton transfer to the leaving group and most of the catalytic contribution derives from a general base

catalysis. On the other hand, the reported β_{LG} value for cleavage under alkaline conditions (where the leaving groups depart as alkoxy anions) is equal to -1.28. In the **AuNP1**-catalysed process, β_{LG} is less negative, since the substrate may be coordinated to the metal complex (Lewis acid catalysis).

4. Studies on the Hydrolysis of Uridine 3'-p-nitrophenyl Phosphate.

Taking advantage of the reactivity and ease in monitoring of the cleavage of uridine 3'-*p*-nitrophenyl (**LG$_7$**) phosphate (UpPNP), it was decided to perform a more detailed UV-Vis-based kinetic study in the presence of **AuNP1**.

The first experiment involved a titration of UpPNP in the presence of **AuNP1**, which aimed to follow Michaelis-Menten-like kinetics. While simple nucleic acids' models like HPNP or BNP revealed a saturation profile (typical for an enzyme-like behaviour), UpPNP displayed a different result. Once the concentration of the substrate substantially increased, the hydrolytic reactivity dropped down (*Fig.6.19.(a)*).

Conversely, increasing the concentration of **AuNP1**, keeping the same amount of UpPNP, yielded longer increase in the reactivity than expected (*Fig.6.19.(b)*). Obtained results clearly indicate an inhibition in the phosphodiester cleavage once UpPNP was present in a larger excess in comparison to nanozyme **1**.

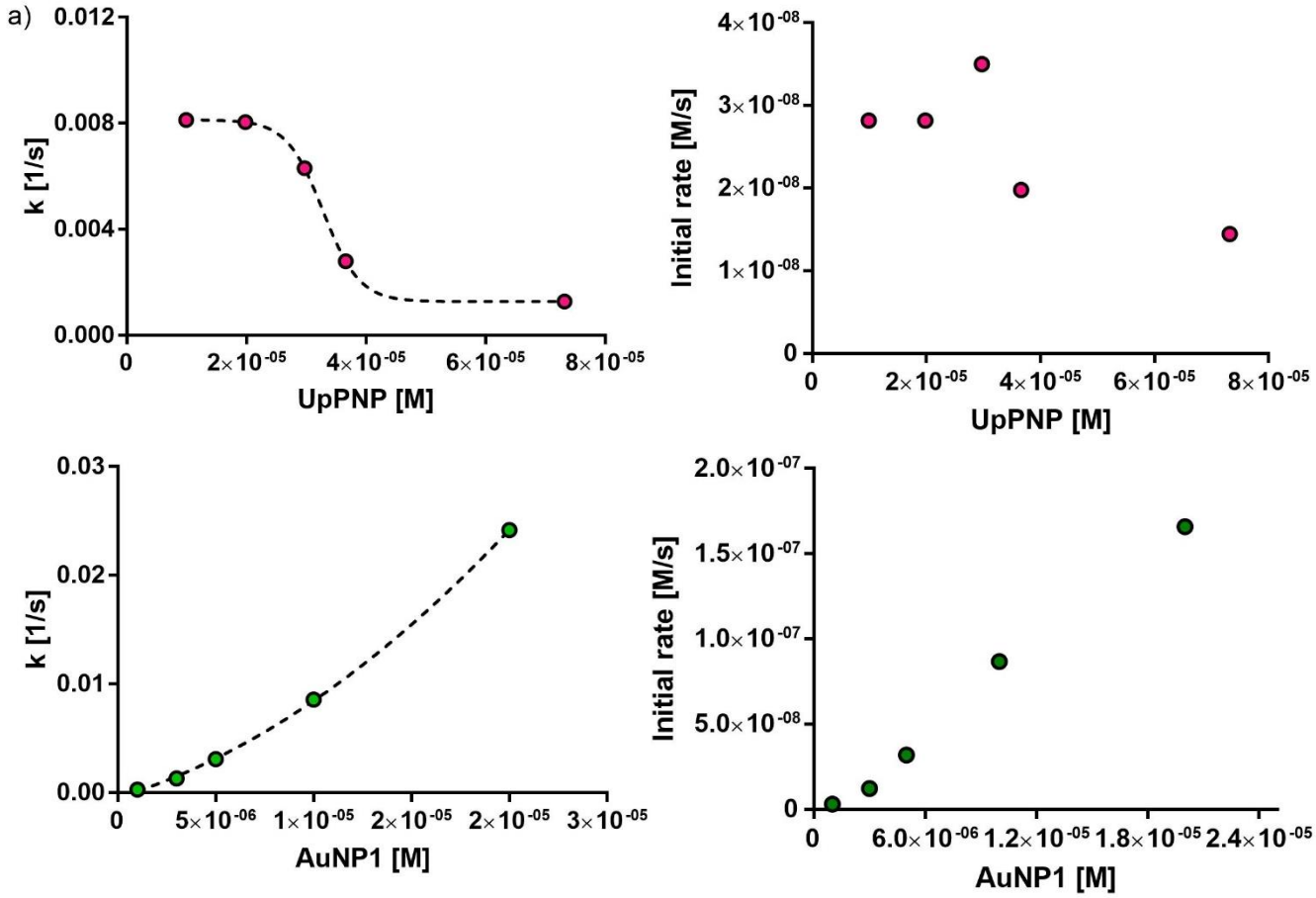

Fig.6.19. The hydrolysis of uridine 3′-*p*-nitrophenyl phosphate as the function of the rate constant (left) / initial rate (right) *vs* increasing concentration of the substrate *(a)* or **AuNP1** *(b)*.
Conditions: [**AuNP1**] = [Zn(II)] = 5.0 x 10^{-6} M, [HEPES]= 0.01 M, [UpPNP]= 3.0 x 10^{-5} M, pH 7.5, 25 °C in H_2O.

The reason for this observed phenomenon may be, as was previously analysed in *paragraph 2*, the interaction of aza-macrocycles with uracil. Kimura and Lönnberg reported a strong interaction between uracil and aza-dodecanes, thus it is likely that aza-cyclic rings complexed with Zn(II) are prone to interact with the nucleobase. However, progressing with the excess of UpPNP, the interaction between TACN-Zn(II) complex and uracil was competing with binding to phosphates, thus blocking Lewis-acid catalytic properties (indeed, one bimetallic Zn(II)-TACN unit can interact with two uracil bases simultaneously). Conversely, increasing the concentration of **AuNP1** yielded more available bimetallic sites, being the possible reason for the observed exponential increase in the catalytic activity.

To confirm the uracil-inhibiting properties in the phosphodiester cleavage by **AuNP1**, the competitive inhibition studies of HPNP cleavage in the presence of increasing concentration of uridine were performed (*Fig.6.20.*).

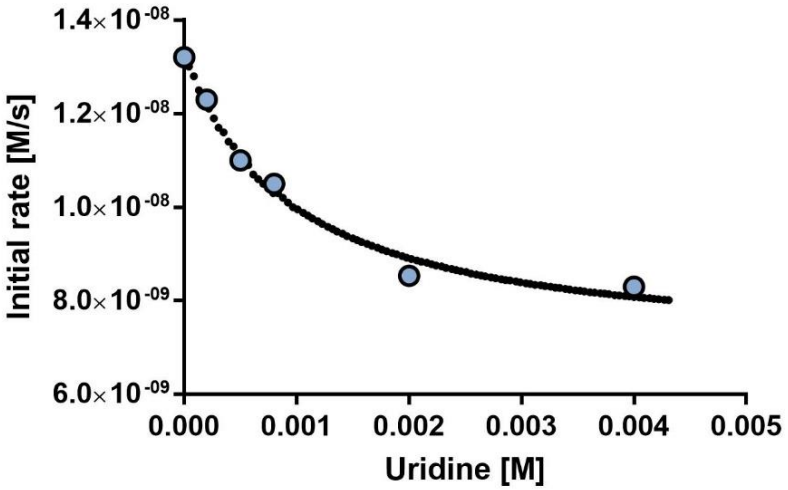

Fig.6.20. Inhibition kinetics of the hydrolysis of HPNP by **AuNP1** by progressive addition of uridine. Conditions: [**AuNP1**] = [Zn(II)] = 5.0×10^{-5} M, [HEPES] = 1.0×10^{-2} M, [HPNP] = 1.0×10^{-5} M; pH = 7.5, 40 °C in H_2O.

The progressive addition of uridine was able to inhibit the efficiency of the cleavage of HPNP by **AuNP1**, most probably due to the phosphate-uracil competition in binding to Zn(II)-TACN complex. However, it is important to underline that the amount of uridine needed to be in large excess by comparison to HPNP to observe any inhibiting effect.

Afterwards, pH-dependent kinetic studies were performed, which results are depicted in *Fig.6.21.* On the contrary to previously presented bell-shaped pH-profiles of another RNA model substrate HPNP, the result of UpPNP cleavage in the presence of **AuNP1** resembles the sigmoidal trend indicating that only one acid/base equilibrium is kinetically relevant.

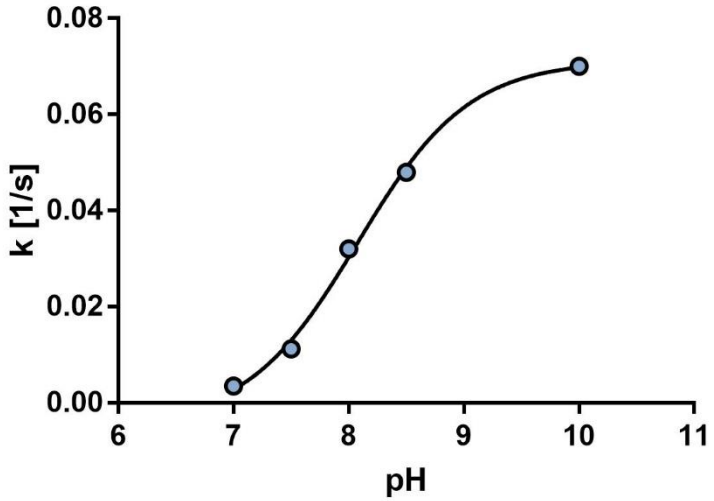

Fig.6.21. The function of reaction rate vs pH of the hydrolysis of uridine 3'-*p*-nitrophenyl phosphate by **AuNP1**. Conditions: [**AuNP1**] = [Zn(II)] = 5 x 10^{-6} M, [UpPNP] = 3.0 x 10^{-5} M, [buffers] = 1.0 x 10^{-2} M, T = 25°C in H_2O. Data fitted with Boltzman function.

In the case of pH profile for HPNP, the first deprotonation (p*Ka* = 7.9) had a positive impact on the catalysis (activation of the nucleophile), while the second p*Ka* (9.3) reflected a deprotonation of the second Zn(II)-coordinated water molecule, which saturateed its coordination sphere and therefore hampered the coordination to phosphates (*Fig.4.17.*, *Chapter 4*). In terms of the pH profile for uridine 3'-*p*-nitrophenyl phosphate, the first deprotonation also reflects activation of the nucleophile, suggesting a similar apparent critical p*Ka* (8.1) as with HPNP. However, further increase of pH was not diminishing the nanoparticles efficiency, which instead, was reaching a plateau. Accordingly, **AuNP1** seem to act as a general-base catalyst in the cleavage of UpPNP, hence upon increasing the pH, the amount of active nucleophile increases. Simultaneously, due to the possible interaction of Zn(II)-TACN complex with uracil, deprotonation of the second zinc-bound water molecule does not affect the phosphate-catalyst binding. In summary, one Zn(II)-TACN unit from a bimetallic catalytic site of **AuNP1** may be involved in the uracil binding, that keeps the second zinc complex in an optimal position towards the internal nucleophile of UpPNP, resulting in its activation.

*5. Kinetic Studies with 1,3-di(1,4,7-triazonan-1-yl)propan-2-ol (**4e**).*

The reactivity of **AuNP1** in the cleavage of nucleotides was compared with the zinc complex of already presented ligand (**4e**), whose synthesis was adapted from Kimura's reported protocol.[49] Taking advantage of the well-known crystal structure of Zn_2(**4e**), good reactivity in phosphodiester cleavage and the presence of a linked bimetallic unit constituted by two Zn(II)-TACN complexes, its studies were aimed to better understand and compare the interaction of Zn(II)-TACN-based **AuNP1** with uracil models.

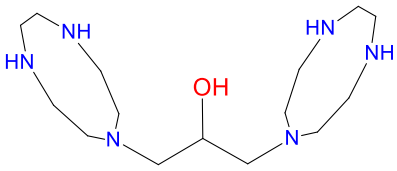

4e

The phosphodiester cleavage of HPNP, uridine 3'-*p*-nitrophenyl phosphate and uridylyl 3',5'-uridine (UpU) by Zn_2(**4e**) were thoroughly studied by Morrow *et al*.[50], [51] Comparing the reactivity of HPNP and UpPNP in the presence of Zn_2(**4e**), the authors claimed that the former was more strongly stabilized by the bimetallic catalyst than uridine 3'-*p*-nitrophenyl phosphate, mostly due to steric interactions between the catalyst and portions of non-reacting substrate ($\Delta\Delta G‡$ = 9.5 and 7.1 kcal x mol^{-1} for HPNP and UpPNP, respectively). Further studies with UpU showed its better stabilization ($\Delta\Delta G‡$ = 9.3 kcal x mol^{-1}) with Zn_2(**4e**) compared to UpPNP. Their justification inferred stronger interactions between the catalyst and C(5') oxyanion of the leaving group at the transition state rather than a stabilization of C(2') nucleophilic oxyanion of UpPNP. The researchers noticed a correlation between the number of uracil bases and the binding affinity for Zn(II)-TACN, based on inhibition studies with dimethyl phosphate. Better catalyst-substrate stabilization for UpU was probably influenced by interactions between the bimetallic Zn(II)-TACN and $N^-(3)$ of two uracil's pyrimidine rings. However, these interactions were considered as relatively weak. Furthermore, the authors observed a different effect of increased concentration of the catalyst for the cleavage of UpU and UpPNP (*Fig.6.22.(a),(b)*). Studies with the former substrate developed a small downward curvature under

almost 100-fold excess of the catalyst vs substrate *(Fig.6.22.(a)*), whereas the latter nucleotide revealed a saturation profile, even working with lower excess of catalyst (30-fold) than in the case of UpPNP *(Fig.6.22.(b)*). To conclude on the studies with Zn_2(**4e**) in phosphodiester cleavage, the authors claimed that more efficient catalysts should allow for a sufficient conformational flexibility for bulky nucleotides, followed by tethering a cationic core to a nucleoside recognition.

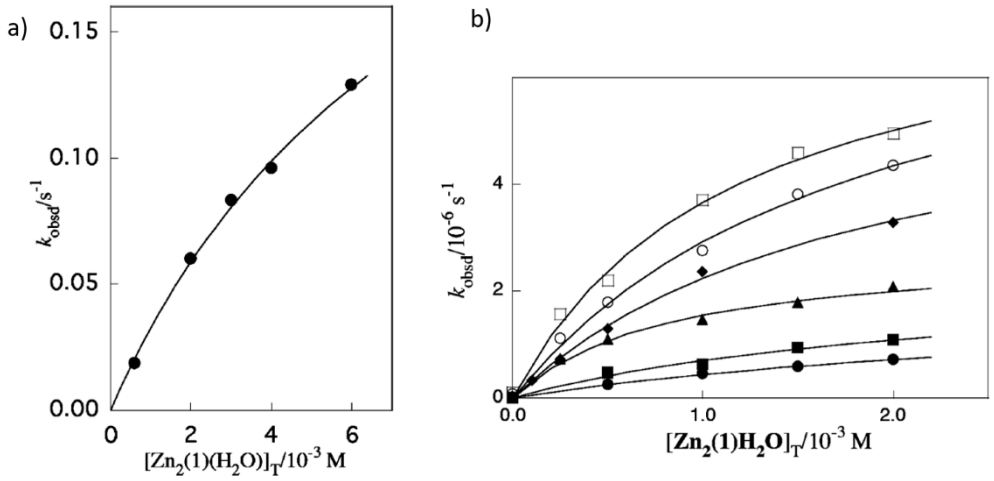

Fig.6.22. The first-order rate constant vs increasing concentrations of Zn_2(**4e**) in the cleavage of UpPNP (a) at pH 7.0 and UpU (*b*) at pH from 7.0 (●) to 9.8 (□).

The structural flexibility of adjacent zinc complexes of TACN, at the same time maintaining their optimal distance enabling creation a bimetallic unit, can be achieved with gold nanoparticles. Comparing the reactivity of **AuNP1** to Zn_2(**4e**) in the cleavage of RNA model substrates, nanozymes are 33- and 125-times more efficient in the hydrolysis of HPNP and UpPNP respectively, working with excess of both substrates in respect to catalysts (*Fig.6.23.*). While the presence of the bulky uracil evidently decreased the complex-substrate stability in the case of rigid Zn_2(**4e**), with **AuNP1** it can be easily accommodated, possibly providing the additional interaction with the catalyst.

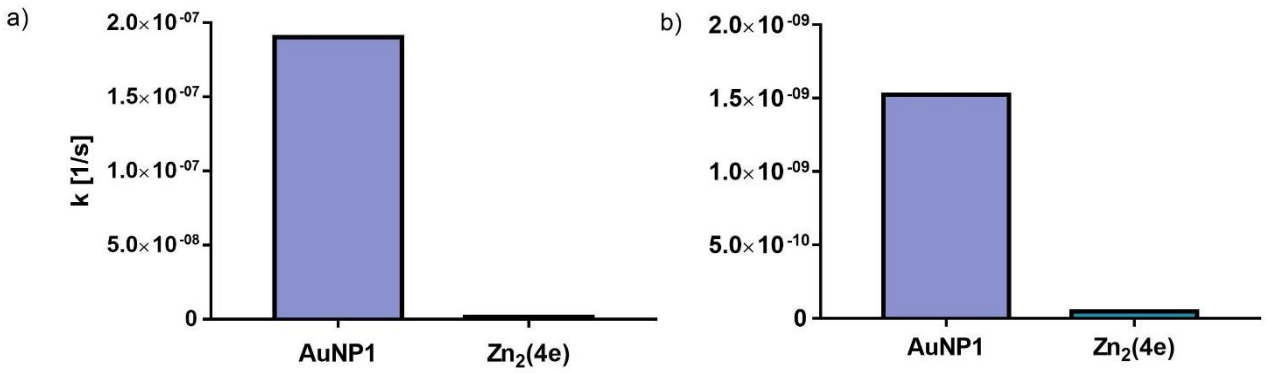

Fig.6.23. The reactivity of **AuNP1** and Zn_2(**4e**) in the cleavage of UpPNP (*a*) and HPNP (*b*). Conditions: [catalyst] = 5 x 10^{-6} M, [substrate] = 3.0 x 10^{-5} M, [HPNP] = 1.0 x 10^{-2} M, T = 25°C in H_2O.

As reported in *Fig.6.19(a),* increasing the concentration of UpPNP in the presence of **AuNP1** yielded a drop in the catalytic reactivity. However, the experiment performed under the same conditions with Zn_2(**4e**) resulted a linear trend. This may suggest a weak substrate binding to zinc-TACN complex (*Fig.6.24.*).

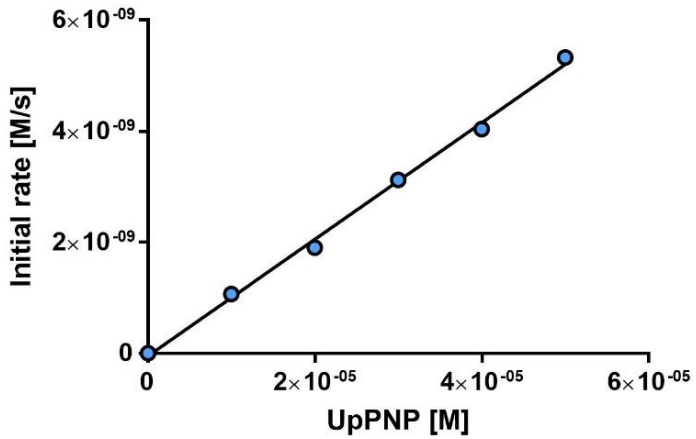

Fig.6.24. The hydrolysis of uridine 3′-*p*-nitrophenyl phosphate by Zn_2(**4e**) as the function of the initial rate *vs* increasing concentration of UpPNP. Conditions: [Zn_2(**4e**)] = 5.0 x 10^{-6} M, [HEPES]= 0.01 M, pH 7.5, 25 °C in H_2O.

The last studies were aimed at investigation of the relevance of the leaving group departure in the presence of Zn_2(**4e**). As with **AuNP1**, the cleavage pathway first led the formation of the cyclic phosphate diester (**2**), which was eventually cleaved into two isomeric phosphate monoesters (**3**) and (**4**) (*Fig.6.16*). Moreover, in this case it was possible to follow the cleavage of all phosphates, including the least reactive among studied RNA models, uridine 3'-(**LG**$_1$) phosphate. Collected data points depicted in *Fig.6.25*. (showing the abundance of different species present in the reaction mixtures) are clearly less scattered than those obtained with **AuNP1**, likely due to the greater stability of Zn_2(**4e**) compared to nanoparticles.

Furthermore, alike to **AuNP1** no isomerisation was observed throughout the course of uridine 3'-(LG) phosphates' cleavage in the presence of Zn_2(**4e**). Therefore, both discussed bimetallic catalysts were not able to stabilize dianionic penta-coordinated phosphorane.

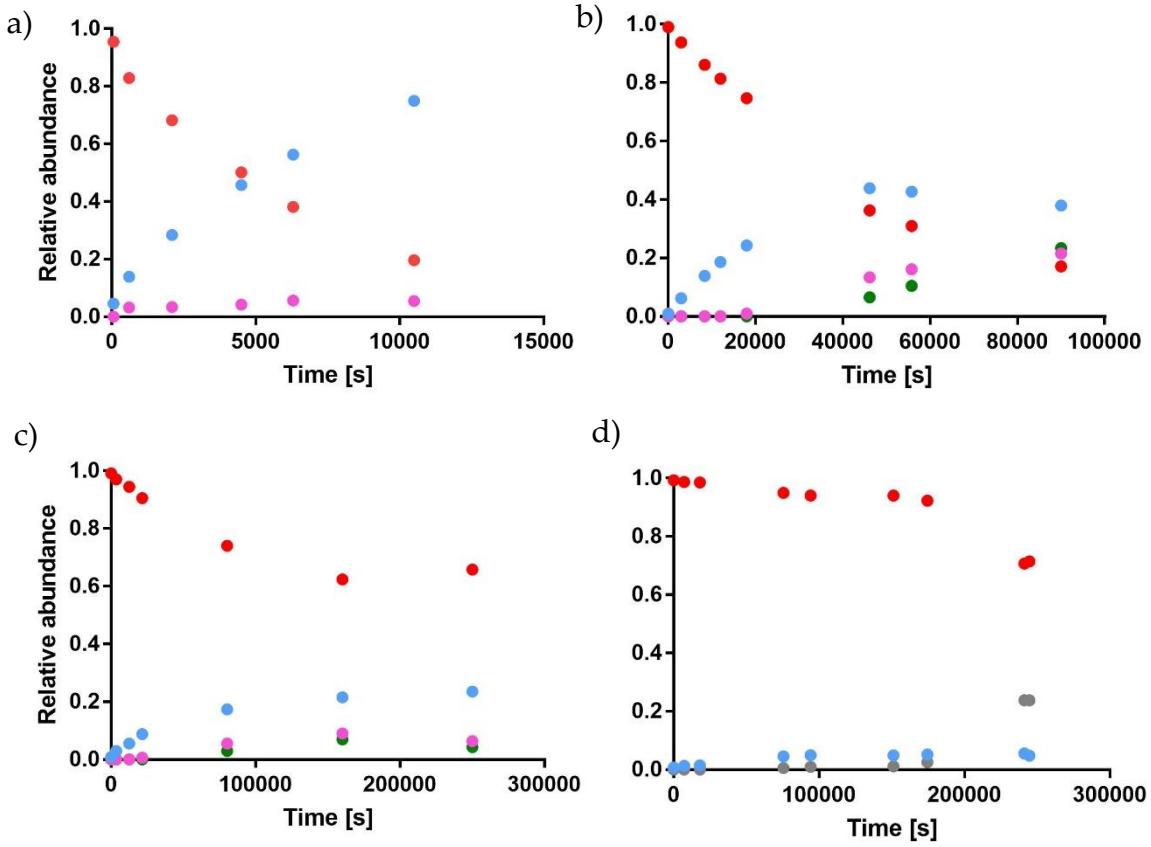

Fig.6.25. Dependence of the relative abundance *vs* time in cleavage of uridine 3′-(**LG**) phosphates by Zn_2(**4e**). Conditions: [Zn_2(**4e**)] = 5.0 x 10^{-5} M, [nucleosides]= 3.0 x 10^{-5} M, [HEPES]= 0.01 M, pH 7.5, 40 °C in H_2O. (a, $\mathbf{LG_4}$), (b, $\mathbf{LG_3}$), (c, $\mathbf{LG_2}$) and (d, $\mathbf{LG_1}$); red: uridine 3′-(**LG**) phosphate (**1**); blue: uridine 2′,3′-phosphate (**2**); pink: uridine 3′-phosphate (**3**); green: uridine 2′-phosphate (**4**).

As presented below in *Fig.6.26.*, the Brønsted plot trend is linear and reveals a β_{LG} equal to -0.59. This indicates that through the p*K*a of all studied leaving groups there was no change in the mechanism. Moreover, the slope of the Brønsted plot is comparable to one that can be drawn from studies performed by Mikkola *et al.* (β_{LG} = -0.66).[14] Both values are lower than that observed for the nanoparticle-based catalysis (β_{LG} = -0.86), indicating a less pronounced charge development in the transition state. This may suggest some assistance in leaving group departure by Zn_2(**4e**), although the major contribution still comes from a general base catalysis.

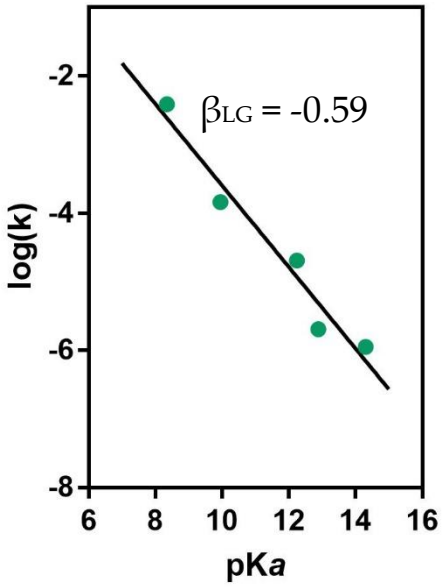

Fig.6.26. The Brønsted plot of uridine 3'-(LG) phosphates hydrolysis promoted by Zn_2(**4e**). Conditions: [Zn_2(**4e**)] = 5.0 x 10^{-5} M, [nucleosides]= 3.0 x 10^{-5} M, [HEPES]= 0.01 M, pH 7.5, 40°C in H_2O (R-square = 0.94298).

The reported value of the p*K*a for the kinetically relevant nucleophile in the reaction catalyzed by Zn_2(**4e**) (a Zn(II)-bound water molecule) is 7.8.[51] Accordingly, at the applied pH for all performed kinetic experiments (7.5), both general acid and base catalysis is possible. The position of two zinc ions in Zn_2(**4e**) alters to what could be attained in a dinuclear catalytic site of **AuNP1**, where two Zn(II) complexes are not held together in a precise geometry by the ligand. It may lead a different coordination of the substrate to the catalyst, allowing (at least partially) a general acid catalytic contribution in the case of Zn_2(**4e**).

6. Concluding Remarks.

Studies on the leaving group departure in uridine 3′-(LG) phosphates cleavage by **AuNP1** revealed a mechanism that did not change throughout the explored p*K*a range of leaving groups. Furthermore, a great negative value of the Brønsted constant suggested a significant development of anionic charge in the transition state.

The cleavage of uridine 3′-(LG) phosphates resulted in the formation of three products – cyclic phosphate (**2**), uridine 3′-phosphate (**3**) and uridine 2′-phosphate (**4**) (*Fig. 6.16*.). Considering the presented studies, the mechanism of the cleavage of uridine 3′-(LG) phosphates by **AuNP1** may be considered as concerted. At the same time, throughout the course of studies with both, aryl and alkyl LGs, no isomerisation was observed. Consequently, **AuNP1** were not able to protonate dianionic penta-coordinated species, resulting with its instability and inability to pseudorotate.
In terms of the catalytic role of **AuNP1** catalytic role, it appears that nanozymes efficiency relies mostly on a general base catalysis through the activation of the intramolecular nucleophile and very little (if any) contribution to the departure of the leaving group.

Additional studies with uridine 3′-*p*-nitrophenyl phosphate, and the zinc complex of 1,3-di(1,4,7-triazonan-1-yl)propan-2-ol (**4e**), provided additional information about Zn(II)-TACN interactions with uracil. The kinetics performed with UpPNP (*Fig. 6.19.(a)*) yielded a drop in the catalytic reactivity upon increasing the substrate's concentration, which can be interpreted as uracil-phosphate competition for Zn(II)-TACN binding. This was supported by competing inhibition experiments of HPNP cleavage in the presence of uridine (*Fig.6.20*.). However, uracil-zinc complex interactions cannot be considered as strong, since to observe inhibiting properties, uridine had to be present in a great excess compared to HPNP.

The reactivity and catalytic properties of **AuNP1** *vs* Zn_2(**4e**) in nucleotide cleavage revealed that, due to conformational flexibility, nanoparticles **1** were able to easily accommodate bulky substrates, contrary to what happens with the rigid Zn_2(**4e**). Therefore, **AuNP1** better stabilized electrostatic interactions between the catalyst and substrate's transition state. What is more, **AuNP1** may also benefit from many weak uracil - Zn(II)-TACN interactions, which may help in positioning the catalyst closer to electrophile. Working with an excess of UpPNP, Zn_2(**4e**) revealed a linear trend, evident for a weak substrate-catalyst binding (*Fig.6.24.*).

Lastly, results of studies on uridine 3'-(**LG_1**-**LG_5**) phosphates cleavage in the presence of Zn_2(**4e**) showed also a linear Brønsted plot (*Fig.6.26.*) and the obtained β_{LG} value (-0.59) may indicate either a modest bond breaking of the leaving group in the transition state or its protonation (different than that observed with **AuNP1**). With both studied catalysts, the initially formed cyclic phosphate (**2**) was eventually converted into the two isomeric phosphate monoesters (**3** and **4**). The amount of the intermediate cyclic phosphate (**2**) detected in the HPLC profiles clearly depended on the relative rate of formation of (**2**) and (**3** and **4**) and the time frame the reaction was followed.

7. *References of Chapter 6.*

[1] S. Mikkola, T. Lönnberg, H. Lönnberg, *Beilstein Journal of Organic Chemistry* **2018**, *14*, 803-837.

[2] H. Korhonen, S. Mikkola, N. H. Williams, *Chemistry – A European Journal* **2012**, *18*, 659-670.

[3] M. Kosonen, E. Youseti-Salakdeh, R. Strömberg, H. Lönnberg, *Journal of the Chemical Society, Perkin Transactions 2* **1997**, 2661-2666.

[4] S. Mikkola, E. Stenman, K. Nurmi, E. Yousefi-Salakdeh, R. Strömberg, H. Lönnberg, *Journal of the Chemical Society, Perkin Transactions 2* **1999**, 1619-1626.

[5] S. Kuusela, H. Lönnberg, *Journal of Physical Organic Chemistry* **1993**, *6*, 347-356.

[6] R. Breslow, D. L. Huang, *Proceedings of the National Academy of Sciences* **1991**, *88*, 4080.

[7] A. M. Davis, A. D. Hall, A. Williams, *Journal of the American Chemical Society* **1988**, *110*, 5105-5108.

[8] M. K. Stern, J. K. Bashkin, E. D. Sall, *Journal of the American Chemical Society* **1990**, *112*, 5357-5359.

[9] S. Kuusela, M. Rantanen, H. Lönnberg, *Journal of the Chemical Society, Perkin Transactions 2* **1995**, 2269-2273.

[10] S. Kuusela, H. Lönnberg, *Nucleosides and Nucleotides* **1998**, *17*, 2417-2427.

[11] D. Wahnon, R. C. Hynes, J. Chin, *Journal of the Chemical Society, Chemical Communications* **1994**, 1441-1442.

[12] K. O. A. Chin, J. R. Morrow, *Inorganic Chemistry* **1994**, *33*, 5036-5041.

[13] S. Kuusela, H. Lönnberg, *Journal of the Chemical Society, Perkin Transactions 2* **1994**, 2301-2306.

[14] H. Korhonen, T. Koivusalo, S. Toivola, S. Mikkola, *Organic & Biomolecular Chemistry* **2013**, *11*, 8324-8339.

[15] T. Gajda, A. Jancsó, S. Mikkola, H. Lönnberg, H. Sirges, *Journal of the Chemical Society, Dalton Transactions* **2002**, 1757-1763.

[16] A. Jancsó, S. Mikkola, H. Lönnberg, K. Hegetschweiler, T. Gajda, *Chemistry – A European Journal* **2003**, *9*, 5404-5415.

[17] N. H. Williams, J. Chin, *Chemical Communications* **1996**, 131-132.

[18] H. Aït-Haddou, J. Sumaoka, S. L. Wiskur, J. F. Folmer-Andersen, E. V. Anslyn, *Angewandte Chemie International Edition* **2002**, *41*, 4013-4016.

[19] C. L. Hannon, E. V. Anslyn, in *Bioorganic Chemistry Frontiers* (Eds.: H. Dugas, F. P. Schmidtchen), Springer Berlin Heidelberg, Berlin, Heidelberg, **1993**, pp. 193-255.

[20] H. Lönnberg, R. Strömberg, A. Williams, *Organic & Biomolecular Chemistry* **2004**, *2*, 2165-2167.

[21] Q. Wang, H. Lönnberg, *Journal of the American Chemical Society* **2006**, *128*, 10716-10728.

[22] S. Liu, A. D. Hamilton, *Bioorganic & Medicinal Chemistry Letters* **1997**, *7*, 1779-1784.

[23] M. Yashiro, A. Ishikubo, M. Komiyama, *Chemical Communications* **1997**, 83-84.

[24] F. Vella, *Biochemical Education* **1983**, *11*, 121-122.

[25] T. R. Cech, *Science (New York, N.Y.)* **1987**, *236*, 1532.

[26] J. A. McClarin, C. A. Frederick, B. C. Wang, P. Greene, H. W. Boyer, J. Grable, J. M. Rosenberg, *Science (New York, N.Y.)* **1986**, *234*, 1526.

[27] E. Kikuta, M. Murata, N. Katsube, T. Koike, E. Kimura, *Journal of the American Chemical Society* **1999**, *121*, 5426-5436.

[28] E. Kikuta, S. Aoki, E. Kimura, *JBIC Journal of Biological Inorganic Chemistry* **2002**, *7*, 473-482.

[29] E. Kimura, M. Kikuchi, H. Kitamura, T. Koike, *Chemistry – A European Journal* **1999**, *5*, 3113-3123.

[30] E. Kimura, H. Kitamura, K. Ohtani, T. Koike, *Journal of the American Chemical Society* **2000**, *122*, 4668-4677.

[31] S. Aoki, E. Kimura, *Journal of the American Chemical Society* **2000**, *122*, 4542-4548.

[32] E. Kimura, T. Shiota, T. Koike, M. Shiro, M. Kodama, *Journal of the American Chemical Society* **1990**, *112*, 5805-5811.

[33] T. Koike, E. Kimura, I. Nakamura, Y. Hashimoto, M. Shiro, *Journal of the American Chemical Society* **1992**, *114*, 7338-7345.

[34] E. Kimura, T. Koike, T. Shiota, Y. Iitaka, *Inorganic Chemistry* **1990**, *29*, 4621-4629.

[35] C. Rossiter, R. Mathews, J. Morrow, *Inorganic chemistry* **2006**, *44*, 9397-9404.

[36] G. C. Silver, P. Gantzel, W. C. Trogler, *Inorganic Chemistry* **1995**, *34*, 2487-2489.

[37] O. Iranzo, A. Y. Kovalevsky, J. R. Morrow, J. P. Richard, *Journal of the American Chemical Society* **2003**, *125*, 1988-1993.

[38] S. Liu, A. D. Hamilton, *Chemical Communications* **1999**, 587-588.

[39] P. International Union of, C. Applied, D. Commission on Equilibrium, E. P. Serjeant, B. Dempsey, P. International Union of, C. Applied, D. Commission on

Electrochemical, *Ionisation constants of organic acids in aqueous solution*, Pergamon Press, Oxford; New York, **1979**.

[40] H. Almer, R. Strömberg, *Journal of the American Chemical Society* **1996**, *118*, 7921-7928.

[41] D. P. L. Green, T. Ravindranathan, C. B. Reese, R. Saffhill, *Tetrahedron* **1970**, *26*, 1031-1041.

[42] B. E. Griffin, M. Jarman, C. B. Reese, *Tetrahedron* **1968**, *24*, 639-662.

[43] J. Stawinski, R. Strömberg, *Current Protocols in Nucleic Acid Chemistry* **2001**, *4*, 2.6.1-2.6.15.

[44] P. J. Garegg, T. Regberg, J. Stawiński, R. Stromberg, *Chem. Scr.* **1986**, *26*, 59-62.

[45] J. Stawinski, M. Thelin, *Nucleosides and Nucleotides* **1990**, *9*, 129-135.

[46] J. Jankowska, M. Sobkowski, J. Stawiński, A. Kraszewski, *Tetrahedron Letters* **1994**, *35*, 3355-3358.

[47] J. E. Marugg, M. Tromp, E. Kuyl-Yeheskiely, G. A. van der Marel, J. H. van Boom, *Tetrahedron Letters* **1986**, *27*, 2661-2664.

[48] A. Jancsó, S. Mikkola, H. Lönnberg, K. Hegetschweiler, T. Gajda, **2003**, *9*, 5404-5415.

[49] E. Kimura, S. Aoki, T. Koike, M. Shiro, *Journal of the American Chemical Society* **1997**, *119*, 3068-3076.

[50] M.-Y. Yang, J. P. Richard, J. R. Morrow, *Chemical Communications* **2003**, 2832-2833.

[51] A. O'Donoghue, S. Y. Pyun, M.-Y. Yang, J. R. Morrow, J. P. Richard, *Journal of the American Chemical Society* **2006**, *128*, 1615-1621.

Chapter 7

1. Materials and Instruments.

Solvents and all commercially available reagents were purchased from Sigma or Fluka and used as received. Chromatography columns were carried out on Macherey-Nagel silica gel 60 (70-230 mesh). TLC analyses were performed using Merck 60 F_{254} precoated silica gel glass plates.

NMR spectra were recorded using a Bruker AV III 500 spectrometer operating at 500 MHz for ^{1}H, 125.8 MHz for ^{13}C. Transmission Electron Microscopy (TEM) images were taken on Jeol 300 PX Electron Microscope (one drop of the concentrated AuNPs solution was placed on the sample grid and utilized solvent was allowed to evaporate itself). ESI-MS mass spectra were obtained with an Agilent Technologies LC/MSD Trap SL Mass Spectrometer. Thermogravimetric Analysis (TGA) runs were performed using a Q5000 IR model TA instrument from 30 to 1000°C under a continuous air flow (on 0.8 - 2 mg of nanoparticle sample).

$Zn(NO_3)_2$ concentration was determined by Atomic Absorption Spectroscopy technique, using Perkin Elmer 1100 instrument. Utilized for the kinetic experiments buffers are following: 2-morpholinoethanesulfonic acid (MES), 4-(2-hydroxyethyl)-1-piperazine-ethanesulfonic acid (HEPES), 4-(2-hydroxyethyl)-1- piperazine-propanesulfonic acid (EPPS), 2-[N-cyclohexylamino]ethanesulfonic acid (CHES), 3-[cyclohexylamino]1-propanesulfonic acid (CAPS).

2. HPNP, BNP and Plasmid DNA Cleavage – Experimental Details.

HPNP/BNP cleavage: Kinetic experiments were performed with Varian Cary 50 spectrophotometer equipped with thermostatic multiple cell holders. AuNPs aqueous stock solution concentrations, being approximated as a [TACN units], were determined by Zn(II) dependent kinetic experiments. HPNP/BNP conversion was monitored by the increase of the absorption at 400 nm of *p*-nitrophenoxide. The initial rate of each run was calculated by a linear fitting of kinetics profiles (considered conversion did not overpass 10-15%). HPNP/BNP concentration dependent kinetic experiments were fitted with the Origin 8.0 software, in accordance to Michaelis-Menten equation:

$$v = \frac{v_{max}[HPNP]}{K_M + [HPNP]}$$

Where v is the reaction initial rate, v_{max} is the limiting reaction rate in the experimental conditions and K_M is the binding constant of HPNP/BNP (substrate) to the nanoparticles (catalyst). For **AuNP1-3** k_{cat} values were obtained by dividing v_{max} by [Zn(II)]/2 (since the reaction is considered to occur in bimetallic sites).

Plasmid DNA cleavage: Reactions were performed incubating plasmid DNA, pBR322 (Gibco BRL; 19 μM base pairs) at 37°C in the presence/absence of Zn(II) in 20 mM HEPES (apart from pH-dependent kinetic studies) at indicated time. A gel was prepared by mixing and heating an agarose powder with TAE buffer and 10% SDS (sodium dodecyl sulfate) to dissociate AuNPs from DNA. As a DNA loading dye, a mixture containing bromophenol blue, glycerol, 10% SDS and 0.1 M pH 7.5 HEPES was used. Loaded gels were run for 1.5 hour at 100 V until the dye line was approximately 80% of the way down gels. Resolved bands were visualized by staining gels in ethidium bromide and subsequently photographed. The quantification of different plasmid forms was performed using a BioRad Gel Doc 1000 apparatus interfaced to a PC workstation.

3. *Synthetic Protocols.*

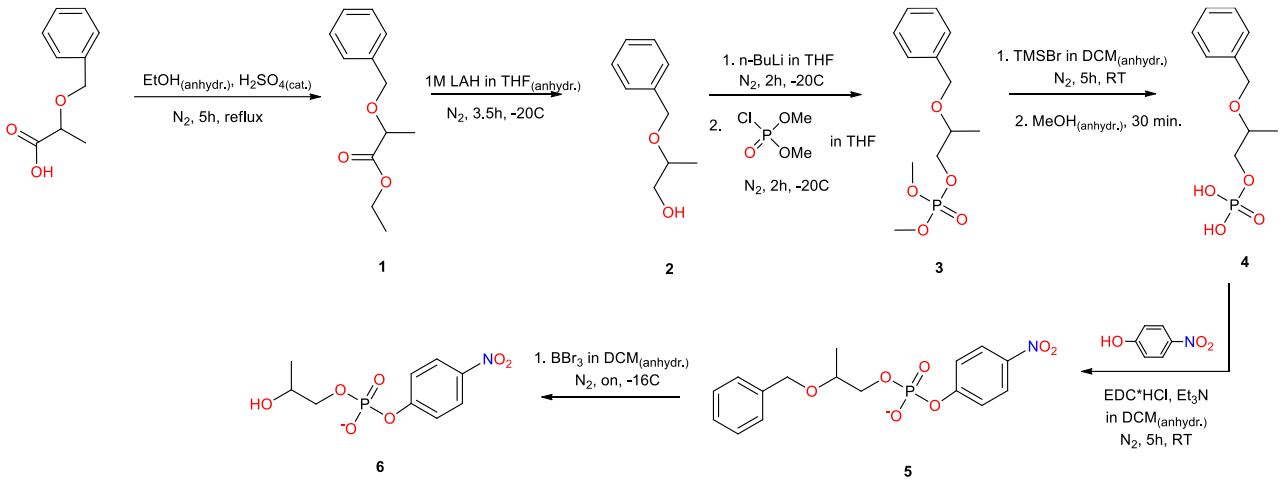

Scheme E.1

Ethyl 2-(benzyloxy)propanoate (**1**): In a two-neck round-bottom flask, (*R*)-2-(benzyloxy)propanoic acid (1.0 g, 5.4 mmol) was dissolved in 10 mL of anhydrous ethanol. Afterwards, a few drops of 98% sulphuric acid were added and resulting mixture was refluxed for 5 hours under nitrogen. The crude was cooled down and concentrated *in vacuo*. The residue was neutralized with saturated solution of sodium bicarbonate and extracted with ethyl acetate. Collected organic phases were washed with brine and eventually dried over magnesium sulphate. The ethyl acetate was evaporated and the pure product collected as a white solid (97% yield). [1], [2], [3], [4]

^{1}H-NMR ($CDCl_3$, 500 MHz), δ: 7.28-7.16 (m, 5H), 4.60 (d, J = 11.6 Hz, 1H), 4.35 (d, J = 11.6 Hz, 1H), 4.14-4.10 (m, 2H), 3.95 (q, J = 6.9 Hz, 1H), 1.34 (d, J = 6.9 Hz, 3H), 1.20 (t, J = 7.1 Hz, 3H)

^{13}C-NMR ($CDCl_3$, 500 MHz), δ: 173.7, 138.0, 129.0, 128.8, 128.2, 74.46, 72.38, 72.38, 61.23, 19.10, 14.63

ESI-MS (m/z): 209.0 $[M + H]^+$, 231.0 $[M + Na]^+$

2-(Benzyloxy)propan-1-ol (**2**): In a three-neck round-bottom flask equipped with thermometer, (**1**) (1.1g, 5.3 mmol, 1.0 eq.) was dissolved in 10 mL of anhydrous tetrahydrofuran under nitrogen. The mixture was cooled down to -20°C in an ice-acetone

bath and then lithium aluminium hydride (1M LAH in THF; 6.4 mL, 1.2 eq.) was added dropwise for 1 hour. After the addition was complete, the reaction was stirred at room temperature for 3.5 hours. Next, the reaction mixture was hydrolysed with saturated aqueous solution of NH_4Cl, ending up with the precipitation of a white solid. The mixture was filtered off, washed with THF and the filtrate was consecutively concentrated. The oily residue was extracted with ethyl acetate, collected organic phases were washed with brine and dried over magnesium sulphate. Desired product formed a colourless oil (75% yield).

^{1}H-NMR ($CDCl_3$, 500 MHz), δ: 7.27-7.17 (m, 5H), 4.57 (d, J = 11.6 Hz, 1H), 4.40 (d, J = 11.6 H, 1H), 3.62-3.57 (m, 1H), 3.54-3.51 (m, 1H), 3.43-3.39 (m, 1H), 1.09 (d, J = 6.2 Hz, 3H)
^{13}C-NMR ($CDCl_3$, 500 MHz), δ: 138.8, 128.9, 128.1, 75.93, 71.19, 66.77, 16.25
ESI-MS (m/z): 167.0 $[M + H]^+$, 189.0 $[M + Na]^+$

2-(Benzyloxy)propyl dimethyl phosphate (**3**): In a three-neck round-bottom flask equipped with thermometer, (**2**) (654 mg, 3.9 mmol, 1.0 eq.) was dissolved in 20 mL of anhydrous THF. The mixture was cooled down to -20°C in the ice-acetone bath and afterwards n-butyl lithium (2.5M solution in hexane; 1.6 mL, 4.1 mmol, 1.1 eq.) was added dropwise for 2 hours. After the whole addition the reaction was stirred at room temperature for 2 hours. After that time, the mixture was cooled down to -20°C and next dimethyl chlorophosphate (620 mg, 460 μL, 4.3 mmol, 1.1 eq.) was added dropwise for 30 minutes. When the addition was complete, the reaction mixture was stirred at room temperature for 2.5 hours. The crude was cooled down and hydrolysed with saturated aqueous solution of NH_4Cl, ending up with the precipitation of a white solid. The mixture was filtered off, washed with THF and the filtrate was consecutively concentrated. The oily residue was extracted with ethyl acetate, the organic phase was additionally washed with saturated solution of sodium bicarbonate and brine. Collected organic phases were dried over magnesium sulphate and after evaporation of the solvent the remaining yellow oil was purified by flash chromatography (ethyl acetate/hexane 55/45-66/34). The desired product was obtained as a colourless oil (86% yield).

^{1}H-NMR ($CDCl_3$, 500 MHz), δ: 7.27-7.17 (m, 5H), 4.54-4.49 (m, 2H), 3.97-3.94 (m, 2H), 3.71-3.65 (m, 7H), 1.13 (d, 3H)

^{13}C-NMR ($CDCl_3$, 500 MHz), δ: 138.42, 127.8, 127.7, 73.41, 71.24, 70.41, 54.37, 16.61

^{31}P-NMR ($CDCl_3$, 500 MHz), δ: 1.31

ESI-MS (m/z): 275.1 $[M + H]^+$, 297.1 $[M + Na]^+$, 313.0 $[M + K]^+$

2-(Benzyloxy)propyl dihydrogen phosphate (**4**): In a two-necked round-bottom flask previously purged with nitrogen, (**3**) (204 mg, 0.74 mmol, 1.0 eq.) was dissolved in 20 mL of anhydrous DCM. Afterwards bromotrimethyl silane (566.4 mg, 488 μL, 3.7 mmol, 5.0 eq.) was added dropwise. When the addition was complete, the mixture was left stirring at room temperature for 5 hours under nitrogen. The crude was concentrated *in vacuo* and remaining orange oil was re-dissolved in 20 mL of methanol. The mixture was consecutively stirred for 30 minutes, then the methanol was removed. The obtained oily product was used without any additional purification in the next step (quantitative yield).

^{1}H-NMR ($CDCl_3$, 500 MHz), δ: 7.37-7.24 (m, 5H), 4.56-4.44 (m, 2H), 4.00-7.70 (m, 3H), 1.12 (d, 3H)

^{13}C-NMR ($CDCl_3$, 500 MHz), δ: 137.7, 128.9, 128.4, 74.19, 71.80, 70.29, 16.85

^{31}P-NMR ($CDCl_3$, 500 MHz), δ: -0.620

ESI-MS (m/z): 247.0 $[M + H]^+$, 269.0 $[M + Na]^+$

2-(Benzyloxy)propyl (4-nitrophenyl) phosphate (**5**): In a two-necked round bottom flask previously purged with nitrogen, (**4**) (183 mg, 0.73 mmol, 1.0 eq.) was dissolved in 20 mL of anhydrous DCM. The mixture was cooled down in an ice-bath for 15 minutes and afterwards triethylamine (TEA; 393.3 mg, 508 μL, 3.7 mmol, 5.0 eq.) and *N*-(3-dimethylaminopropyl)-*N*′-ethyl-carbodiimide hydrochloride (EDC*HCl; 419 mg, 2.2 mmol, 3.0 eq.) were added. After 10 minutes more, *p*-nitrophenol (101.5 mg, 0.73 mmol, 1.0 eq.) solubilized in 5 mL of DCM was added dropwise. When the addition was complete, the mixture was stirred at room temperature for 8 hours under nitrogen. The crude was

concentrated *in vacuo* and purified by column chromatography (chloroform/ methanol 100/0-70-30) yielding a white solid (33% yield).

^{1}H-NMR ($CDCl_3$, 500 MHz), δ: 8.08 (d, J = 9.0 Hz, 1H), 7.89 (d, 8.5 Hz, 2H), 7.26-7.11 (m, 6H), 6.86 (d, J = 8.8 Hz, 1H), 4.40-4.20 (m, 2H), 3.89-3.46 (m, 3H), 0.93 (d, 3H)

^{31}P-NMR ($CDCl_3$, 500 MHz), δ: -6.20

ESI-MS (m/z): 365.9 $[M - H]^-$, 368.1 $[M + H]^+$, 390.1 $[M + Na]^+$, 412.1 $[M + 2Na]^+$

2-Hydroxypropyl *p*-nitrophenyl phosphate (**6**): In a two-necked round bottom flask previously purged with nitrogen, (**5**) (531 mg, 1.45 mmol, 1.0 eq.) was dissolved in 10 mL of anhydrous DCM. The mixture was cooled down in the ice-acetone bath for 20 minutes and afterwards boron tribromide (BBr_3; 1M in DCM; 5.8 mL, 5.8 mmol, 4.0 eq.) was rapidly added. The mixture was allowed to warm up to room temperature and left stirring overnight under nitrogen. Afterwards the crude was cooled down in an ice-bath followed by the hydrolysis of remaining BBr_3 by adding a water. The resulting mixture was concentrated *in vacuo* and purified by preparative RP HPLC (36-minute run, RT=15.4 min., 0-100% ACN + 0.05% TFA, λ=214 nm). Collected fractions were lyophilised and remaining product was analysed by ESI-MS showing its high purity and desired mass. However, collected fractions enabled to obtain a sufficient amount of material to perform its further characterisation (4% yield).

ESI-MS (m/z): 275.9 $[M - H]^-$

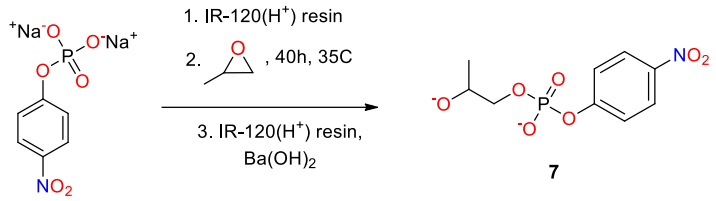

Scheme E.2

2-Hydroxypropyl *p*-nitrophenyl phosphate, barium salt (**7**): 4-nitrophenyl phosphate disodium salt (1.9 g, 5.0 mmol, 1.0 eq.) was dissolved in 10 mL of distilled water. The solution was passed through an ion-exchange resin (IR-120 (H+) resin). The acid effluent was alkalized to pH 8.0 with an aqueous solution of ammonia. Following this, 1,2-epoxypropane (20 mL, 17.0 mmol, 3.4 eq.) was added and the reaction was stirred at 40°C for 2 days and any unreacted epoxide was removed *in vacuo*. The remaining liquid was diluted with a small amount of water and passed through an ion-exchange resin ((IR-120 (H+) resin). The aqueous solution was carefully neutralized to pH 6.5-7.0 with an aqueous solution of barium hydroxide (carbonate-free) and then concentrated *in vacuo* at room temperature until the volume was reduced to 70%. Ethanol (2 vol.) was added and the white precipitate was filtered off. The filtrate was concentrated and added to vigorously stirring 10% solution of ethanol in acetone (300 ml). The mixture was stirred for additional 1 hour. After that time a white precipitate was filtered off and dried under high pressure. Desired compound was obtained as a white fluffy solid (46% yield).[5]

^{1}H-NMR (D_2O, 500 MHz), δ: 8.26 (d, 2H), 7.36 (d, 2H), 4.02-3.82 (m, 3H), 1.15 (d, 3H)

^{13}C-NMR (D_2O, 500 MHz), δ: 157.3, 143.4, 125.8, 120.4, 71.00, 66.48, 17.64

ESI-MS (m/z): 275.8 $[M]^-$

^{31}P-NMR (D_2O, 500 MHz), δ: -4.83, -4.86, -4.89

Elemental Analysis ($C_{18}H_{22}BaN_2O_{14}P_2$): Called- C: 31.35, H: 3.22, N: 4.06; Found- C: 30.95, H: 3.23, N: 3.37

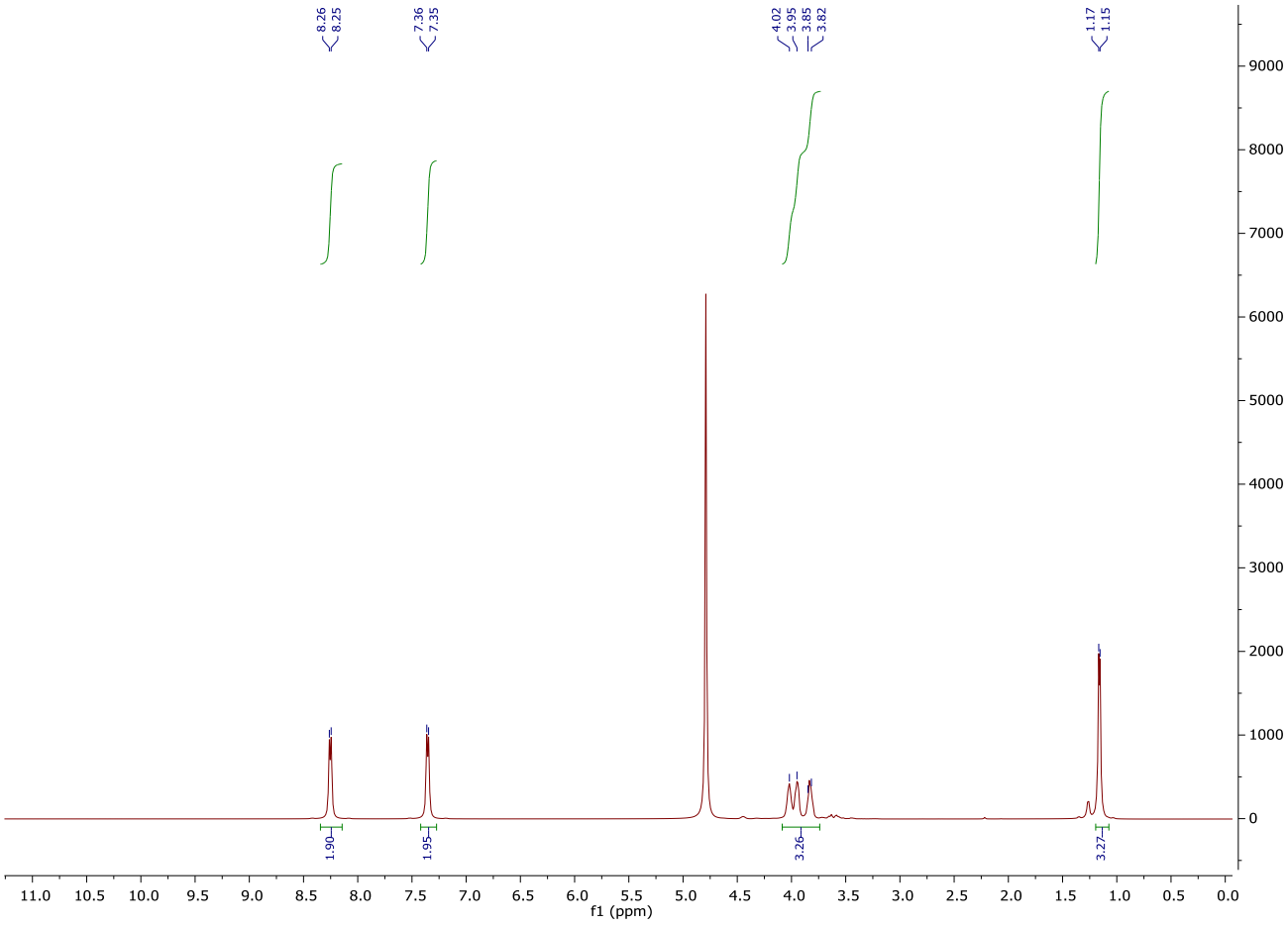

Fig.E.3. ^{1}H-NMR (500 MHz) spectrum of HPNP in D_2O.

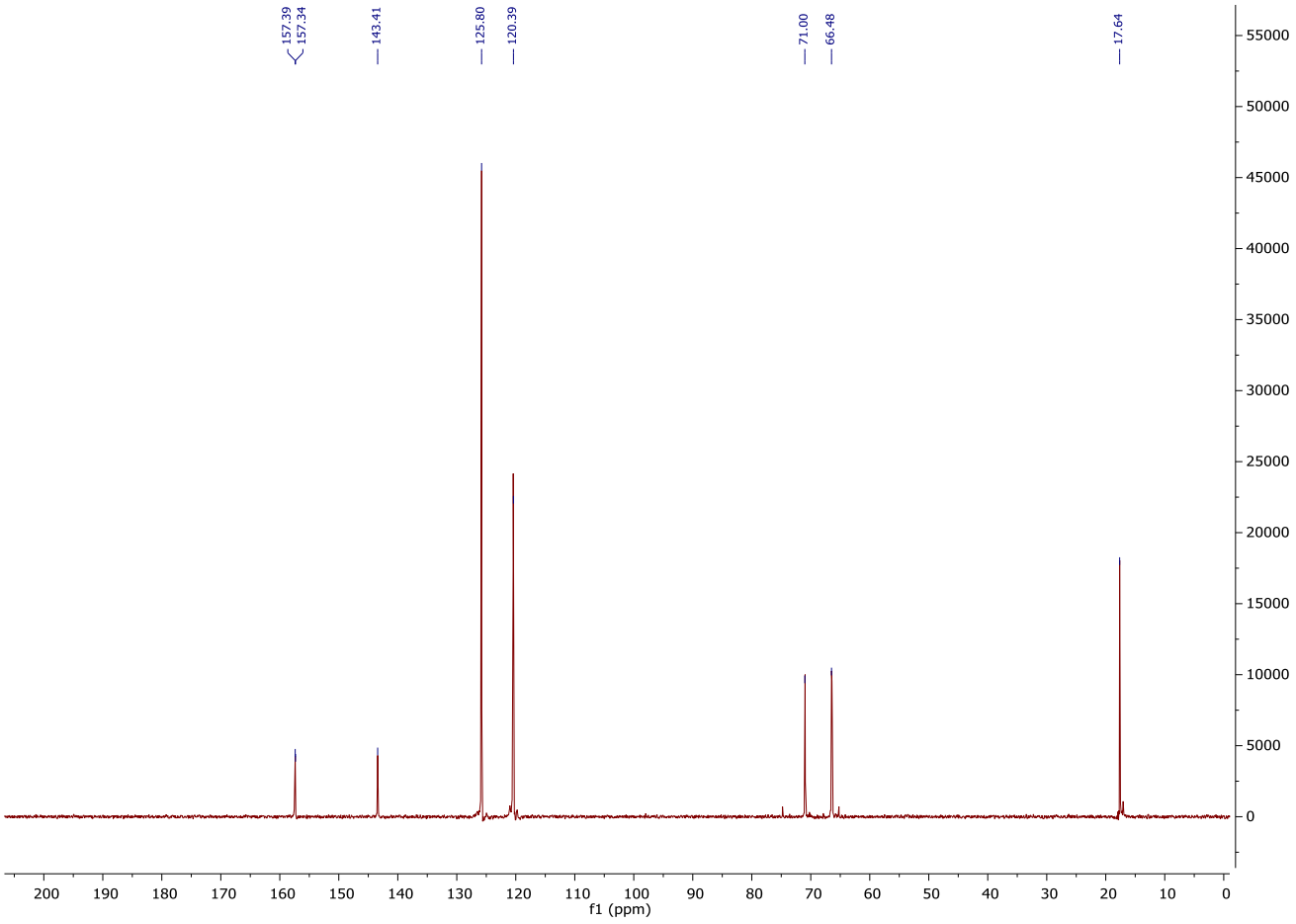

Fig.E.4. ^{13}C-NMR (500 MHz) spectrum of HPNP in D_2O.

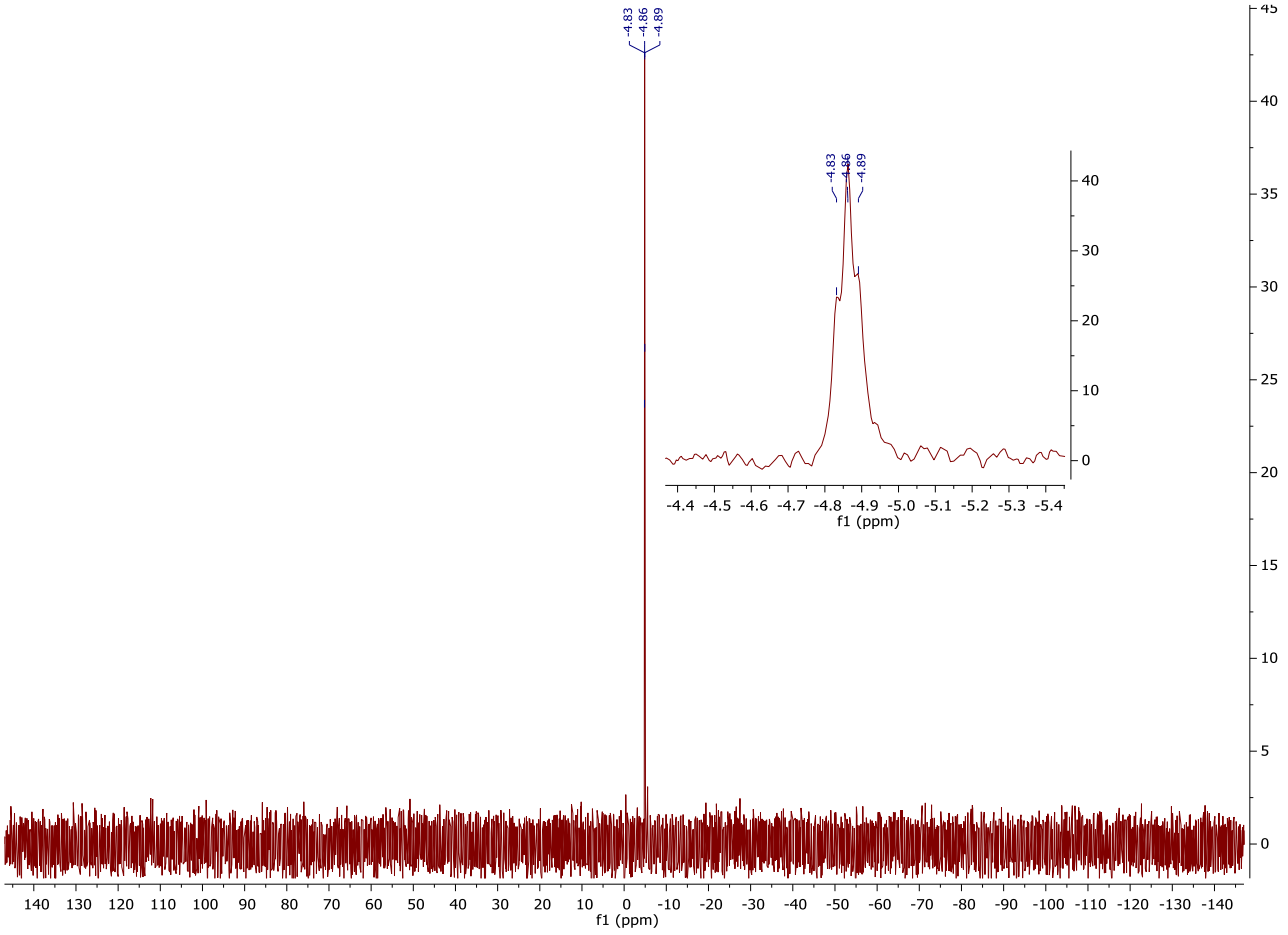

Fig.E.5. ^{31}P-NMR (500 MHz) spectrum of HPNP in D_2O.

3.1. The Synthesis of Gold Nanoparticles.

The synthesis of AuNPs was performed using the method published by Scrimin.[6]

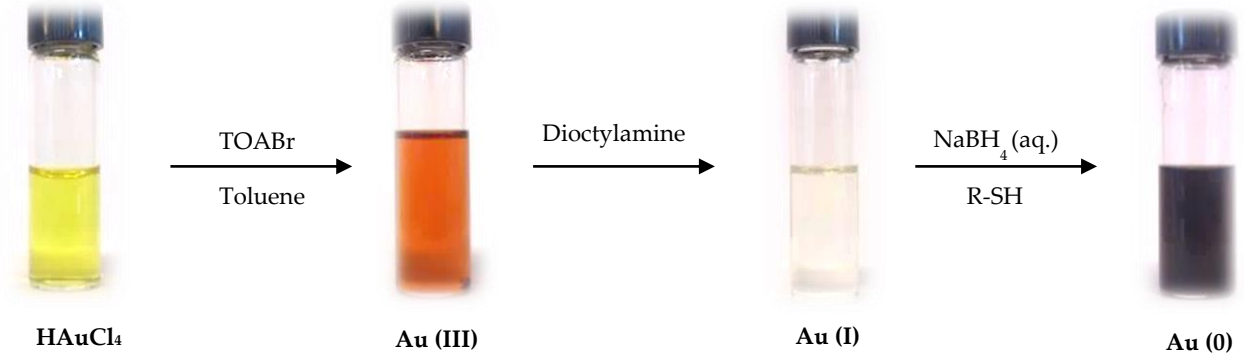

Fig.E.6.[6a]

All the glassware was washed with Aqua Regia and rinsed with distilled water. The aqueous solution of tetrachloroauric (III) acid trihydrate ($HAuCl_4 \cdot 3H_2O$; 50 mg, 0.13 mmol, 1.0 eq.) was extracted with tetraoctylammonium bromide (213 mg, 0.39 mmol, 3.0 eq.) previously dissolved in 125 mL of degassed toluene. To the red-orange organic phase, dioctylamine (628 mg, 786 µL, 2.6 mmol, 20 eq.) was added. The mixture was vigorously stirred at room temperature under nitrogen for 30 minutes. During that time the colour changed from an orange to colourless. The flask was placed in an ice-bath and then aqueous solution of sodium borohydride ($NaBH_4$; 49.1 mg, 1.3 mmol, 10 eq.) was rapidly added. The colour changed immediately to brownish-black due to nanoparticles' formation. After 2-hour stirring, a small amount of left water was removed. Keeping the reaction under an ice-bath, desired thiol (0.26 mmol, 2.0 eq.) dissolved in methanol was added to the solution and then the reaction was left stirring for additional 2 hours. AuNPs were purified by their sonication and washing with different solvents (hexane, toluene, petroleum ether, ethyl acetate and methanol). Eventually, their concentrated solution was applied on the gel permeation chromatography with Sephadex G-25 resin.

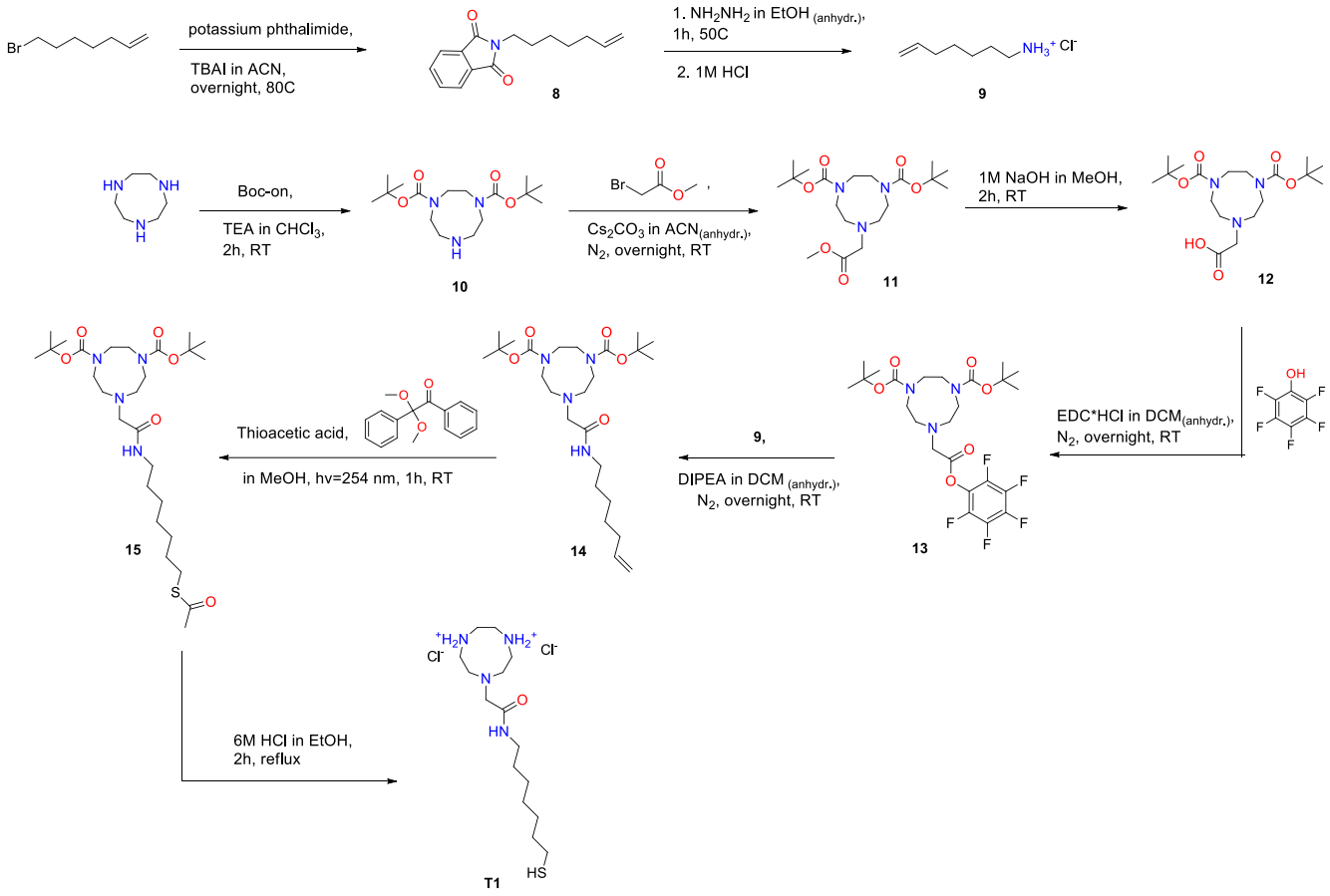

Scheme E.7.

2-(Hept-6-en-1-yl)isoindoline-1,3-dione (8): In a round-bottom flask, tetrabutylammonium iodide (47.1 mg, 0.1 mmol, 0.02 eq.) and potassium phthalimide (2.1 g, 11.3 mmol, 2.0 eq.) were suspended in 30 mL of acetonitrile. 7-bromohept-1-ene (1.0 g, 860 µL, 5.65 mmol, 1.0 eq.) was added dropwise and the resulting mixture was heated up to 80°C for exactly 24 hours. Once the mixture reached room temperature, it was diluted with diethyl ether and passed through a celite plug. The filtrate was concentrated *in vacuo* and the yellow residue was purified by column chromatography (hexane/ethyl acetate 95/5) giving the desired product as a white solid (83% yield).

^{1}H-NMR ($CDCl_3$, 500 MHz), δ: 7.85-7.82 (m, 2H), 7.72-7.69 (m, 2H), 5.82-5.76 (m, 1H), 5.00-4.91 (m, 2H), 3.68 (t, 2H), 2.04 (q, 2H), 1.68 (m, 2H), 1.45-1.34 (m, 4H)

^{13}C-NMR ($CDCl_3$, 500 MHz), δ: 168.9, 139.4, 134.2, 132.6, 123.6, 114.7, 36.44, 34.06, 29.12, 27.11

Hept-6-en-1-amonium chloride (9): In a glass tube (**8**) (500 mg, 1.1 mmol, 1.0 eq.) was dissolved in 10 mL of anhydrous ethanol and heated up to 50°C. Hydrazine (NH_2NH_2 65% monohydrate; 183 mg, 177 μL, 2.7 mmol, 1.5 eq.) was added and the resulting mixture was stirred at reflux for 1 hour under nitrogen. The obtained white slurry was quenched with 10 mL of 6M hydrochloric acid and stirred for an additional 30 minutes. The white solid was filtered off and washed several times with ethanol. The remaining filtrate was concentrated *in vacuo* and the residual aqueous solution was alkalized with 1M sodium hydroxide (pH = 9) and then extracted with chloroform. The collected organic phases were then extracted with 1M hydrochloric acid, water phases concentrated *in vacuo* resulting with desired product as a pale-yellow solid (86% yield).

^{1}H-NMR (D_2O, 500 MHz), δ: 5.95-5.89 (m, 1H), 5.09-4.99 (m, 2H), 3.00 (t, 2H), 2.11-2.07 (m,2H), 1.70-1.66 (m, 2H), 1.45-1.38 (m, 4H)

^{13}C-NMR (D_2O, 500 MHz), δ: 139.7, 114.3, 39.45, 32.70, 27.41, 26.48, 25.01

Di-tert-butyl-1,4,7-triazonane-1,4-dicarboxylate (10): In a round-bottom flask, the white powder of 1,4,7-triazacyclononane (TACN; 1.0 g, 7.74 mmol, 1.0 eq.) together with triethylamine (TEA; 2.32 g, 3.2 mL, 23.0 mmol, 3.0 eq.) was dissolved in 30 mL of chloroform and cooled in an ice bath. [2-(tert-butoxycarbonyloxyimino)-2-phenylacetonitrile] (Boc-on; 3.8 g, 15.5 mmol, 2.0 eq.) dissolved in 20 mL of chloroform was added dropwise over the course of 5 hours. After the addition was complete, the mixture was stirred at room temperature for additional 2 hours. Afterwards the solvent was evaporated and remaining yellow oily residue was washed with 5% aqueous solution of sodium carbonate, brine and 10% aqueous solution of citric acid. The acidic aqueous phase was alkalized with 1M sodium hydroxide to pH 11 and then extracted with chloroform. The chloroform was evaporated and the pure product collected as a clear oil (92% yield).

^{1}H-NMR ($CDCl_3$, 500 MHz), δ: 3.46-3.39 (m, 4H), 3.26-3.29 (m, 4H), 2.89 (m, 4H), 1.45 (s, 18H)

^{13}C-NMR ($CDCl_3$, 500 MHz), δ: 156.0, 155.8, 79.8, 79.7; 52.5, 52.4, 49.8, 49.5, 48.2, 48.09, 28.53

ESI-MS (m/z): 330.3 $[M + H]^+$

Di-tert-butyl-7-(2-methoxy-2-oxoethyl)-1,4,7-triazonane-1,4-dicarboxylate (11): In a two-neck round-bottom flask previously flushed with nitrogen, (**10**) (700 mg, 2.1 mmol, 1.0 eq.) was dissolved in 60 mL of anhydrous acetonitrile. Then caesium carbonate (2.0 g, 6.4 mmol, 3.0 eq.) and methyl bromoacetate (354 mg, 230 μL, 2.1 mmol, 1.0 eq.) were added. The mixture was stirred overnight at room temperature under nitrogen. Acetonitrile was evaporated and the oily crude was purified by column chromatography (petroleum ether/ ethyl acetate 80/20-70/30) yielding the desired product as a colorless oil (83% yield).

^{1}H-NMR ($CDCl_3$, 500 MHz), δ: 3.75-3.73 (t, 3H), 3.54-3.51 (m, 7H), 3.30 (m, 4H), 2.89 (m, 4H), 1.55 (s, 18H)

^{13}C-NMR ($CDCl_3$, 500 MHz), δ: 172.8; 156.0, 79.78, 56.35, 54.56, 54.08, 53.85, 51.64, 51.09, 50.23, 49.80, 28.87

ESI-MS (m/z): 402.3 $[M + H]^+$

2-(4,7-Bis(tert-butoxycarbonyl)-1,4,7-triazonan-1-yl)acetic acid (12): In a round-bottom flask placed in an ice bath, (**11**) (406 mg, 1.0 mmol, 1.0 eq.) was dissolved in 20 mL of methanol. 1 M sodium hydroxide (20 mL) was added dropwise. After the addition, the reaction was stirred for 1 hour at room temperature. Next, methanol was evaporated and the aqueous phase was acidified with 10% aqueous solution of potassium hydrogen sulfate until pH 3 was reached. The product was extracted with ethyl acetate and the collected organic phases were dried over sodium sulfate. After evaporation of the solvents, the desired product was isolated as a white solid (85% yield).

^{1}H-NMR ($CDCl_3$, 500 MHz), δ: 3.44 – 3.31 (m, 10H), 2.83-2.73 (m, 4H), 1.45 (s, 18H)

^{13}C-NMR ($CDCl_3$, 500 MHz), δ: 170.6, 155.3, 80.85, 60.52, 59.74, 53.99, 53.54, 49.87, 48.81, 46.83, 28.34

ESI-MS (m/z): 388.3 $[M + H]^+$

Di-tert-butyl-7-(2-oxo-2-(perfluorophenoxy)ethyl)-1,4,7-triazonane-1,4-dicarboxylate (13): In a two-neck round-bottom flask previously flushed with nitrogen, (**12**) (200 mg, 0.51 mmol, 1.0 eq.) and pentafluorophenol (151 mg, 0.82 mmol, 1.6 eq.) were dissolved in 10 mL

of anhydrous DCM and placed in an ice bath. When the temperature reached 0°C, *N*-(3-dimethylaminopropyl)-*N'*-ethyl-carbodiimide hydrochloride (EDC*HCl; 157 mg, 0.82 mmol, 1.6 eq.) was added. The mixture was stirred overnight at room temperature under nitrogen. The organic solution was washed with saturated aqueous solution of potassium hydrogen sulfate and brine and then dried over magnesium sulfate. After evaporation of the solvents, a brownish oil was purified by column chromatography (dichloromethane/methanol 98/2). The desired product was obtained as a white foam (86% yield).

^{1}H-NMR ($CDCl_3$, 500 MHz), δ: 3.77 (m, 2H), 3.42-3.37 (m, 4H), 3.25-3.21 (m, 4H), 2.84 (m, 4H), 1.45 (s, 18H)

^{13}C-NMR ($CDCl_3$, 500 MHz), δ: 167.7, 155.5, 141.8, 140.2, 139.8, 138.6, 138.2, 136.7, 79.62, 55.27, 53.71, 53.16, 51.37, 50.63, 50.04, 49.27, 28.20

ESI-MS (m/z): 554.3 $[M + H]^+$

Di-tert-butyl-7-(2-(hept-6-en-1-ylamino)-2-oxoethyl)-1,4,7-triazonane-1,4-dicarboxylate (14): In a two-neck round-bottom flask previously purged with nitrogen, (**9**) (68 mg, 0.45 mmol, 1.0 eq.) and (**13**) (252 mg, 0.45 mmol, 1.0 eq.) were dissolved in 10 mL of anhydrous DCM. The flask was placed in an ice bath and after 15 minutes *N,N*-diisopropylethylamine (DIPEA; 175 mg, 235 μL, 1.35 mmol, 3.0 eq.) was added dropwise. After the whole addition, the mixture was stirred at reflux overnight. The mixture was concentrated *in vacuo* and purified by column chromatography (chloroform/ ethyl acetate 80/20-70/30). A clear oil was obtained (80% yield).

^{1}H-NMR (CD_3OD, 500 MHz), δ: 5.85-5.77 (m, 1H), 5.02-4.92 (m, 2H), 4.49 (s, 1H), 3.52-3.41 (m, 6H), 3.23-3.20 (m, 4H), 2.80-2.70 (m, 4H), 2.09-2.02 (m, 2H), 1.55-1.50 (m, 20H), 1.44-1.30 (m, 6H)

ESI-MS (m/z): 483.5 $[M + H]^+$

Di-tert-butyl-7-(2-((7-(acetylthio)heptyl)amino)-2-oxoethyl)-1,4,7-triazonane-1,4-dicarboxylate (15): In a 3 mL quartz cuvette, 2,2-dimethoxy-1,2-diphenylethan-1-one (3.9 mg, 0.01 mmol, 0.05 eq.) was dissolved in 2 mL of degassed methanol. Then (**14**) (148 mg, 0.3 mmol, 1.0 eq.) was added and the solution was treated with nitrogen flow for 15 minutes. Next, thioacetic acid (80 mg, 75 μL, 1.1 mmol, 3.5 eq.) was added to the solution. The reaction was left stirring for 5 hours upon UV irradiation at 254 nm. Following this, the crude was concentrated, washed several times with methanol and purified by column chromatography. The elution was performed using dichloromethane/methanol 90/10. The desired product formed a yellow solid (80% yield).

^{1}H-NMR (CD_3OD, 500 MHz), δ: 3.52-3.40 (m, 6H), 3.22-3.20 (m, 4H), 2.86 (t, 2H), 2.70 (m, 4H), 2.30 (s, 3H), 1.56-1.40 (m, 23H), 1.34-1.27 (m, 7H)

ESI-MS (m/z): 559.3 $[M + H]^+$

7-(2-((7-Mercaptoheptyl)amino)-2-oxoethyl)-1,4,7-triazonane-1,4-diium chloride (T1): In a round-bottom flask, **9** (55 mg, 0.1 mmol) was dissolved in 3 mL of ethanol. Then an equal amount of 6M hydrochloric acid was added dropwise. After the complete addition, the resulting mixture was refluxed for 2 hours. The solvents were evaporated and the crude was dried under high vacuum. Obtained product was used *in situ* without any additional purification in the synthesis of gold nanoparticles (**AuNP1**).

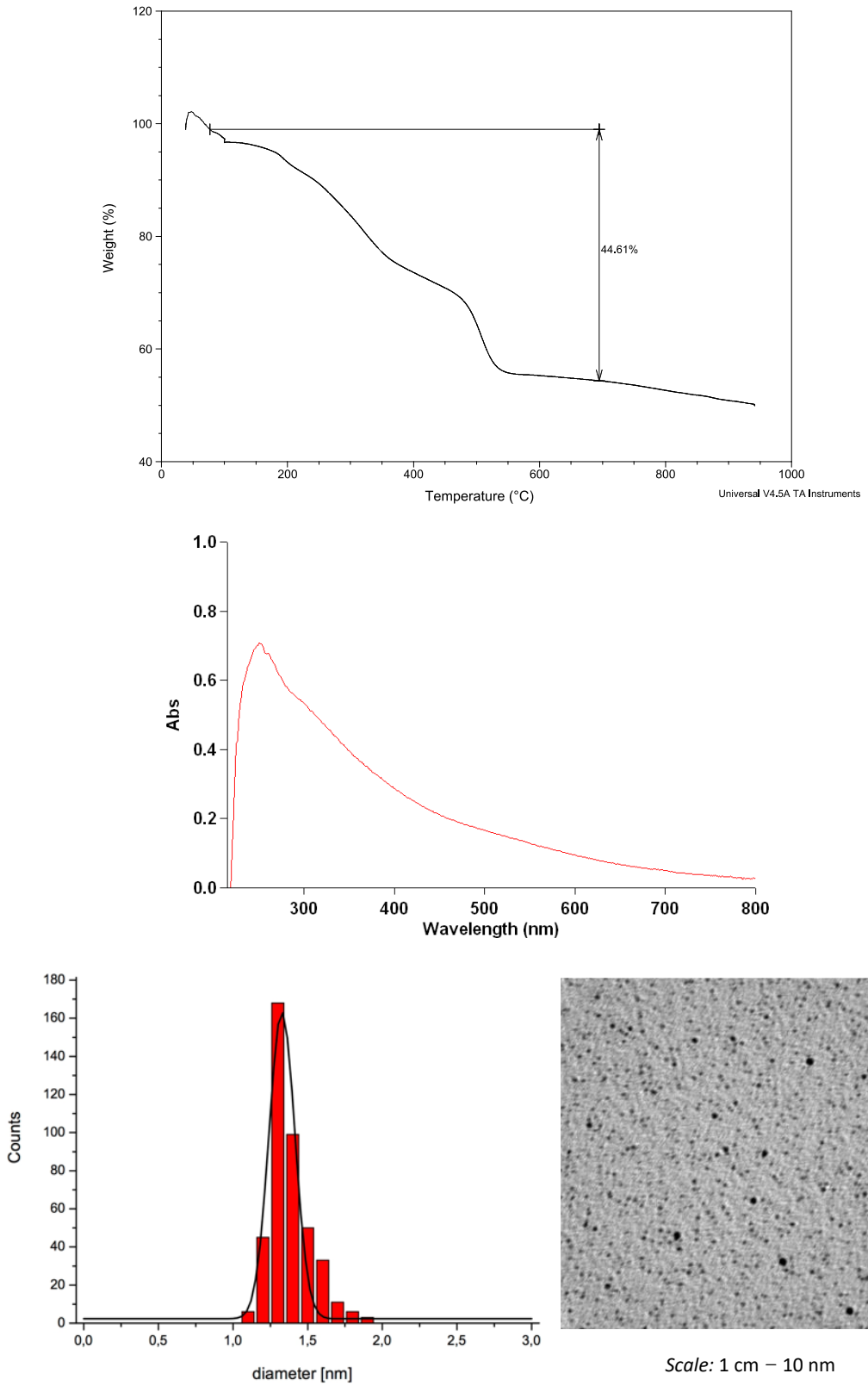

Fig.E.8.

Top: TGA analysis of **AuNP1**. Formula: $Au_{68}(SR)_{34}$
Middle: UV-VIS analysis of **AuNP1**
Bottom: TEM image and size distribution of **AuNP1**. Average diameter = 1.3 nm (± 0.2 nm)

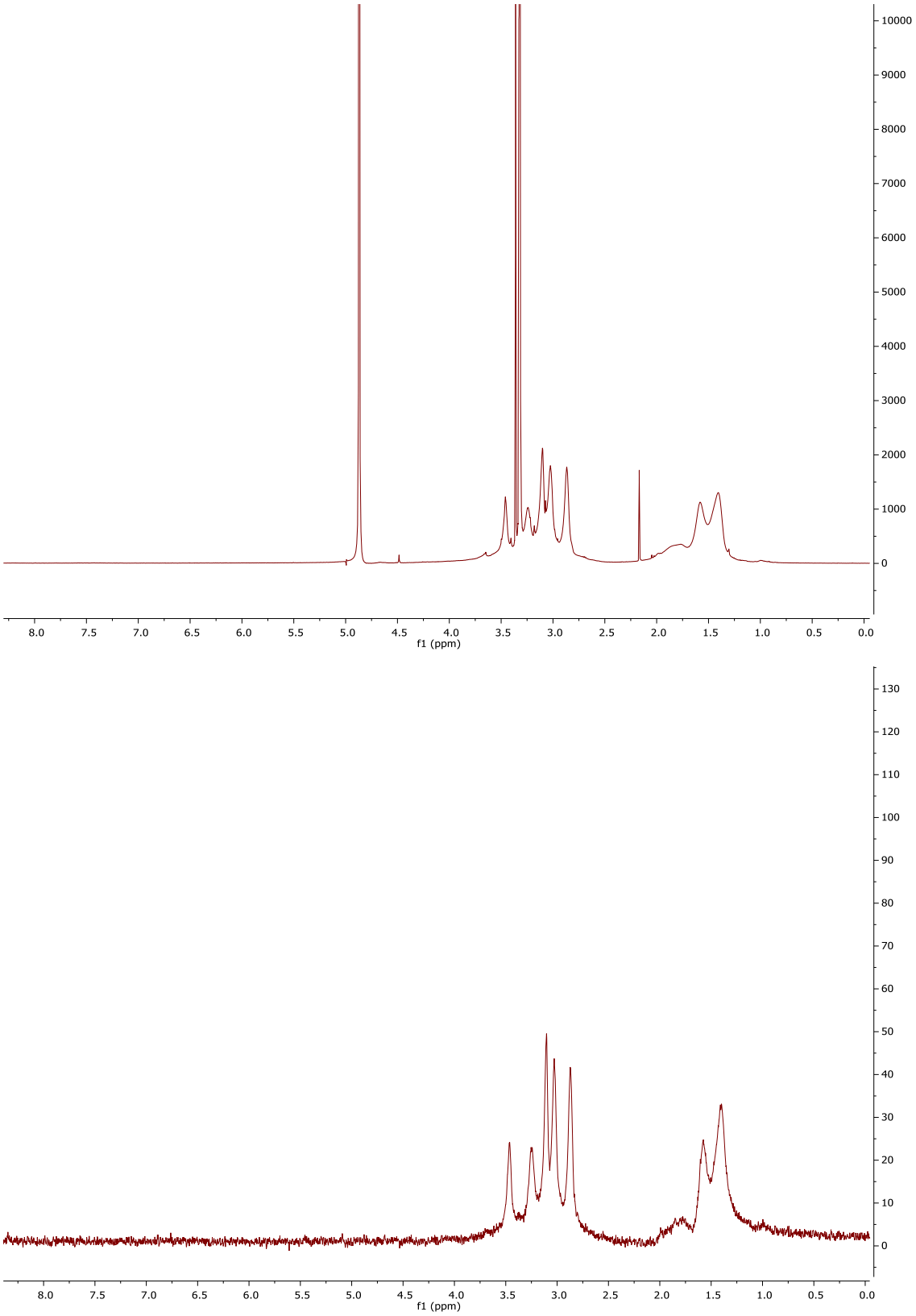

Fig.E.9.

Top: ^{1}H-NMR (500 MHz) spectrum of **AuNP1** in CD_3OD
Bottom: Diffusion-filtered ^{1}H-NMR (500 MHz) spectrum of **AuNP1** in CD_3OD

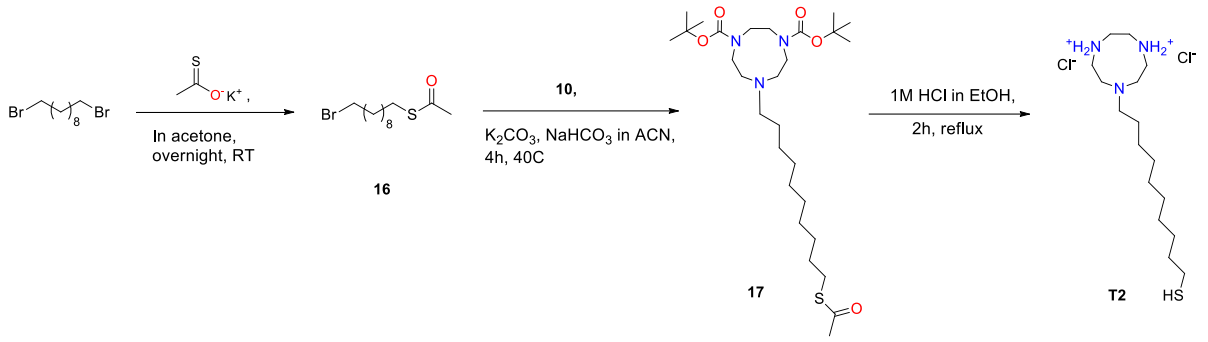

Scheme E.10.

S-(10-Bromodecyl) ethanethioate (16): In a round-bottom flask, 1,10-dibromodecane (4.0 g, 13.3 mmol, 1.0 eq.) was dissolved in 30 mL of acetone. Potassium thioacetate (1.52 g, 13.3 mmol, 1.0 eq.) together with 20 mL of acetone was added. This resulting mixture was stirred overnight at room temperature. Afterwards the solution was concentrated, extracted with ethyl acetate and dried over a Na_2SO_4. After solvent evaporation, the remaining orange oil was purified by column chromatography (petroleum ether/ethyl acetate 98/2-96/4). The desired product was obtained as a white solid (46% yield).

^{1}H-NMR ($CDCl_3$, 500 MHz), δ: 3.40 (t, 2H), 2.86 (t, 2H), 2.32 (s, 3H), 1.83 (q, 2H), 1.56 (q, 2H), 1.56-1.28 (m, 12H)

^{13}C-NMR ($CDCl_3$, 500 MHz), δ: 196.51, 34.49, 33.19, 31.07, 29.87, 29.72, 29.52, 29.44, 29.16, 29.11, 28.53

Di-tert-butyl-7-(10-(acetylthio)decyl)-1,4,7-triazonane-1,4-dicarboxylate (17): In a round-bottom flask previously purged with nitrogen, potassium carbonate (207 mg, 1.5 mmol, 3.0 eq.) and sodium bicarbonate (126 mg, 1.5 mmol, 3.0 eq.) were suspended in 10 mL of anhydrous MeCN. Then (**16**) (177 mg, 0.6 mmol, 1.2 eq.) and (**10**) (165 mg, 0.5 mmol, 1.0 eq.) were added. The mixture was stirred at 60°C for 4 hours. Afterwards, the solvent was removed and resulting oily crude was purified by column chromatography (dichloromethane/methanol 97/3). The desired product was isolated as a yellow oil (40% yield).

^{1}H-NMR (CD_3OD, 500 MHz), δ: 5.85-5.78 (m, 1H), 5.01-4.94 (m, 2H), 3.48-3.21 (m, 8H), 2.63-2.46 (m, 4H), 2.06 (m, 2H), 1.85 (q, 2H), 1.48-1.27 (m, 30H)

ESI-MS (m/z): 544.3 $[M + H]^+$

7-(10-Mercaptodecyl)-1,4,7-triazonane-1,4-diium chloride (T2): In a round-bottom flask (**17**) (54 mg, 0.1 mmol) was dissolved in 5 mL of ethanol. An equal amount of 6M hydrochloric acid was added dropwise. After the addition, the resulting mixture was refluxed for 2 hours. Afterwards, the solvents were evaporated and the crude was dried under high vacuum. Obtained product was used *in situ* without any additional purification in the synthesis of gold nanoparticles (**AuNP2**).

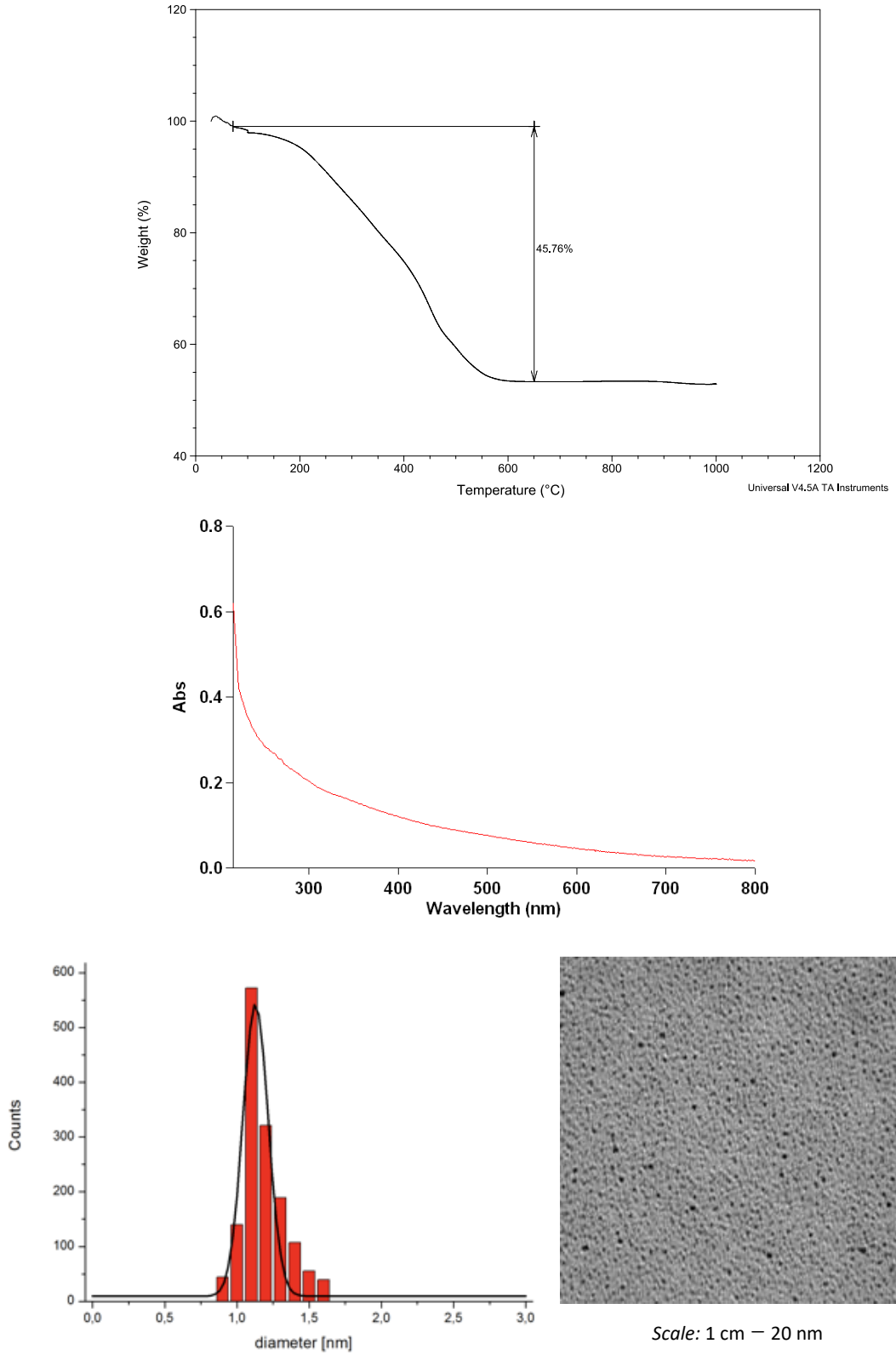

Fig.E.11.

Top: TGA analysis of **AuNP2**. Formula: $Au_{41}(SR)_{23}$
Middle: UV-VIS analysis of **AuNP2**
Bottom: TEM image and size distribution of **AuNP2**. Average diameter = 1.1 nm (± 0.2 nm)

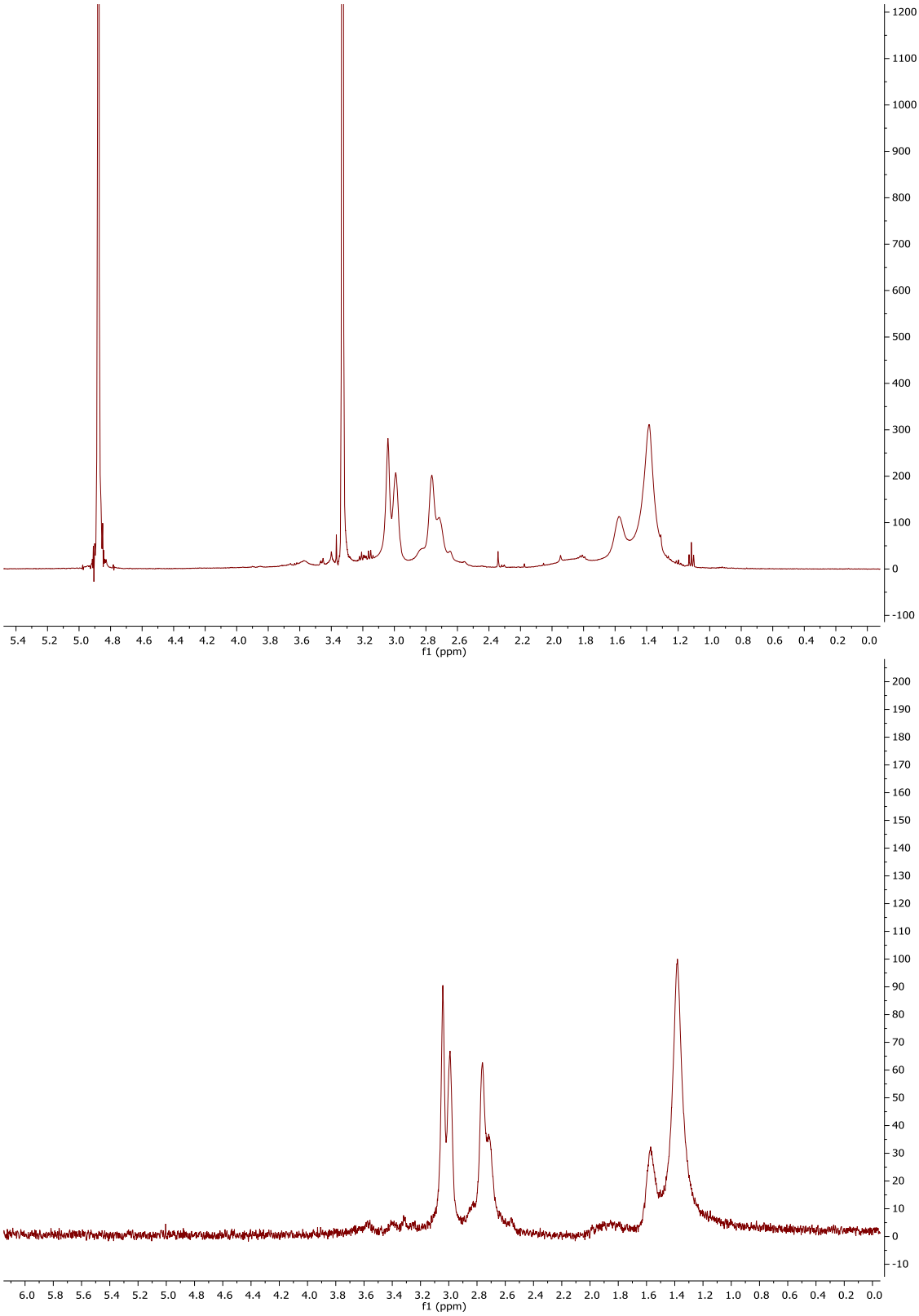

Fig.E.12.

Top: ^{1}H-NMR (500 MHz) spectrum of **AuNP2** in CD_3OD
Bottom: Diffusion-filtered ^{1}H-NMR (500 MHz) spectrum of **AuNP2** in CD_3OD

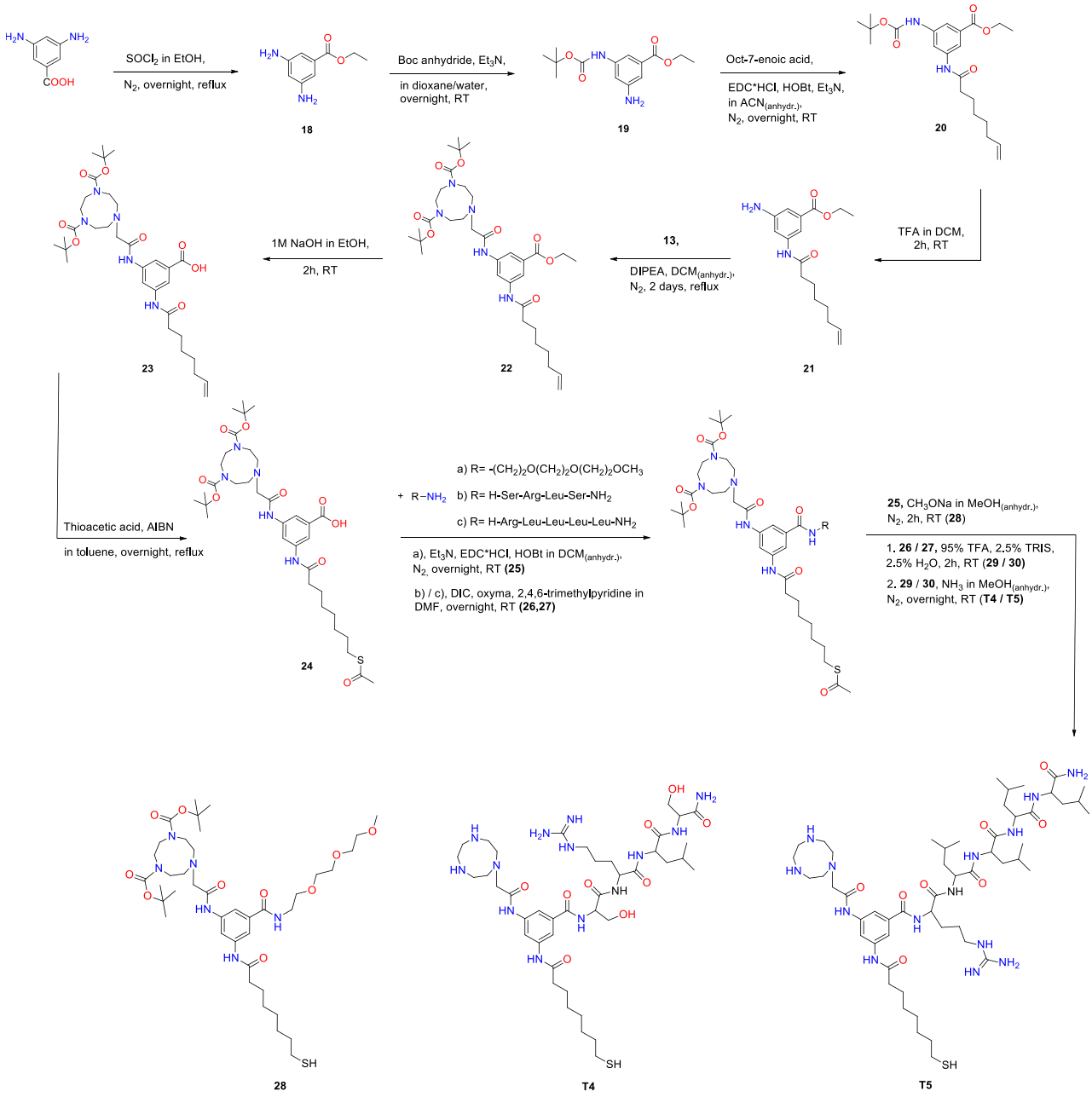

Scheme E.13.

Ethyl 3,5-diaminobenzoate (18): In a two-neck round bottom flask, thionyl chloride ($SOCl_2$; 7.1 g, 4.5 mL, 0.06 mmol, 1.0 eq.) was added dropwise to 15 mL of anhydrous ethanol under nitrogen at 0°C. Afterwards, 3,5-diaminobenzoic acid (2.5 g, 0.17 mmol, 3.0 eq.) was added in 3 portions and the resulting mixture was stirred at reflux overnight. The ethanol and unreacted $SOCl_2$ were evaporated, remaining residue was dissolved in water and alkalized with sat. aqueous solution of $NaHCO_3$. The cloudy mixture was extracted with ethyl acetate,

collected organic phases were washed with water and dried over a $MgSO_4$. Brown glass-like solid was obtained (91% yield).

^{1}H-NMR ($CDCl_3$, 500 MHz), δ: 6.79 (s, 2H), 6.18 (s, 1H), 4.31 (q, 2H), 3.66 (s, 4H), 1.36 (t, 3H)
ESI-MS (m/z): 181.0 $[M + H]^+$

Ethyl 3-amino-5-((tert-butoxycarbonyl)amino)benzoate (19): In a round-bottom flask placed in an ice bath, (**18**) (1.3 g, 7.3 mmol, 1.0 eq.) was solubilized in a mixture of dioxane and water (2:1; 45 mL in total), followed by addition of triethylamine (Et_3N; 1.62 g, 2.3 mL, 16 mmol, 2.2 eq.). Next, di-*tert*-butyl-dicarbonate ($(Boc)_2O$; 1.6 g, 7.3 mmol, 1.0 eq.) was solubilized in 5 mL of dioxane and added dropwise to the mixture. The reaction was stirred at room temperature overnight. The solvents were evaporated and the crude was dissolved in ethyl acetate and washed with 10% aqueous solution of citric acid and water. The collected organic phases were dried over $MgSO_4$, concentrated *in vacuo* and purified by column chromatography (dichloromethane/acetonitrile 95/5-90/10). The desired product formed pale-yellow solid (80% yield).

^{1}H-NMR ($CDCl_3$, 500 MHz), δ: 7.29 (s, 1H), 7.26 (s, 1H), 7.14 (s, 1H), 6.52 (s, 1H), 4.32 (q, 2H), 1.51 (s, 9H), 1.36 (t, 3H)

Ethyl 3-((tert-butoxycarbonyl)amino)-5-(oct-7-enamido)benzoate (20): In a two-neck round-bottom flask previously flushed with nitrogen, (**19**) (1.1 g, 3.9 mmol, 1.2 eq.) was dissolved in 60 mL of anhydrous acetonitrile. Triethylamine (Et_3N; 987 mg, 1.3 mL, 9.8 mmol, 3.0 eq.), hydroxybenzotriazole (983 mg, 6.5 mmol, 2.0 eq.) and oct-7-enoic acid (462 mg, 500 μL, 3.25 mmol, 1.0 eq.) were added. Afterwards the flask was cooled down in an ice-bath and after 15 minutes, *N*-(3-dimethylaminopropyl)-*N'*-ethyl-carbodiimide hydrochloride (EDC*HCl; 1.24 g, 6.5 mmol, 2.0 eq.) was added. The reaction was left stirring at room temperature for 24 hours. Then the mixture was concentrated *in vacuo* and purified by column chromatography (dichloromethane/acetonitrile 95/5-90/10). White solid was obtained (89% yield).

^{1}H-NMR ($CDCl_3$, 500 MHz), δ: 8.04 (s, 1H), 7.82 (s, 1H), 7.69 (s, 1H), 7.23 (s, 1H), 6.62 (s, 1H), 5.84-5.76 (m, 1H), 5.02-4.94 (m, 2H), 4.35 (q, 2H), 2.34 (t, 2H), 2.07 (q, 2H), 1.71 (m, 2H), 1.52 (s, 9H), 1.45-1.36 (m, 9H)

^{13}C-NMR ($CDCl_3$, 500 MHz), δ: 171.8, 166.5, 153.0, 139.6, 139.2, 132.2, 115.4, 114.9, 114.07, 81.41, 61.67, 38.12, 33.94, 29.07, 28.70, 25.72, 14.71

Ethyl 3-amino-5-(oct-7-enamido)benzoate (21): In a two-neck round-bottom flask previously flushed with nitrogen and placed in an ice bath, (**20**) (950 mg, 2.3 mmol, 1.0 eq.) was solubilized in 5 mL of anhydrous dichloromethane. 5 mL of trifluoroacetic acid (TFA) was dissolved in an equal amount of dichloromethane and added dropwise. Afterwards the reaction was stirred at room temperature for 2 hours. The solvent and TFA were evaporated and remaining oil was washed several times with cold diethyl ether. Desired product was isolated as a pale-yellow solid (82% yield).

^{1}H-NMR ($CDCl_3$, 500 MHz), δ: 7.60 (s, 1H), 7.32 (m, 2H), 7.15 (s, 1H), 5.83-5.75 (m, 1H), 5.01-4.93 (m, 2H), 4.34 (q, 2H), 2.95 (s, 2H), 2.36 (t, 2H), 2.05 (m, 2H), 1.71 (m, 2H), 1.38-1.25 (m, 9H)

^{13}C-NMR ($CDCl_3$, 500 MHz), δ: 171.6, 163.4, 147.0, 139.1, 138.8, 131.8, 114.5, 116.7, 110.7, 61.07, 37.73, 33.54, 28.67, 25.37, 14.29

ESI-MS (m/z): 305.2 $[M + H]^+$, 327.2 $[M + Na]^+$

Di-tert-butyl-7-(2-((3-(ethoxycarbonyl)-5-(oct-7-enamido)phenyl)amino)-2-oxoethyl)-1,4,7-triazonane-1,4 dicarboxylate (22): In a two-neck round-bottom flask previously purged with nitrogen, (**21**) (730 mg, 2.4 mmol, 1.0 eq.) and (**13**) (1.7 g, 3.12 mmol, 1.1 eq.) were dissolved in 50 mL of anhydrous dichloromethane. The flask was placed in an ice-bath and after 15 minutes, DIPEA (1.5 g, 2.9 mL, 12.0 mmol, 5.0 eq.) was added dropwise. After the complete addition, the mixture was stirred and refluxed for 2 days. The solution was concentrated and purified by column chromatography (chloroform/acetone 92/8-90/10). The product was isolated as a white solid (56% yield).

^{1}H-NMR (CD_3OD, 500 MHz), δ: 8.20 (s, 1H), 8.01 (m, 2H), 5.87-5.79 (m, 1H), 5.03-4.95 (m, 2H), 4.37 (q, 2H), 3.56-3.70 (m, 10H), 2.91-2.82 (m, 4H), 2.41 (t, 2H), 2.10 (m, 2H), 1.72 (m, 2H), 1.50-1.38 (m, 25H)

^{13}C-NMR (CD_3OD, 500 MHz), δ: 174.5, 172.7, 167.4, 158.0, 157.6, 140.1, 139.9, 132.6, 118.6, 118.3, 117.9, 117.8, 114.93, 114.90, 81.55, 62.75, 62.30, 55.67, 55.36, 54.95, 51.86, 51.45, 37.91,34.71, 29.80, 28.80, 26.68, 26.68, 14.62

ESI-MS (m/z): 674.4 $[M + H]^+$, 699.4 $[M + Na]^+$

3-(2-(4,7-Bis(tert-butoxycarbonyl)-1,4,7-triazonan-1-yl)acetamido)-5-(oct-7-enamido)-benzoic acid (23): In a round-bottom flask placed in an ice-bath, (**22**) (132 mg, 0.2 mmol, 1.0 eq.) was dissolved in 5 mL of ethanol. Next, an equal volume of aqueous 1 M NaOH as ethanol was added dropwise. After the whole addition the cloudy mixture was stirred at room temperature for 2 hours. The solvent was evaporated, residue acidified with saturated aqueous solution of $KHSO_4$ (pH = 4). Afterwards the mixture was extracted with ethyl acetate, collected organic phases were washed with water and dried over a $MgSO_4$. Desired product was collected as a white solid (85% yield).

^{1}H-NMR ($CDCl_3$, 500 MHz), δ: 9.72 (m, 1H), 8.25-7.97 (m, 3H), 7.63 (s, 1H), 5.82-5.77 (m, 1H), 5.01-4.92 (m, 2H), 3.56-3.38 (m, 10H), 2.75 (m,4H), 2.37 (m, 2H), 2.06 (m, 2H), 1.72 (m, 2H), 1.48-1.41 (m, 22H)

^{13}C-NMR ($CDCl_3$, 500 MHz), δ: 174.6, 172.5, 169.0, 157.8, 157.3, 140.5, 139.7, 132.9, 118.5, 118.0, 117.6, 114.8, 81.42, 62.61, 55.51, 54.78, 53.33, 51.63, 51.13, 50.94, 37.75, 34.55, 29.64, 29.60, 28.63, 26.54

ESI-MS (m/z): 646.3 $[M + H]^+$, 668.3 $[M + Na]^+$

3-(8-(Acetylthio)octanamido)-5-(2-(4,7-bis(tert-butoxycarbonyl)-1,4,7-triazonan-1-yl)acetamido)benzoic acid (24): In a round-bottom flask, (**23**) (138 mg, 0.17 mmol, 1.0 eq.) and α,α'-azoisobutyronitrile (AIBN; 14 mg, 0.085 mmol, 0.5 eq.) were dissolved in 20 mL of toluene. Next, thioacetic acid (38.8 mg, 36.4 μL, 0.51 mmol, 3.5 eq.) was added and the reaction mixture was refluxed overnight. The toluene was evaporated and the remaining

oily crude was dried under high vacuum and purified by column chromatography (dichloromethane/methanol 90/10-80/20 with 0.5% addition of TEA). The product was obtained as a pale-yellow solid (80% yield).

^{1}H-NMR (CD_3OD, 500 MHz), δ: 8.17 (m, 1H), 7.95-7.91 (m, 2H), 3.55-3.32 (m, 10H), 2.87-2.81 (m, 6H), 2.38 (t, 2H), 2.30 (s, 3H), 1.70 (m, 2H), 1.57 (m, 2H), 1.48-1.26 (m, 24H)

^{13}C-NMR (CD_3OD, 500 MHz), δ: 197.6, 174.7, 172.5, 157.9, 157.5, 140.2, 139.5, 118.7, 118.2, 117.1, 81.41, 81.34, 62.54, 55.63, 55.35, 54.94, 51.76, 51.50, 51.16, 37.94, 30.70, 30.51, 30.13, 29.90, 29.81, 29.63, 28.81, 26.81

ESI-MS (m/z): 722.4 $[M + H]^+$, 744.4 $[M + Na]^+$

Di-tert-butyl-7-(2-((3-(8-(acetylthio)octanamido)-5-((2-(2-(2-methoxyethoxy)ethoxy)-ethyl)-carbamoyl)-phenyl)-amino)-2-oxoethyl)-1,4,7-triazonane-1,4-dicarboxylate (25): In a two-neck round-bottom flask previously flushed with nitrogen, (**24**) (119 mg, 0.16 mmol, 1.0 eq.) was dissolved in 10 mL of anhydrous acetonitrile. Triethylamine (Et_3N; 49 mg, 67 μL, 0.48 mmol, 3.0 eq.), hydroxybenzotriazole (HOBt; 48 mg, 0.32 mmol, 3.0 eq.) and 2-(2-(2-methoxyethoxy)ethoxy)ethan-1-amine (**(a)**, 31 mg, 0.19 mmol, 1.2 eq.) were added. The flask was placed in an ice-bath and when the mixture reached 0°C, *N*-(3-dimethylaminopropyl)-*N*′-ethyl-carbodiimide hydrochloride (EDC*HCl; 61 mg, 0.32 mmol, 3.0 eq.) was added. The reaction was stirred at room temperature under nitrogen overnight. Then the crude was concentrated and purified by column chromatography (dichloromethane/methanol 96/4). The product was isolated as a pale-yellow solid (71% yield).

^{1}H-NMR ($CDCl_3$, 500 MHz), δ: 8.35-7.64 (m, 3H), 3.68-3.34 (m, 25H), 2.87-2.75 (m, 6H), 2.38-2.32 (m, 5H), 1.69 (m, 2H), 1.56 (m, 2H), 1.48-1.25 (m, 24H)

^{13}C-NMR ($CDCl_3$, 500 MHz), δ: 196.3, 188.2, 171.8, 167.3, 156.6, 156.0, 139.5, 139.0, 135.9, 115.1, 114.9, 114.5, 80.61, 80.42, 71.95, 70.63, 70.55, 70.37, 69.95, 63.70, 59.04, 55.20, 54.21, 53.13, 51.42, 50.21, 49.42, 40.03, 37.63, 30.77, 29.54, 29.16, 28.93, 28.65, 25.52

ESI-MS (m/z): 867.6 $[M + H]^+$

Di-*tert*-butyl 7-(2-((3-(8-(acetylthio)octanamido)-5-((1-((1-((1-((1-amino-3-hydroxy-1-oxopropan-2-yl)amino)-4-methyl-1-oxopentan-2-yl)amino)-5-guanidino-1-oxopentan-2-yl)amino)-3-hydroxy-1-oxopropan-2-yl)carbamoyl)phenyl)amino)-2-oxoethyl)-1,4,7-triazonane-1,4-dicarboxylate and di-*tert*-butyl 7-(2-((3-(8-(acetylthio)octanamido)-5-((1-amino-15-carbamoyl-1-imino-9,12-diisobutyl-17-methyl-7,10,13-trioxo-2,8,11,14-tetraazaoctadecan-6-yl)carbamoyl)phenyl)amino)-2-oxoethyl)-1,4,7-triazonane-1,4-dicarboxylate, (26) and (27): In a two-neck round-bottom flask previously flushed with nitrogen, (**24**) (19 mg, 0.02 mmol, 1.0 eq.) together with collidine (2,4,6-trimethylpyridine; 7.3 mg, 7.8 μL, 0.06 mmol, 3.0 eq.) and *N,N'*-diisopropylcarbodiimide (DIC; 7.5 mg, 9.3 μL, 0.06 mmol, 3.0 eq.) were dissolved in 1 mL of anhydrous DMF. Then, the solution of previously synthesized peptide (**b**) or (**c**) ((the synthesis shown below), 0.024 mmol, 1.2 eq.) with oxyma (ethyl cyano(175ydroxyamino)acetate, 8.5 mg, 0.06 mmol, 3.0 eq.) in 1 mL of anhydrous DMF were added. The mixture was stirred under nitrogen overnight. The solvent was evaporated and the crude purified by preparative RP HPLC (45 min. run, 0-60% ACN + 0.05% TFA, λ=214 nm). The collected fractions were lyophilized yielding a white solid.

LC-MS (m/z) ***26:*** *582.68 $[0.5M + H]^+$, 1164.52 $[M + H]^+$*

LC-MS (m/z) ***27:*** *665.43 $[0.5M + H]^+$, 1329.62 $[M + H]^+$*

Di-tert-butyl-7-(2-((3-(8-mercaptooctanamido)-5-((2-(2-(2-methoxyethoxy)ethoxy)ethyl)-carbamoyl)phenyl)-amino)-2-oxoethyl)-1,4,7-triazonane-1,4-dicarboxylate (28): In a two-neck round-bottom flask previously flushed with nitrogen, (**25**) (86 mg, 0.1 mmol) was solubilized in 10 mL of anhydrous methanol. Sodium methoxide (11 mg, 0.2 mmol, 2.0 eq.) was added. The mixture was stirred at RT under nitrogen for 2 hours. Next methanol was evaporated and the crude was dried under high vacuum. Obtained product, being a precursor of (**T3**), was used *in situ* without any additional purification in the synthesis of gold nanoparticles.

Once AuNPs were formed and purified, Boc-protecting groups were removed by dissolving AuNPs in anhydrous dichloromethane and slow addition trifluoroacetic acid in DCM (until gold nanoparticles started precipitating). The mixture was stirred for 2 hours, solvent and acid were evaporated and gold nanoparticles were purified again on a 25-Sephadex column, using MeOH as an eluent (**T3**, **AuNP3**).

7-(2-((3-(8-(acetylthio)octanamido)-5-((1-((5-((amino(iminio)methyl)amino)-1-((1-((1-amino-3-hydroxy-1-oxopropan-2-yl)amino)-4-methyl-1-oxopentan-2-yl)amino)-1-oxopentan-2-yl)amino)-3-hydroxy-1-oxopropan-2-yl)carbamoyl)phenyl)amino)-2-oxoethyl)-1,4,7-triazonane-1,4-diium and 7-(2-((3-(8-(acetylthio)octanamido)-5-((1-amino-15-carbamoyl-1-iminio-9,12-diisobutyl-17-methyl-7,10,13-trioxo-2,8,11,14-tetraazaoctadecan-6-yl)carbamoyl)phenyl)amino)-2-oxoethyl)-1,4,7-triazonane-1,4-diium (29) and (30): In a two-neck round-bottom flask previously flushed with nitrogen and placed in an ice bath, (**26**) / (**27**) (0.1 mmol, 1.0 eq.) was solubilized in 5 mL of anhydrous dichloromethane. Trifluoroacetic acid (TFA; 15 mL, 0.2 mmol, 2.0 eq.) was dissolved in an equal amount of dichloromethane and added dropwise. Afterwards the reaction was stirred at room temperature for 4 hours. The solvent and TFA were evaporated and remaining yellow oil was precipitated from a cold *tert*-buthylmethyl ether. Both compounds were obtained as a white solid (54-62%).

Next, the solution of ammonia in methanol (2.0 eq.) was added and the mixture was stirred at room temperature overnight (the reaction was monitored by ^{1}H NMR). The solvents were evaporated and the crude was dried under high vacuum. Without any additional steps the product with a free thiol group was used *in situ* in the synthesis of gold nanoparticles (**T4,5**; **AuNP4,5**).

3.2. *The Solid-phase Synthesis of Peptides.*

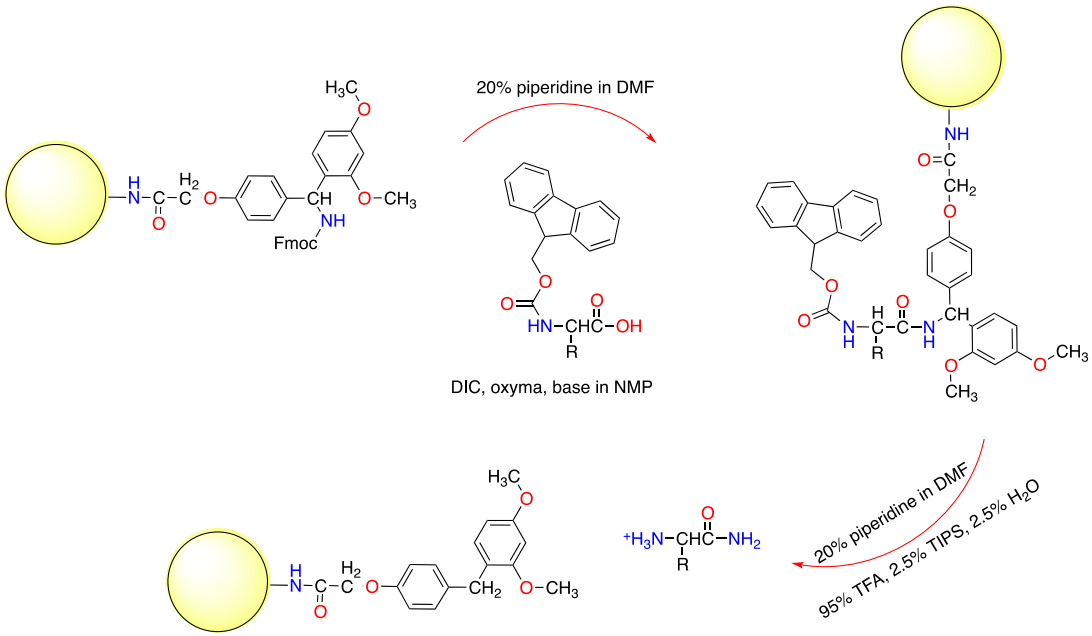

Scheme E.14.

H-Ser-Arg-Leu-Ser-NH$_2$ and H-Arg-Leu-Leu-Leu-Leu-NH$_2$ (b) and (c): In a 25 mL volume syringe equipped with a filter, 1.0 g of the resin (TentaGel S RAM) was added. It was swelled in 15 mL of dichloromethane for 30 minutes. Afterwards the solvent was filtered off and the Fmoc groups were deprotected with 20% solution of piperidine in *N,N*-dimethylformamide (15-minute stirring). Next, all liquids were filtrated and the resin was washed with 1-methyl-2-pyrrolidone (NMP), methanol and dichloromethane. Simultaneously the protected amino acid (amounts depicted in the table below), oxyma (ethyl cyano(hydroxyamino)acetate; 177.5 mg, 1.0 eq.), *N,N'*-diisopropylcarbodiimide (DIC; 157.7 mg, 193.5 μL, 1.0 eq.) and collidine (2,4,6-trimethylpyridine; 151.5 mg, 162.7 μL, 1.0 eq.) were dissolved in 5 mL of *N*-methyl-2-pyrrolidon and sonicated. Resulting mixture was poured on the resin.

Compound	MW [g/mol]	Quantity [mg]	mmol
Fmoc-Ser(tBu)-OH	383.4	479.3	1.25
Fmoc-Leu-OH	353.5	441.8	1.25
Fmoc-Arg(Pbf)-OH	648.7	810.9	1.25

Table E.15.

A total volume was adjusted using dichloromethane (up to 15 mL) and then everything was stirred for 1 hour. Afterwards the solvents were filtrated, resin washed with NMP, MeOH and DCM. The Fmoc group of the last coupled amino acid was deprotected by 20% solution of piperidine in DMF. The liquids were again filtered off and the resin washed with NMP, MeOH and DCM. Described steps were repeated until desired peptide was built. After the last coupling, the cocktail made from 95% (v) of TFA, 2.5% (v) of triisopropylsilane and 2.5% (v) of water was poured into dry resin (15 mL in total), in order to cleave the peptide from the solid platform. The concoction was stirred for 2 hours. Next the crude was quenched and washed several times with cold *tert*-butylmethyl ether. The protocol yielded a formation of desired compounds with high purity.

LC-MS (m/z ***b)****: 461.41* $[M + H]^+$

LC-MS (m/z ***c)****: 626.50* $[M + H]^+$

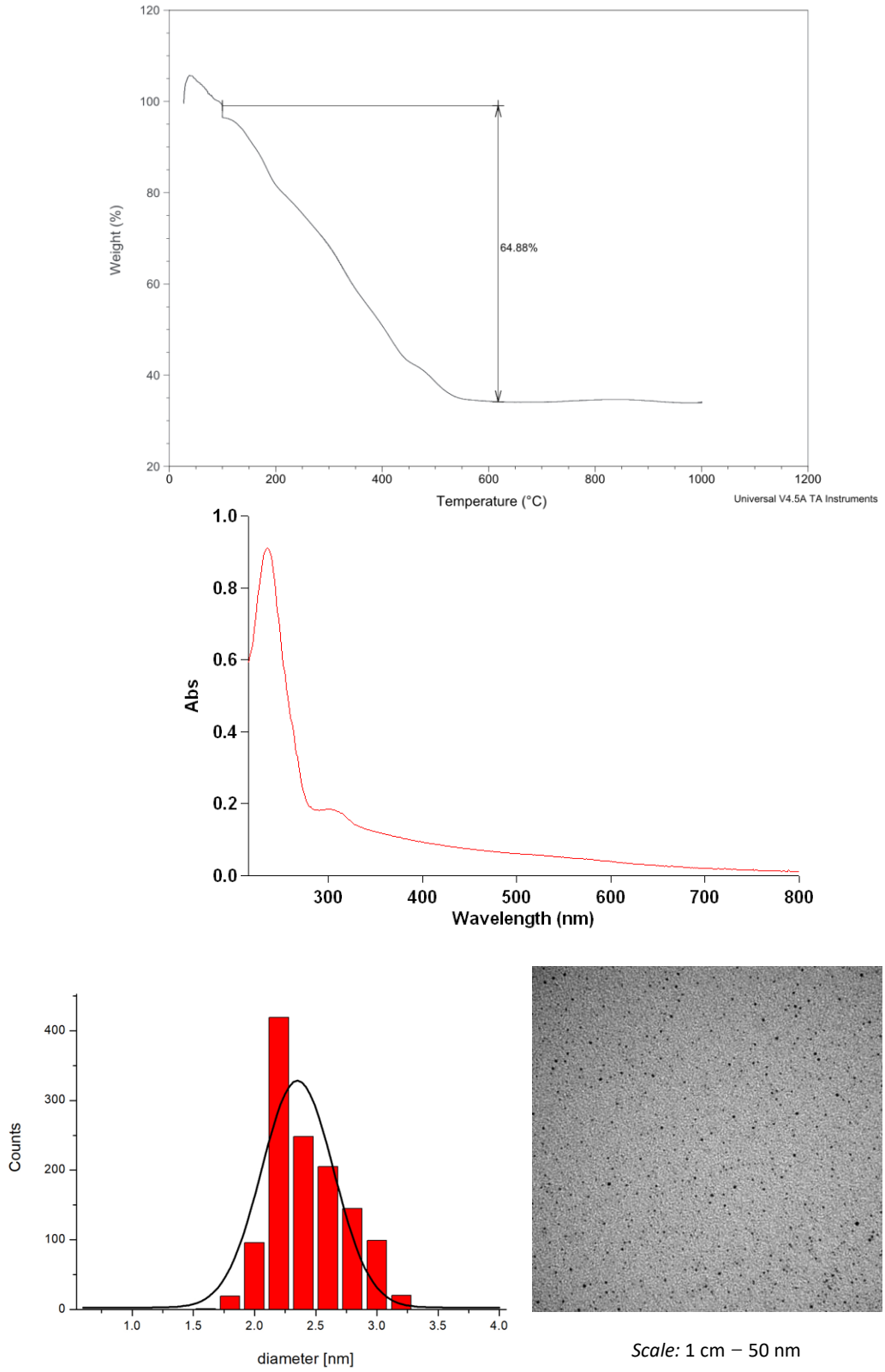

Fig.E.16.

Top: TGA analysis of **AuNP3**. Formula: $Au_{376}(SR)_{211}$
Middle: UV-VIS analysis of **AuNP3**
Bottom: TEM image and size distribution of **AuNP3**. Average diameter = 2.3 nm (± 0.3 nm)

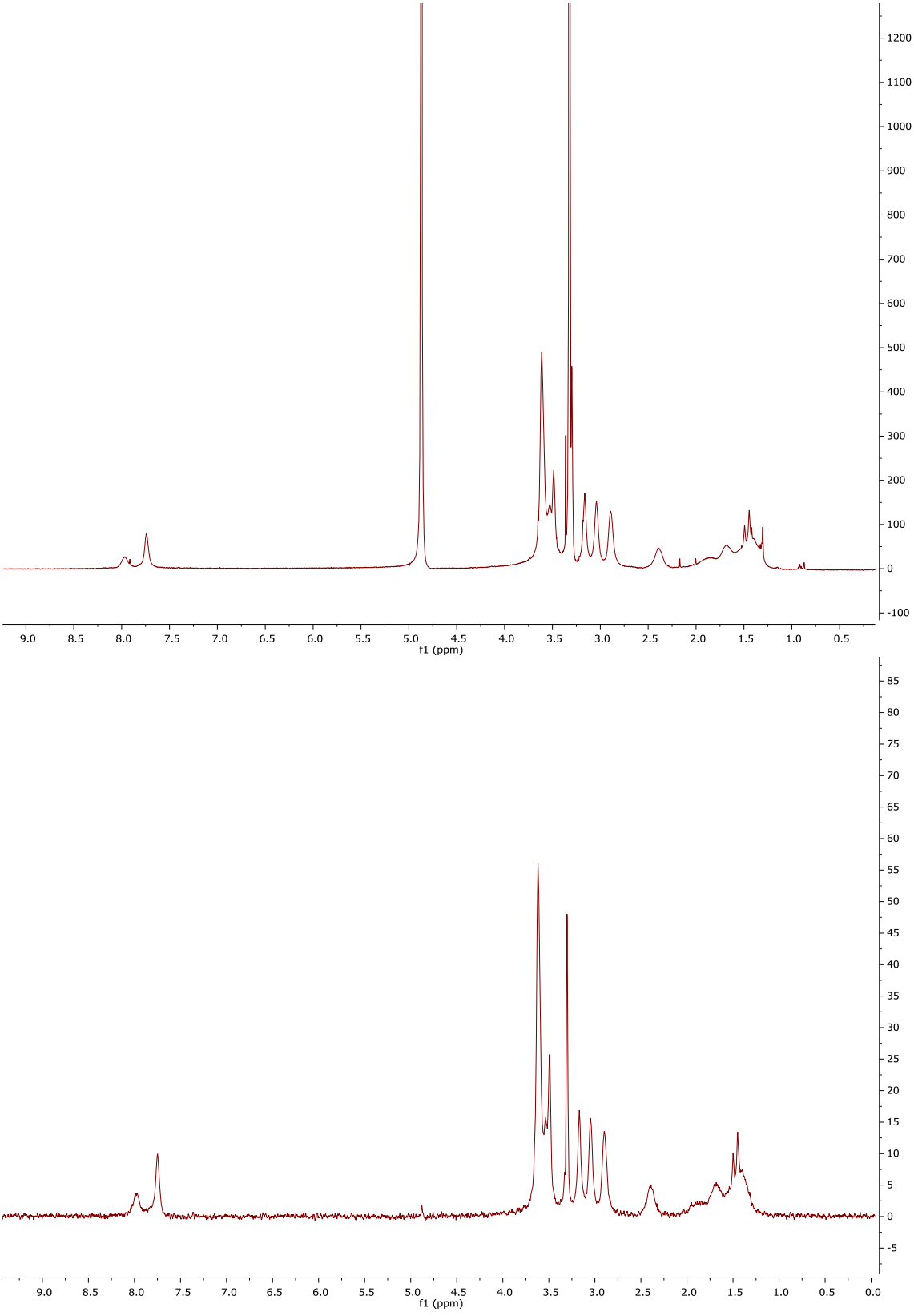

Fig.E.17.

Top: ^{1}H-NMR (500 MHz) spectrum of **AuNP3** in CD_3OD
Bottom: Diffusion-filtered ^{1}H-NMR (500 MHz) spectrum of **AuNP3** in CD_3OD

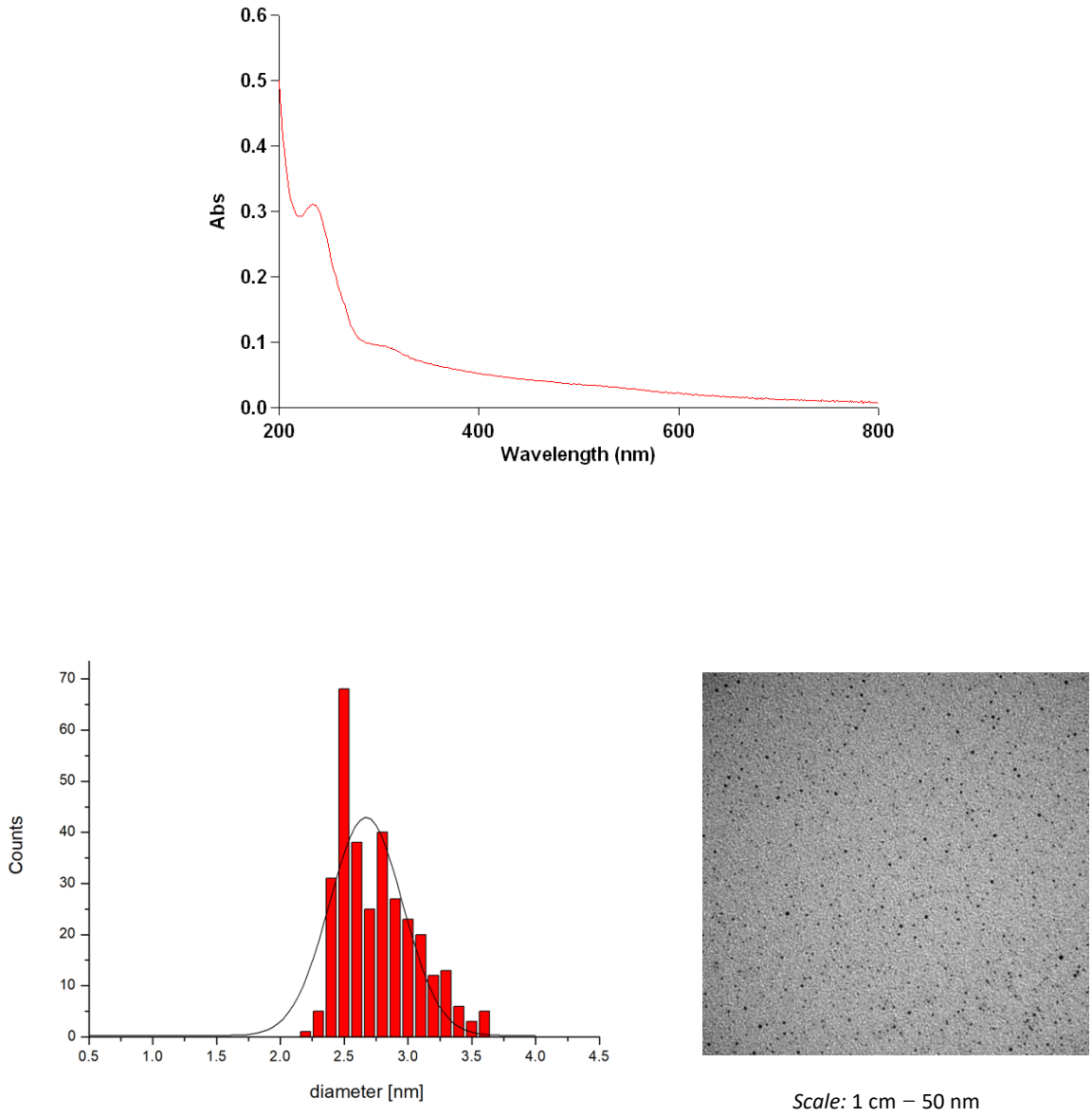

Fig.E.18.

Top: UV-VIS analysis of **AuNP4**
Bottom: TEM image and size distribution of **AuNP4**. Average diameter = 2.6 nm (± 0.3 nm)

*TGA analysis of **AuNP4** was not studied due to a very small amount of obtained nanoparticles.

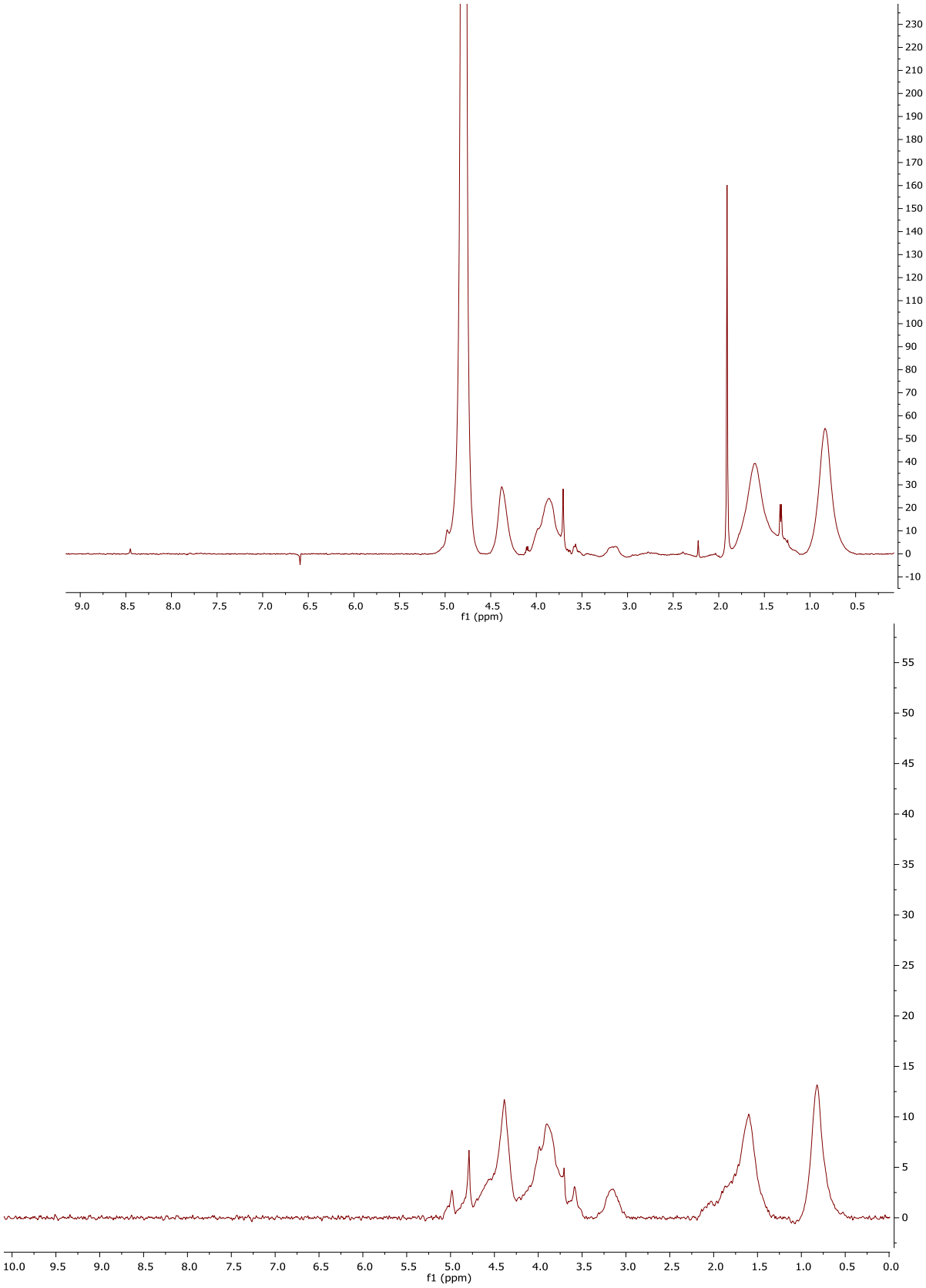

Fig.E.19.

Top: ^{1}H-NMR (500 MHz) spectrum of **AuNP4** in D_2O
Bottom: Diffusion-filtered ^{1}H-NMR (500 MHz) spectrum of **AuNP4** in D_2O

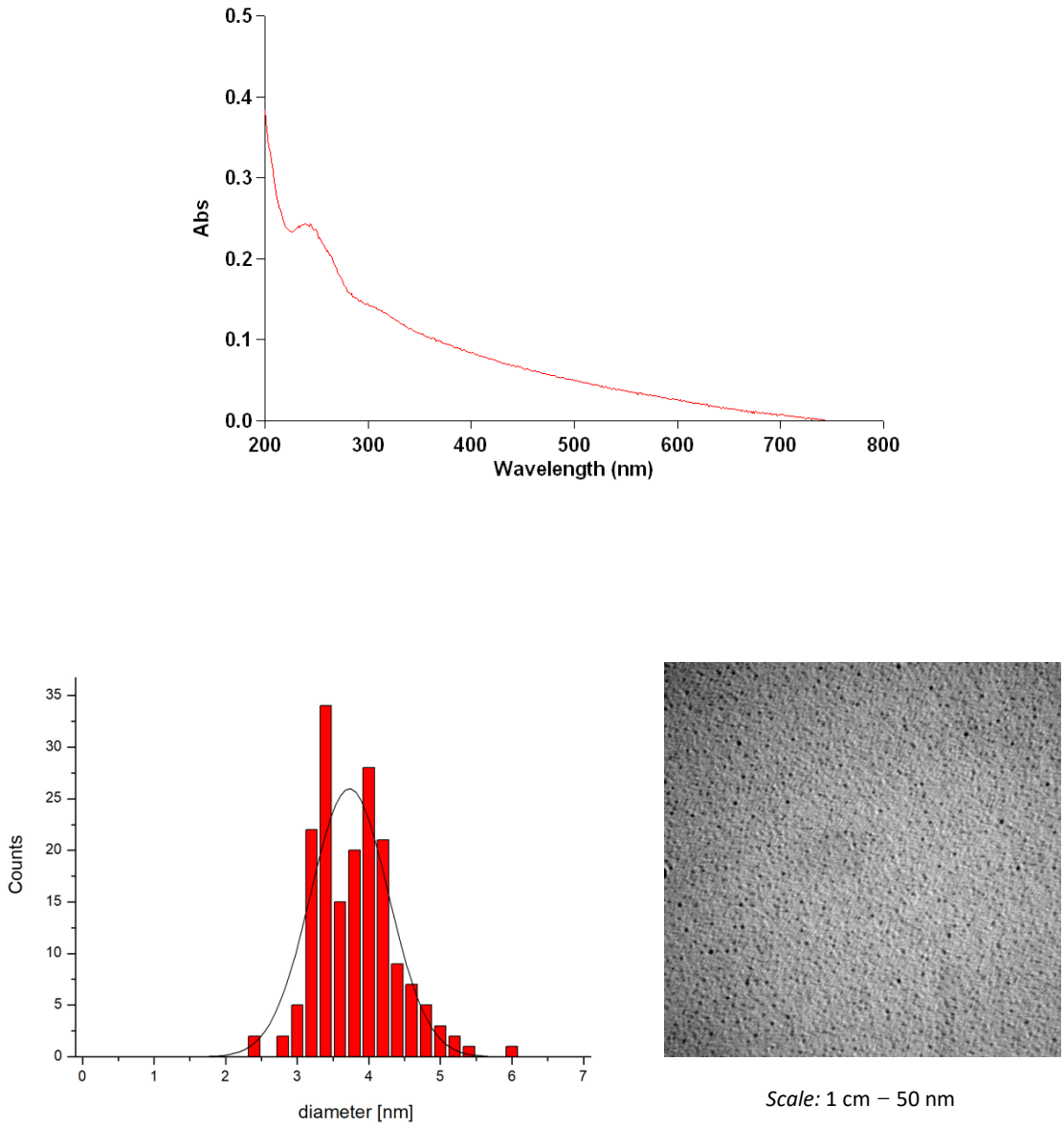

Fig.E.20.

Top: UV-VIS analysis of **AuNP5**
Bottom: TEM image and size distribution of **AuNP5**. Average diameter = 3.7 nm (± 0.5 nm)

*TGA analysis of **AuNP5** was not studied due to very small amount of obtained nanoparticles.

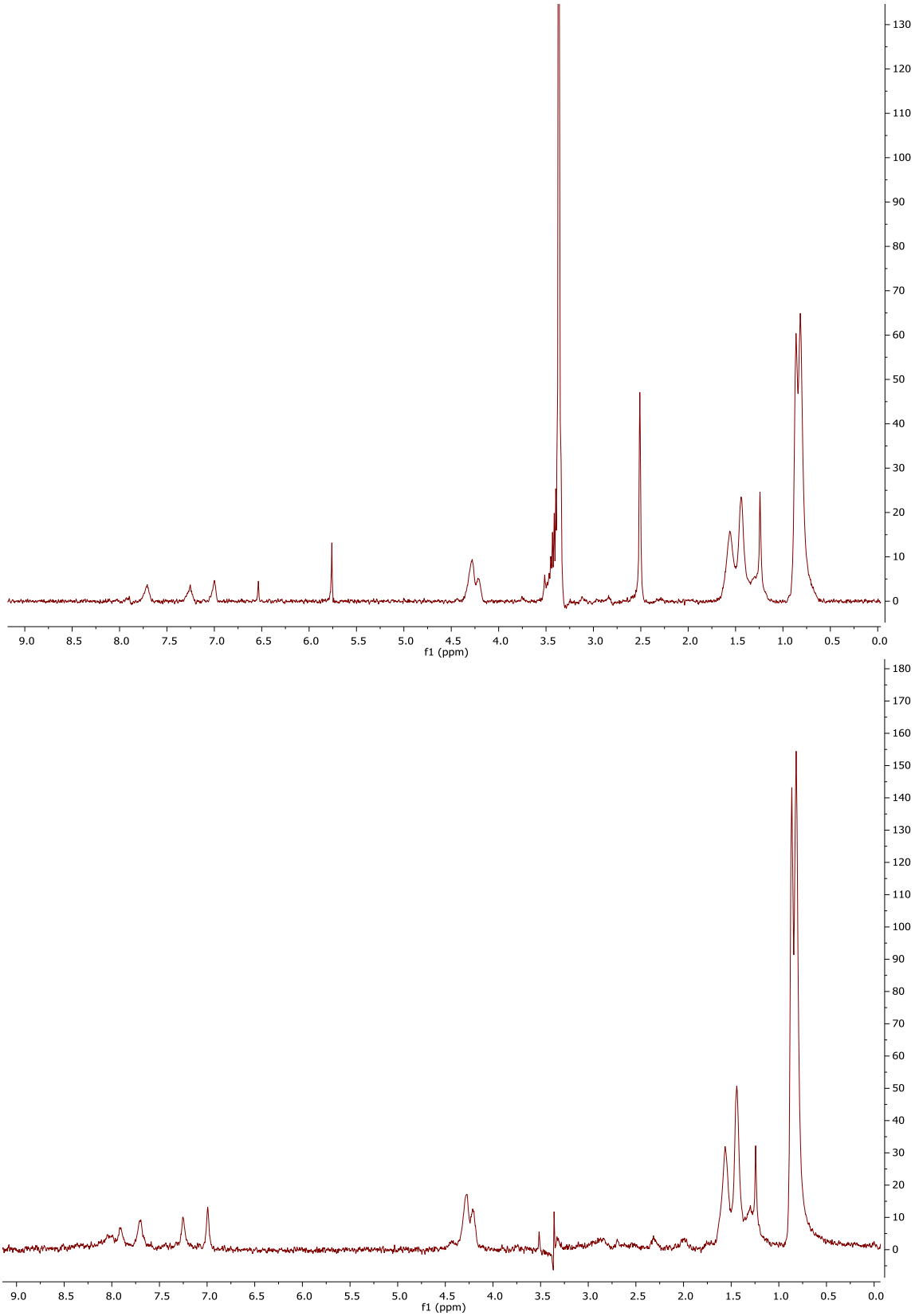

Fig.E.21.

Top: ^{1}H-NMR (500 MHz) spectrum of **AuNP5** in d-DMSO
Bottom: Diffusion-filtered ^{1}H-NMR (500 MHz) spectrum of **AuNP5** in d-DMSO

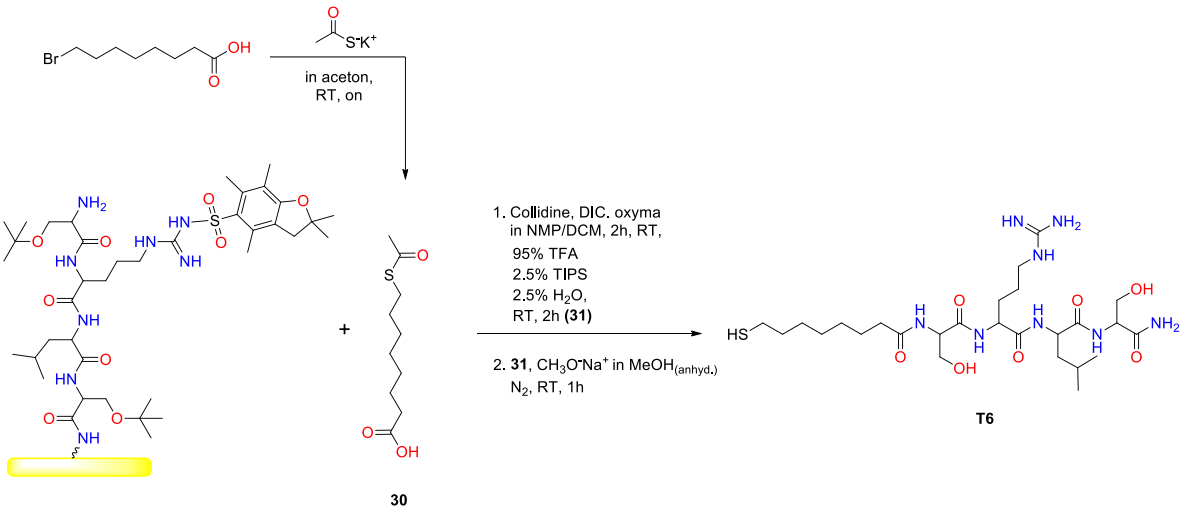

Scheme E.22.

8-(acetylthio)octanoic acid (30): In a round-bottom flask, 8-bromooctanoic acid (2.0 g, 9.0 mmol, 1.0 eq.) was dissolved in 40 mL of acetone. Potassium thioacetate (2.25 g, 19.7 mmol, 2.0 eq.) together with 20 mL of acetone was added. This resulting mixture was stirred overnight at room temperature. Afterwards the solution was concentrated, re-dissolved in DCM and filtrated. The filtrate was concentrated again and remaining orange oil was purified by column chromatography (DCM/ACN 100/0-90/10). The desired product was obtained as an orange solid (89% yield).

^{1}H-NMR ($CDCl_3$, 500 MHz), δ: 2.85 (t, J = 7.3 Hz, 2H), 2.34 (t, J = 7.5 Hz, 2H), 2.33 (s, 3H), 1.65-1.53 (m, 4H), 1.39-1.29 (m, 6H)

^{13}C-NMR ($CDCl_3$, 500 MHz), δ: 196.5, 180.0, 34.30, 31.04, 29.80, 29.47, 29.10, 28.93, 24.95

ESI-MS (m/z): 216.9 $[M - H]^-$

1-amino-6-((1-((1-amino-3-hydroxy-1-oxopropan-2-yl)amino)-4-methyl-1-oxopentan-2-yl)carbamoyl)-9-(hydroxymethyl)-8,11,20-trioxo-19-thia-2,7,10-triazahenicosan-1-iminium (31): The synthesis of H-Ser-Arg-Leu-Ser-NH_2 (**a**) on the solid platform was performed as described before. After the last coupling with serine, (**30**) (273 mg, 1.25 mmol, 1.2 eq.), oxyma (ethyl cyano(hydroxyimino)acetate; 117.5 mg, 1.25 mmol, 1.0 eq.), *N,N'*diisopropylcarbodiimide (DIC; 157.7 mg, 193.5 µL, 1.25 mmol, 1.0 eq.) and collidine

(2,4,6-Trimethylpyridine; 177.5 mg, 1.25 mmol, 1.0 eq.) were dissolved in 5 mL of *N*-methyl-2-pyrrolidon and sonicated. Resulting mixture was poured on the resin. A total volume was adjusted using dichloromethane (up to 15 mL) and then everything was stirred for 2 hours. The solvents were filtrated, resin washed with NMP, MeOH and DCM, respectively. Then the cocktail made from 95% (v) of TFA, 2.5% (v) of triisopropylsilane and 2.5% (v) of water was poured into dry resin, in order to cleave the peptide derivative from the solid platform. The concoction was stirred for 2 hours. Afterwards, the crude was quenched and washed several times with cold *tert*-butylmethyl ether. The whole protocol was repeated 5 times. Desired product yielded a formation of a desired compound as a yellowish solid with a high purity (59% yield).

^{1}H-NMR (CD_3OD, 500 MHz), δ: 4.43-4.39 (m, 4H), 3.89-3.84 (m, 4H), 3.24-3.20 (t, 2H), 2.91-2.86 (t, 2H), 2.37-2.31 (m, 5H), 1.65-1.55 (m, 11H), 1.33-1.20 (m, 6H), 0.94-0.88 (m, 6H)
TOF MS ES(-): 661.3680, 662.3705, 663.3687

1-amino((5-((1-((1-amino-3-hydroxy-1-oxopropan-2-yl)amino)-4-methyl-1-oxopentan-2-yl)amino)-4-(3-hydroxy-2-(8-mercaptooctanamido)propanamido)-5-oxopentyl)amino)methaniminium (T6): In a two-neck round-bottom flask previously flushed with nitrogen, (**31**) (66 mg, 0.1 mmol, 1.0 eq.) was solubilized in 5 mL of of anhydrous methanol. Then sodium methoxide (11 mg, 0.2 mmol, 2.0 eq.) was added. The mixture was stirred at RT under nitrogen for 1 hour. Next the methanol was evaporated and the crude was dried under high vacuum. Obtained product was used *in situ* without any additional purification in the synthesis of gold nanoparticles (**AuNP6**).

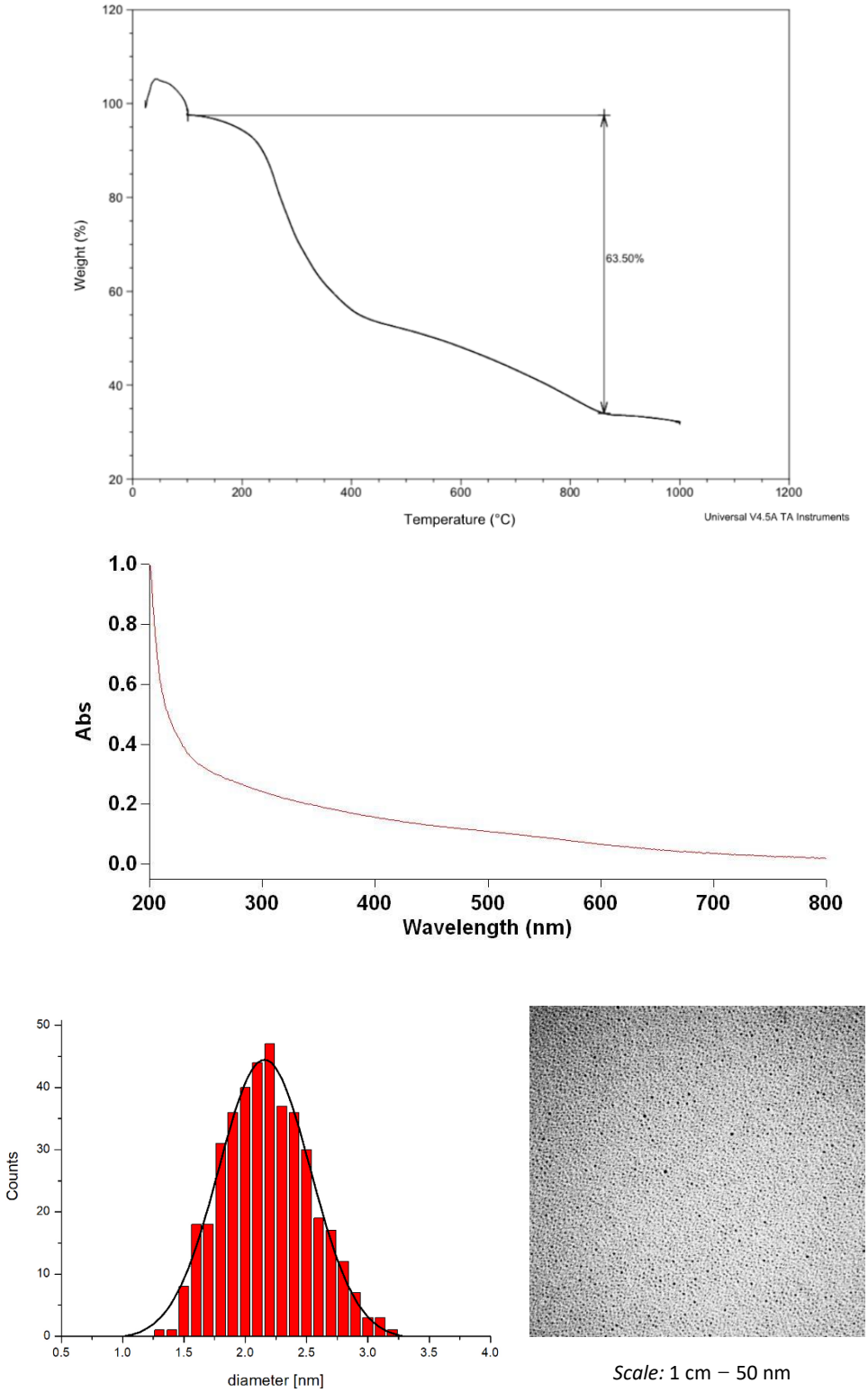

Fig.E.23.

Top: TGA analysis of **AuNP6**. Formula: $Au_{329}(SR)_{181}$
Middle: UV-VIS analysis of **AuNP6**
Bottom: TEM image and size distribution of **AuNP6**. Average diameter = 2.2 nm (± 0.4 nm)

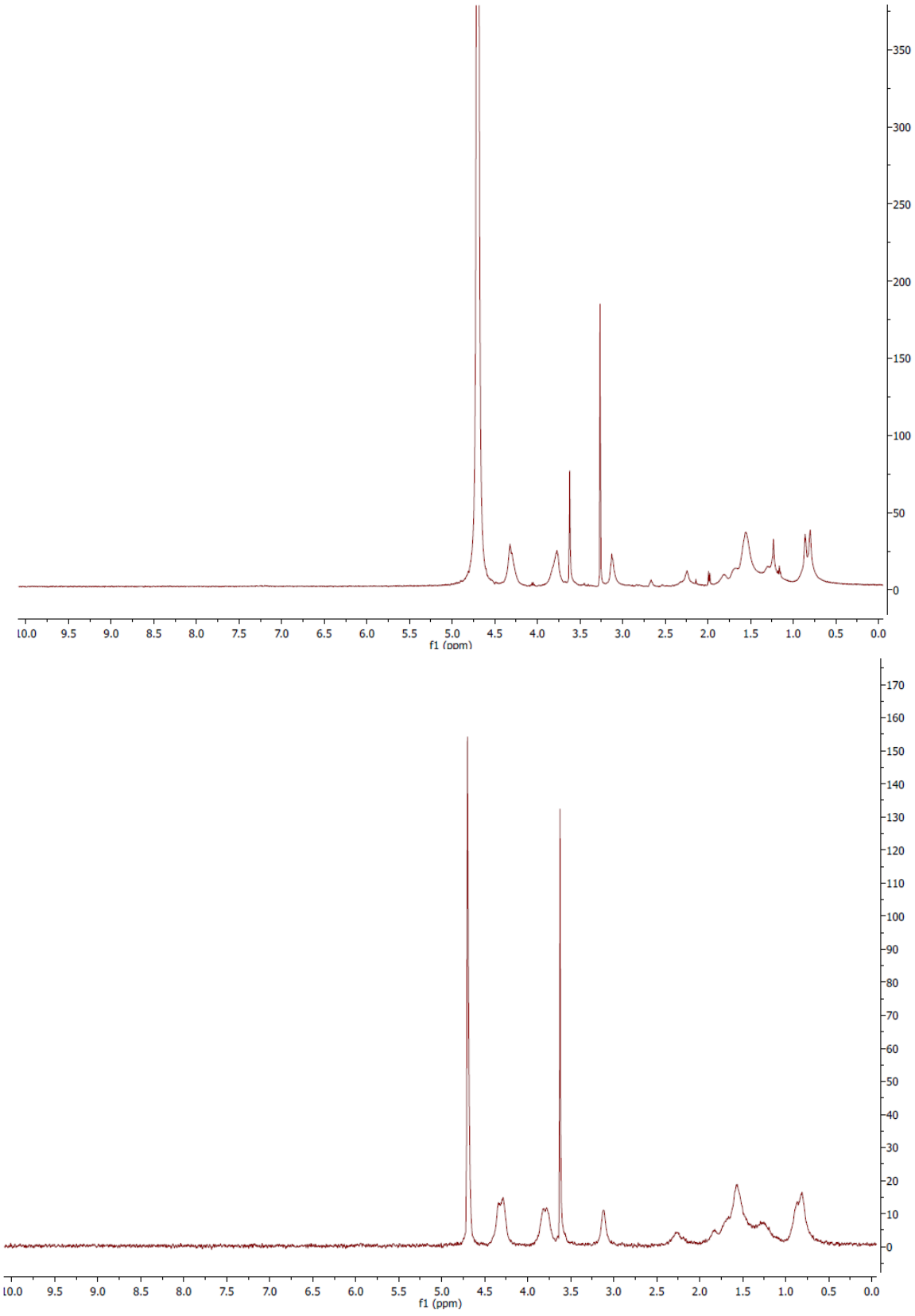

Fig.E.24.

Top: ^{1}H-NMR (500 MHz) spectrum of **AuNP6** in CD_3OD
Bottom: Diffusion-filtered ^{1}H-NMR (500 MHz) spectrum of **AuNP6** in CD_3OD

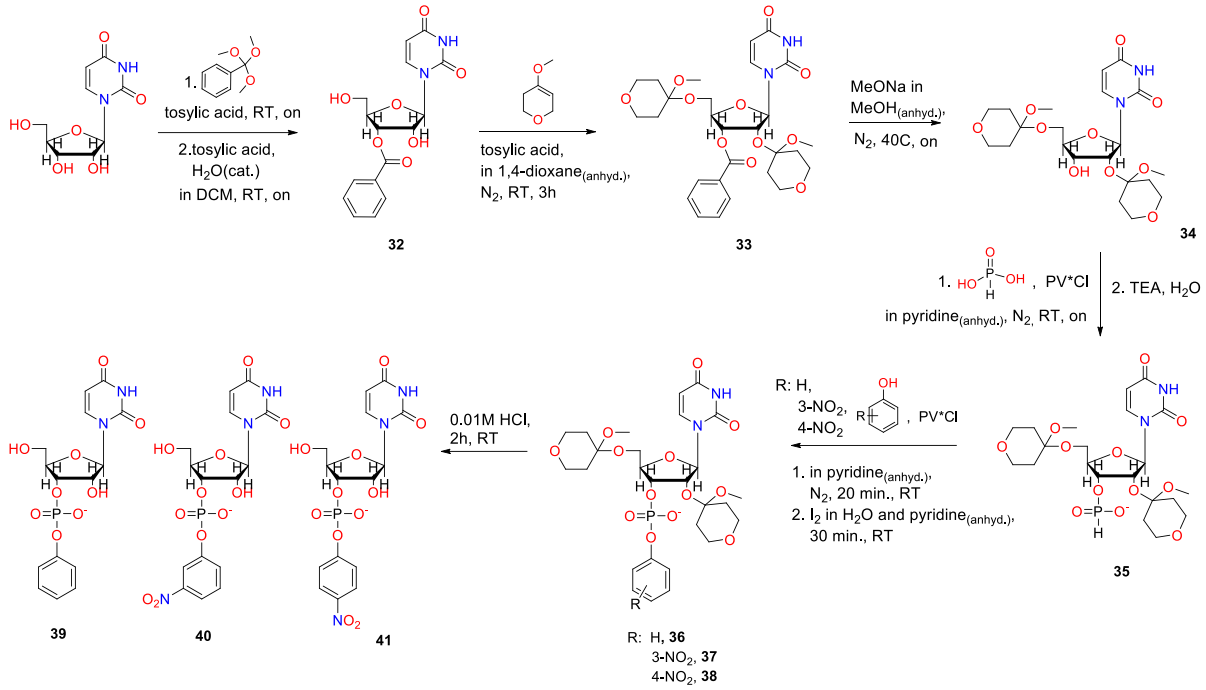

Scheme E.25.

3′-Benzoyluridine (32): In a two-neck round-bottom flask previously flushed with nitrogen, uridine (1.0 g, 4.1 mmol, 1.0 eq.) was added to the solution of trimethyl orthobenzoate (547 mg, 5.2 mL, 3.0 mmol, 0.7 eq.) and tosylic acid (500 mg, 3.0 mmol, 0.7 eq.) in 10 mL of anhydrous tetrahydrofuran. The mixture was stirred overnight at room temperature. Afterwards, a small amount of methanolic sodium methoxide was added to neutralize the products. The mixture was concentrated *in vacuo* and purified by silica gel column chromatography (chloroform/methanol 95/5-90/10). Isolated product yielded with a diastereomeric mixture of 2′,3′-methoxybenzylideneuridine as a colourless glass. The mixture was further hydrolysed: **1** (800 mg, 2.2 mmol, 1.0 eq.) together with tosylic acid (25 mg, 0.13 mmol, 0.1 eq.) was solubilized in dichloromethane followed by the addition of 2 mL of water. The resulting mixture was stirred overnight at room temperature. All volatiles were removed from the reaction and the residue was solubilized in ethanol. Next, the alcohol was evaporated and this process repeated 3 times. The remaining white solid was recrystallized from ethanol resulting in a white foamy solid (42% yield).[7], [8]/

^{1}H-NMR (d-DMSO, 500 MHz), δ: 11.40 (s, 1H), 8.05 (m, 2H), 7.92 (d, J = 8.1 Hz, 2H), 7.71-7.76 (m, 1H), 7.58-7.55 (m, 2H), 5.94 (d, J = 6.9 Hz, 1H), 5.84 (d, J = 6.1 Hz, 1H), 5.73 (d, J = 8.1 Hz, 1H), 5.38 (m, 1H), 5.34 (t, 1H), 3.67 (m, 2H)

^{13}C-NMR (d-DMSO, 500 MHz), δ: 164.5, 162.5, 150.4, 140.0, 133.0, 129.0, 128.2, 101.87, 86.75, 82.21, 73.13, 71.40, 60.55

ESI-MS (m/z): 349.0 $[M + H]^+$, 371.1 $[M + Na]^+$, 346.9 $[M - 2H]^-$

2′,5′-O-Bis(methoxytetrahydropyranyl) 3′-benzoyluridine (33): In a two-neck round-bottom flask previously flushed with nitrogen, (**32**) (400 mg, 1.1 mmol, 1.0 eq.) was solubilized in 10 mL of anhydrous 1,4-dioxane. Tosylic acid (20 mg, 0.1 mmol, 0.1 eq.) and 4-methoxy-5,6-dihydropyran (377 mg, 369 μL, 3.3 mmol, 3.0 eq.) were added. The mixture was stirred at room temperature under nitrogen for 3 hours. After solvent evaporation, remaining brown oil was solubilized in dichloromethane and washed with saturated aqueous solution of sodium bicarbonate. Organic phases were dried over a sodium sulfate and deprived of the solvent. The crude was purified by column chromatography (chloroform/methanol 96/4), resulting with desired compound as a white solid (39% yield).

^{1}H-NMR ($CDCl_3$, 500 MHz), δ: 8.60 (s, 1H), 8.11 (d, J = 8.4 Hz, 1H), 7.85 (d, J = 8.2 Hz, 1H), 7.62 (m, 1H), 7.50 (m, 2H), 6.36 (d, J = 7.6 Hz, 1H), 5.79 (d, J = 8.2 Hz, 1H), 5.41 (m, 1H), 4.63 (d, J = 7.5 Hz, 1H), 3.82-3.45 (m, 10H), 3.26 (s, 3H), 3.20 (s, 3H), 3.05 (m, 3H), 1.97-1.62 (m, 8H)

ESI-MS (m/z): 575.1 $[M - H]^-$, 599.2 $[M + Na]^+$

2′,5′-O-Bis(methoxytetrahydropyranyl)uridine (34): In a two-neck round-bottom flask previously flushed with nitrogen, (**33**) (160 mg, 0.3 mmol, 1.0 eq.) was dissolved in 5 mL of anhydrous methanol. Next a sodium methoxide (32 mg, 0.5 mmol, 2.0 eq.) was added. The mixture was heated up to 40°C and stirred overnight under nitrogen. The crude was concentrated and purified by column chromatography (chloroform/methanol 97/3). The product was obtained as a white foamy solid (92% yield).

^{1}H-NMR (CD_3OD, 500 MHz), δ: 7.99 (d, J = 8.2 Hz, 1H), 6.14 (d, J = 6.3 Hz, 1H), 5.80 (d, J = 8.1 Hz, 1H), 4.48 (d, J = 6.4 Hz, 1H), 4.19 (m, 2H), 3.82-3.52 (m, 10H), 3.26 (s, 3H), 3.19 (s, 3H), 1.92-1.73 (m, 8H)

^{13}C-NMR (CD_3OD, 500 MHz), δ: 165.8, 152.4, 142.3, 103.2, 100.7, 99.46, 88.28, 85.54, 73.83, 72.36, 65.85, 61.00, 36.04, 35.32, 34.91

ESI-MS (m/z): 471.1 $[M - H]^-$, 495.2 $[M + Na]^+$, 511.2 $[M + K]^+$

2′,5′-O-Bis(methoxytetrahydropyranyl)uridine 3′-H-phosphonate triethylammonium salt (35): In a two-neck round-bottom flask previously flushed with nitrogen, (**34**) (94 mg, 0.2 mmol, 1.0 eq.) (previously dried by repeated evaporation of added pyridine) was dissolved in 1 mL of 1M solution of pyridinium H-pyrophosphonate in anhydrous pyridine (1M solution was prepared by adding 0.5 eq. mol of pivaloyl chloride to 2M solution of H_3PO_3 in anhydrous pyridine). The mixture was stirred overnight under nitrogen. The reaction was hydrolysed by addition of 1 mL of triethylamine and 1 mL of water and stirred for additional 1 hour. The crude was concentrated and purified by column chromatography (dichloromethane/methanol 85/15 + 0.5% of TEA). The product was isolated as a white foamy solid (42% yield).

^{1}H-NMR (CD_3OD, 500 MHz), δ: 7.97 (d, J = 8.1 Hz, 1H), 7.73 (s, 1H), 6.19 (m, 1H), 5.80 (d, J = 8.1 Hz, 1H), 4.69 (d, J = 5.4 Hz, 1H), 4.57 (m, 1H), 4.40 (s, 1H), 3.78-3.46 (m, 10H), 3.29 (s, 3H), 3.24 (s, 3H), 1.90-1.62 (m, 8H)

^{31}P-NMR (CD_3OD, 500 MHz), δ: 6.34 (d, J = 9.4 Hz), 2.46 (d, J = 9.4 Hz)

TOF MS ES(-): 421.3265, 535.2698, 536.2782

2′,5′-O-Bis(methoxytetrahydropyranyl)uridine 3′-(aryl phosphate) Triethylammonium Salt (36-38): The appropriate phenol (0.084 mmol, 1.2 eq.) and (**35**) (45 mg, 0.07 mmol, 1.0 eq.) was dried several times by evaporation of added pyridine and left under high vacuum for 1 hour. The solid was re-dissolved in 1 mL of anhydrous pyridine and next pivaloyl chloride (17 mg, 17 μL, 0.14 mmol, 2.0 eq.) was added. The reaction was stirred for 20 minutes at room temperature under nitrogen. Then 4% solution of iodine with 2% of

water in pyridine (1 mL) was added and after 10-minute stirring, H_2O (100 μL), pyridine (3 mL) and triethylamine (1 mL) were added. After 15-minutes, the solvents were evaporated, and the crude was dried under high vacuum. The solid residue was washed several times with toluene to remove the excess of iodine. Evaporation of toluene yielded with a brownish solid, which was purified by column chromatography (eluent: chloroform/methanol 95/5 + 0.5% of TEA). Additionally, all crudes were purified with by preparative-HPLC, resulting with desired phosphates (**36**; 30-min. gradient of 0-66% acetonitrile mixed with 10% triethylammonium acetate buffer (pH 6.5); RT: 26.94 min.); (**37**; 30-min. gradient of 0-100% acetonitrile mixed with 10% triethylammonium acetate buffer (pH 6.5); RT: 22.98 min.); (**38**; 30-min. gradient of 0-80% acetonitrile mixed with 10% triethylammonium acetate buffer (pH 6.5); RT: 25.80 min.).

*TOF MS ES(-) **36**: 627.1351*

*TOF MS ES(-) **37**: 672.0973*

*TOF MS ES(-) **38**: 672.1407*

Uridine 3′-(aryl phosphate) Triethylammonium Salts (39-41): The appropriate protected aryl nucleoside phosphate (**36-38**) (2.5 *μ*mol*)* was dissolved in 0.01 M HCl (50 *μ*L*)* in an Eppendorf vial and stirred for 2 hours. Afterwards, water was added (200 *μ*L). The stock solutions of deprotected compounds were subsequently used for the kinetic studies.

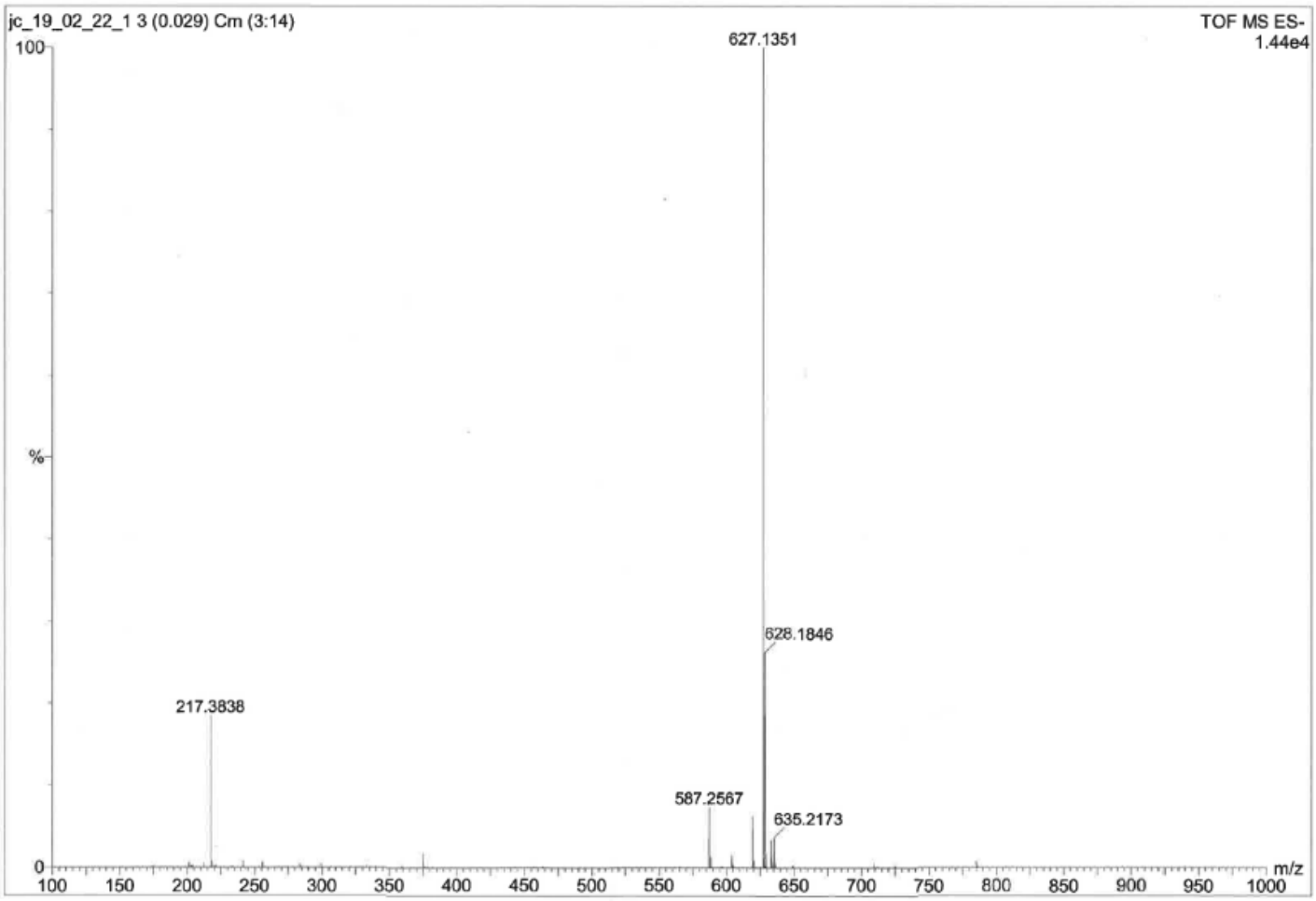

Fig.E.26. TOF MS ES(-) spectrum of (**36**). MW: 627.55

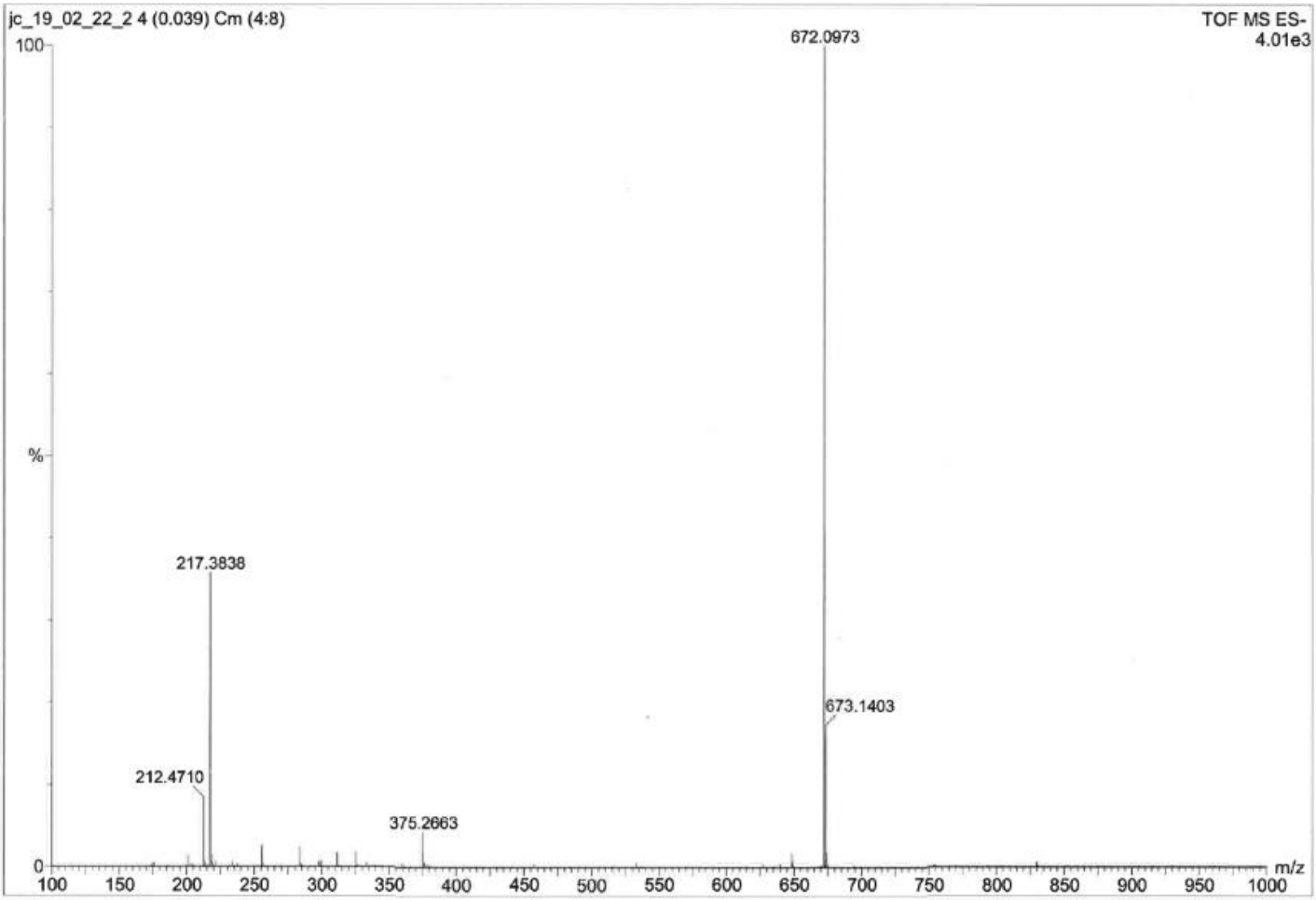

Fig.E.27. TOF MS ES(-) spectrum of (**37**). MW: 672.18

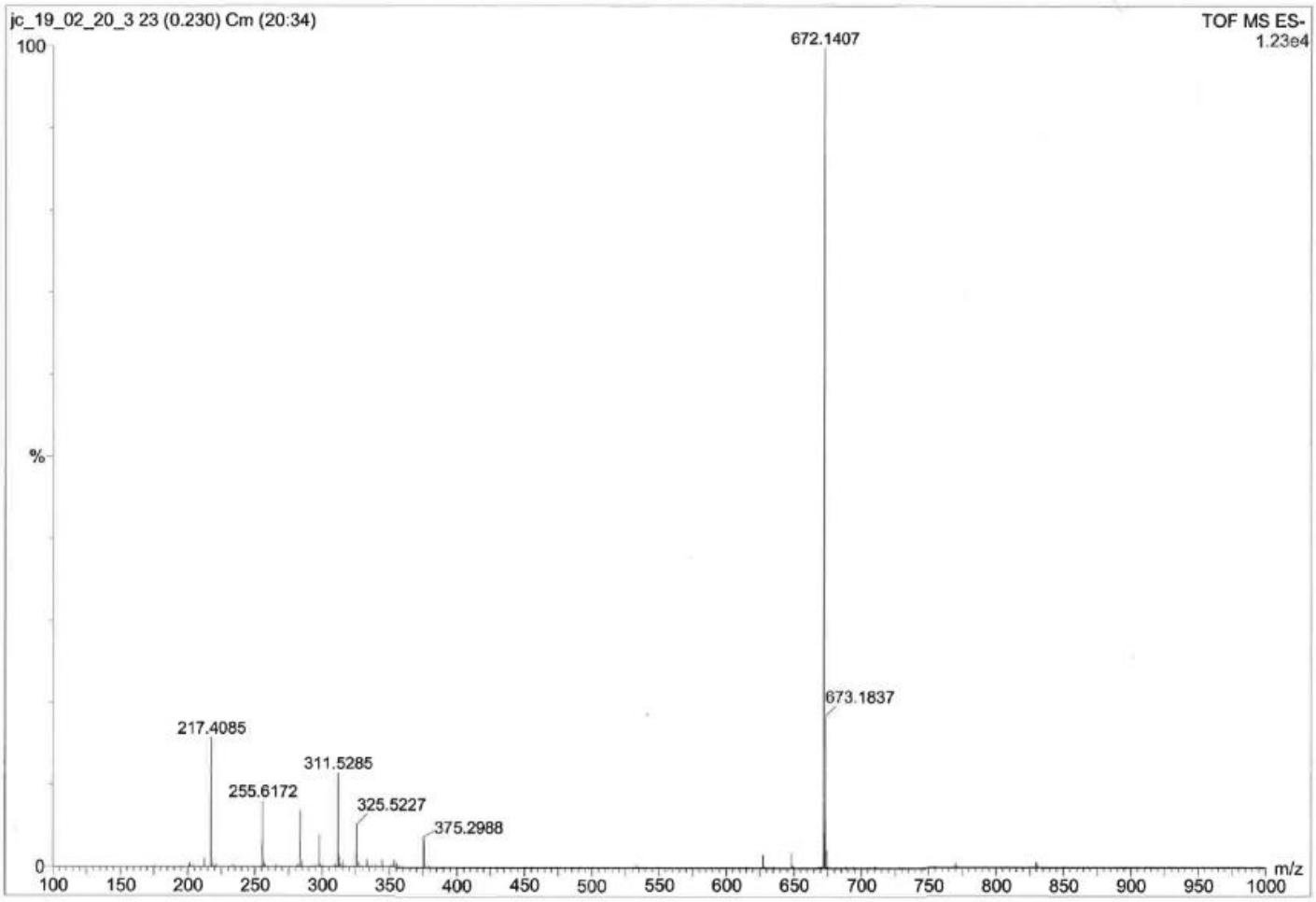

Fig.E.28. TOF MS ES(-) spectrum of (**38**). MW: 627.18

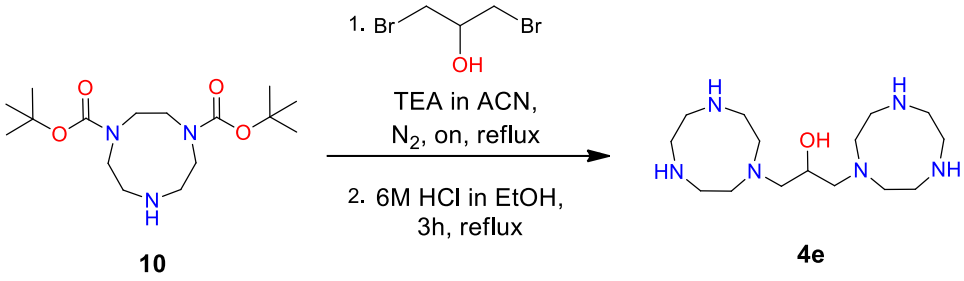

Scheme E.29.

1,3-di(1,4,7-triazonan-1-yl)propan-2-ol (4e): In a two-necked round-bottom flask previously purged with nitrogen, (**10**) (690 mg, 2.1 mmol, 2.0 eq.) was dissolved in 40 mL of anhydrous acetonitrile. Afterwards, triethylamine (318 mg, 438 µL, 3.1 mmol, 3.0 eq.) was added dropwise. Next, 1,5-dibromo-propan-2-ol (229 mg, 107 µL, 1.1 mmol, 1.0 eq.) was added in one portion. The resulting mixture was refluxed overnight under nitrogen. The crude was cooled down and concentrated *in vacuo*. The residue was purified by column chromatography (dichloromethane/methanol 95/5-90/10 + 0.05% TFA). After collection of desired product and its detection by ESI-MS, di-Boc-protected (**4e**; 730 mg, 1.0 mmol) was dissolved in 5 mL of ethanol and treated with 5 mL of 6M HCl. The mixture was refluxed for 2 hours and afterwards concentrated *in vacuo.* The residual solid was washed a several times with ethanol and left for drying out. Desired product was formed as a white solid (75% overall yield).[9]

^{1}H-NMR (D_2O, 500 MHz), δ: 4.27-4.25 (m, 1H), 3.67-3.61 (m, 8H), 3.35-3.33 (m, 8H), 3.17-3.11 (m, 4H), 3.07-3.03 (m, 4H), 2.81-2.78 (m, 2H), 2.68-2.65 (m, 2H)

^{13}C-NMR (D_2O, 500 MHz), δ: 65.93, 58.64, 48.23, 43.80, 42.16

ESI-MS (m/z): 158.1 $[0.5M + H]^+$, 315.3 $[M + H]^+$

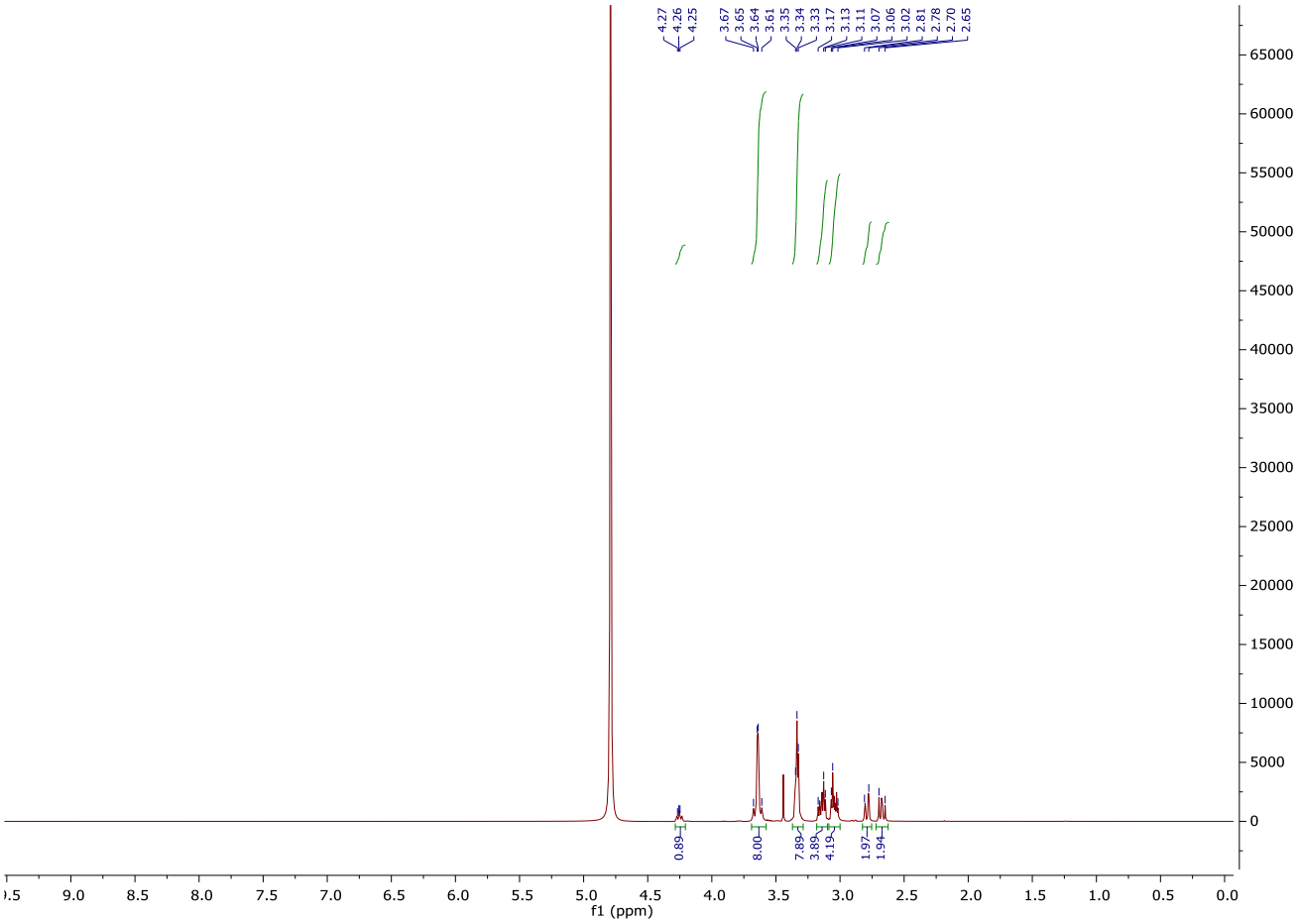

Fig.E.30. ^{1}H-NMR (500 MHz) spectrum of (**4e**) in D_2O.

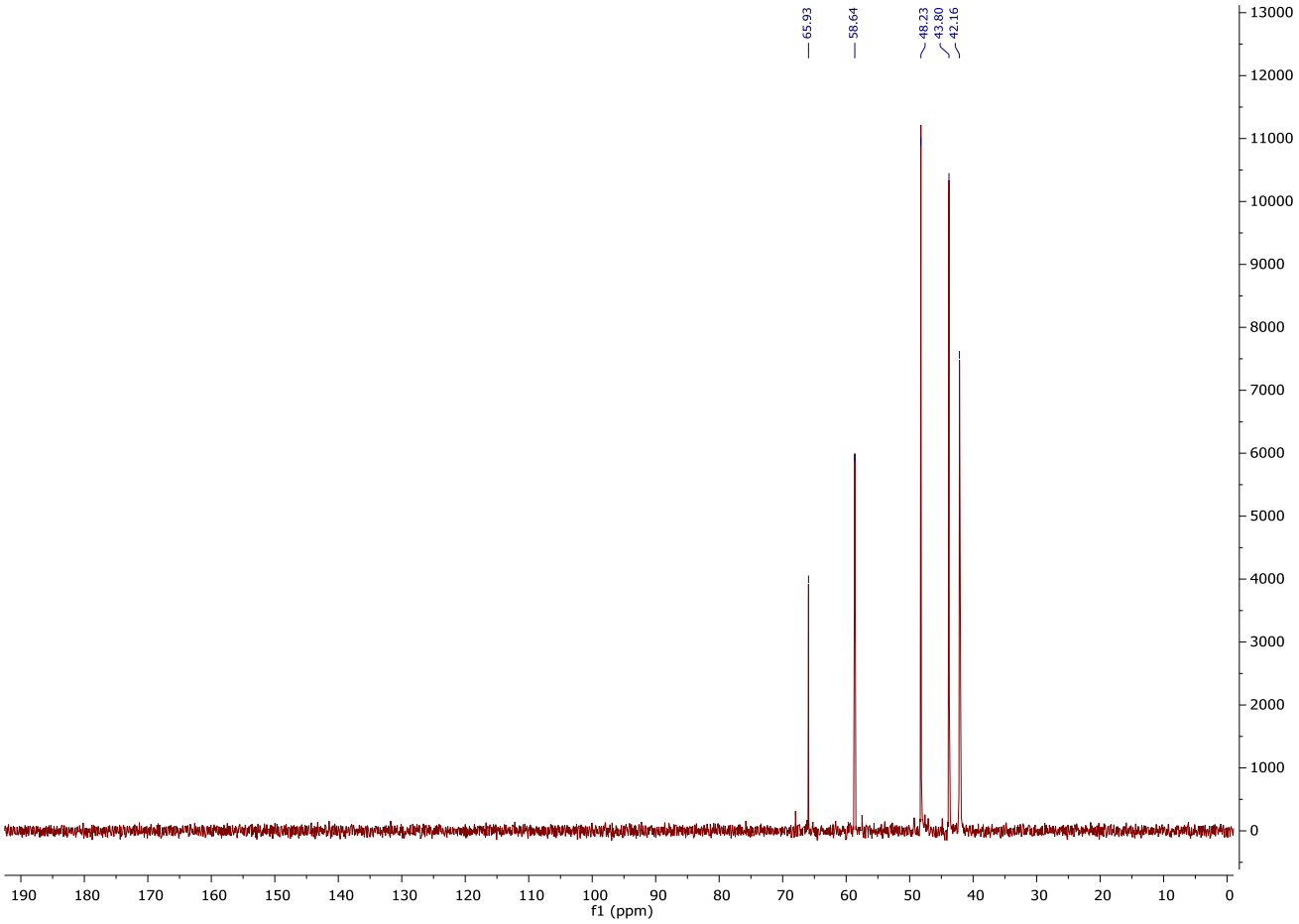

Fig.E.31. ^{13}C-NMR (500 MHz) spectrum of (**4e**) in D_2O.

4. The Plasmid DNA Cleavage – Agarose Gel Pictures.

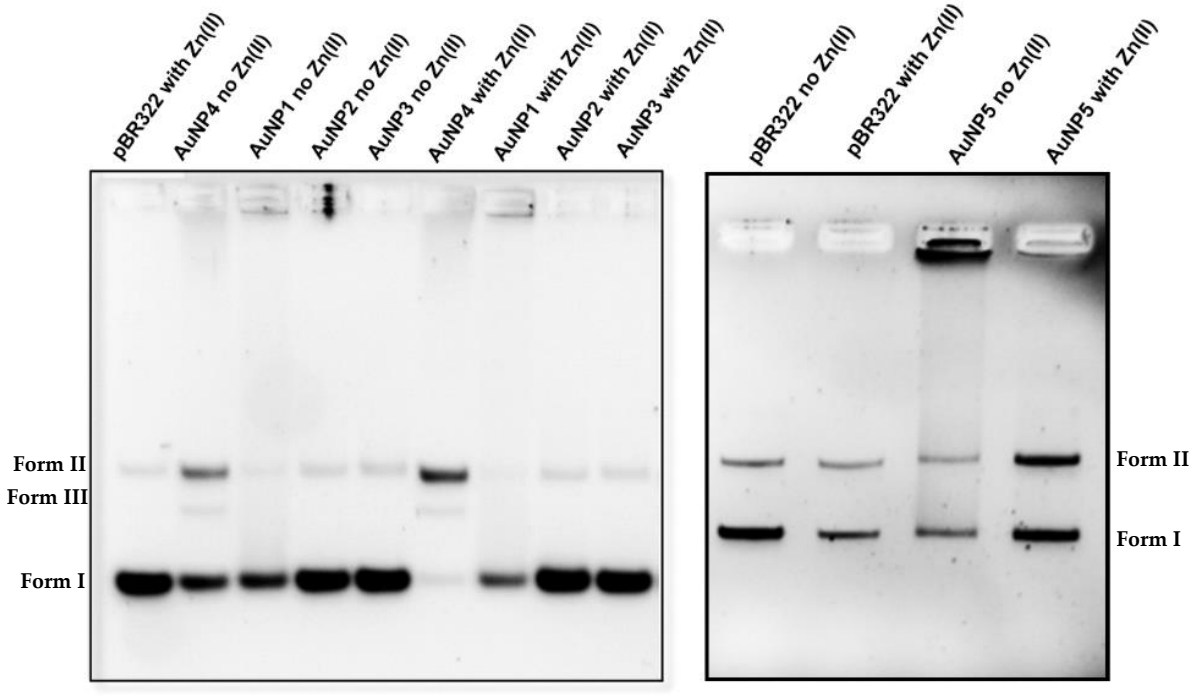

Fig.E.32. The agarose gel of the plasmid DNA cleavage after 24-hour incubation with **AuNP1-4** (left) and **AuNP5** (right).
Conditions: [nanozyme] = 45 μM, [pBR322 DNA] = 19.3 μM/bp, [HEPES] = 20 mM, 37°C, pH 7.5 in H_2O.

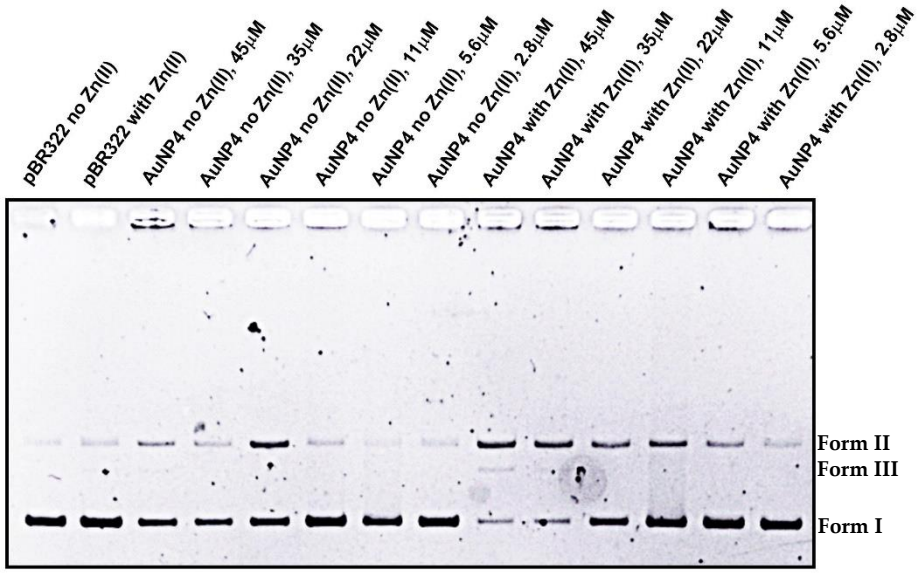

Fig. E.33. The agarose gel of the plasmid DNA cleavage by **AuNP4** after 1-hour incubation.
Conditions: [pBR322 DNA] = 19.3 μM/bp, [HEPES] = 20 mM, 37°C, pH 7.5 in H_2O.

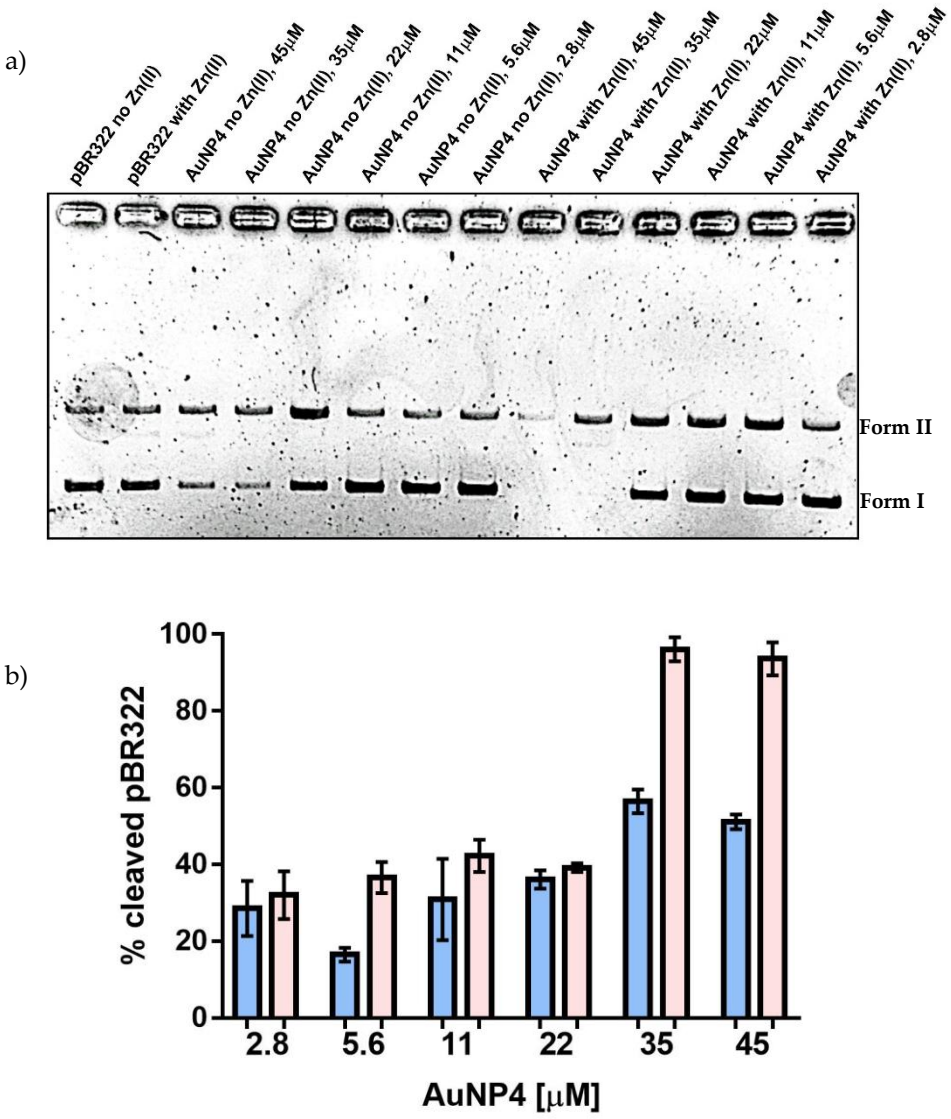

Fig. E.34. The agarose gel (*a*) and its quantification (*b*) of the plasmid DNA cleavage by **AuNP4** after 24-hour incubation.
Conditions: [pBR322 DNA] = 19.3 μM/bp, [HEPES] = 20 mM, 37°C, pH 7.5 in H_2O.

5. Uridine 3′-(LG) Phosphate Cleavage – Experimental Details.

	t_R/min				
Leaving group	**Substrate**	**(2)**	**(3)**	**(4)**	**HEPES**
-CH_2CH_2Cl (LG_1)	9.813	2.129	2.197	2.348	2.393
-CH_2CHCl_2 (LG_2)	13.073				
-CH_2CCl_3 (LG_3)	14.357				
-Ph (LG_4)	13.508				

Table E.35. Retention times of uridine 3′-(**LG_1-LG_4**) phosphates, cyclic phosphate (**2**), uridine 3′-phosphate (**3**), uridine 2′-phosphate (**4**) and HEPES.

The reactions of uridine 3′-(**LG_1-LG_4**) phosphates were carried out in Eppendorf tubes. The temperature of reaction solutions was controlled by a water bath thermostat, set at 40°C. The reactions' progress was followed by Agilent Technologies 1260 Infinity RP HPLC on Phenomenex Kinetex 5u XB-C18 100A (150 x 4.6 mm) column and the flow rate being 1.0 mL x min^{-1}. Aliquots were withdrawn (20 μL) from the reaction mixtures at appropriate intervals and UV-detection at 260 nm was employed for the analysis. A step-wise elution was applied, using as eluents the mixtures of water (A) and acetonitrile (B) with 0.02% TFA (0-8 min. (2% B), 8-10 min. (10% B), 10-15 min. (30% B), 15-25 min. (80% B), 25-30 min. (90%B), 30-36 min. (100%B), 36-37 min. (0%B)). The legitimacy of interpreted results was confirmed by (**2**) and (**3**) standards, purchased in Biosynth®Carbosynth (*Fig. E.40*). The rate constants of the cleavage were calculated by following a decrease of substrate's signal on chromatogram, as the function of time. Obtained results gave the final rate constants upon applying the integrated rate-law of the first-order processes.

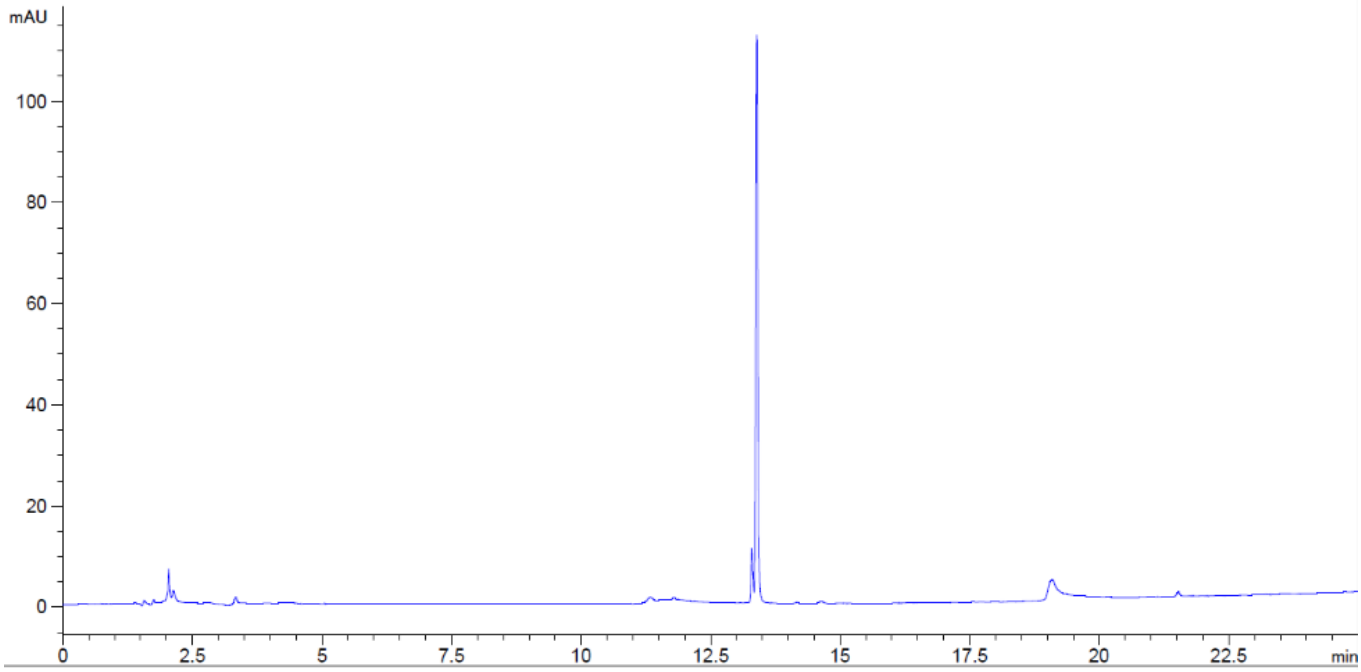

Fig. E.36. The HPLC chromatogram of uridine 3′-(**LG**$_4$) phosphate in the presence of the catalyst and HEPES at time 0.

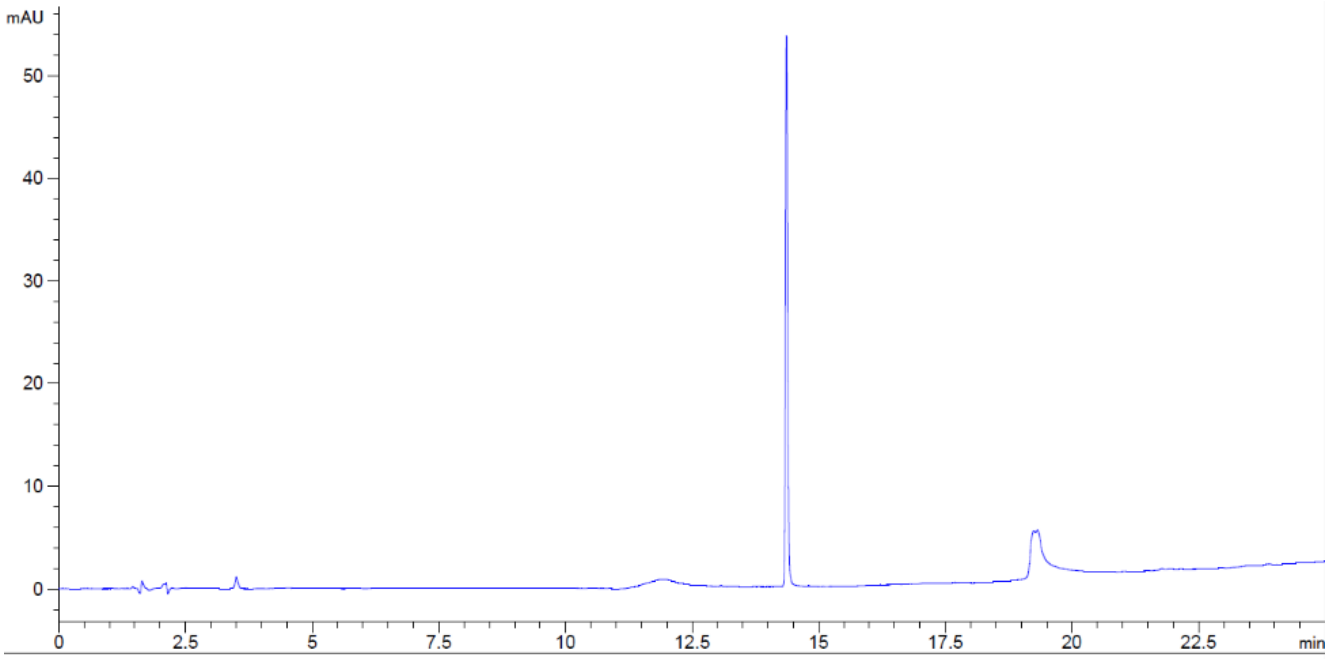

Fig. E.37. The HPLC chromatogram of uridine 3′-(**LG**$_3$) phosphate in the presence of the catalyst and HEPES at time 0.

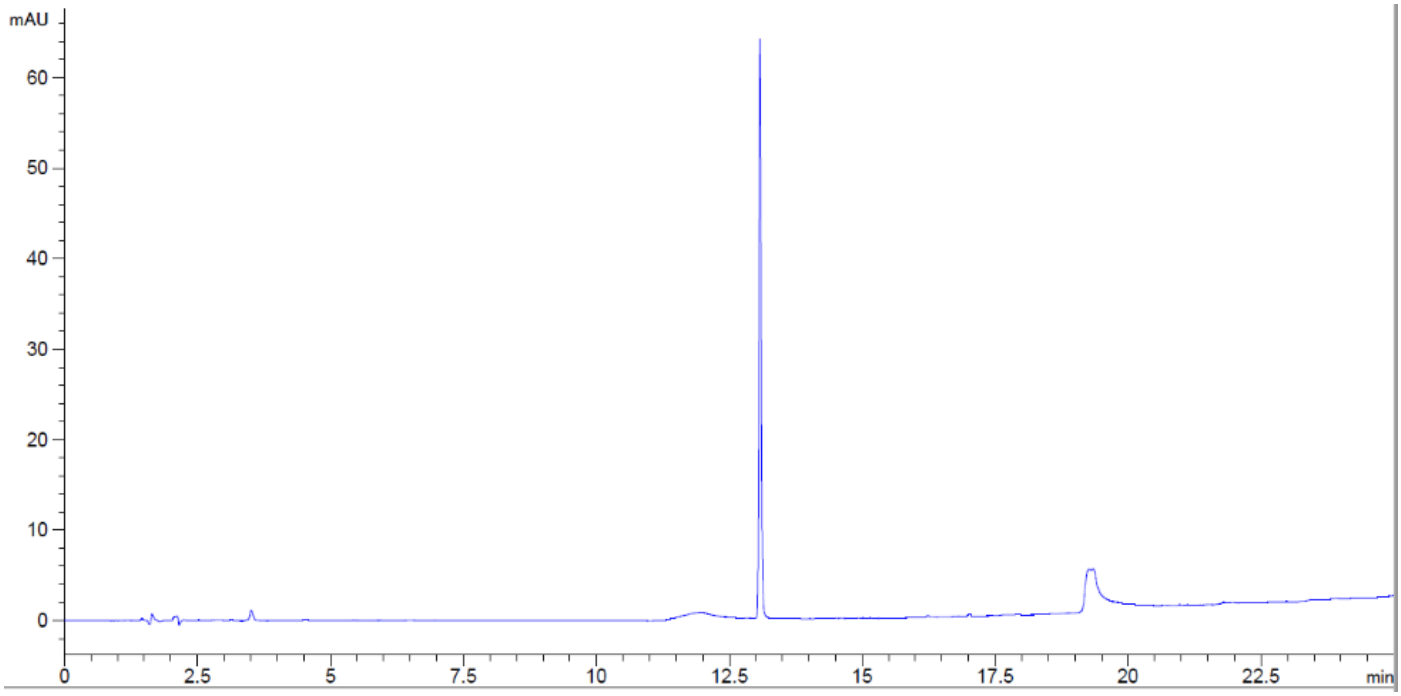

Fig. E.38. The HPLC chromatogram of uridine 3′-(**LG**$_2$) phosphate in the presence of the catalyst and HEPES at time 0.

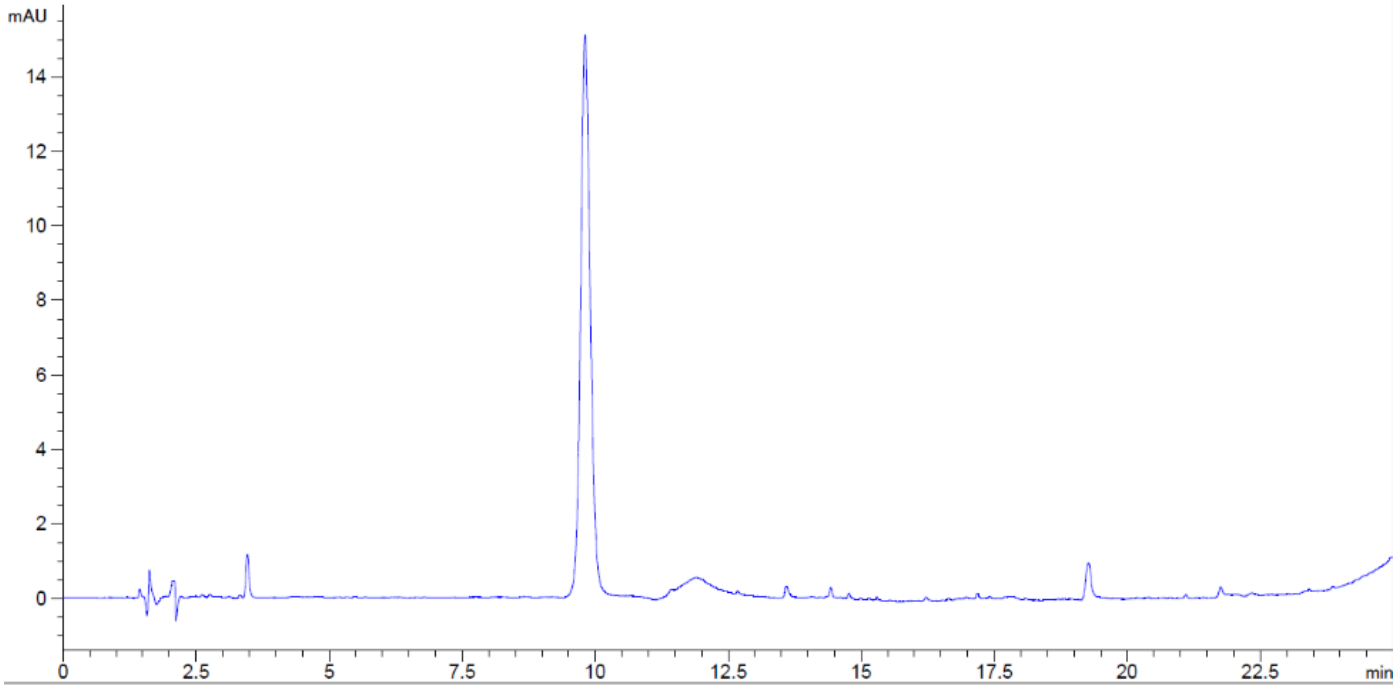

Fig. E.39. The HPLC chromatogram of uridine 3′-(**LG**$_1$) phosphate in the presence of the catalyst and HEPES at time 0.

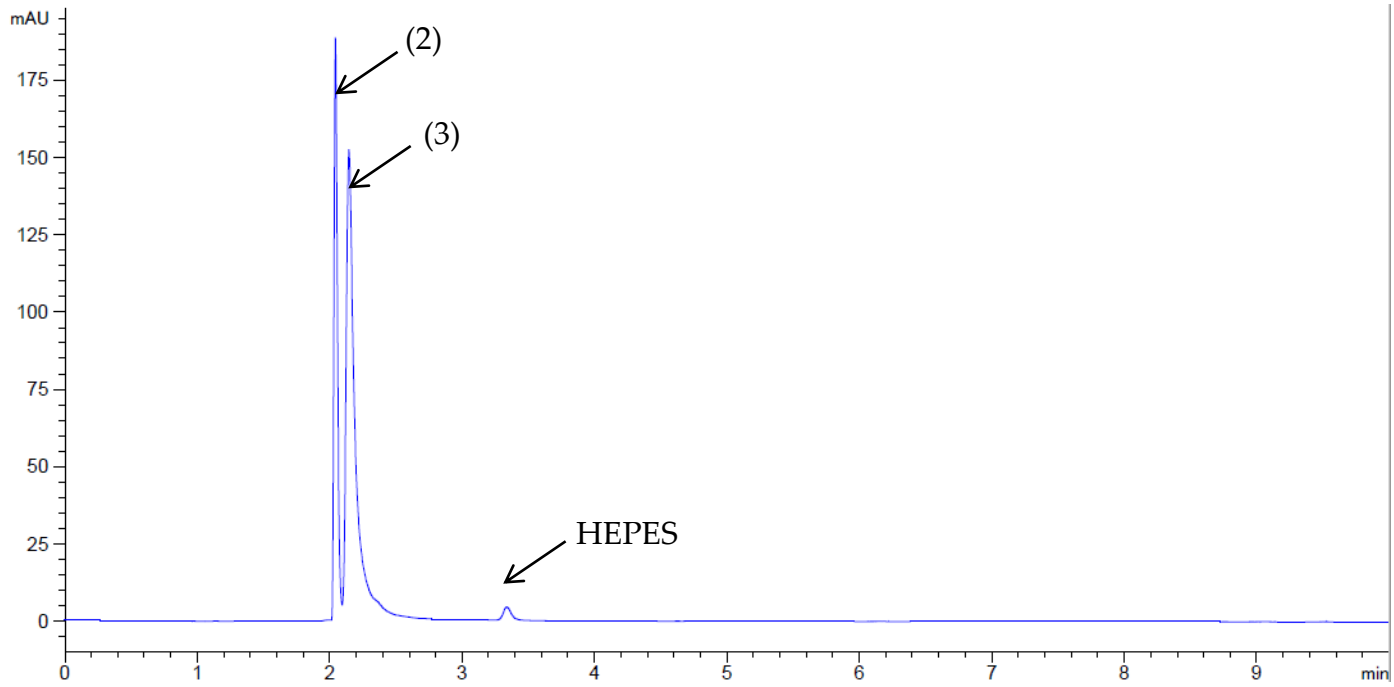

Fig. E.40. The HPLC chromatogram of uridine-2′,3′-monophosphate (**2**) and uridine 3′-monophosphate (**3**) standards in HEPES buffer.

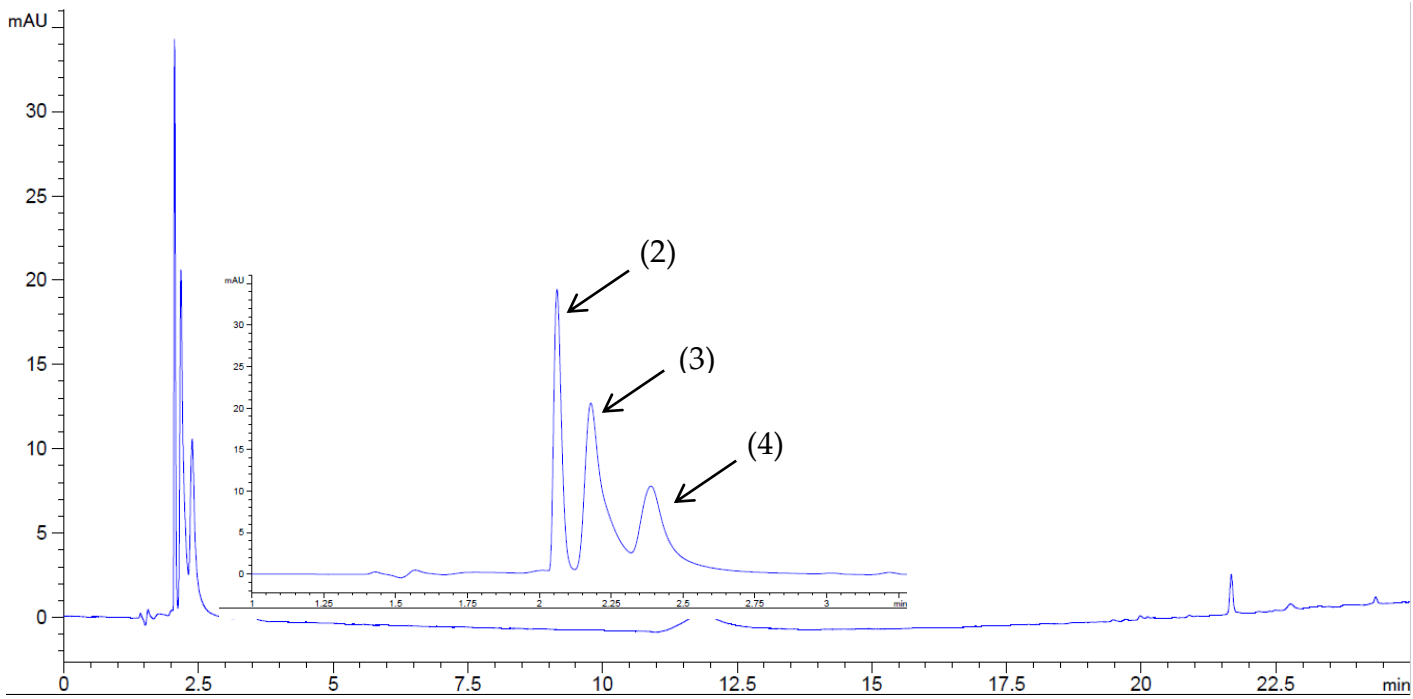

Fig. E.41. The HPLC chromatogram of uridine-2′,3′-monophosphate (**2**) standard cleavage after 48-hour incubation with Zn_2(**4e**) in HEPES.

The hydrolysis of uridine 3′-(**LG6**, **LG7**) phosphates was followed by UV-Vis spectrophotometer, monitoring the change of the absorbance vs time at 238 and 400 nm, respectively. The kinetic experiments were performed at 20, 25 and 30°C in each case (when **AuNP1** were applied as a catalyst). The results were plotted as ln(k) against 1/T and from the linear regression, the rate constants at 40°C were calculated (*Fig.E.42.*).

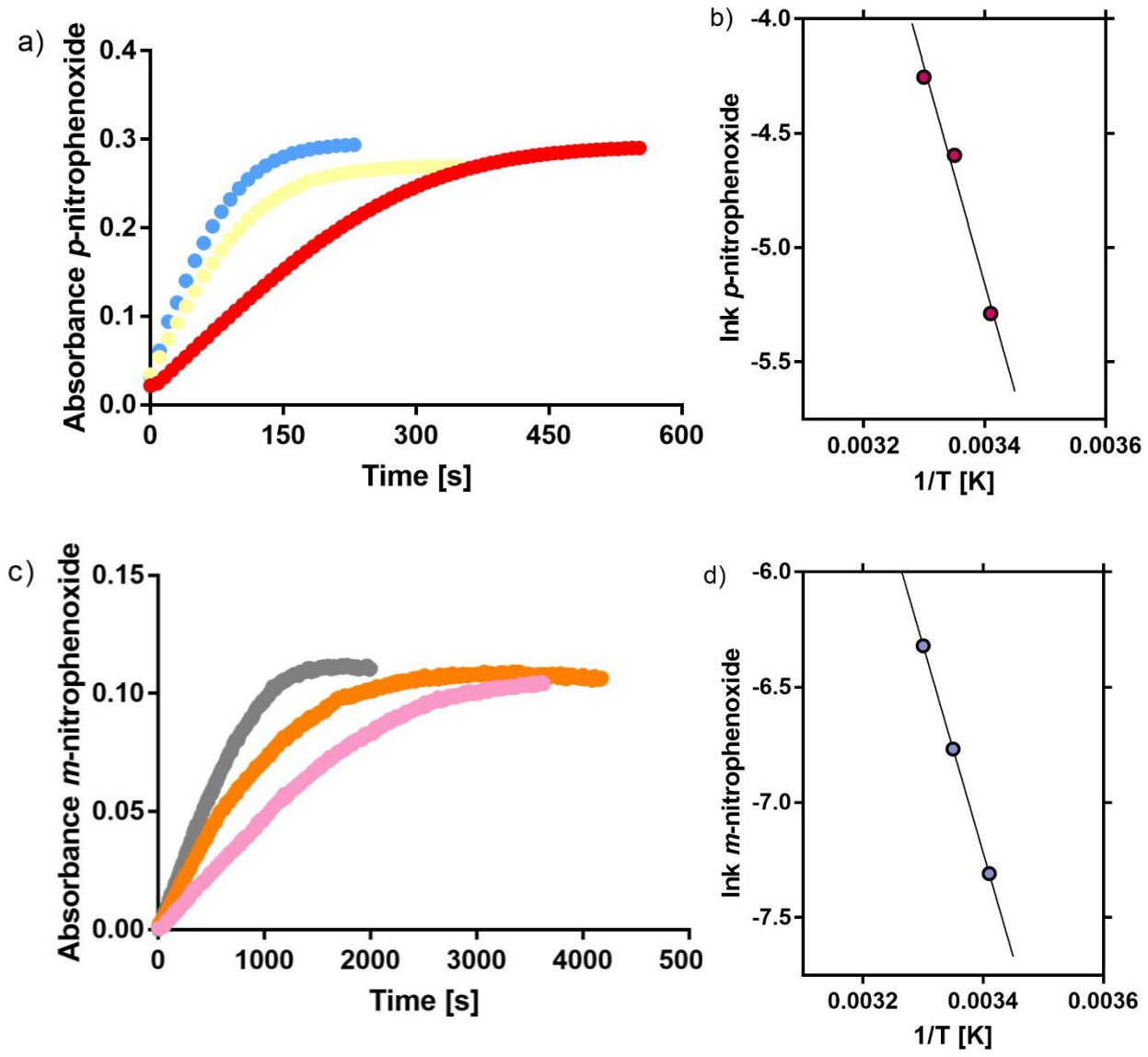

Fig. E.42. The increase of the absorbance vs time for the cleavage of uridine 3′-*p*-nitrophenyl (*a*) / *m*-nitrophenyl (*c*) phosphate in the presence of **AuNP1** at 20, 25 and 30°C;
the linear regression of rate constants as the function of ln(k) against 1/T (*b*, *d*).

6. *References of Chapter 7.*

[1] L. Qian, Y. Xu, H. Arai, J. Aoki, T. M. McIntyre, G. D. Prestwich, *Organic Letters* **2003**, *5*, 4685-4688.

[2] T. Humphry, S. Iyer, O. Iranzo, J. R. Morrow, J. P. Richard, P. Paneth, A. C. Hengge, *Journal of the American Chemical Society* **2008**, *130*, 17858-17866.

[3] Y. Xu, L. Qian, G. D. Prestwich, *Org Lett* **2003**, *5*, 2267-2270.

[4] J. Eldo, S. Heng, E. R. Kantrowitz, *Bioorganic & Medicinal Chemistry Letters* **2007**, *17*, 2086-2090.

[5] D. M. Brown, D. A. Usher, *Journal of the Chemical Society (Resumed)* **1965**, 6558-6564.

[6] F. Manea, C. Bindoli, S. Polizzi, L. Lay, P. Scrimin, *Langmuir : the ACS journal of surfaces and colloids* **2008**, *24*, 4120-4124.

[6a] Figures were modified from Dr. A. Cazzolaro's PhD thesis; **2014**, Padova.

[7] H. Almer, R. Strömberg, *Journal of the American Chemical Society* **1996**, *118*, 7921-7928.

[8] D. P. L. Green, T. Ravindranathan, C. B. Reese, R. Saffhill, *Tetrahedron* **1970**, *26*, 1031-1041.

[9] E. Kimura, S. Aoki, T. Koike, M. Shiro, *Journal of the American Chemical Society* **1997**, *119*, 3068-3076.

Acknowledgements

The period of my PhD was the biggest challenge and adventure that I have ever experienced in my entire life. 3 years ago I came to Italy not knowing anyone, being far away from family and friends and focusing everything what I had to achieve my goals. And I absolutely do not regret it.

The person who trusted my knowledge and experience, gave the opportunity to be completely independent as a researcher and was always patient, helpful and understanding, is my supervisor, Prof. Paolo Scrimin. I would not have been able to ask for a better mentor than you and I feel like I was given more than I deserved. Thank you for everything.

My PhD would not have been the same without Prof. Fabrizio Mancin. Thank you so much for your knowledge, time you dedicated me to explain matters I was struggling with, for your patience and kindness. It was an honour to work with you.

I cannot forget about people who definitely made me feel at ease thorough my last 3 years in Italy. Thanks to Lucy for making the beginning of my PhD easier and more eventful, to Kuba and Alvaro for the coolest office team I have ever had, and to Daniele, Yanchao, Sun, Samuele, Giordano, Nicola, Federico, Riccardo, Sara and Rui. I am flattered I could work with and meet you.

I would like to thank all MMBio community which enabled me to work with the world-class experts, made me better and more confident in presenting my work, as well as trained in diverse fields. Particularly, I would like to thank Dr. Tamis Darbre and Prof. Roger Strömberg for sharing their knowledge while hosting and supervising me in their laboratories. Furthermore, I am grateful for the opportunity of spending a few months in Prof. Claudia Sissi's group, where I learnt how to work with plasmid DNA.

Last, but definitely not least, I would like to thank people the closest to my heart, who have been a great support, inspiration and motivation for me.

Mum, dad and Ola. Thank you for absolutely everything. I would not be the same person, in the same place without your love, care and faith in everything I do. I hope I was able to make you proud of me.

Jacob. Meeting you during my PhD was the best thing that could have happened to me. You made me feel happier, stronger and more confident than I have ever been. Thank you for your invaluable knowledge, patience, comments and dedicated time whenever I needed your help. Thank you for everything, my love.

PhD is not only a time when we are developing our skills, knowledge and we are truly becoming independent scientists. This time is a real exam of our determination, patience, resistance and dedication for something that we are passionate about, even if it yields lack of any private life or spare time. But if you really want something, you can achieve everything. Just believe in yourself.

* * *

Okres doktoratu był niewątpliwie najważniejszym i najcięższym testem dla mnie nie tylko jako naukowca, ale i także jako kobiety. Trzy lata temu przyjechałam do Padwy nie znając tu nikogo, mając rodzinę i przyjaciół kilka tysięcy kilometrów ode mnie, będąc zdaną tylko na siebie i na swoje marzenia, determinację. I wcale nie żałuję swojej decyzji.

Osobą, która zaufała mojej wiedzy i doświadczeniu, dała możliwość bycia kompletnie niezależnym badaczem i która była zawsze cierpliwa, pomocna i wyrozumiała, jest mój promotor, Prof. Paolo Scrimin. Nie byłabym w stanie poprosić o lepszego mentora niż Ty i mam wrażenie, że dostałam więcej, niż na to zasługiwałam. Dziękuję Ci z całego serca za wszystko.

Mój doktorat nie byłby taki sam bez Prof. Fabrizio Mancin. Dziękuję Ci za Twoją wiedzę, czas, który mi poświęciłeś tłumacząc nieznane mi pojęcia, za Twoją cierpliwość i życzliwość. To był honor pracować z Tobą.

Nie mogę zapomnieć o ludziach, którzy ułatwili mi mój 3-letni pobyt we Włoszech. Dziękuję Lucy za wsparcie i obecność na początku mojej kariery doktoranckiej, Kubie i Alvaro ogromną dawkę humoru, ale także doświadczenia i wiedzy. Dziękuję również Daniele, Yanchao, Sun, Samuele, Giordano, Nicola, Federico, Riccardo, Rui i Sara. To był zaszczyt Was poznać i z Wami pracować.

Ogromne podziękowania dla członków grantu MMBio, którzy umożliwili mi pracę ze światowej klasy ekspertami w dziedzinie chemii i biologii, sprawili, że stałam się pewniejsza siebie w prezentowaniu swojej pracy oraz poszerzyli moją wiedzę i umiejętności na wielu płaszczyznach. W szczególności chciałabym podziękować Dr. Tamis Darbre i Prof. Roger Strömberg za ich gościnność i opiekę podczas mojego pobytu w ich laboratoriach. Jestem także wdzięczna za możliwość pracowania w grupie Prof. Claudia Sissi, gdzie zostałam wytrenowana w pracy z DNA.

Na koniec chciałabym podziękować osobom najbliższym mojemu sercu, którzy byli, są i będą dla mnie największym wsparciem, motywacją i inspiracją.
Mamo, Tato, Olu. Dziękuję za wszystko. Nie mogłabym być tą samą Asią, w tym samym miejscu, bez Waszej miłości, troski i wiary we wszystko, co robię. Mam nadzieję, że możecie być teraz dumni z Waszej Pani Doktor.

Jacob. Spotkanie Ciebie podczas robienia doktoratu było najlepszą rzeczą, jaka mi się mogła wydarzyć w moim życiu. Sprawiłeś, że jestem szczęśliwsza, silniejsza i pewniejsza siebie niż kiedykolwiek byłam. Dziękuję za Twoją nieocenioną wiedzę, cierpliwość, cenne uwagi i czas, który mi poświęciłeś kiedykolwiek potrzebowałam Twojej pomocy. Dziękuję Ci, mój kochany.

Doktorat jest prawdziwym egzaminem nie tylko dla naszych umiejętności i wiedzy, ale przede wszystkim sprawdza naszą wytrwałość, cierpliwość, poświęcenie i determinację. To czas, kiedy trzeba poświęcić swoje hobby i życie prywatne dla czegoś, co jest naszą zawodową pasją. Ale jeśli czegoś się bardzo chce, to można osiągnąć wszystko. Wystarczy tylko uwierzyć w siebie.